Designing Novel Thiosemicarbazone Cu(I) Complexes against Gram Positive Methicillin Susceptible *Staphylococcus Aureus* and Methicillin Resistant *Staphylococcus Aureus*

by

Anjana Madusanka De Silva Delpe Acharige

B.Sc. (Hons), Northumbria University, 2013

AN ABSTRACT OF A DISSERTATION

submitted in partial fulfillment of the requirements for the degree

DOCTOR OF PHILOSOPHY

Department of Chemistry
College of Arts and Sciences

KANSAS STATE UNIVERSITY
Manhattan, Kansas

2021

Abstract

Bacteria are microscopic, single cell organisms that can exist anywhere on earth. There are good bacteria that live synergistically inside the human body. Due to the disequilibrium in their proliferation and rapid transmission among hosts, they can be pathogenic to hosts. Misadministration of antibiotics directly assists bacteria to become multidrug resistant. Methicillin resistant *Staphylococcus aureus* (MRSA), gram positive multidrug resistant pathogenic bacteria, are categorized into the "serious" threat category, according to the CDC, and can cause major skin infections or even death. In response to the growing need for new antibiotics, it is worth uncovering the host-derived antibacterial immune response. Copper's antibacterial characteristics have attracted interest from many research groups because they tend to show promising host-derived bactericidal effects. Cu(I) ions show more prominent antibacterial properties than Cu(II) ions via the formation of hydroxy radicals and displacement of Fe from Fe-S cluster proteins. During bacterial infections, activated macrophages increase the intake of Cu(I) ions through elevated expression of the copper importer, CTR1. Trafficking of Cu(I) ions into activated macrophages involves copper importers CTR1, chaperones ATX1, CCC2 and ATP7A- copper-transporting ATPases. Similarly, bacteria activate the copper chaperone CopZ to deliver excess Cu(I) ions to CopA and CopB efflux pumps in order to resist the bactericidal activity of Cu(I) ions. All these copper trafficking proteins consist of common metal binding domain "MXCXXC". In this thesis, novel organic ligands for Cu(I) complexes are being explored for the treatment of multi drug resistant gram positive bacteria, such as *Staphylococcus aureus*.

Thiosemicarbazones are promising candidates for complexation with Cu(I) and it has been demonstrated that the complexation of thiosemicarbazone with Cu(I) can enhance its antibacterial properties. In this research, extended versions of thiourea or thiosemicarbazone derivatives

(abbreviated as NNSN) were the main focus in order to study the structure activity relationship against MSSA and MRSA. At initial stages, NNSN derivatives contained different substituted pyrazoles and 4-chlorophenyl groups. Based on the results, the substitution of electron donating groups at pyrazole's 3C enhanced the antibacterial activity. Having amine, methyl and benzyl ether groups at 3C increased activity against MSSA and MRSA. However, the anti-bacterial activity of amine substituted NNSN compounds was diminished due to the structural isomerization. EDG substitution at 4C did not contribute to the antibacterial activity as those derivatives showed less activity *in vitro.* To date, the results proved that EDG substitution at 3C of the pyrazole ring and the thionyl center enhanced the copper dependent antibacterial properties of our NNSN candidates.

Designing Novel Thiosemicarbazone Cu(I) Complexes against Gram Positive Methicillin Susceptible *Staphylococcus Aureus* and Methicillin Resistant *Staphylococcus Aureus*

by

Anjana Madusanka De Silva Delpe Acharige

B.Sc. (Hons), Northumbria University, 2013

A DISSERTATION

submitted in partial fulfillment of the requirements for the degree

DOCTOR OF PHILOSOPHY

Department of Chemistry
College of Arts and Sciences

KANSAS STATE UNIVERSITY
Manhattan, Kansas

2021

Approved by:

Major Professor
Prof. Dr. Stefan H. Bossmann

Copyright

Abstract

Bacteria are microscopic, single cell organisms that can exist anywhere on earth. There are good bacteria that live synergistically inside the human body. Due to the disequilibrium in their proliferation and rapid transmission among hosts, they can be pathogenic to hosts. Misadministration of antibiotics directly assists bacteria to become multidrug resistant. Methicillin resistant *Staphylococcus aureus* (MRSA), gram positive multidrug resistant pathogenic bacteria, are categorized into the "serious" threat category, according to the CDC, and can cause major skin infections or even death. In response to the growing need for new antibiotics, it is worth uncovering the host-derived antibacterial immune response. Copper's antibacterial characteristics have attracted interest from many research groups because they tend to show promising host-derived bactericidal effects. Cu(I) ions show more prominent antibacterial properties than Cu(II) ions via the formation of hydroxy radicals and displacement of Fe from Fe-S cluster proteins. During bacterial infections, activated macrophages increase the intake of Cu(I) ions through elevated expression of the copper importer, CTR1. Trafficking of Cu(I) ions into activated macrophages involves copper importers CTR1, chaperones ATX1, CCC2 and ATP7A- copper-transporting ATPases. Similarly, bacteria activate the copper chaperone CopZ to deliver excess Cu(I) ions to CopA and CopB efflux pumps in order to resist the bactericidal activity of Cu(I) ions. All these copper trafficking proteins consist of common metal binding domain "MXCXXC". In this thesis, novel organic ligands for Cu(I) complexes are being explored for the treatment of multi drug resistant gram positive bacteria, such as *Staphylococcus aureus*.

Thiosemicarbazones are promising candidates for complexation with Cu(I) and it has been demonstrated that the complexation of thiosemicarbazone with Cu(I) can enhance its antibacterial properties. In this research, extended versions of thiourea or thiosemicarbazone derivatives

(abbreviated as NNSN) were the main focus in order to study the structure activity relationship against MSSA and MRSA. At initial stages, NNSN derivatives contained different substituted pyrazoles and 4-chlorophenyl groups. Based on the results, the substitution of electron donating groups at pyrazole's 3C enhanced the antibacterial activity. Having amine, methyl and benzyl ether groups at 3C increased activity against MSSA and MRSA. However, the anti-bacterial activity of amine substituted NNSN compounds was diminished due to the structural isomerization. EDG substitution at 4C did not contribute to the antibacterial activity as those derivatives showed less activity *in vitro.* To date, the results proved that EDG substitution at 3C of the pyrazole ring and the thionyl center enhanced the copper dependent antibacterial properties of our NNSN candidates.

Table of Contents

List of Figures

List of Schemes

List of Tables

List of Abbreviations

ABC	ATP-binding cassette
AMR	Antimicrobial resistance
CDC	Centers for Disease Control and Prevention
DCM	Dichloromethane
DMF	Dimethylformamide
DMT	Drug/Metabolite Transporter
2-DOS	2-deoxystreptamine
EDG	Electron donating group
EWG	Electron withdrawing group
GN	Gram Negative
GP	Gram Positive
GSH	Glutathione
GSSG	Glutathione disulfide
h	Hours
IM	Inner Membrane
IMP	Integral Membrane Protein
HIV	Human Immunodeficiency virus
HTS	High Throughput screening
LPS	Lipopolysaccharide
MATE	Multidrug And Toxic compound Extrusion

MBD	Metal Binding Domain
MDR	Multi-Drug Resistant
MFS	Major Facilitator Superfamily
MIC	Minimum Inhibitory Concentration
MRSA	Methicillin-Resistant Staphylococcus Aureus
MSSA	Methicillin-Susceptible Staphylococcus Aureus
NHE	Normal Hydrogen Electrode
NMR	Nuclear Magnetic Resonance
NPV	Net Present Value
OM	Outer Membrane
PACE	Proteobacterial Antimicrobial Compound Efflux
PBP	Penicillin Binding Proteins
PMA	Phosphomolybdic Acid
PTC	Peptidyl Transferase
RND	Resistance-Nodulation-Cell Division
ROS	Reactive Oxygen Species
SA	Staphylococcus Aureus
SAR	Structure Activity Relationship
SMR	Small Multidrug Resistance
TLC	Thin Layer Chromatography
TM	Transmembrane
TSC	Thiosemicarbazone

UPLC-MS	Ultra Performance Liquid Chromatography Mass Spectrometry
VRE	Vancomycin Resistant *Enterococci*
VRSA	Vancomycin Resistant *Staphylococcus aureus*

Acknowledgements

Before anything else, I would like to express gratitude to Prof. Bossmann, for being a supportive advisor, a great mentor and a great empowering leader. I don't think that I have enough words to express how blessed I am to being in your group. From the very first day, I realize that you are such a helpful teacher and supervisor, but for me, you gave me life lessons to name one incident, I still remember your exact words when I talk about my daughter's recurrent ear infections. Then the second most important phrase you told me, "show who you are". Again, I appreciate the great support you gave me always, thank you for trusting me, guiding me, and encouraging me. And I take this opportunity to show my gratitude to Katrin. Katrin, you are the backbone of our group. You were always there to help all of us.

I would like to acknowledge my committee members: Dr. Smith, Dr. Om Prakash, Dr. Rafferty, Dr. Sues and outside-chair Dr. Revathi for your support and willingness to help me during my Ph.D. career.

I would like to thank Kansas State University, especially Dr. Aakeroy and other graduate committee members for allowing me to pursue my Ph.D. here. I am glad to acknowledge our department head Dr. Higgins, all organic faculty especially Dr. Santosh, other faculty members also for their support I had. Without them, we can't conduct our research smoothly. Therefore, I would like to acknowledge Dr. Simon Sham, Dr. Leila Maurman for keeping both the NMR machines up and running conditions, Mr. Michael Hilton and Dr. Singha for supervising teaching laboratories, their guidance especially Michael's teaching advice. Then, I like to remember the

support I received from Mr. Ron Jackson, Mr. Tobe Eggers and our amazing Mr. James Hodgson. Mr. James helped me and our group a lot, his glassblowing ability is exceptional.

My heartfelt gratitude goes to all my teachers who taught me from grade 1 to this moment. I especially need to mention Mr. Dimuthu Harshana Amarasiri, who was my chemistry tutor and taught me Chemistry for my advanced level exams. And he was the first person who made chemistry very interesting subject for me. Then I would like to mention my previous supervisor Dr. Dinara Gunesekera. I was very blessed to meet him at SLINTEC because he was a great mentor who polished my organic knowledge and my lab skills. Moreover, I would like to mention Dr. Marcus Durrant and Dr. Rohan Perera because they were always with me when I needed them most.

I would like to thank the endless list of my friends here at KSU and in all other countries also who were very supportive and cheered during all the tough times. And with all the respect, most Venerable Priyarathana Thero, Venerable Rahula Thero at Kansas Meditation Center for their advice and support my family and I gained during our tough times.

Last, but not least, my family; my mother, father and brother. Without my father's financial support and their blessings, I am not here today. There was a huge shadow behind me, it was my father (father in-law), sadly he is not here with us now, but always in my heart, and I know he always with us to guide us to go to the success. However, I am very happy to have my second mother (mother in-law), her blessing is always with me. Here comes the best part in my life, my loving wife Achini and my daughter Renadee. All the credits should go to my wife (she is my best friend too), because she sacrificed her valuable time and her wealth to help me to achieve my goals.

1. Introduction

1.1 Bacteria and bacterial Infections

Bacteria are microscopic, single cell organisms that can be found living in nearly every habitat on the face of the earth varying from the deep ocean[1] to inhospitable volcanic vents.[2] In addition, billions of bacteria live inside the guts of humans and animals as well as the surface of plant roots.[3, 4] Even though, there are vast numbers of bacterial species, both identified and yet to be identified, only a few varieties consistently cause human diseases.[5] Despite the presence of bacteria in the human body, they do not necessarily cause any infections until they begin to multiply and disturb the state of equilibrium.[6] Conversely, nonpathogenic bacteria cooperate with the ecological system in many ways, such as aiding in the digestion of food,[7] supplying essential nutrients (for instance vitamin K),[8] degrading waste material,[9] aiding the biosynthesis of some antibiotics[10], and much more. Based on the cell wall composition and Gram stain test, bacteria are classified into two broad categories: Gram positive (GP) and Gram negative (GN) bacteria.[11]

To date, accurate data on the prevalence of GP-positive and GP-negative infections world-wide are not available.[12] Although it is generally accepted in the global health care community that there is a large clinical and public burden associated with antimicrobial resistance (AMR), it is challenging to obtain reliable data on morbidity and mortality caused by AMR. Since accurate data on GP and GN infections are not available, accurate modeling of current and future infection rates is sheer impossible. Therefore, significant investments have to be made to facilitate "comprehensive, population-based surveillance data from low-, middle-, and high-income countries.[12] A recent high-profile report of the future occurrence of and mortality because of AMR estimated that "10 million people will die every year due to AMR" by the year of 2050.[13] It should

also be mentioned that it is impossible to ascertain and/or predict the prevalence of GN and GP infections accurately. However, in the opinion of the Centers for Disease Control and Prevention (CDC), both pose a significant health risk.[14]

In general, treating Gram-positive bacteria is generally perceived to be easier than Gram-negative bacteria. This is caused by the structure of the GN bacterial cell wall. The multiple layered protection of the GN bacteria cell wall facilitates an additional resistance to antibiotics, because two cell membranes have to be crossed before the antibiotic can find its target.[11] In that sense, GN bacterial infections are harder to treat compared to GP bacterial infections.[15] The major differences between the cell membranes of GP and GN bacteria is that the GP membranes features one thick, multi-layered peptidoglycan layer that is associated with teichoic acids, whereas the GN cell membrane featured a thin peptidoglycan layer, a periplasmic space, and a second outer membrane. The GP cell membranes are low on lipids and lipopolysaccharides. This makes them generally more susceptible to antibiotics. GN membranes are rich in lipids and lipopolysaccharides and feature channel porins. Most importantly, their (GN bacteria) outer membrane can alter the hydrophobic properties and show mutations in porins so that GN bacteria can show enhanced resistance to antibiotics.[16]

However, some notable GP bacteria are causing fatal infections, such are *Staphylococcus aureus*, *Staphylococcus epidermidis*, *Streptococcus pneumoniae*, *Bacillus anthracis* and etc.[17] The currently observed rapid increase in bacterial infections is mainly caused by the phenomenon called “drug resistance”. CDC studies demonstrated that about 33% of all Americans (including legal aliens) carry S. aureus in their nose. This means that 332,575,000 Americans x 0.33 = 109,749,750 people with S. aureus.[18] About 2 percent of these are MRSA infections, 2,194,995.

About 8-10 percent of these cases require treatment. It is noteworthy that these statistics did not significantly change since 2016.[19]

1.2 A History of Antibiotics and the Development of Bacterial Resistance

Bacterial resistance to antibiotics is an intrinsic problem that has been recognized almost since the dawn of the antibiotic era.[20] However, during the last two decades, bacterial resistance has become one of the central problems of Global Health.[21] There are two factors, which are responsible for this development: 1) From a genetic perspective, the occurrence of resistance is inevitable, and 2) The antibiotic pipeline is drying up. In the US, the health system is burdened every year by an additional $20 billion in additional health care costs due to the occurrence of resistant infections, concurrent with at least 8 million additional hospital days. The cost for antimicrobials has exceeded 30% of the hospital pharmacy budgets in the US.[22]

1.2.1 Why has Pharmaceutical Investment Diminished?

One of the main causes for diminished interest in the development of antibiotics is that they are prescribed only for clearly specified durations, whereas drugs developed for chronic illnesses (e.g., hypertension or diabetes) will be administered for much longer times. Therefore, the drugs for chronic illnesses are much more profitable than antibiotics.[23, 24] There are also emerging regulatory hurdles for new antibiotics. Concise guidelines for clinical trials of new antibiotics are absent, which have slowed down the development of new antibiotics. Clinical pharma companies have developed a metric called net present value (NPV), which is used to determine in what future drug development projects they would like to invest.[23, 24] A typical NPV for the development of an antibiotic drug is around 100, whereas a typical cancer drug is around 300, and a neuroscience drug can reach more than 700.[23, 24]

As Fair and Tor reported in 2014, "Since 1998 AstraZeneca, GlaxoSmithKline, Merck, Johnson & Johnson, and Pfizer/Wyeth have been the only major pharmaceutical companies to develop an antibiotic past phase I clinical trials. Sanofi Aventis, Eli Lilly, Bristol-Myers Squibb, GlaxoSmithKline, Proctor and Gamble, Roche, and Wyeth have all greatly curtailed, eliminated, or spun off their antibiotic R&D divisions. In fact, as of 2013 there are only four multinational pharmaceutical companies with antibiotics divisions left."[21]

1.2.2 Human Factors are Drivers of Emerging Bacterial Resistance

There are several major ways in which humans, especially in highly industrialized countries like the US and Europe, greatly accelerate the occurrence of bacterial resistance: 1) Historically, US doctors overprescribe antibiotics for symptoms that are not caused by bacterial infections. According to estimations from the Center for Disease Control and Prevention (CDC), about 50% of the antibiotics in the US are being prescribed unnecessarily.[22] This practice is causing additional healthcare costs of > $1 billion per year. Consequently, human (mis)use of antibiotics has accelerated their evolution towards drug resistance and increased survival capabilities.[25]

1.2.3 Gram-positive and Gram-negative Pathogens

Table 1 summarizes the most dangerous pathogens and their observed resistances against antibiotics to date.

Table 1.1 Bacterial Threats in 2021[21]

Bacterium	Gram Stain	Respiration	Resistances
Staphylococcus aureus	+	Facultative anaerobe	β-lactams, glycopeptides
Enterococci	+	Facultative anaerobe	β-lactams, glycopeptides, aminoglycosides

Streptococcus pneumoniae	+	Aerotolerant anaerobe	β-lactams, macrolides, quinolones
Clostridium difficile	+	Obligate anaerobe	β-lactams, quinolones
Mycobacterium tuberculosis	+	Aerobe	Rifamycins, quinolones, aminoglycosides
Escherichia coli	-	Facultative anaerobe	β-lactams, quinolones, aminoglycosides
Pseudomonas aeruginosa	-	Facultative anaerobe	All classes
Acinetobacter	-	Facultative anaerobe	All classes
Klebsiella pneumoniae	-	Facultative anaerobe	β-lactams, quinolones, aminoglycosides
Enterobacter	-	Facultative anaerobe	β-lactams, quinolones
Neisseria gonorrhoeae	-	Aerobe	β-lactams, quinolones, tetracyclines, macrolide

Since the 1990s resistant gram-positive bacteria are a major threat with methicillin (MRSA) and vancomycin (VRSA) resistant *Staphylococcus aureus*, vancomycin resistant *Enterococci* (VRE), penicillin resistant *Streptococcus pneumonia*, and multi-drug resistant (MDR) *Clostridium difficile.*[21] *Staphylococcus aureus* is a gram-positive, facultative anaerobic pathogen with both hospital- and community-acquired strains. Many *S. aureus* strains have evolved from opportunistic to aggressively pathogenic.[26] About 60% of all humans are intermittent carriers of *S. aureus* on their skin. 20% are persistent carriers.[27] Furthermore, *S. aureus* is prone to forming biofilms on medical surfaces and especially clinical devices.[28] MRSA is responsible for the majority of nosocomial infections.[29] At the height of the MRSA threat in 2009, before improved clinical disinfection measures haves somewhat decreased the prevalence of MRSA infections, MRSA caused 19,000 deaths and more than $3 billion in additional health care costs in the US.[30] Year-by-year, MRSA kills more people than HIV/AIDS and tuberculosis together.[31] It should be noted that b-lactam resistance in MRSA arises from the expression of the *mecA* gene, which encodes for PBP 2a, which is a low affinity penicillin binding protein.[32] This gene, like virtually all other resistance genes, can be shared among bacteria.[22]

While the waning development of new antibiotics focused on gram-positive bacteria from 1990-2010, drug-resistant tuberculosis and numerous drug-resistant gram-negative strains have evolved.[21] Currently, the health-care threat of gram-positive bacteria is becoming eclipsed by gram-negative pathogens.[22] Principally, the health threat by gram-negative bacteria is even more troublesome, because they feature outer membranes that are more difficult to penetrate and a higher prevalence of efflux pumps for drugs.[33] The main gram-negative threats are multi- (MDR) and pan- (PDR) drug resistant *Escherichia coli*, *Pseudomonas aeruginosa*, *Acinetobacter*, *Klebsiella pneumoniae*, *Enterobacter*, and *Neisseria gonorrhoeae*.[34, 35]

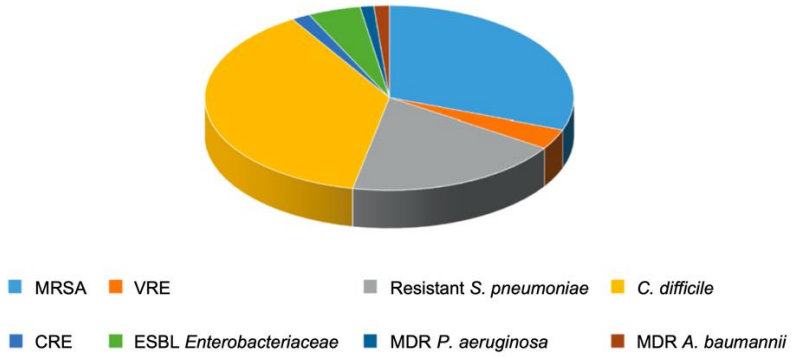

Figure 1.1 Death caused by distinct classes of bacteria in the US (average percentages from 2000 to 2014).[21]

1.2.4 The Gram-negative Cell Envelope

There are three fundamental layers in the cell envelope of Gram-negative bacteria: the outer membrane (OM), the peptidoglycan cell wall, and the cytoplasmic or inner membrane (IM). The two concentric membrane layers surround an aqueous cellular compartment, the periplasm.[36] The outer membrane is the distinguishing feature of gram-negative bacteria, because it is not found in gram-positives.[36] It is of great importance that the OM is a lipid bilayer, but not a phospholipid

bilayer. Phospholipids are confined to the inner leaflet of the OM, whereas the outer leaflet is composed of glycolipids with lipopolysaccharide (LPS) as principal component. Lipid A is formed by a disaccharide of 1-6'-connected hexosamines. Acylation in 2- and 3-positions forms connections with LPS.[37] Almost all proteins of the OM are either lipoproteins or β-barrel proteins.[38] Lipoproteins feature covalently attached lipid moieties. The β-barrel proteins form β-sheets that form "cylinders" (outer membrane proteins, OMPs).[36] Some of these cylinders (e.g. OmpF) permit passive diffusion of small molecules. The OM serves as a highly selective permeability barrier of gram-negatives, which significantly decreases drug diffusion into the actyl muramic acid, which are cross-linked by penta- peptide side chains.[39] Peptidoglycan is a rigid biopolymer.[39,40] Therefore, it determines the shape of gram-negative bacteria. The OM is attached to the deeper peptidoglycan through the lipoprotein Lpp.[41]

The periplasm is generally more viscous than the cytoplasm because it contains a significantly higher concentration of proteins than the latter. Due to cellular compartmentalization, gram-negative bacteria are capable of sequestering and degrading xenobiotic compounds, such as antibiotics. In evolutionary terms, the biological functions of the periplasm can be understood as a precursor to the lysosomes of eukaryotic cells.[42] In contrast to eukaryotic cells, bacteria do not possess intracellular organelles.[36] Therefore, all biochemical processes that are performed in eukaryotes in association with specific membranes, are performed in the inner membrane (IM). Contrary to the OM, the IM is a phospholipid bilayer.[43]

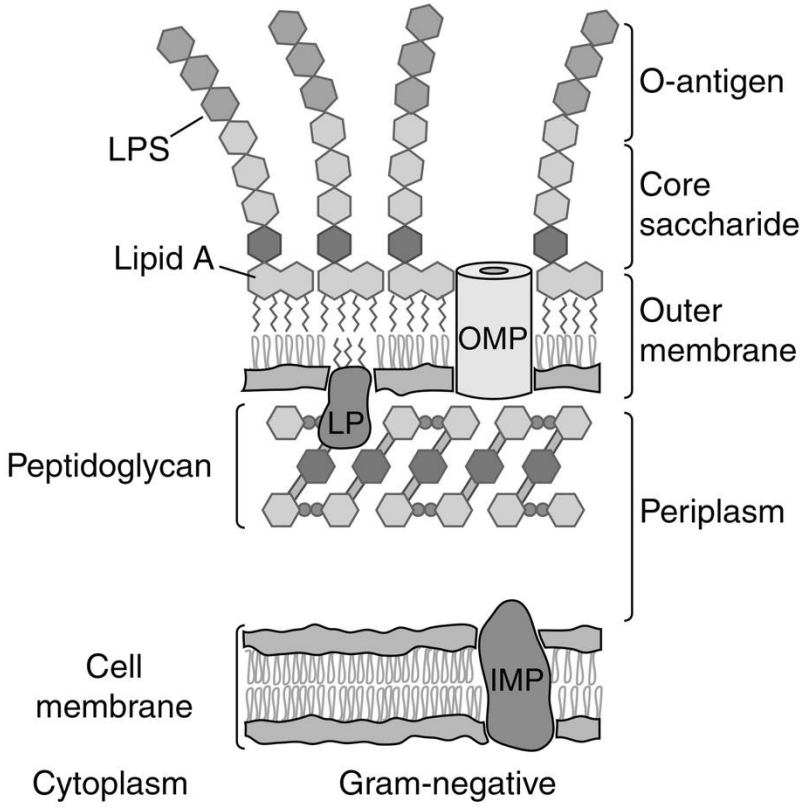

Figure 1.2 Gram-negative cell envelope: IMP, integral membrane protein; LP, lipoprotein; LPS, lipopolysaccharide; Lipid A: innermost of the three regions of LPS; OMP, outer membrane protein.[36]

1.2.5 The Gram-positive Cell Envelope

The most significant difference between the cell envelopes of gram-negatives and gram-positives is that in the latter there is no outer membrane (OM).[21] This means that gram-positive bacteria are significantly less protected from their environment and also pertains to antibiotic treatment. Therefore, it is a common rule that significantly higher concentrations of antibiotics have to be used to kill gram-negative pathogens than are required for gram-positive pathogen.[26] Because of the absence of the stabilizing OM, the peptidoglycan layer of gram-positive bacteria is much thicker (30-100 nm in diameter) and forms multilayered structures.[36] These peptidoglycan layers are interconnected by anionic teichoic acids, which are biopolymers comprised mainly of glycerol

phosphate, glucosyl phosphate, and ribitol phosphate repeats. Teichoic acids are covalently tethered to peptidoglycan, whereas lipoteichoic acids are attached to the head groups of membrane lipids.[44] In gram-positives peptidoglycan, teichoic acids and lipoteichoic acids make up together approx. 60 percent of the total weight of the cell envelope. The bacterial surfaces of gram-positives are covered with attached functional proteins, which show some similarities to the proteins found in the periplasm of gram-negative bacteria.[45, 46]

In general, the chemical structure of peptidoglycan in gram-positive and -negative bacteria is similar. As already discussed, the major differences are the significantly greater thickness and the layered structure of peptidoglycan in gram-positive bacteria, together with their attachment to teichoic acids. It should be noted that *S. aureus* and other gram-positive bacteria feature stem peptides that serve multiple functions, such as the covalent attachment of a variety of enzymes (e.g. the transpeptidase PBP2A in *S. aureus* strains that are resistant to β-lactams)[47] and other peptides on unknown functions to date.[48, 49]

Surface proteins facilitate the ability of *S. aureus* to adhere to the host tissue, for instance during skin infections. Although there is a lot of variability, surface proteins usually consist of teichoic acids and proteins binding to host extracellular matrix components, such as fibronectin, fibrinogen, and elastin.[50]

The inner cell membrane and the cytoplasm of gram-positive bacteria are again similar to these cell organelles of gram-negative organisms. In conclusion, gram-positive organisms are more vulnerable to antibiotics, because their cell envelope does not protect them as efficiently as the cell-envelope of gram-negative bacteria. Furthermore, gram-negative bacteria possess efflux pumps that are capable of actively removing xenobiotic chemicals (drugs) from the bacteria.[36] Due to the thickness of the bacterial cell envelope in gram-positive bacteria, efflux pumps are rare. This

again results in better treatment efficacies of gram-positive bacteria, such as (resistant) *S. aureus*.[21,51]

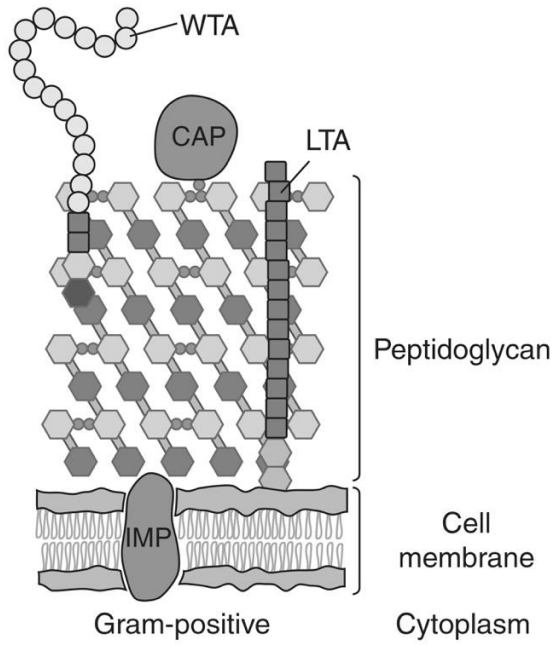

Figure 1.3 Gram-positive cell envelope: CAP: covalently attached protein; IMP, integral membrane protein; LPS, LTA, lipoteichoic acid; WTA, wall teichoic acid.[36]

1.2.6 Efflux Pumps in Gram-negative Bacteria

Transmembrane (TM) pump proteins that are present in numerous biological systems with the exception of gram-positives, can either actively take up nutrients etc. or remove unwanted (toxic) substances.[52] The evolution of these systems occurred much earlier than the invention of antibiotics.[37] Therefore, gram-negative bacteria repurpose their efflux pumps to resist against antibiotics. This does not prohibit further evolution to remove antibiotics even more effectively.

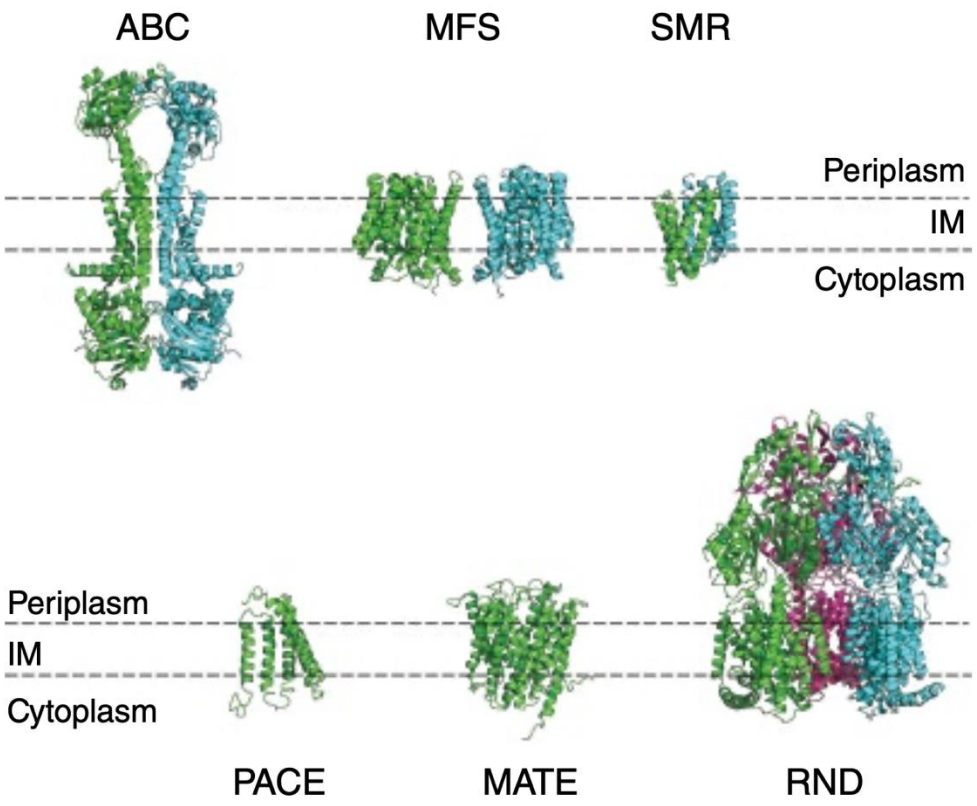

Figure 1.4 General architecture and relative sizes of the principal classes of MDR-transporters (drawn at the same scale). Where oligomeric state is known, separate protomers have been colored distinctly. ABC-, MFS-, and SMR-families appear to function as dimers, while the RND-transporter family members form trimeric assemblies. As stoichiometry of PACE- and MATE-transporters hasn't been conclusively established, they are shown as monomers. The position of the inner membrane (IM) is relative.[37]

1.2.7 ABC Transporters

This class of transporters requires ATP-binding for functionality. They feature an ATP-recognition sequence (ATP-binding cassette (ABC) transporters). The structures and functions of the usually dimeric ABC transporters vary in different gram-negative bacteria.[53] To date, only a few ABC transporters have been discovered that can facilitate multi-drug efflux, for instance the MacB-family capable of removing macrolides. The exact function of ABC transporters remains unknown. However, they require ATP binding and subsequent hydrolysis to facilitate a conformation change required for the transport of drugs from the cytoplasm.[37]

1.2.8 MFS Transporters

Different from ABC transporters, all other five known families of efflux pumps are so-called "secondary transporters" that utilize ion gradients for facilitating transport. The Major Facilitator Superfamily (MFS) is the largest group of transporters.[37] MFS transporters are known to facilitate all three possible transport types (symport, antiport, and facilitated diffusion) and MFS transporters are formed by either 12 or 14 TM helices.[54] They contain a narrow inner pore, which is operated by a rocker-switch type movement of a single binding site.[55] Binding of either a symporting substrate or an antiporting substrate is possible. This process determined the directionality of MFS transporters.[37]

1.2.9 SMR Transporters

The co-called Small Multidrug Resistance (SMR) family belongs to the drug/metabolite transporter (DMT) superfamily.[37] Due to their small size and structure, SMR efflux pumps can only transport lipophilic compounds, such as quaternary ammonium compounds and cationic dyes. All SMR efflux pumps function by means of drug/proton antiport that is facilitated by a rocker-switch type mechanism.[56, 57] Similar to MFS transporters, SMR proteins feature no cytoplasmic or periplasmic regions, but they are much smaller (4 TM helices per monomer).[58]

1.2.10 MATE Transporters

Multidrug And Toxic compound Extrusion (MATE) efflux pumps consist of 12 TM helices, which go through major conformational changes that are triggered by substrate binding.[59, 60] Transport in MATE transporters is driven by electrochemical potential, antiporting protons, or sodium and potassium cations.[37]

1.2.11 RND Transporters

The Resistance-Nodulation-Cell Division (RND) transporters are the most important family of efflux pumps in gram-negative bacteria.[37] RND efflux pumps are swiftly up-regulated in response to antibiotic therapy. They are capable of providing a wide non-specific resistance.[61] Contrary to most other transporter systems, RND efflux pumps operate unidirectionally and remove drugs from the cytoplasm and transport them to the exterior of the bacterium.[37] RND transporters form trimeric assemblies. Each protomer possesses three main domains.[62] One domain, which is formed by 12 TM helices, is located within the inner membrane. The other two domains reside in the periplasm. They facilitate the assembly with auxiliary periplasmic and outer membrane proteins.[63] The membrane domain's function is to couple proton transport to drug extrusion.[63]

The periplasmic domains form two large loops located between TM-helices TM 1 and TM 2, and TM 7 and TM 8, respectively.[37] The upper part of this periplasmic structure or "TolC-docking domain" facilitates binding to the outer membrane factor (OMF) family of channel proteins.[62] The lower part of the periplasmic domain can undergo a coordinated peristaltic pump-like structural transition to achieve drug efflux.[64,65] This process has also been described as "alternating-access cycle", because a drug molecule is captured on the periplasmic side and subsequently squeezed through the protein toward the center-top of the RND-trimer and eventually released into the exit conduit formed by the outer membrane proteins of OMF-family.[37]

1.2.12 PACE Transporters

The Proteobacterial Antimicrobial Compound Efflux (PACE) family is the most recently discovered group of efflux pumps. No structural or mechanistic information is available to date.

What is known is that PACE efflux pumps can also be found outside the group of proteobacteria.[66, 67]

1.2.13 The Pipeline of New Antibacterial Agents

Over the last decades, the number of antibacterial agents has steadily declined.[21] This is in part, because historically, new compounds were developed that belonged to already established classes of antibiotics in order to decrease developmental risk.[68] Between 1981 and 2005 the classes of cephalosporins, penicillins, quinolones, and macrolides accounted for 73% of all new antibiotics.[69] It should also be noted that the cellular targets available in virtually all bacteria are generally limited to cell wall or protein biosynthesis, or DNA/RNA inhibition.[21] In the long run, we need new classes of antibiotics, because resistance mechanisms in bacteria often eliminate the efficacy of whole classes of antibiotics. Contrary to the classic approach of developing antibiotics, copper(I)-activated antibacterial agents will hit multiple targets, making it more difficult to develop resistance mechanisms.[70]

The new first in class antibiotics introduced for human use are the streptogramin combination quinupristin / dalfopristin in 1999, the oxazolidinone linezolid in 2000, the lipopeptide daptomycin in 2003, the pleuromutilin retapmulin in 2007, the macrolactone fidaxomicin in 2011, and the diarylquiniline bedaquiline in 2012.[21] Linezolid and bedaquiline are fully synthetic drugs, whereas the others are natural products.[21] It should be noted that the majority of antibiotics that were introduced to the marked within the last 40 years are semisynthetic. These include the β-lactams meropenem and tazobactam, the aminoglycoside amikacin, the macrolide azithromycin, the tetracycline tigecycline, the rifamycin rifampicin, and the glycopeptide

telavancin.[21,69] In contrast, fully synthetic antibiotics, which are also being developed in this thesis, are quite rare.

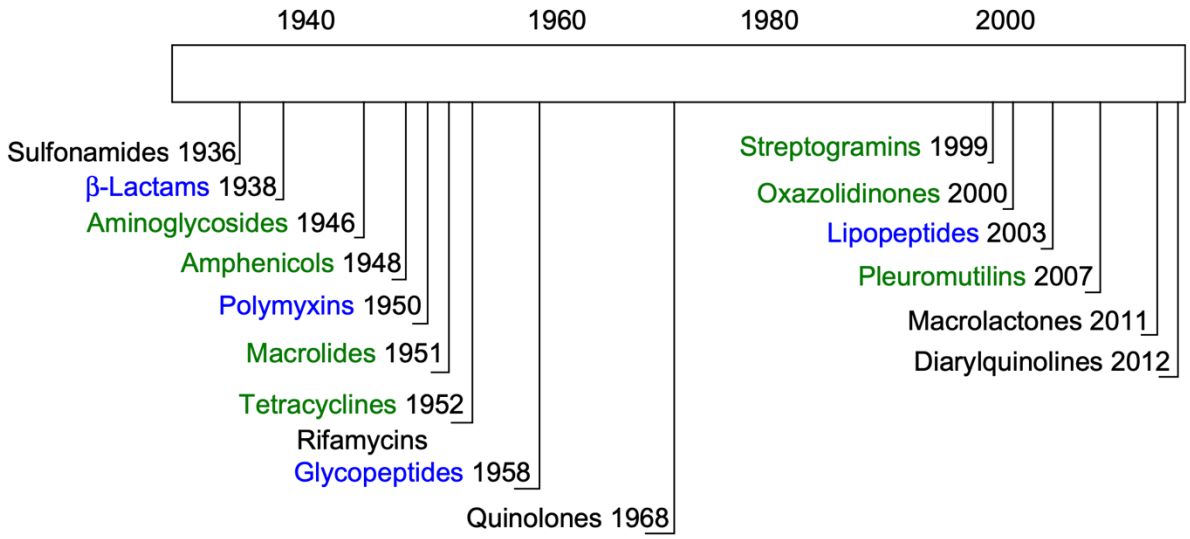

Figure 1.5 Timeline of first clinical introduction of antibiotic classes. Classes targeting bacterial cell walls or membranes are highlighted in blue. Classes targeting the ribosome are highlighted in green.[21]

1.2.14 A History of Established Antibiotic Classes

1.2.14.1 Sulfonamides

Sulfonamides, which are clinically used since 1936, are structurally diverse, but they all have the aryl sulfonamide group in common.[71] They inhibit dihydropteroate synthetase, which is absent in mammals. Inhibition of this enzyme causes repressed DNA replication and, therefore, bacteriostatic activity against aerobic gram-positive and -negative bacteria. Their use has substantially decreases due to resistance and other health issues, as for instance the Stevens-Johnson syndrome.[72]

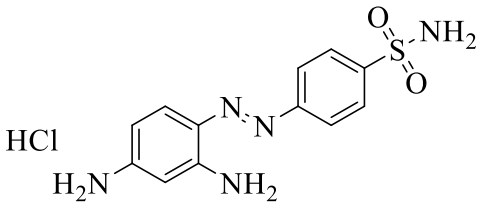

Prontosil

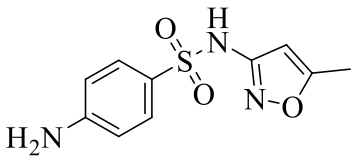

Sulfamethoxazole

Figure 1.6 Sulfonamides[21]

Note that no compound numbers were assigned to the drugs discussed in this chapter, because the information presented here serves as a background for the development of drugs with NNSN motif. No derivatives of drugs discussed here were synthesized in this thesis.

1.2.14.2 β-lactams

The active pharmacophore of β-lactams is their four-membered β -lactam ring. The first β -lactams antibiotic was benzylpenicillin (penicillin G) in 1928, which arrived in the clinic in 1938.[73] Currently, there are 28 members from three subclasses: penicillins, cephalosporins, and carbapenems.[74] Antibacterial activity is achieved by acting as a suicide substrate for penicillin binding proteins (PBPs), also known as transpeptidases. This process inhibits peptidoglycan biosynthesis, which leads to a bacterial stress response and consequent lysis. β-lactams are still first-line antibiotics, because peptidoglycan biosynthesis occurs in gram-positive and -negative bacteria alike.[75] Resistance, which has greatly increased during the last two decades is achieved by a wide range of bacterial β-lactamases.[21] According to the Ambler classification system, there are four recognized classes of β-lactamases: class A (KPCs and most ESBLs), class B (MBLs (metallo-beta-lactamases)), class C (AmpC β-lactamases), and class D (OXAs).[76]

β-Lactams have been improved by means of semi-synthetic modifications. The introduction of bulky side chains (e.g. methicillin and oxacillin) led to a significant increase in

stability against hydrolysis by β-lactamases.[21] Aminopenicillins (e.g. ampicillin and amoxicillin) feature a broader spectrum especially against gram-negative bacteria.[21]

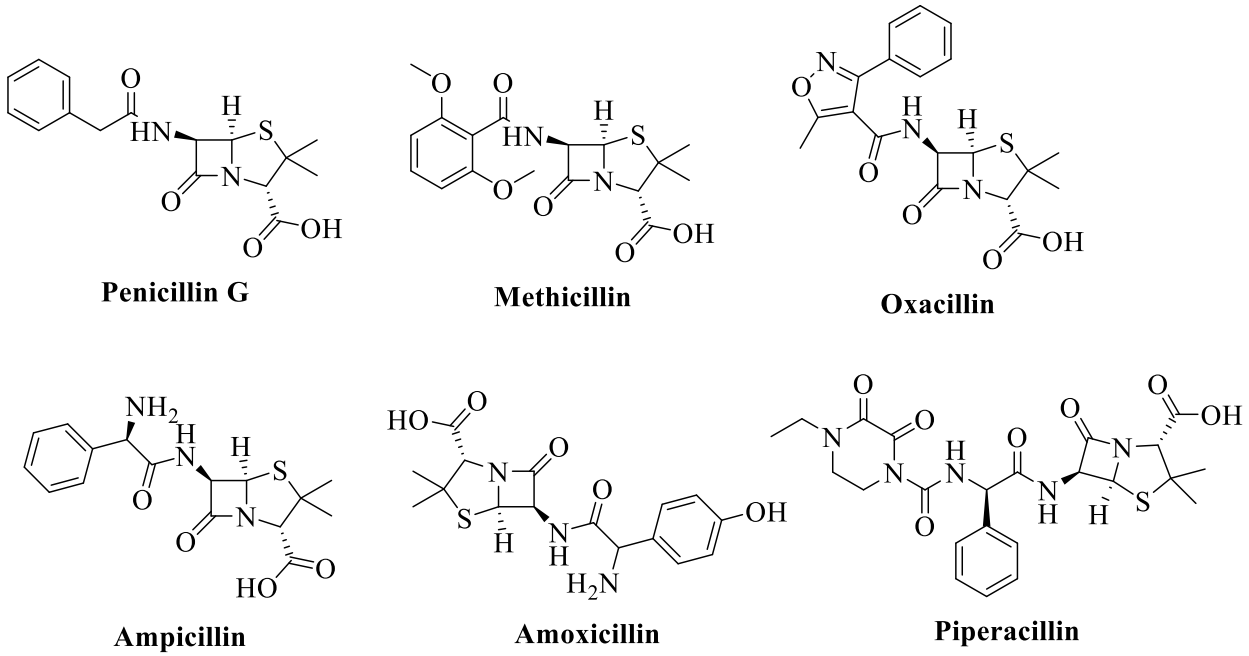

Figure 1.7 Penicillin subclass β-lactams[21]

The first cephalosporin was discovered in 1948 (cephalosporin C). Again, better cephalosporins were developed following a semi-synthetic approach. This led to increased β-lactam stability towards enzymatic hydrolysis and improved pharmacokinetics due to better membrane permeability of gram-negatives.[21] It is noteworthy that the 5th generation, ceftaroline (2010) shows increased activity against MRSA, but not gram-negatives due to β-lactamase sensitivity.[21]

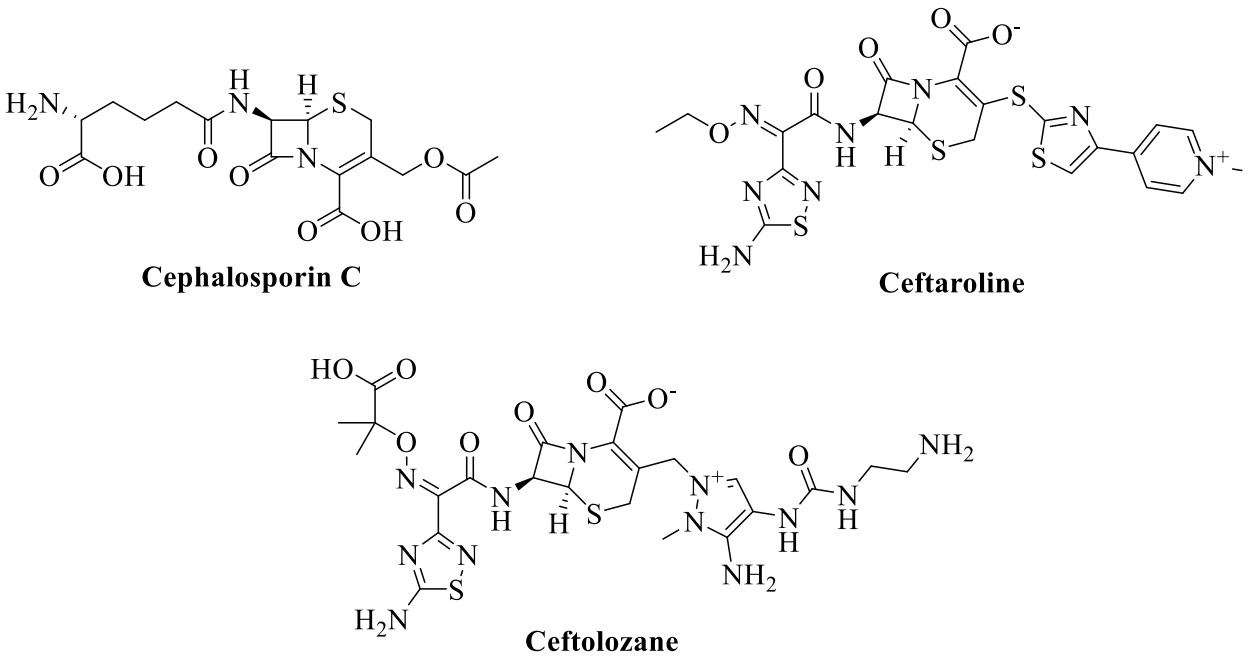

Figure 1.8 Cephalosporin subclass β-lactams[21]

The first carbapenem to be discovered was imipenem in 1976.[21] Carbapenems are active against numerous anaerobic gram-negative bacteria due to their stability against β-lactamases (especially ESBLs).[77] However, due to the constant evolution of β-lactamases, resistance against carbapenems is continuously increasing. Doripenem, which was approved in the US in 2007, is active against many gram-negative bacteria, but it is not highly active against MRSA.[78]

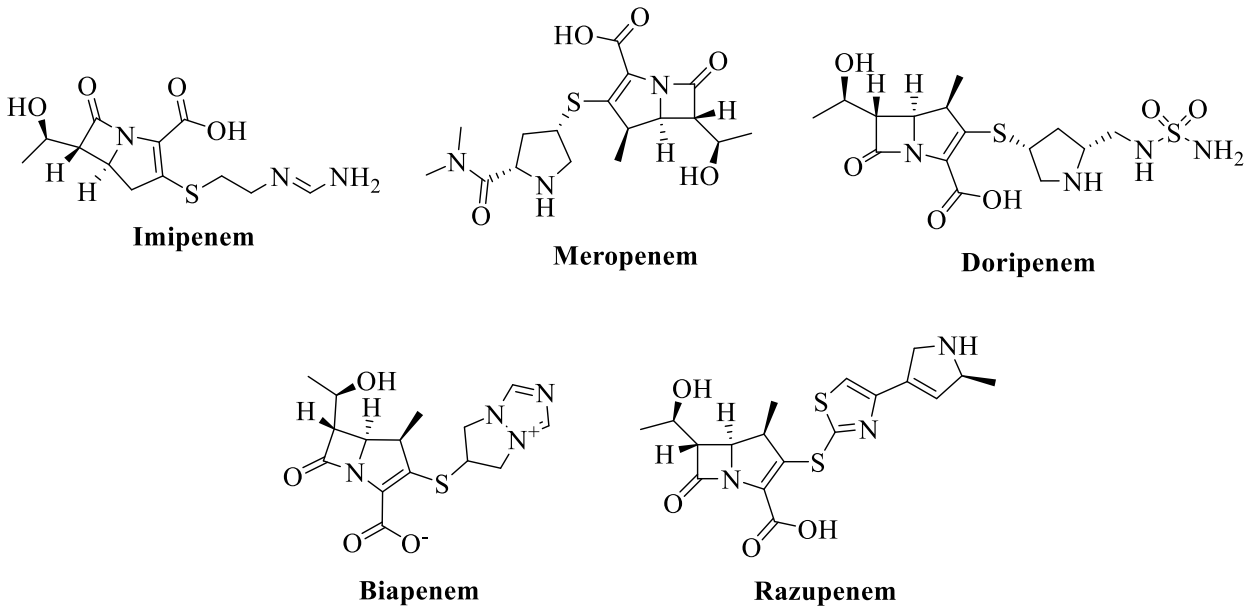

Figure 1.9 Carbapenem subclass β-lactams.[21]

The only FDA-approved monobactam, aztreonam, was discovered in 1981. It is active only against gram-negative bacteria.[21]

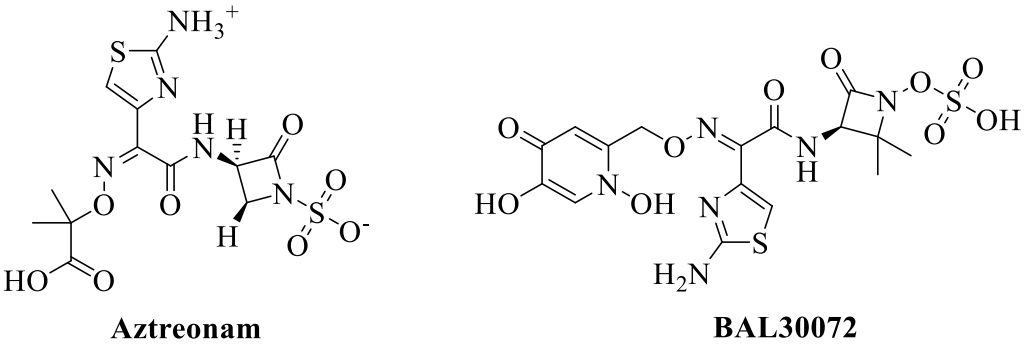

Figure 1.10 Monobactams.[21]

1.2.14.3 Aminoglycosides

Aminoglycosides are comprised of amino-sugars that are linked through glycosidic bonds to a 2-deoxystreptamine (2-DOS) core.[21] Streptomycin was the first aminoglycoside (discovered in 1943, first clinical application in 1946).[51] The target of aminoglycosides is the 30S ribosomal subunit (A-site within the 16S rRNA) causing mistranslation of proteins and subsequent cell death. Aminoglycosides are the only class of translation inhibiting antibiotics that is broadly bactericidal.[21] The definition of bactericidal is that the antibiotic kills the bacterium.[79] They are active against most gram-positive and -negative bacteria, as well as *M. tuberculosis*. However, their uptake is severely limited under anaerobic conditions. It should also be noted that aminoglycosides cause nephrotoxicity and ototoxicity.[21] Therefore, they are considered a last resort and certainly not first-line antibiotics. During the last two decades, resistance has been observed particularly in gram-negatives due to increased MexXY and ABC transporter activity. Whereas a large number of aminoglycosides are natural products, some newer drugs are the result of semi-synthetic approaches (e.g. amikacin, clinically introduced in 1976, and plazomycin, launched in 2018).[73]

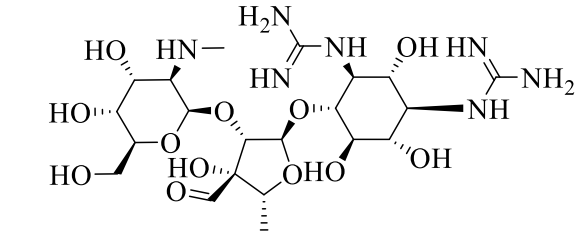

Streptomycin

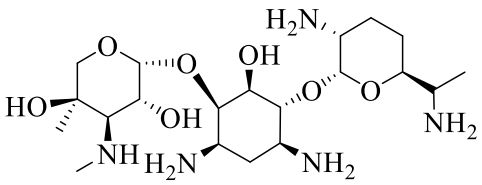

Gentamicin C2

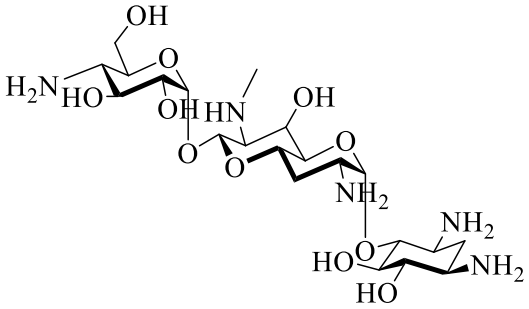

Apramycin

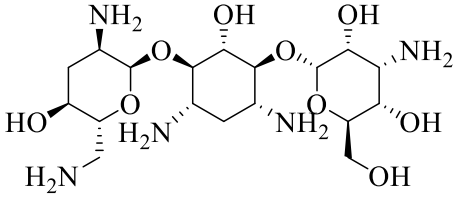

Tobramycin

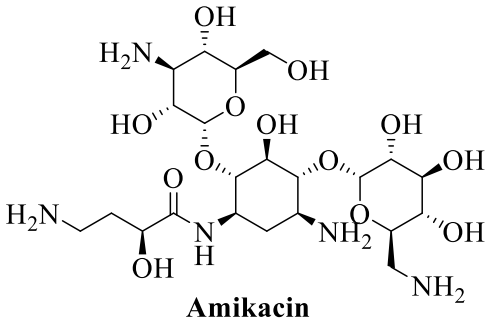

Amikacin

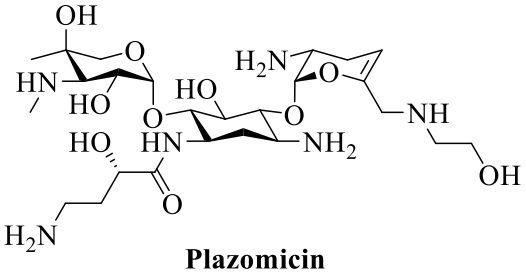

Plazomicin

Figure 1.11 Aminoglycosides.[21]

1.2.14.4 Amphenicols

Chloramphenicol, the only amphenicol that is FDA approved, was discovered in 1946 and introduced to the clinic in 1948.[51] Amphenicols target the center of peptidyl transferase (PTC) of the 50S ribosomal subunit thus inhibiting translation. Chloramphenicol is a typical broad-band antibiotic. However, there have been always questions regarding the safety of amphenicols.[80] Resistance has been observed via methylation of the C8 position of A2503 of the 23S rRNA (target

modification).[81] Increased acetyltransferase activity and increased efflux pump efficacy have also been established as common resistance mechanisms against amphenicols.[21]

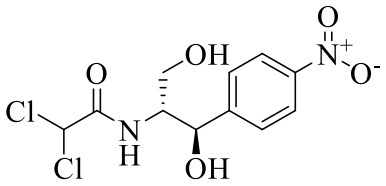

Chloramphenicol

Figure 1.12 Structure of Chloramphenicol.[21]

1.2.14.5 Macrolides

Macrolides are macrocyclic lactones with deoxy-sugars (usually cladinose and desosamine). Erythromycin was the first macrolide that was discovered in 1949 and introduced to the clinic in 1951.[51] Macrolides target the 50S ribosomal subunit. They are capable of blocking the exit tunnel and of inhibiting elongation of translation.[21] Like aminoglycosides, macrolides display broad spectrum antibacterial activities against aerobic and anaerobic gram-positive and -negative bacteria. Resistance against macrolides has been achieved during bacterial evolution by means of target modification.[21] Recently, macrolide-modifying enzymes have been isolated.[82] However, it is safe to assume that especially in gram-negative bacteria, efflux pumps are the main culprits in bacterial resistance.[83] As in other classes of antibiotics, semi-synthetic approaches yielded the best results in terms of developing/retaining broad-band activities and activities against gram-negatives. Examples are azithromycin, clarithromycin, and roxithromycin, which are popular first line antibiotics.[26] Telithromycin is the first ketolide. It is available since 1997.[21]

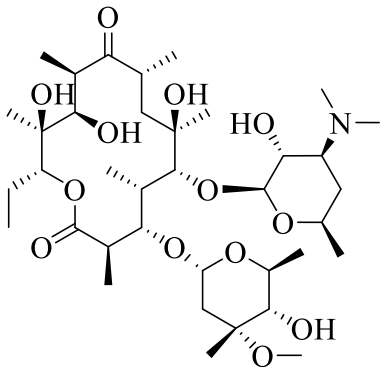

Erythromycin

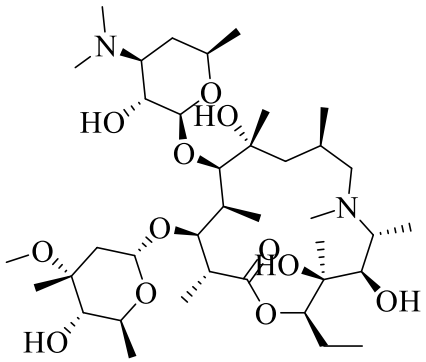

Azithromycin

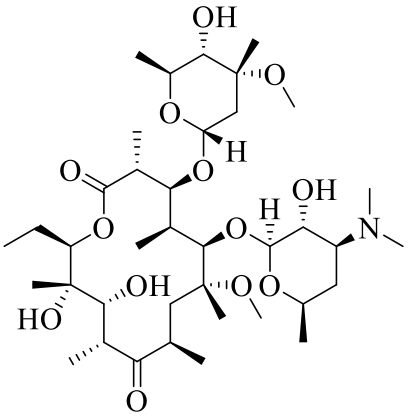

Clarithromycin

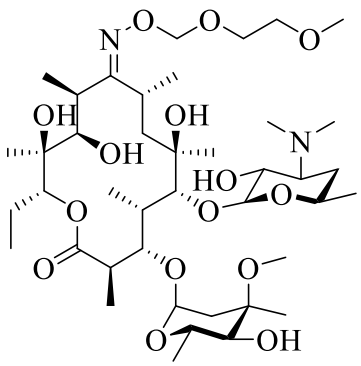

Roxithromycin

Figure 1.13 Macrolides.[21]

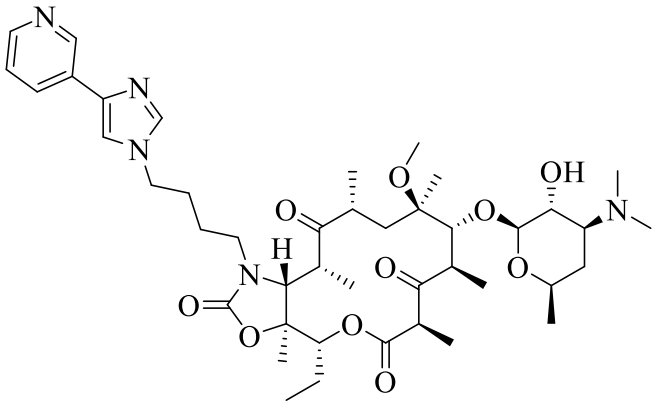

Telithromycin

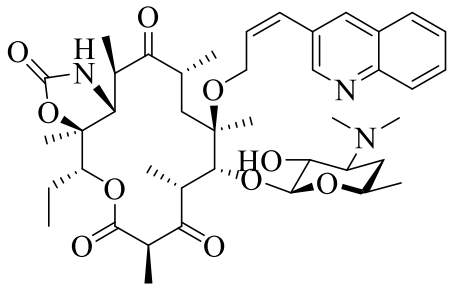

Cethromycin

Figure 1.14 Ketolides.[21]

1.2.14.6 Tetracyclines

All tetracyclines have an octahydrotetracene basic structure in common. Chlortetracycline was the first tetracycline (discovered in 1945, first clinical application in 1952).[21] Tetracyclines are broad spectrum antibiotics, which are bacteriostatic. The term "bacteriostatic" means that the drug stops the proliferation of a bacterium but does not necessarily kill it.[79] Tetracyclines are popular first line therapy drugs, because they exhibit side effects less often than other antibiotics. Tetracyclines target the 30S ribosomal subunit and block aminoacyl tRNA access.[51] Resistance against tetracycline occurs due to ABC and other efflux pumps or via target modification.[21] It should be noted that a tetracycline metabolizing enzyme, TetX, is also known.[51, 84] Similarly to other classes of antibiotics, their early members are natural products (tetracycline, oxytetracycline, and demeclocycline), but later members are semi-synthetic.[21, 51]

Early members of this class were natural products (tetracycline, oxytetracycline, and demeclocycline), but later members (doxycycline and minocycline) were semi-synthetic.[51] Eravacycline (FDA-approved in 2018[85]) has broad activity against numerous MDR pathogens, such as MRSA, *C. difficile*, and others.[21]

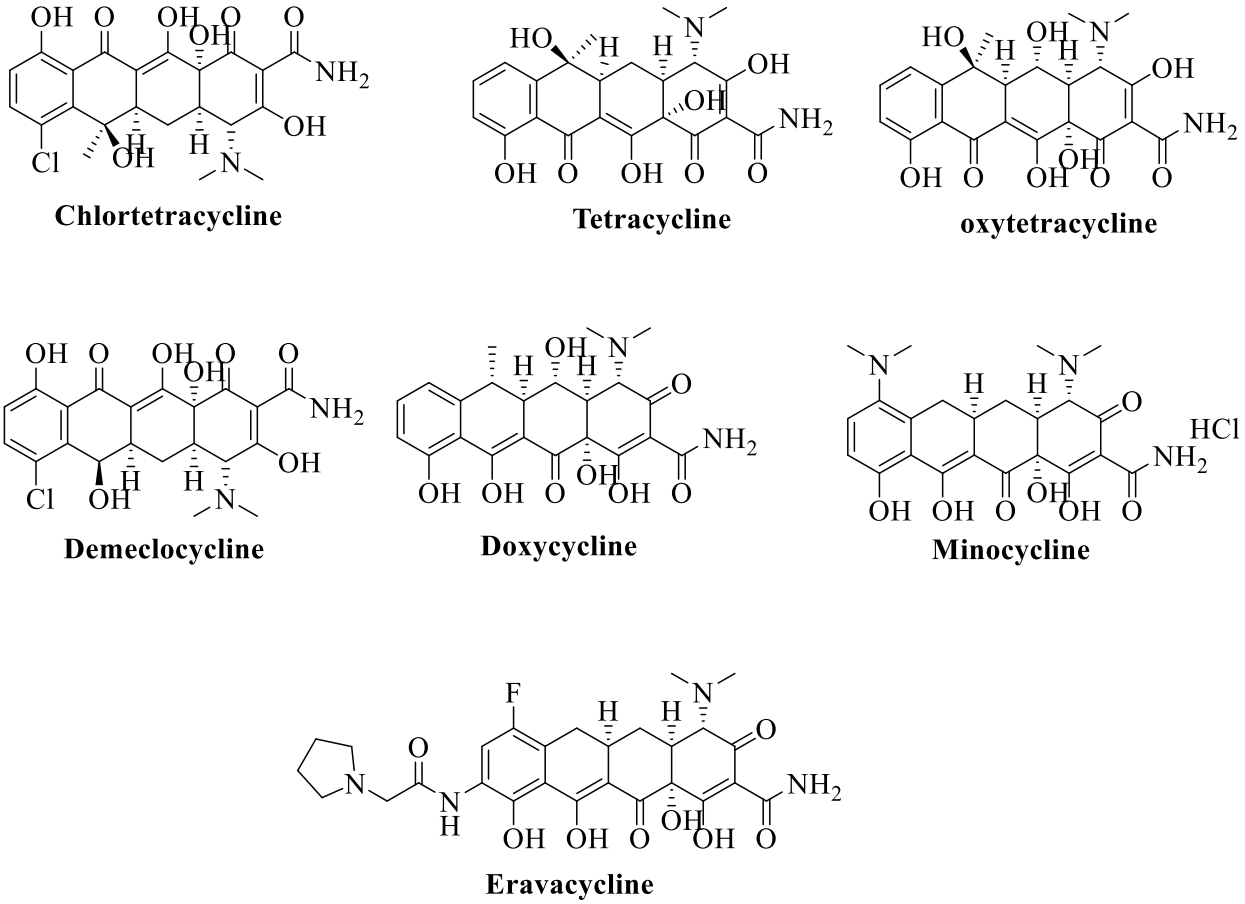

Figure 1.15 Tetracyclines.[21]

1.2.14.7 Rifamycins

The group of rifamycins is characterized by macrocyclic structures that include an aromatic group. Technically, they are ansamycin antibiotics.[26] The semi-synthetic rifampicin was discovered 1957. It appeared in the clinic in 1958.[21] Rifamycins bind the b-subunit of RNA polymerase and are bactericidal against gram-positives and *M. tuberculosis*, but bacteriostatic against gram-negatives due to their inability to effectively cross their cell walls.[86] Target modifications and the activation of efflux pumps are recognized resistance mechanisms.[51] It is noteworthy that rifampicin, isoniazid, and pyrazinamide remain the first line combination therapy against *M. tuberculosis* to date.[74] Rifaximin was FDA-approved in 2004.[85]

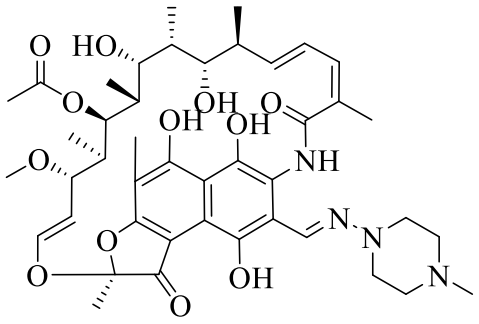

Rifamycin

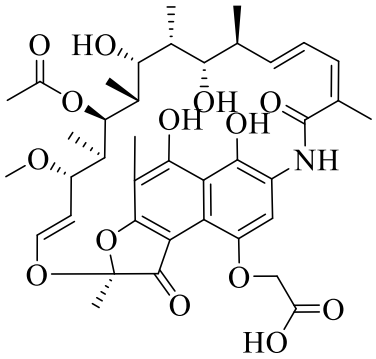

Rifamycin B

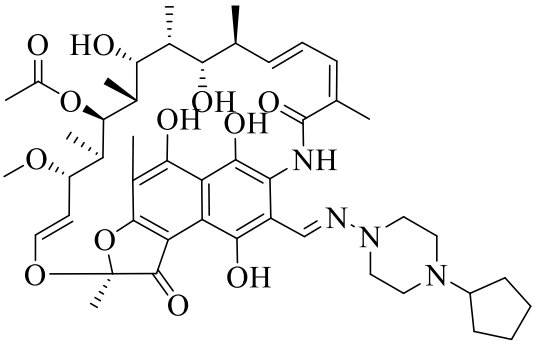

Rifapentine

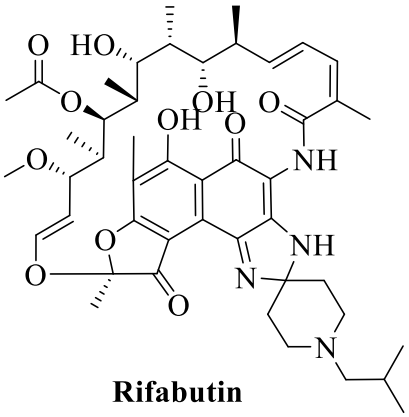

Rifabutin

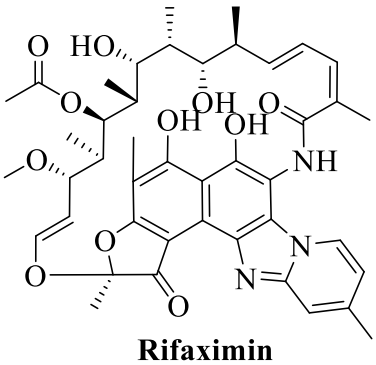

Rifaximin

Figure 1.16 Rifamycins[21]

1.2.14.8 Glycopeptides

The class of glycopeptides consists of macrocyclic peptides featuring interspersed bridged aromatic groups and saccharide side chains that are attached by means of glycosidic bonds.[21] Vancomycin was the first glycopeptide, discovered in 1952, clinical application in 1958.[26] Glycopeptides inactivate cell wall synthesis in gram-positive organisms by binding the terminal D-Ala-D-Ala dipeptide of peptidoglycans.[21] This binding event blocks their use as substrates for PBPs and transglycosylases. The evolutionary response in gram-positive bacteria has created five vancomycin-resistant phenotypes due to target modification.[87] As for all antibiotics with higher molecular masses, efflux pumps are less effective that for antibiotics with smaller molecular weight.[51] Whereas vancomycin resides in the periplasm of bacteria, teicoplanin features a membrane-anchor. Telavancin was FDA-approved in 2009.[85] It has a secondary mechanism of action by means of membrane-depolarization. Telavancin is especially suited to treat MRSA infections including biofilms.[88] Oritavancin, FDA-approved in 2014, is very active against MRSA and VRSA.[85] Dalbavancin was FDA-approved in 2021 for skin infections by multi-resistant gram negatives.[85]

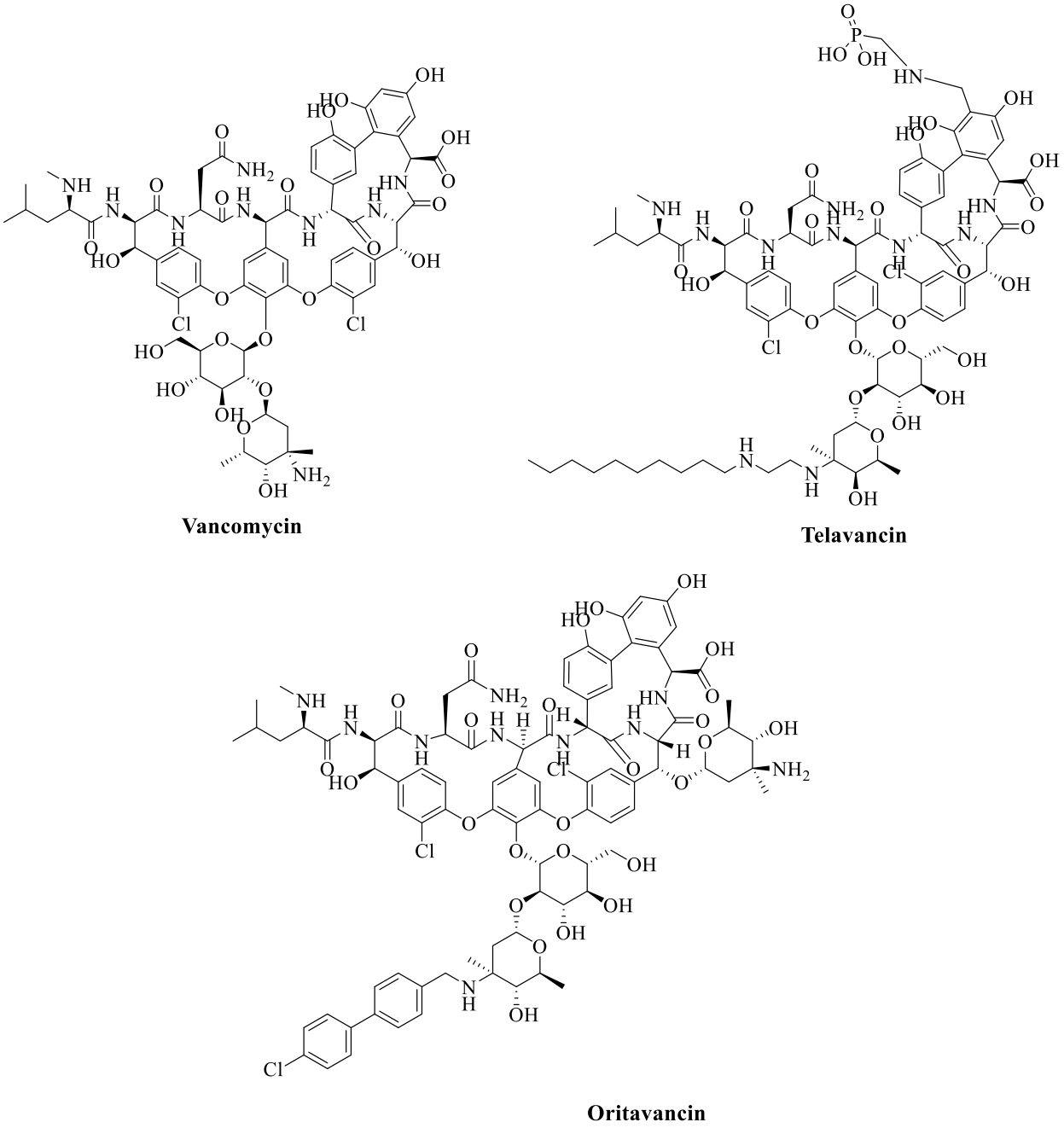

Figure 1.17 Vancomycin and derivatives.[21]

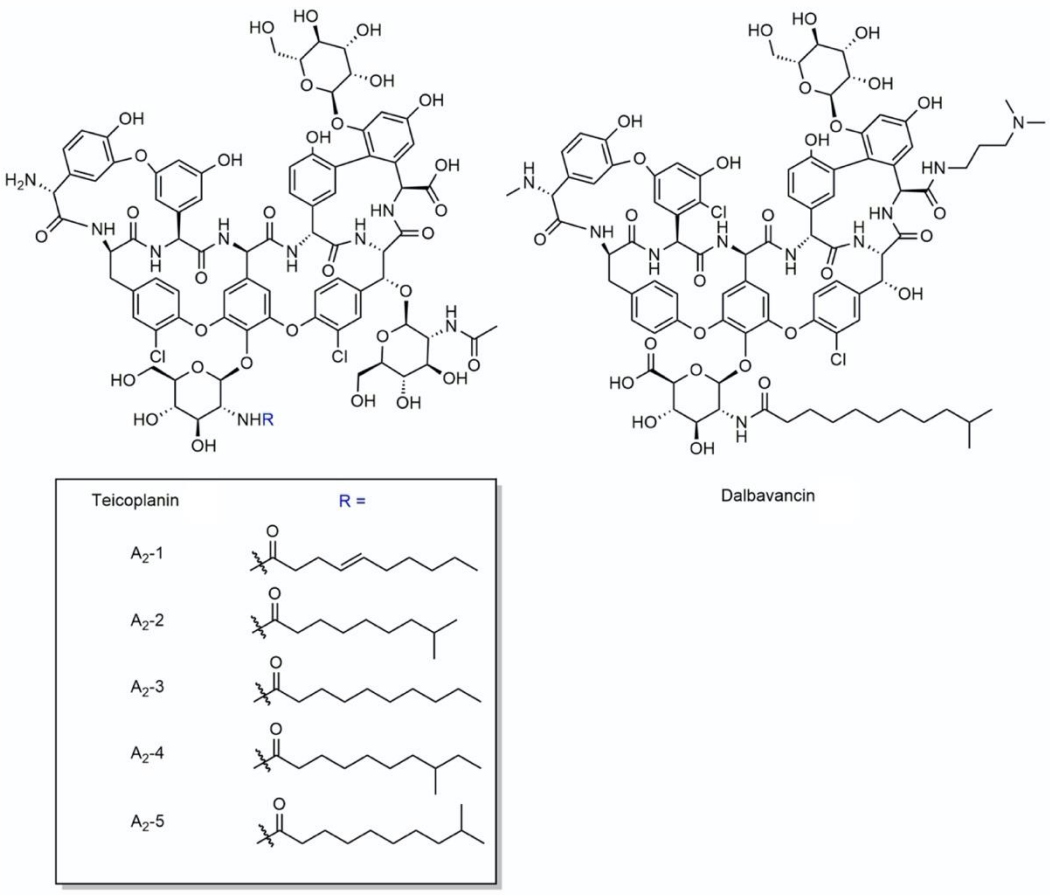

Figure 1.18 Teicoplanin and Dalbavancin.[21]

1.2.14.9 Quinolones

Quinolone antibiotics feature a quinolone core and a N-linked ring of fused ring-system. Nalidixic acid was discovered in 1962.[21] Ciprofloxacin, which is a fully synthetic quinoline, was introduced to the clinic in 1968.[26] Quinolines target topoisomerases II (DNA gyrase) and IV, which leads to inhibition of DNA replication.[21] Most quinolones are bactericidal and have a very broad spectrum activity (gram-positives, -negatives, and *M. tuberculosis*). Resistance occurs by means of target modification and efflux pumps.[51]

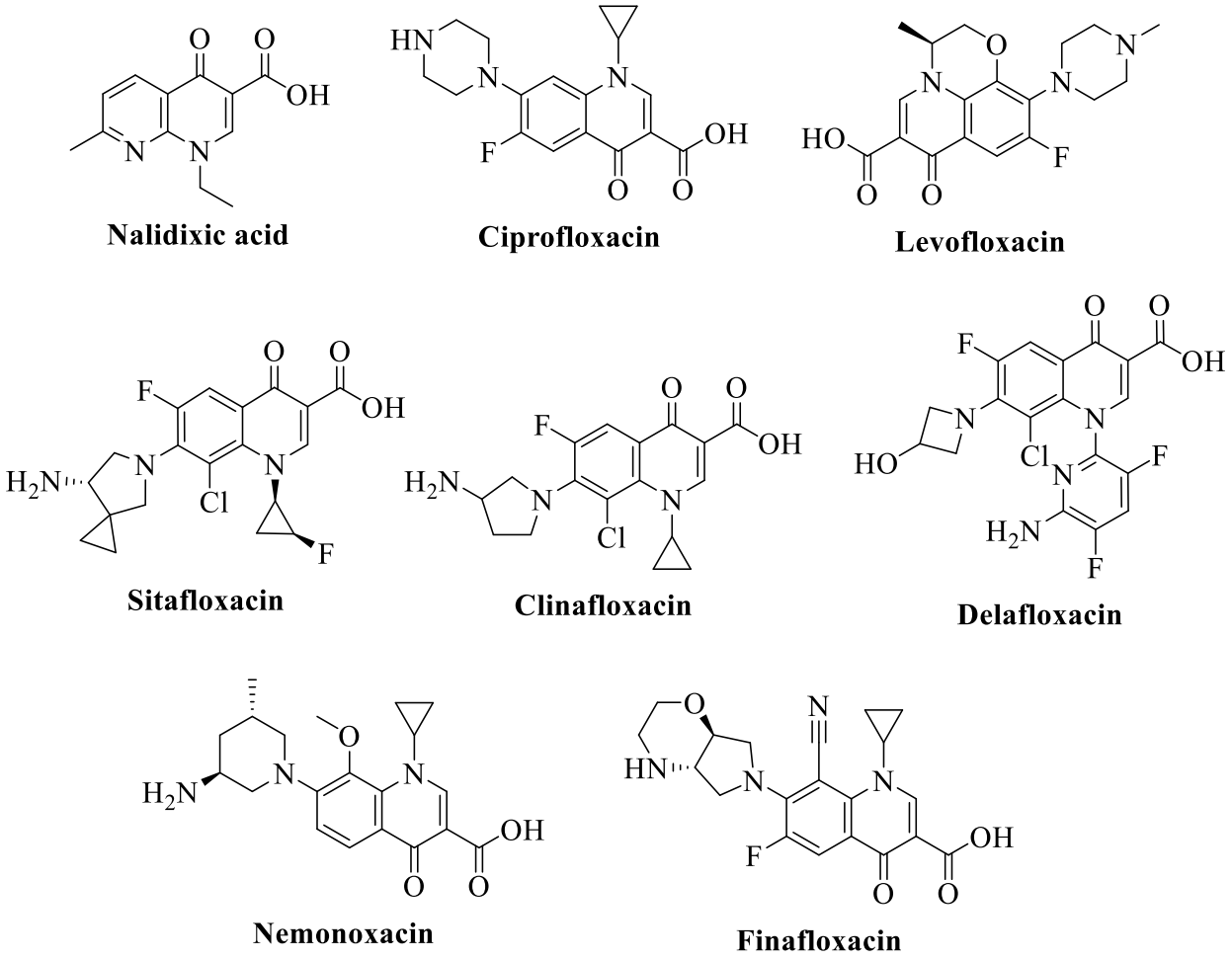

Figure 1.19 Quinolones.[21]

1.2.14.10 Oxazolidinones

This group of antibiotics is also defined by their heterocyclic oxazolidinone core. Linezolid was discovered in 1995, and FDA-approved in 2000.[85, 89] Oxazolidine antibiotics bind to the 50S ribosomal subunit, thus blocking peptide bond formation.[21] Their antibacterial action results in bacteriostatic activity against gram-positives and *M. tuberculosis*.[21] Target modification has been observed in *S. aureus*.[90] Linezoid is currently being used to treat MRSA infections.[21] Radezolid was FDA-approved in 2012 and tedizolid in 2014.[85] Both oxazolidones were develop to address

poor pharmacokinetics and to enhance activity against linezolid-resistant *Staphylococci*, including MRSA strains.[21]

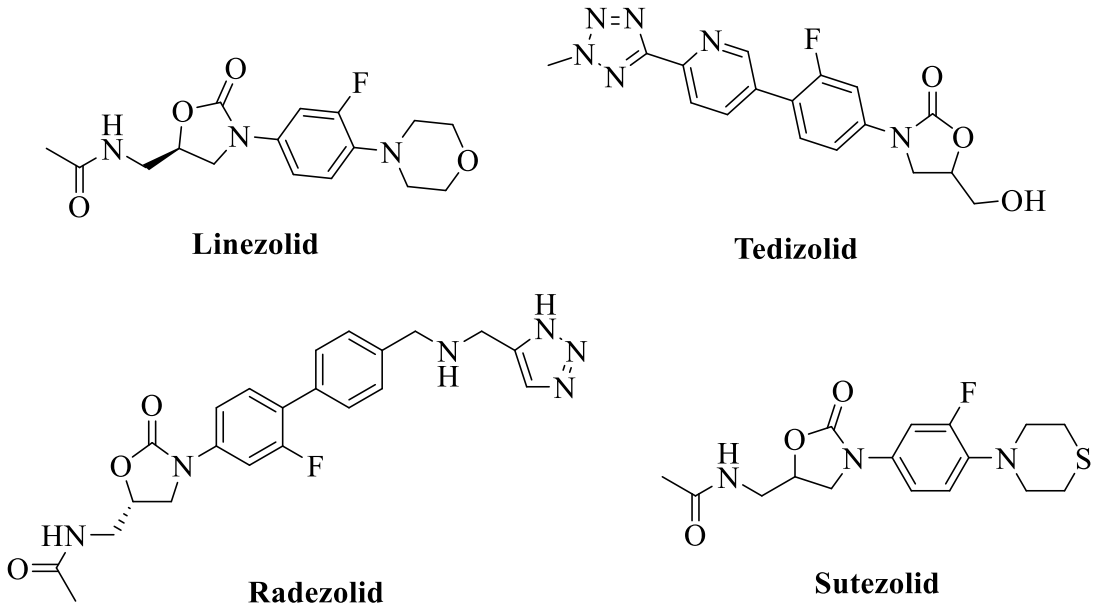

Figure 1.20 Oxazolidinones.[21]

1.2.14.11 Lipopeptides

This class of antibiotics has the following structural hallmarks: a cyclic depsipeptide that is capped with a peptidyl side chain featuring a saturated alkyl chain.[21] The first lipopeptide was daptomycin that was discovered in 1985 but only used in the clinic starting in 2003.[26] The function principle of lipopeptides is membrane-depolarization of gram-positive bacteria. The resulting potassium influx leads to membrane lysis.[21] Daptomycin resistance is still sporadic. *S. aureus* strains with thickened cell walls have been observed. Wall thickening is caused by increased production of teichoic acids and subsequent D-alanylation.[91] Daptomycin is highly active against MRSA.[92]

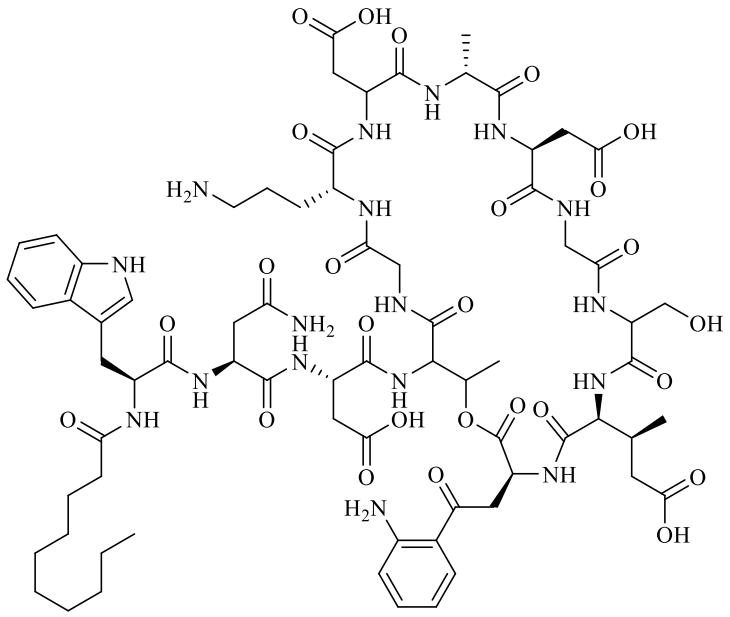

Daptomycin

Figure 1.21 Daptomycin.[21]

It should be noted that further classes of antibiotics are in development[21], among them streptogramins[51,93], polymyxins[94,95], pleuromutilins[96], macrolactones[51], and diarylquinolines[97]. However, since the major challenge of my thesis consisted in the development of copper(I)-activated drugs against MRSA and other *S. aureus* strains, and neither of these classes of antibiotics is of importance for treating MRSA, they are only quoted here because a comprehensive report is being attempted here.

Table 1.2 Critically important antibiotics.[21]

Class or Subclass	Primary Target	Important Members
Penicillins	Penicillin binding proteins	Pencillin G and V, ampicillin, amoxicillin, piperacillin, azlocillin, carbenicillin, mezlocillin, ticarcillin
Cephalosporins	Penicillin binding proteins	Cefixime, cefotaxime, cefpodoxime, ceftazidime, ceftizoxime, cefoperazone, ceftriaxone, cefepime, cefpirome, cefoselis
Carbapenems	Penicillin binding proteins	Ertapenem, faropenem, imipenem, meropenem

Aminoglycosides	30S ribosomal unit	Amikacin, arbekacin, gentamicin, netilmocin, tobramycin, meropenem
Macrolides	50S ribosomal unit	Azithromycin, clarithromycin, erythromycin, midecamycin, roxithromycin, spiramycin, telithromycin
Tetracyclines	30S ribosomal unit	Tigecycline
Rifamycins	RNA polymerase	Rifabutin, rifampin, rifaximin
Glycopeptides	Peptidoglycan units	Teicoplanin, vancomycin
Quinolones	Topoisomerase II and IV	Cinoxacin, nalidixic acid, pipemidic acid, ciprofloxacin, enoxacin, gatifloxacin, gemifloxacin, levofloxacin, lomefloxacin, moxifloxacin, norfloxacin, ofloxacin, sparfloxacin
Oxazolidinones	50S ribosomal unit	Linezolid
Lipopeptides	Cell Membrane	Daptomycin

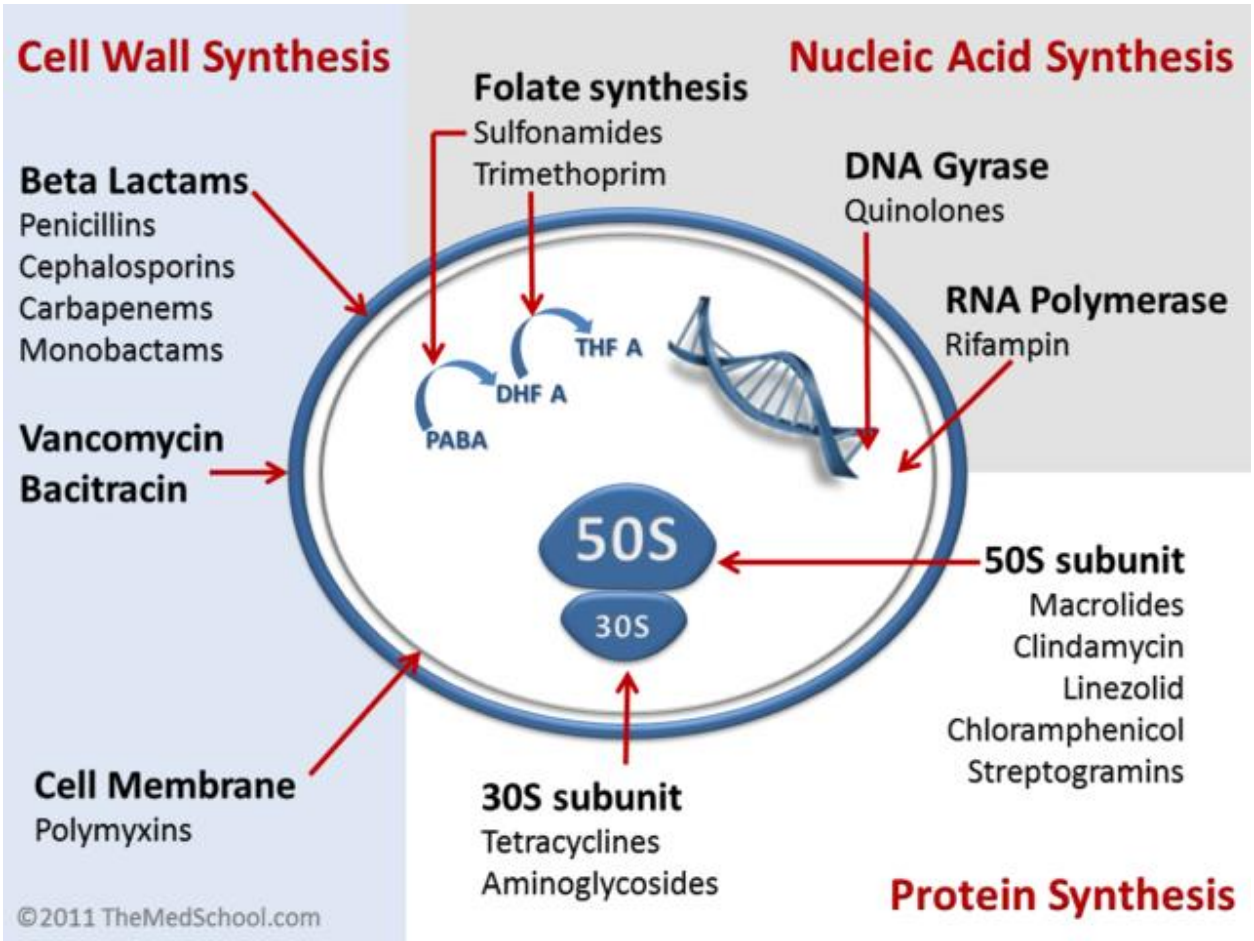

Figure 1.22 Drug Targets in both, GP and GN bacteria.[39]

1.3 Structural Comparison of Current Antibiotics against MRSA and the Class of Antibiotics Possessing NNSN Motifs for Copper(I)-Activation.

With the exception of the classes of antibiotics that are based on core aromatics (sulfonamides, amphenicols) or heterocycles (quinolones, oxazolidinones, diarylquinolines), virtually all other classes of antibiotics are natural products or semi-synthetic derivatives thereof.[21] Consequently, their structures are diverse and very complex. This results in synthetic hurdles, high prices for and/or limited availability. Although complete data sets do not exist, it is safe to assume that most of the bacterial infections and consequent deaths occur in the developing world. The class of NNSN compounds offers a structurally simple and effective way to treat MRSA and other *S. aureus* strains, as will be demonstrated in this thesis.

1.4 NIH-Recommended Therapy for MRSA Infections

As already discussed, methicillin-resistant *Staphylococcus aureus* (MRSA) is frequently the cause of serious nosocomial infections. The glycopeptide vancomycin is still the most important antibiotic for treating MRSA, followed by telavancin, which is also a glycopeptide.[98] Whereas resistance to vancomycin is on the rise, telavancin is especially suited for treating MRSA infections. The lipopeptide daptomycin is increasingly used as first-line antibiotic for MRSA as well.

This is based on the following considerations. In addition to fast developing bacterial resistance, vancomycin is a slow-acting bactericidal, which is a severe disadvantage when treating bacteremia and endocarditis. Telavancin and daptomycin are also bactericidal but act much faster than vancomycin. Telavancin has the advantage that it requires an order of magnitude lower

concentration for successful treatment. Vancomycin and daptomycin are active in the low micromolar range, telavancin in the high nanomolar range.[98]

Second-line drugs for MRSA are ceftaroline, a cephalosporin (β-lactam), and linezoid, an oxazolidinone.[98] Both drugs are active in the mid-micromolar range and show significant side effects, such as vomiting, diarrhea, abdominal pain, headaches, red blood cell and platelet deficiencies, as well as becoming prone to yeast infections.[85] Note that all drugs can be applied locally for MRSA skin infections and intravenously for MRSA infections within the body.[21]

What are the main disadvantages of current MRSA therapies? Apart from the significant side effects, the use of glycopeptides and lipopeptides is very expensive. Therefore, this kind of therapy is limited to the richer nations. β-lactams contain several stereocenters and oxazolidinones at least one. Oxazolidinones are easier to produce, almost as easy as compounds with a NNSN motif. Therefore, the final costs for oxazolidinones and compounds with NNSN motif should be similar. Both would be available in developing nations unless political barriers are created. The central advantage of copper(I)-activatable NNSN drugs is that their toxicity will be targeted to activated phagosomes. These drugs won't be toxic in the absence of copper(I) and are activated upon copper(I)-binding.

1.5 Copper: Geology, and Human History and Biology

The US Geological Survey has estimated that there are approx. 6.3 billion metric tons of copper that can be mined by humans.[99] The absolute copper on planet Earth could be 10-1000 times higher, depending on the unknown concentrations of copper in the Earth's mantle and core. Copper was of interest to our ancestors. The Bronze Age (3500 BC to 500 BC) is characterized by mining copper and tin for the fabrication of tools, utensils, ornaments and weapons.[100,101] Increased

contact with copper caused a slow biochemical adaptation. In today's human adults, copper concentrations between 1.4 and 2.1 mg per kg of body weight are measured.[102] This means that a typical human contains between 0.1 and 0.2 grams of copper.

Figure 1.23 Human Artifacts from the European Bronze Age.[103]

1.6 Importance of Copper in Mammals

Although the historical evidence is scarce, there is some clear archeological evidence that shows the use of copper as a medicine by ancient human civilizations dating back to 5th millennium BC.[104] Furthermore, the Smith Papyrus, which is one of the oldest Egyptian medical texts has described copper-based sterilization applications.[105] Similarly, there are many records from other civilizations including Rome, Greece and China that cited the use of copper or copper alloys for sterilization and other medical benefits.[105] Copper is abundant in nature and one of the essential

elements for many organisms to sustain a multitude of biological functions including free radical scavenging, electron transfer, as well as oxygen binding, storage and transport, oxidation catalysis and much more.[106] Moreover, it is well known that there are 25 or more copper containing enzymes, which facilitate the aforementioned biological functions.[107] This concept has recently attracted much attention, due to its medical attractiveness. Over the last three decades, numerous studies have demonstrated copper's anticancer[108] and antibacterial[109] properties. A few studies have described the antiviral properties of copper as well.[110] It should be noted that Cu(I) is tightly regulated in the human body and that Cu(II) is virtually absent, except as cofactor in copper-containing enzymes involved in oxidation catalysis (tyrosinase, galactose oxidase, hemocyanin, ceruloplasmin, ascorbate oxidase, cytochrome c oxidase, superoxide dismutase, amine oxidase, lysyl oxidase, dopamine-β-hydroxylase, and peptidylglycine α-amidating monooxugenase).[107] Copper homeostasis in mammals requires complex regulation processes.[111] Cu(I) and Cu(II) are taken up through ion channels across basolateral intestinal membranes. Luminal copper is reduced t^{o}u(I) for effective storage in CTR1(High affinity copper uptake protein 1) in mammalian bodies.[112] It should be emphasized that the binding constants of Cu(I) by CTR1 and other Cu(I)-binding proteins, such as Atox1 (Antioxidant Protein 1) and ATP7B (ATPase Copper Transporting Beta) are extraordinarily high. They range from K_B's = 10^{14} to 10^{16} M^{-1}.[113] Cu(I) excretion proceeds via bile secretion by the liver.[112] These Cu(I)-complexes are too stable for virtually any Cu(I)-binding antibiotics to successfully compete. Therefore, a biochemical process called nutritional immunity[114, 115], in which Cu(I) is delivered to activated phagosomes, is becoming increasingly of interest for copper-activated antibiotic treatment strategies. Since essentially only Cu(I) is available for complexation with copper-activated antibiotics,[112] I will focus on compounds designed for Cu(I) complexation in this thesis.

1.7 Copper antibacterial properties

Although copper has multiple medicinal properties, its antibacterial characteristics have attracted interest from many research groups over the last three decades which is clearly visible from the number of publications published each year dating back to 1972. An exponential growth of publications in refereed journals has been observed during the last decade. Even though this study is exclusively concerned with copper complexes' antibacterial properties, there is sufficient evidence to demonstrate that some bacterial strains can be rapidly killed on metallic copper surfaces. This phenomenon is termed "contact killing", which has been utilized in the apparel industry to roll out copper infused fabrics for self-cleaning clothes.[116] Another application is fabricating hospital surfaces with copper or copper alloys, which reduce the exposure of patients to pathogenic bacteria and thereby reduce hospital acquired infections.[117] Even though copper is essential for many living organisms, it can be toxic if free copper(II) ions get accumulated in healthy cells, which seems to play a key role in copper's antibacterial properties.[118] However, this is not the strategy that is pursued here, because Cu(II) exists on surfaces[117] and in copper-transporting nanoparticles[119] but only Cu(I) is available in mammalian cells and blood circulation.[112]

There are few mechanisms that elucidate the copper ion's lethal role against invading pathogens. In addition, the exact modes of action of free copper ions binding to sensitive cellular targets have not yet been clearly elucidated. It is noteworthy that among copper's most prominent oxidation states, Cu^{+}, which is abundant in the cytoplasm due the presence of the reductant Glutathione (GSH), has significant antibacterial properties. The standard redox potential of Cu^{2+}/ Cu^{+} is +0.155 V (vs. normal hydrogen electrode (NHE)) (Equation 1).[120] This means that the

estimated redox potential of Cu^{2+}/ Cu^{+} at physiological pH is near +0.1 V. [120] This is not taking into account potential Cu(I) or Cu(II) complexation in living systems (pH ~7). The major reducing agent in prokaryotic and eukaryotic cells is Glutathione (GSH), which possesses a redox potential of -0.24 V (Equation 2) under cytoplasmic conditions for the GSH/GSSG (Glutathione disulfide) redox couple.[121] Moreover, the cytoplasm controls the ratio of GSH/GSSG and always favors the reduced GSH form.[121]

Equation 1 $Cu^{2+} + e^{-} \rightarrow Cu^{+} \quad E \approx +1.0V$

Equation 2 $2\,GSH \rightarrow GSSH \quad E \approx -0.24\,V$

Based on these redox potentials, copper is present as Cu(I) in the cytoplasm, as already discussed above. The link between the innate immune system and Cu^{+} ions plays a vital role at the sites of pathogenic attacks.[122] Upon the detection of infections, the rapid influx of macrophages attempts to engulf the pathogens. Moreover, activated macrophages accumulate Cu^{+} ions to fight against pathogenic bacteria in activated phagosomes after they have been engulfed. This is part of a global strategy of mammalian cells to fight bacteria, which is called *nutritional immunity* (starving pathogens of trace minerals (iron and zinc) and increasing the concentration of copper in activated phagosomes).[123,124]

Copper(I) secretion to activated phagosomes is facilitated by the high affinity copper transporter CTR1 and activated copper ATPase "ATP7A".[125,126] Although virtually all bacteria require micronutrients, such as Fe, Zn, Mn, and Ni, high accumulation of Cu^{+} ions can show bactericidal effects. Although the reported concentrations of copper in activated phagosomes vary considerably in the literature,[123] it can be conservatively estimated that at least 50 μmol is present in activated phago(lyso)somes.[123, 127]

The precise role of the Cu^+ ion in innate immune systems remains to be further studied, but current studies reveal that the following bactericidal mechanisms can play a major role in macrophage derived antibacterial activity:

1) Cytoplasmic cuprous ions can react with hydrogen peroxide in Fenton-like chemistry to generate highly reactive hydroxyl radicals (or in other terms reactive oxygen species "ROS"), which can potentially damage bacterial DNA, react with membrane lipids and lead to the disintegration of bacterial cell membrane components. Similarly, ROS can react with the side chains of certain proteins/enzymes causing dysfunction of their biological activities.[128]
2) The ROS is enhanced by the ability of Cu(I) to disrupt cell membranes. This leads to leakage of sugars, glutamate, and potassium. This considerably weakens the bacteria and their ability to clear Cu(I) by means of efflux pumps.
3) Cu(I) decreases the osmotic pressure in bacteria. This effect further weakens their cell membranes.
4) Cu(I) binds to numerous peptides with thiol- or amine-functions that are not designed for copper-binding. "Inappropriate Cu(I)-Binding" leads often to the loss of function.
5) Cu(I) acts as chemical hydrolase of sugar-phosphate bonds. Therefore, it is able to hydrolyze DNA and RNA.

1.8 Copper(I)-Activated Drugs

The concept of copper(I)-activation is based on a discovery by Dr. Michael Niederweis, Dr. Olaf Kutsch, and Dr. Frank Wolschendorf at the University of Birmingham, Alabama in 2013. They recognized that the NIH-recommended standard conditions for testing drug candidates for *M. tuberculosis* were unable to ascertain activity of isoniazid,[129] which is together with rifampicin

and pyrazinamide still the first-line treatment of *M. tuberculosis* infections.[130] This discovery was the starting point of the development of the concept of copper(I)-activation. The Bossmann group joined this endeavor in 2013 in order to provide organic expertise and to synthesize lead compounds.[131] This thesis has contributed significantly to this endeavor.

In 2014, Wolschendorf et al. demonstrated copper(I)-activation of neocuproine, disulfiram, and thiocarlide for treating MSSA (*methicillin-susceptible S. aureus*) and MRSA (*methicillin-resistant S. aureus*) in-vitro.[132] In 2016, an extensive library search[70,133] identified several heterocyclic compounds capable of copper(I)-binding and subsequent activation. The lead compound, which is a thiourea with a tethered pyrazole and an aromatic unit is shown in Figure 1.24. It has a minimum inhibitory concentration (MIC) of 0.6 μmol against *S. aureus* clinical isolate SA3 (resistant to ampicillin, clindamycin, erythromycin, penicillin, and tetracycline). This is distinctly more effective than vancomycin (MIC > 2 μmol) and almost as effective as telavancin.

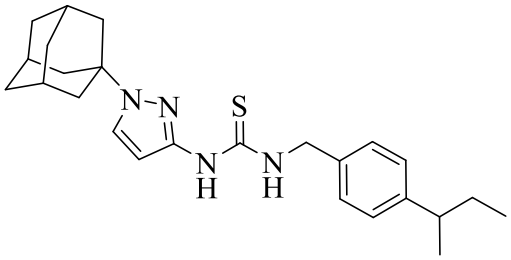

Figure 1.24 Early lead compound for copper(I)-activated treatment of MRSA[70]

Since then, the group of researchers from UAB and Kansas State have explored several new binding motifs for copper(I) against MRSA and against *M. tuberculosis*.[134,135,136,137] This research led to a patent disclosure in 2020.[138] The research of this thesis was concerned with discovering structure-activity relationships (SRA) of compounds with NNSN-motif and with upscaling key steps required for future application of compounds with NNSN-motif in the clinic.

The experimental approach pursued here is conceptionally different from competing approaches, in which either copper(I/II)-complexes with organic ligands,[139,140,141,142,143,144] metal-organic-frameworks[145,146] or nanoparticles capable of releasing significant concentrations of Cu(II) will be employed,[147,148,149,150,151,152,153] which then will be reduced to Cu(I) after cellular uptake by glutathione.[154] The general advantage of copper(I)-activation within phagosomes is that collateral toxicity and the rapid deactivation of the antibiotic by copper homeostasis will be avoided.[155] Note that the chapter on copper-semithiocarbazones has been included in this thesis, because this class of compound has chemical similarities to the class of novel NNSN-compounds that was synthesized in this thesis.

1.8.1 Response of *S. aureus* to Copper Stress

The co-evolution of pathological bacteria and human hosts has led to arsenals of copper chaperones, copper pumps, and copper storage proteins on both sides. The result is copper homeostasis at the host-pathogen interface.[156,157,158]

1.8.2 The Human Response

In humans, inflammatory agents, such as bacterial lipopolysaccharides (LPS) that are being released from the surface of invading bacteria upregulate the expression of the CRT1 copper importer. The function of CRT1 is to import copper(I) that is stored in ceruloplasmin across the plasma membrane. The copper chaperone ATOX1 binds copper(I) in the cytoplasm and delivers it to the ATP7A copper pump in the trans-Golgi network. As the name indicates, ATP7A is an ATPase. Upon copper(I)-uptake, ATP7A partially relocates to the membranes of phagolysosomes

where it releases copper(I) into this compartment. Note that the concentration of copper(I) within activated phagolysosomes (after uptake of bacteria) can reach up to > 150 micromoles per liter.[159]

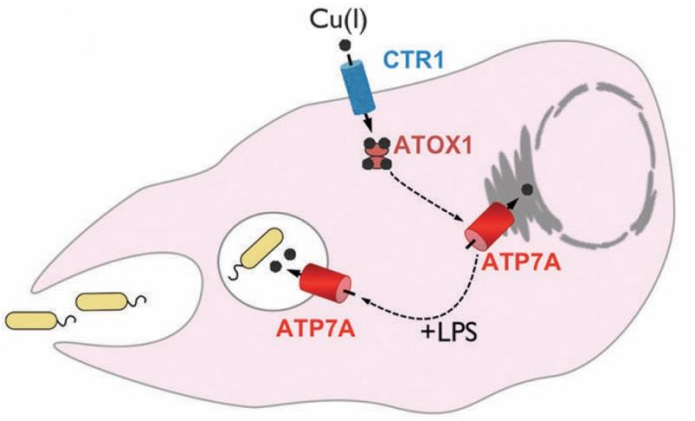

Figure 1.25 Delivery of Cu(I) to activated phagosomes. Upon activation, CRT1 imports copper through the cell membrane, which is collected by the copper chaperone ATOX1 and then delivered to the copper pump ATP7A copper pump in the trans-Golgi network. ATP7A shuttles between trans-Golgi network and phagosomes. It delivers Cu(I) into the phagosomes and then reloads.[156]

1.8.3 The Bacterial Response

When *S. aureus* is engulfed by an activated phagosome, the copper(I) concentration within the phagosome increases (see Figure 1.25). Cu(I) is capable of diffusing through the cell envelope of gram-positive organisms, such as *S. aureus*.[160] Once the Cu(I) concentration in the cytoplasm of *S. aureus* increases, it binds to the CsoR transcriptional regulator.[161] This process leads to the derepression (enhanced expression upon a stimulus) of the copAZ and copBL operons. Both operons act together and turn on CsoZ expression. CsoZ acts as cytosolic Cu(I)-buffer and copper-chaperone, which delivers the collected Cu(I) to the efflux pumps CopA and CopB. Both, CopA and CopB are ATPases. Note that CopA and CopB deliver Cu(I) only across the inner membrane of *S. aureus*, but not beyond the thick peptidoglycan. CopL is also expressed in response to increased Cu(I) in the cytosol. CopL is a membrane-bound, copper-binding lipoprotein that

features Cu(I)-binding sites at the surface of *S. aureus*. CopL prevents cytosolic uptake and re-uptake by binding extracellular Cu(I).[161]

Investigations of several members of copper metallochaperone proteins revealed that the majority of them contain common structural characteristics, including a short metal binding domain (MBD) and a conserved sequence of the binding site $MX^1CX^2X^3C$.[162] These "X' positions can be varied with respect to each protein and usually X^1 consists of histidine, threonine, or serine. In contrast, X^2 and X^3 positions tend to feature hydrophobic or polar uncharged residues, such as alanine, glycine, and serine.[162] In most cases, methionine (MX^1) has very limited interaction with the copper center as it is located too far, whereas CX^2X^3C closely coordinates with the metal ion as sulfur atoms from two cysteines bind linearly on both sides of the Cu(I) ion. It is very clear that having two sulfur atoms in close proximity enhanced affinity for Cu(I), which enables copper chaperones to escort the Cu(I) ion to the specific location such as from CTR1 to ATX1 followed by Ccc2, eventually reaching the phagolysosome. However, the copper defense systems of many bacteria, CopZ, CopA and CopB, also consists of very similar MBDs. Hence, the Cu(I) ions are exported from the bacterial cell to extracellular space effectively before bactericidal effects can occur.

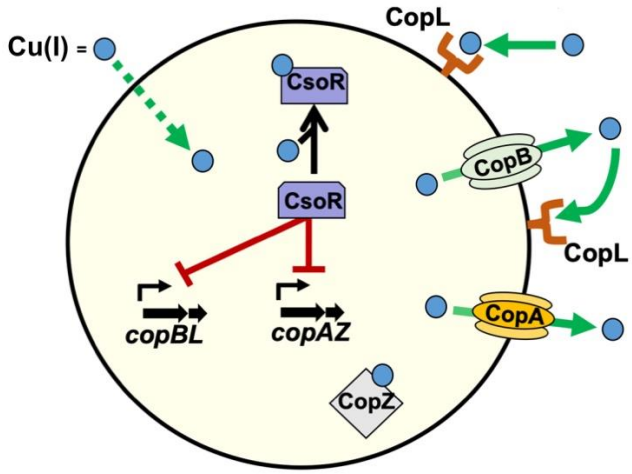

Figure 1.26 Cu(I) binds to CsoR, which leads to derepression of CopAZ and copBL operons and, subsequently, to CsoZ expression. CsoZ delivers Cu(I) to the efflux pumps CopA and CopB. External Cu(I) is sequestered by CopL.[161]

1.8.4 What is the pH of Phagosomes?

Macrophages are the major type of defensive cells involved in a response to a bacterial infection. Macrophages can be either M1- or M2-polarized. M1 polarization of macrophages is induced by pro-inflammatory signaling, among them bacterial infection, Toll-like receptor ligation, and exposure to the T-helper 1 cytokine interferon-γ (IFN-γ). M1-polarized macrophages show an increased capacity to clear bacteria after taking them up in their activated phagosomes. The M2-phenotype of macrophages is stimulated by the STAT-6–activating cytokines interleukin-4 (IL-4) and/or IL-13. M2-polarized macrophages are suppressors of inflammation. They are involved in tissue repair and remodeling, and the uptake and proteolytic degradation of apoptotic cell debris.[163,164]

Canton et al. proved by means of ratiometric pH-measurements in phagosomes of M1- and M2-polarized macrophages that the pH-evolution within the first 30 min. proceeds entirely differently, depending on macrophage polarization.[163] Their results are shown in Figure 1.27 Whereas the pH in phagosomes of M2-polarized macrophages decreases from the initial pH = 7.1

± 0.1 to about pH = 5 within 10 min, the pH in phagosomes of M1-polarized macrophages varies between 7 and 9. It is noteworthy that the phagosomes of M1-polarized macrophages also reach pH = 5 after 24h.[163] However, they have a window of several hours in which the pH is very suitable for the binding of Cu(I) to targets, such as NNSN compounds. Based on these findings, we postulate the paradigm that copper(I)-activation of NNSN compounds occurs immediately after the bacteria have been engulfed by the phagosome and that they act sufficiently quickly to be either bactericidal or bacteriostatic.

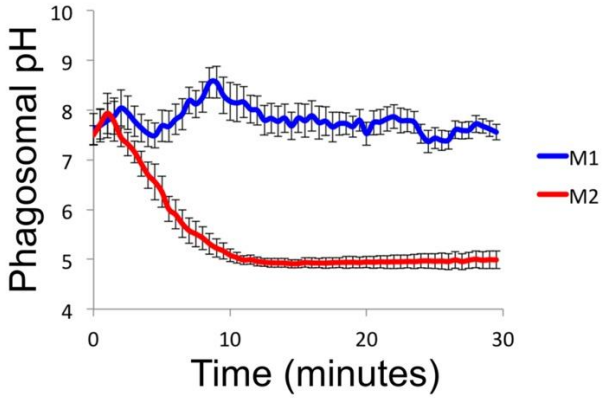

Figure 1.27 pH-evolution during the first 30 min. in the phagosomes of M1- and M2-polarized macrophages.[163]

1.9 Copper Complexes of Thiosemicarbazone (TSC)

On our voyage to explore possible organic ligands capable of copper-binding, TSCs were promising candidates for further studies, as TSCs have been widely studied in medicinal chemistry due to their broad array of biological activities.[165] Most of them are well known for their antimicrobial,[166] antiviral,[167] antiparasitic,[168] antifungal[169] and anticancer[170] properties (Figure 1.28b). TSCs have been intensively studied as drug candidates due to the stereochemistry of the azomethine imine functionality and the presence of several hydrogen bond donors and acceptors (Figure 1.28a).[171]

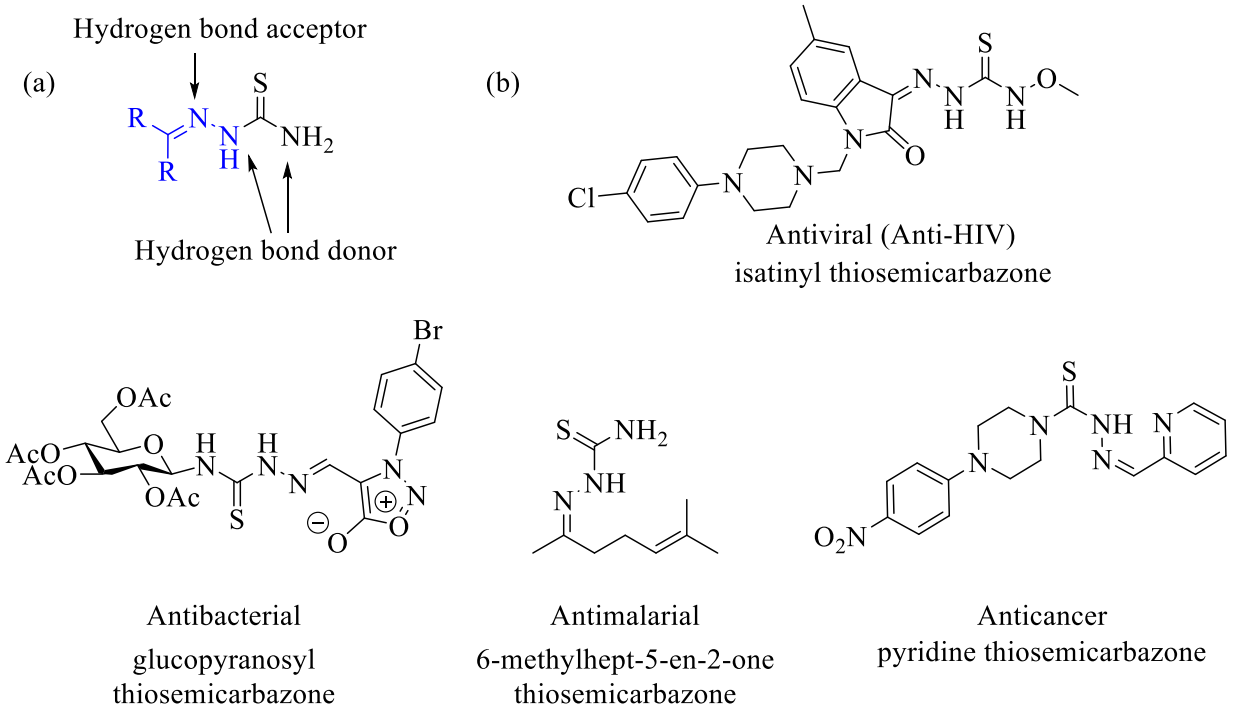

Figure 1.28 Structures of thiosemicarbazone derivatives and corresponding medicinal properties. (a) Generic structure of thiosemicarbazone is assigned with blue color. (b) Thiosemicarbazone derivatives with antiviral, antibacterial, antimalarial and anticancer properties.[166, 167, 168, 169, 170, 171]

It has been demonstrated that the complexation of thiosemicarbazone with Cu(I) or Cu(II) ions can enhance its antibacterial (10 µM to 2 µM),[172] antifungal (>600 µM to 1.5 µM)[173] and anticancer (100 µM to 0.3 µM)[174] properties significantly (Figure 1.29). It should be noted that the literature on Copper-Thiosemicarbazone complexes features both, Cu(I) and Cu(II) complexes. Since Cu(II) will be quickly reduced to Cu(I) under biological conditions, which are also relevant for direct bacterial uptake before phagosomal uptake or ex-vivo, there is serious doubt that the Cu(II)-complexes that have been reported are responsible for the observed antibacterial, antifungal, or anticancer activities.

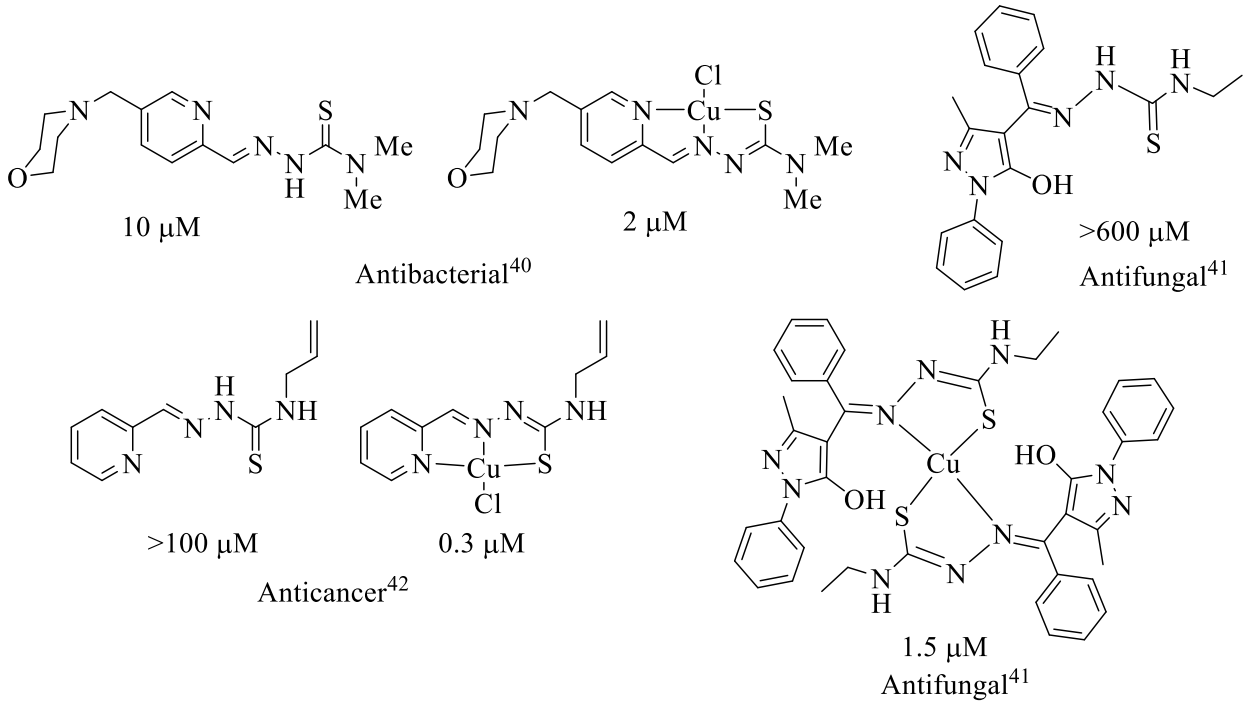

Figure 1.29 Thiosemicarbazone and Cu(II) complexes as antibacterial, antifungal and anticancer molecular candidates.[172, 173, 174]

It has been suggested that increased bioactivity may be attributed to the enhanced lipophilicity of copper complexes.[175] Once Cu(I/II) ions are complexed with thiosemicarbazone ligands, there may be an increase in their lipophilicity, which boosts their cell membrane permeability.[176] For instance, the structure activity relationship (SAR) of copper complexes with 8-hydroxyquinoline derivatives showed high cytotoxic activity with only log P values between 1.5 to 3, which is in agreement with this paradigm.[177] It should be noted that we have tested the ability of Cu(I) to boost the antibacterial activity of NNSN-compounds. We have not synthesized Cu(I/II) complexes and used them as therapeutics. Therefore, enhanced permeability of Cu(II) is not an option in the research conducted here. However, NNSN-compounds may increase the permeability for Cu(I). Although this does not appear to be a major therapeutic pathway in Cu(I)-resistant pathogens, as for instance MRSA and MSSA, it cannot be completely discarded at this time.

1.10 Copper-Binding Complexes in Nature

Recent progress by means of X-ray crystallography of Cu(I/II) complexes and Electron Paramagnetic Resonance of Cu(II) has unlocked the structures of active sites of virtually all known copper-containing enzymes and enzyme models.[107] Principally, this information is important for the potential binding geometry of Cu(I) binding to antibiotics with NNSN-motif.

Table 1.3 Types of copper containing sites and main ligands.

Type	Mononuclear site		
	Type 1	Type 2	Nu_B
UV spectroscopy	Strong absorption band at ~600 nm and (in some proteins) 450 nm	Absorptions at ~ 700 nm	Absorptions at ~ 610 nm
Main ligands	His, Cys, (Met)	His, Asp, (Tyr)	His
Geometry	Distorted tetragonal Trigonal planar	Distorted tetragonal	Trigonal pyramid
Type	Dinuclear site		
	Type 3	Cu_A	
UV spectroscopy	Absorptions at ~ 700 nm	Strong absorption bands at ~480 nm and ~ 530-580 nm, absorption band at 800 nm	
Main ligands	His, (Tyr)	His, Cys, (Met)	
Geometry	Tetragonal	Trigonal planar	
Type	Trinuclear site	Tetranuclear site	
	Type 4 (Type 2 + Type 3)	Cu_Z	

UV spectroscopy	Absorptions at ~ 330 and ~600nm	Strong absorption at ~640 nm
Main ligands	His	His, S^{2-}
Geometry	Trinuclear site	$_{4}$-S^{2-} tetranuclear copper cluster

As can be discerned from the data compiled by Tishchenko et al.,[107] the copper-binding sites in enzymes can be classified in type 1, 2, 3, and 4. Types 1 and 2 are mononuclear, type 3 is dinuclear, and type 4 is trinuclear (combination of type 2 and type 3). A tetranuclear site exists in N_2O reductase. Although mixed Cu(I)/Cu(II) valences can occur in types 2, 3, and 4, type 1 active sites are of particular interest for this thesis. This group comprises the so-called small blue proteins (cupredoxins), and the phytocyanin family.[107] As shown in Figure 1.30 the typical binding site in type 1 copper enzymes has the shape of an irregular tetrahedron. This is a clear indication that type 1 copper can rapidly change its oxidation state from Cu(II), which required square planar coordination to Cu(I) that prefers tetrahedral coordination geometries.[107] An irregular tetrahedron requires minimal energy for site reorganization if a change of redox state occurs.[107] Since stable Cu(I)-NNSN crystals could not be obtained by means of X-ray crystallography, we have assumed an irregular tetrahedron as the most likely coordination geometry of Cu(I) in NNSN compounds, following nature's example. As in the general structure shown in Figure 1.30, at least one of the corners of the irregular tetrahedron (marked with an X) can be taken up by a solvent molecule (water) or an anion from the aqueous buffer solution.

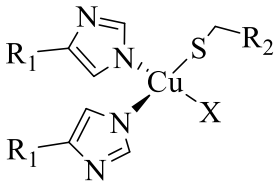

Figure 1.30 General structure of the copper environment in type 1 enzymes.[107]

1.11 Central Hypothesis

My thesis research was guided by the following central hypothesis: Copper on surfaces has been very successful against microbes. However, copper is toxic to human (mammalian) organisms. Therefore, copper is tightly controlled in the human body. Except as co-factor of enzymes, copper(I) virtually only exist in Cu(I) storage proteins. Cu(II) is present only in enzymes and is immediately reduced to Cu(I) by gluthatione and other reductants in the human body.[178] The only location where free Cu(I) is present is in activated phagosomes and in some solid tumors. Free Cu(I) reacts with multiple targets in bacteria, as described above: It weakens their cell membranes, increases ROS, hydrolyzes DNA and RNA, and deactivates multiple proteins via "inappropriate binding". This is conceptionally different from most classic drugs that were designed against a specific target.[179] The compounds with NNSN motif that are the major topic of my thesis are designed to be relatively weak Cu(I) binders. They cannot compete with Cu(I) storage proteins, but they can form complexes with free Cu(I) in activated phagosomes. By forming Cu(I)-complexes they are capable of forming reactive iminium cations. This will enhance the ability of Cu(I) to cause oxidative stress (ROS).[180,181]. Iminium cations are also known as typrosine phosphatase B inhibitors, [182] and to undergo Diels-Alder and Michael reactions with multiple targets.[183] By targeting multiple sites in bacteria, their chances of becoming resistant are diminished. Therefore, this strategy is, in my opinion, well-suited for the treatment of multi-resistant bacteria, such as MRSA.

2. Preliminary Work and Current Approach

2.1 Identification of Copper Hits Against MSSA and MRSA

This collaborative research was initiated with the use of a high throughput screening (HTS) method, which played a leading role in the drug discovery process. Using HTS enables researchers to uncover the distinctive interaction between copper(I) ions and compounds that already exist in chemical libraries as well as their synergistic inhibitory activity.[115] Dalecki *et al*. have used this copper biased combinatorial screening method to identify possible copper dependent targets against *Staphylococcus aureus (*SA*).*[115] Of the 10,000 compounds that were screened, 53 compounds showed copper dependent antibacterial activity (Figure 2.1a). These 53 targets were further categorized into two groups: thiourea (45 targets) and non-thiourea derivatives (8 targets). Most interestingly, 33 out of those 45 hits contained a traditional thiourea core (blue,) and the rest of the 12 hits consisted of extended versions of the thiourea core, which was abbreviated as "NNSN" (red). Moreover, the 12 NNSNs possessed nitrogen containing heterocycles as shown in Figure 2.1b. In order to investigate whether these NNSN moieties could be further optimized for a lead compound, a narrow structure activity relationship (SAR) was performed with 9 commercially available pyrazolyl thiourea derivatives containing adamantane at pyrazole's 1N.

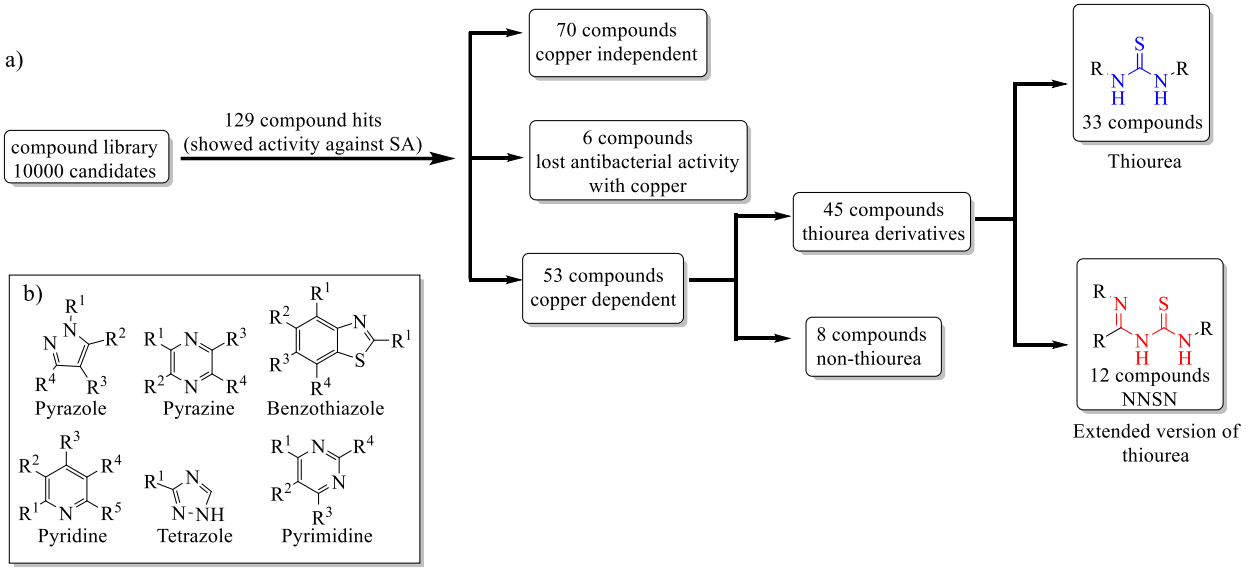

Figure 2.1 (a) A HTS method was utilized to find 33 thiourea (blue) targets and 12 extended versions of thiourea (red) "NNSN" targets. (b) 12 NNSNs featuring thiourea targets were found with six possible nitrogen containing heterocycles.

The selection of adamantyl in the 1N position is hypothesized to increase the overall pharmacophore properties of the targeted compounds (as shown in Table 2.1) as it possesses a broad spectrum of medicinal properties such as antiviral,[184] antibacterial,[185] anticancer,[186] and antidiabetic (Type 2 Diabetes) effects.[187] In contrast to the pyrazolyl side, molecule's right hand side employed six different substituted phenyl rings, a furan ring and two other cyclic derivatives. As shown in Table 2.1, out of these nine analogs, compound 9 demonstrated the best copper dependent antibacterial activity against *S. aureus* with a minimum inhibitory concentration (MIC) of 0.3 µM.[115] Based on the overall SAR study, it suggested that having aromatic heterocyclic pyrazole and phenyl rings may enhance the copper dependent antibacterial activity. Thus, it is essential to retain these two moieties when synthesizing a library. Due to the lesser availability of adamantyl substituted pyrazole, the initial syntheses were started by replacing the adamantyl ring with methyl, *t*-butyl and hydrogen substituents.

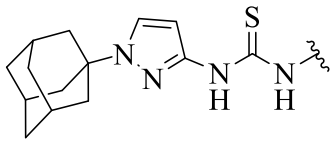

Table 2.1 Minimum inhibition concentration values of pyrazolyl derivatives against the strain SA3.

Compound No	Structure	MIC (µM)	Compound No	Structure	MIC (µM)
1	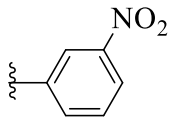	10	**6**	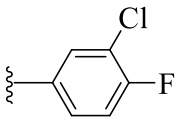	2.5
2	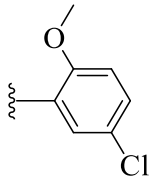	5-10	**7**	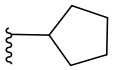	1.25
3	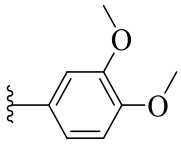	5-10	**8**	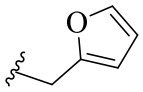	0.6
4	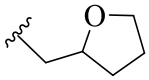	5-10	**9**	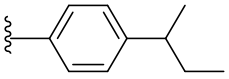	0.3
5	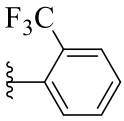	2.5			

2.2 Preliminary Synthesis of NNSN Candidates

In order to access the extended thiourea version NNSN, 1N substituted 3-amino pyrazoles were reacted with 4-choloro phenyl isothiocyanate as shown in Scheme 2.1. Isothiocyanate's "C" is sandwiched between two electronegative atoms of sulfur and nitrogen so that the middle carbon is electrophilic. In that case, many nucleophiles can attack the electrophilic "C" easily under mild conditions. Although the pyrazole's pyridine like "N" atom tends to show nucleophilic character, in the presence of a base pyrazole's 1N-H can be deprotonated and undergo the nucleophilic attack. Additionally, the aromaticity of the pyrazole can be diminished when the pyridine like N attacks an electrophile. Therefore, in order to maintain the aromaticity and in the presence of a base, pyrazole's pyrrole like N is more prone to act as a nucleophile.

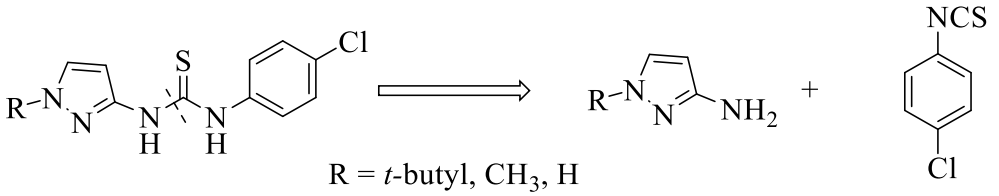

Scheme 2.1 Retrosynthesis of N-substituted thiourea derivatives.

1N substituted 3-amino pyrazole derivatives **10**, **11** (Scheme 2.2) were synthesized by reacting corresponding hydrazines with 2-chloroacrylonitrile in the presence of K_2CO_3/$NaHCO_3$ additives (1:2 molar ratio).[188] According to the original publication, the purpose of the additives was to minimize the formation of 5-aminopyrazole derivatives and to deprotonate of the hydrazine hydrogens.[188] However, the advantage of one derivative over the other is not clearly described. The resulting pyrazoles are hydrophilic, and they tend to dissolve in aqueous layer rather than organic solvents. Here, the continuous extraction method was employed to improve the pyrazole extraction into the organic phase.

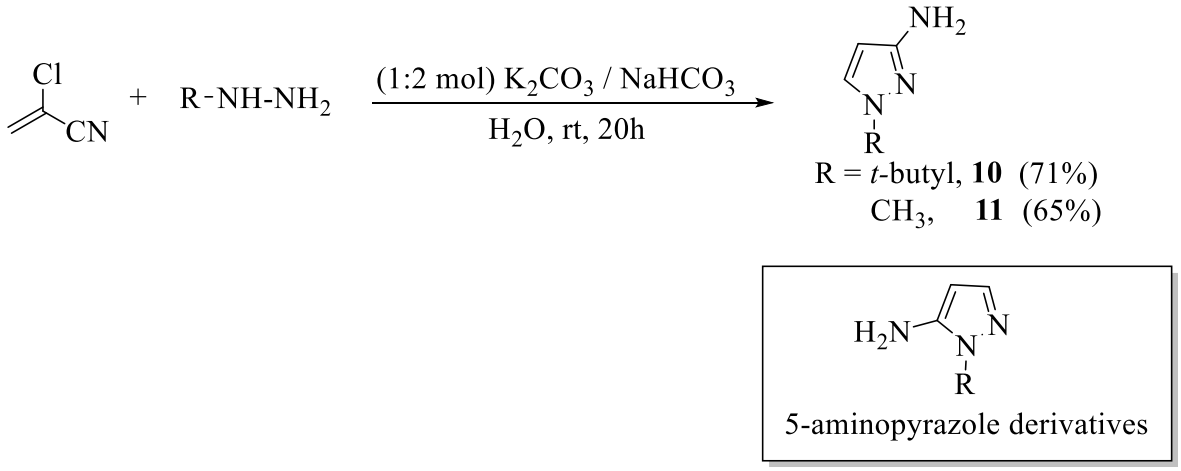

Scheme 2.2 Synthesis of 3-aminopyrazole derivatives consisting of 1N substituted with methyl, *t*-butyl, and hydrogen. Refer Appendix A.1 for the proposed mechanistic discussion.

After that **10**, **11 and 12** were reacted with 4-chlorophenyl isothiocyanate under mild reaction conditions to provide thiourea derivatives **13**, **14**, **15** and thiosemicarbazone **16**. 3-amino pyrazole **12** was commercially available for purchase. Except for compound **13**, the rest of the compounds were synthesized using reflux conditions for 16-18 hours. For compound **13**, instead of refluxing, K_2CO_3 was used as a base at room temperature overnight in a dimethyl formamide (DMF) medium.

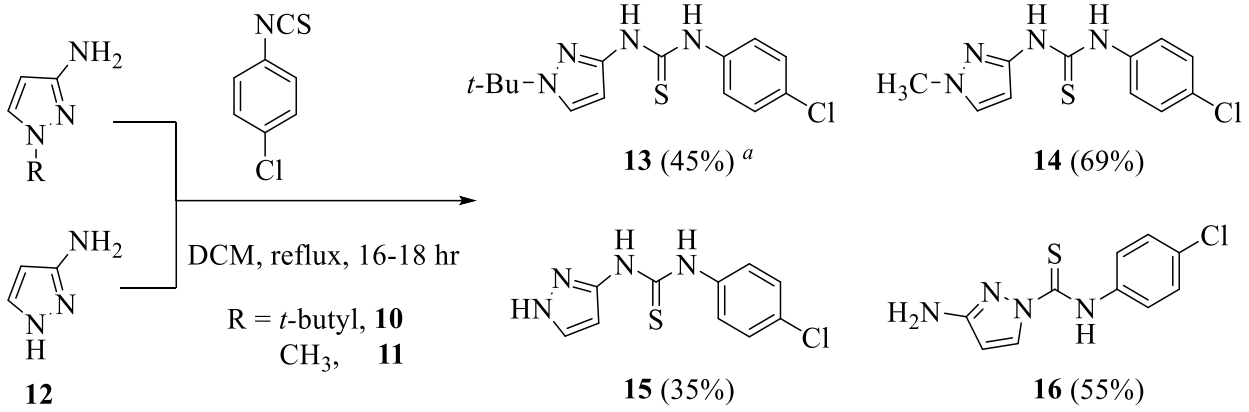

Scheme 2.3 Syntheses of thiourea derivatives 13, 14,15 and thiosemicarbazone 16 by reacting 3-aminopyrazole derivatives and 4-chlorophenyl isothiocyanate. [a]1 eq. of K_2CO_3 was used in DMF at room temperature overnight.

During the reaction between 3-aminopyrazole **12** and 4-chlorophenyl isothiocyanate, there were two major spots visible on the TLC plate (thin layer chromatography) and it was determined that **15** and **16** are structural isomers. Although there are three nucleophilic nitrogen atoms present in **15** and **16**, the heterocyclic N can be disregarded as it would undergo a reversible dearomatization/aromatization process, which would leave the heterocyclic NH group and the primary amine at 3C as potential nucleophiles. The paradigm for the observed reactivity is shown in Scheme 2.4. The autocatalytic conversion reaction begins with an intermolecular nucleophilic attack of two molecules **16**, which leads to a series of consecutive equilibrium reactions, which end with the formation of one molecule of **15** and the reformation of one molecule of **16.** Note that only the constructive reaction steps are shown in Scheme 2.4.

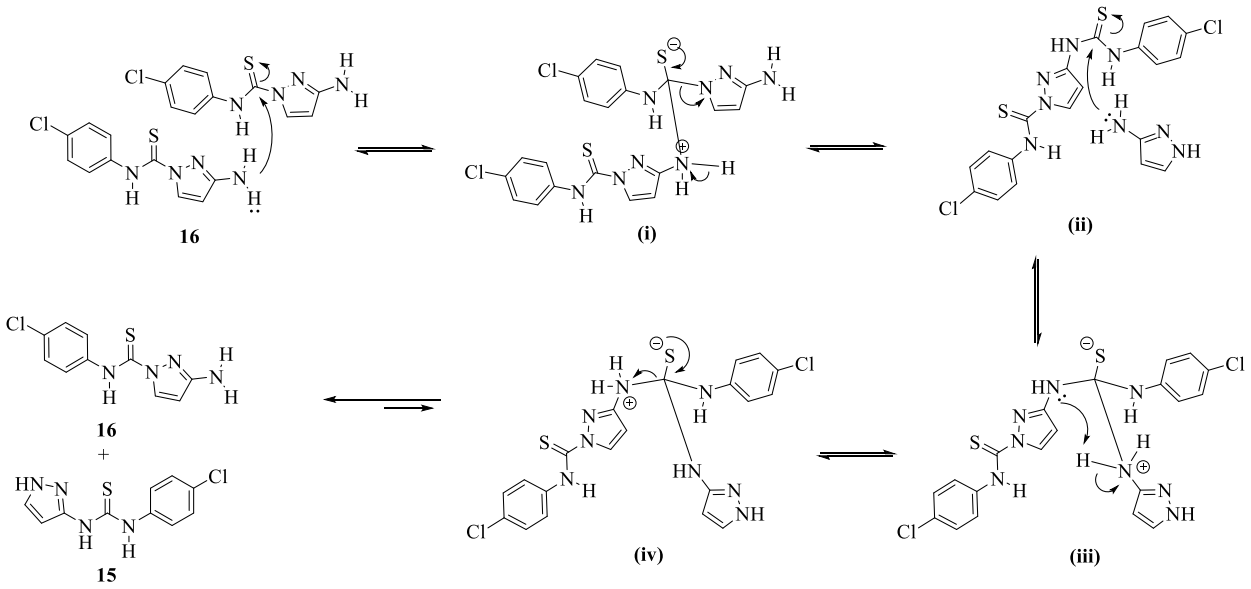

Scheme 2.4 Proposed reaction mechanism for the isomerization of 15 to 16. Only the necessary electron pair and vital deprotonation/protonation steps are shown: The reaction starts with two compounds 16 reacting with each other via nucleophilic attack of the primary heterocyclic amine group. This leads to the tetrahedral carbon addition intermediate (TCAI) (I). This intermediate reacts rapidly under elimination of 3-amino pyrazole to the metastable compound (II). Then, the former leaving group of 3-amino pyrazole undergoes a nucleophilic attack via its more nucleophilic primary amine group. This process leads to the second TCAI

(III). The reprotonation step from TCAIs (III) and (IV) is vital for the observed product formation. IV then reacts under elimination to a molecule 15 and a molecule 16.

After their synthesis was completed, compounds **13**,**14**,**15** and **16** were tested against methicillin susceptible *S. aureus* (MSSA) and MRSA. This biological data (Table 2.2) suggested that displacement of the adamantyl group did not affect the antibacterial properties against MSSA significantly. However, the antibacterial activity of **13** and **14** against MRSA was 8-fold decreased compared to MSSA values. Most interestingly, compound **16** exhibited the most antibacterial activity among the four compounds which indicated the importance of an EDG at the pyrazole's 3C.

Table 2.2 Minimum inhibitory concentration values of thiourea derivatives 13, 14, 15 and thiosemicarbazone 16.

Compound	MSSA MIC (µM)	MRSA MIC (µM)
13	0.6	5
14	1.25	5
15	1.25	2.5
16	0.07	1.25

Based on all the results, thiosemicarbazone **16** was selected for further analysis because it still possessed the NNSN motif in the molecule as we highlighted early. However, compound **16**'s antibacterial activity decreased over time, requiring an investigation into this sudden decline. Hence, a time dependent NMR screen was performed on compound **16** for ten days (Figure 2.2). In the ^{1}HNMR spectrum of compound **16**, there was a peak at 5.71 ppm (integrated intensity represents 2H) which diminished significantly after three days. Similarly, two new peaks appeared at 12.7 and 11.8 ppm. Between the 5th and 10th day (Figure 2.2), there were no significant changes and peak intensities were stable. This NMR evidence suggested that compound **16** changed into

its structural isomer compound **15** when it was dissolved in a polar solvent. This result indicated that the presence of free amine in the pyrazole ring can trigger structural isomerization into its thermodynamically more favorable form. This NMR analysis suggested that presence of free amine at 3C of thiosemicarbazone's pyrazole (compound **16**) can drive to the structural isomer (compound **15**) in polar solvent media as the charges on S and N atoms (as shown in Scheme 2.4) can be solvent stabilized. This further highlights the importance of substitution of different functional group to 3C instead of amine groups.

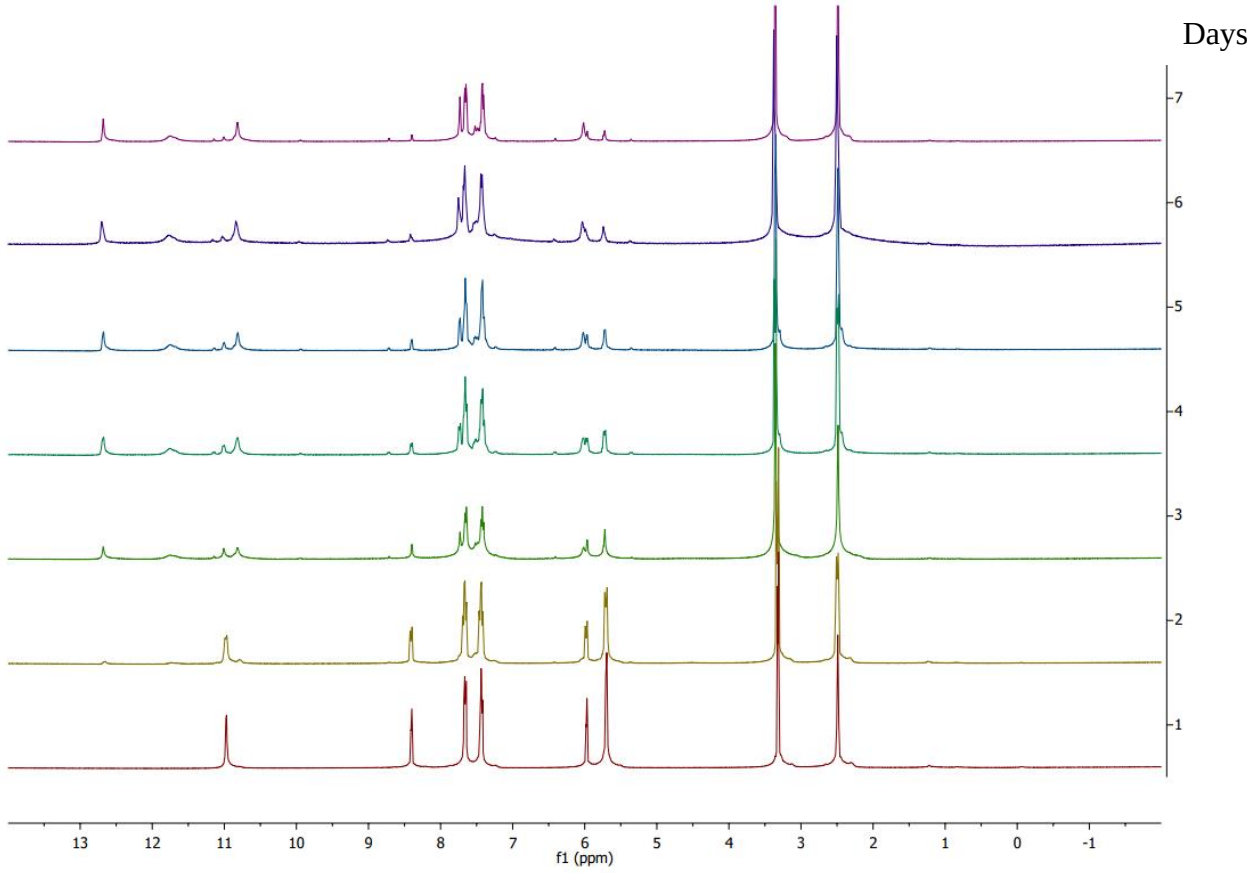

Figure 2.2 Time dependent NMR profile of compound 16 to determine any possible isomerization.

After utilizing the thionyl functionality, it was worth determining the importance of this thionyl moiety by displacing it with a carbonyl functionality. Hence, two pyrazole derivatives with 1N

substituted were reacted with 4-chlorophenyl isocyanate and 4-chlorobenzylisocyanate to obtain compounds **17**-**20**. They were biologically tested for their copper dependent antibacterial activity against MSSA and all of them were biologically inactive and did not show any bactericidal effect. Except for compound **19**, the rest of them in fact showed an inverse effect with copper. It was hypothesized that the antibacterial activity can be attributed to the complexation of Cu(I) by the NNSN motif. However, Cu(I) is a soft acid which prefers to complex with soft ligands.[189] Therefore, the inverse antibacterial effect can be attributed to the poor complexation of Cu(I) with urea derivatives. This suggested that the thionyl motif was important for the copper dependent bactericidal effect.

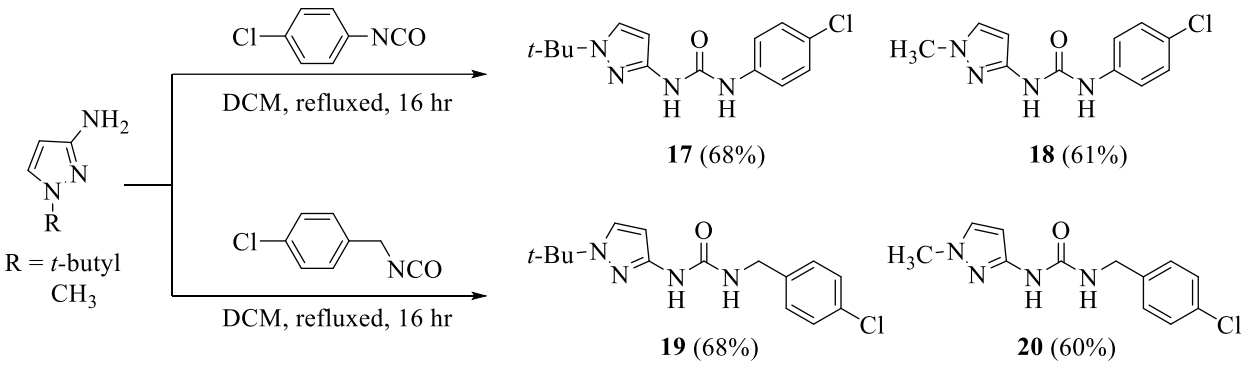

Scheme 2.5 Syntheses of urea derivatives 17-20. 1 eq. of 3-aminopyrazole derivative was dissolved in DCM and introduced to the 1 eq. of phenyl isocyanate or benzyl isothiocyanate dissolved in DCM and refluxed for 16 hr.

Then SAR was performed for the para position of the phenyl ring. So, the para position was substituted with EWGs such as -NO_2, -F, -Cl, -Br and EDGs including -CH_3, and -OCH_3. Phenyl isothiocyanates were reacted with pyrazole to generate compounds **21**-**26** as shown in Scheme 2.6. Compound **21** was synthesized without any additional base in DCM at room temperature. The presence of the EWG NO_2 in the para position may have enhanced the electrophilicity of the isothiocyanate "C" as electron density was pulled the NO_2 group. Therefore, the nucleophilic pyrazole N could attack the isothiocyanate center easily using mild conditions.

However, syntheses of compounds **22-26** required additional base, K_2CO_3, as they decreased the overall electrophilicity of the isothiocyanate "C" by delocalizing more electron density toward to isothiocyanate moiety. Additionally, compound **22** was synthesized in THF because 4-fluorophenyl isothiocyanate showed higher solubility in THF than DMF.

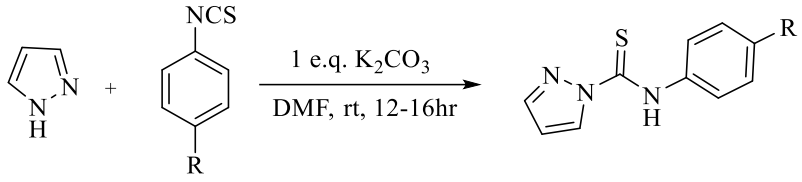

R = NO_2,	**21**	(65%)[a]
F,	**22**	(55%)
Cl,	**23**	(62%)
Br,	**24**	(60%)
-OCH_3,	**25**	(65%)
-CH_3	**26**	(68%)

Scheme 2.6 Reaction of pyrazole with different para substituted isothiocyanates. [a]1 eq. of pyrazole and 1 eq. of 4-nitrophenyl isothiocyanate in DCM were stirred at room temperature for 20 hr. Compounds 22-26 were synthesized using 1 eq. of K_2CO_3 in DMF at room temperature overnight.

Among these six derivatives (Table 2.3), compound **23** with the Cl substitution showed the best copper dependent antibacterial activity against a pathogenic MRSA strain. In contrast to chlorine, other two halogen substitutions did not show similar activity with copper. Natalia Molchanova *et* al and Gentry *et al.* have described in their studies that chlorination of certain molecules (including bromination) can enhance their therapeutic effect due to the higher cell permeability through elevated lipophilicity and self-assembling character.[190,191] Therefore, compound **23**'s increased activity can be likely attributed to the enhanced lipophilicity and self-assembling properties.

Table 2.3 Minimum inhibitory concentrations values of thiosemicarbazones 21-26 after changing the para substitution on the phenyl ring.

Compound	MIC (μM)	Compound	MIC (μM)
21	10	24	10
22	>10	25	10
23	1.25	26	5

It is worth investigating the antibacterial properties of 3-aminopyrazole with different para substituted isothiocyanates. Therefore, the aforementioned isothiocyanate derivatives were reacted with 3-aminopyrazole. As shown in Scheme 2.7, 3-aminopyrazole dissolved in DCM was added to the para substituted isothiocyanate dissolved in DCM and refluxed overnight to obtain compounds **27-31**. No additional base was required to deprotonate the N-H of the pyrazole as the primary amine was basic enough to carry out the desired reaction. It was interesting to observe that no additional base was required even with EDGs. Then compounds **27-31** were tested against a MSSA strain and results are further discussed below.

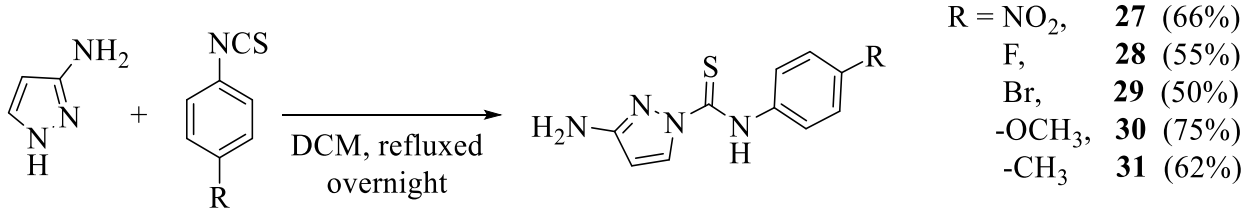

Scheme 2.7 Reaction of 3-aminopyrazole with different para substituted isothiocyanates. 1 eq. of 3-aminopyrazole was mixed with 1eq. of isothiocyanate in DCM and refluxed for overnight without any bases.

As mentioned in Table 2.4, a bacterial study revealed that almost all the tested compounds with a primary amine showed elevated copper dependent antibacterial activity against GP MSSA.

In contrast to the results in Table 2.3, compound **27** showed a 33-fold, compound **16** demonstrated an 18 fold, and the bromine substitution of compound (**29**) showed an 8-fold increase in activity as compared to **21**, **23** and **24**. Thus these synthesized compounds have shown that substitution of pyrazole's 3C position with electron donating substituents is important to increase the antibacterial properties of thiosemicarbazone derivatives.

Table 2.4 Minimum inhibitory concentrations values of thiosemicarbazones 16, 27-31 after changing the para substitution in the phenyl ring and positioning a primary amine at the 3C of the pyrazole.

Compound	MIC (μM)	Compound	MIC (μM)
16	0.07	29	1.25
27	0.3	30	10
28	10	31	2.5

My research efforts were then directed toward checking the antibacterial activity of the pyrazole which was substituted with EWG and EDG at the 4C. The 4C position can be easily functionalized via electrophilic aromatic substitution as pyrazole's 4C possesses higher nucleophilic character as compared to the 3C and 5C.[192] Pyrazole was nitrated with concentrated H_2SO_4 and HNO_3 to obtain a white colored solid compound **32** (Scheme 2.8). Unlike the usual nitration, instead of forming a nitronium ion by mixing H_2SO_4 and HNO_3 mineral acids, pyrazole can be initially dissolved in excess concentrated H_2SO_4 acid and then HNO_3 can be added separately dropwise. Afterward, the reaction was heated to 60 $^{\circ}$C for 90 minutes. Compound **32** was reacted with 4-chlorophenyl isothiocyanate in the presence of NaH and dry THF to obtain yellow colored product, **33**.

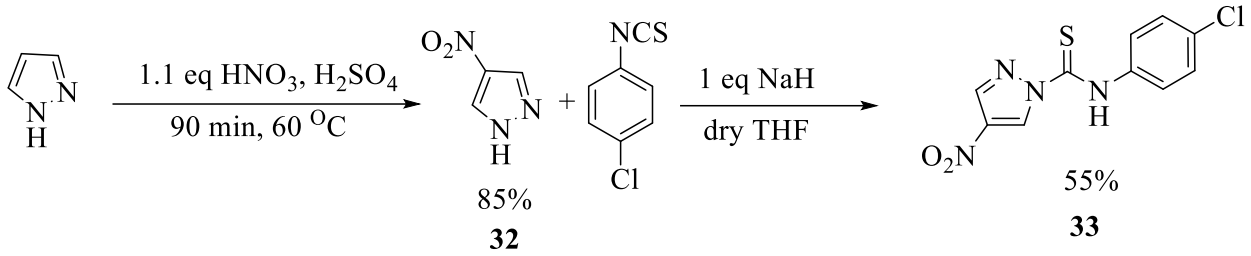

Scheme 2.8 Synthesis of compound 32 by nitrating the pyrazole under acid conditions. Then 32 was introduced to 4-chlorophenyl isothiocyanate to obtain compound 33.

In order to introduce an EDG to pyrazole's 4C, 4-nitropyrazole, **32** was reduced to 4-aminopyrazole **34** using iron powder under acidic condition as shown in Scheme 2.9 with ethanol as the solvent.[193] Although compound **34** was isolated in 86% yield, scaling up the reduction was difficult because the iron powder was attracted to the stirring bar and this prevented it from stirring effectively. Therefore, the reduction step was performed with Pd/C catalyst more efficiently. As mentioned in Scheme 2.9, the reduced compound **34** was introduced to 4-chlorophenylisothiocyanate to obtain compound **35** with an amine substitution at 4C of the pyrazole ring. This reaction was first set up in DCM but the reaction did not proceed to completion as **34** showed partial solubility in DCM. Therefore, DMF was utilized in which most of the pyrazole substrates showed elevated solubility.

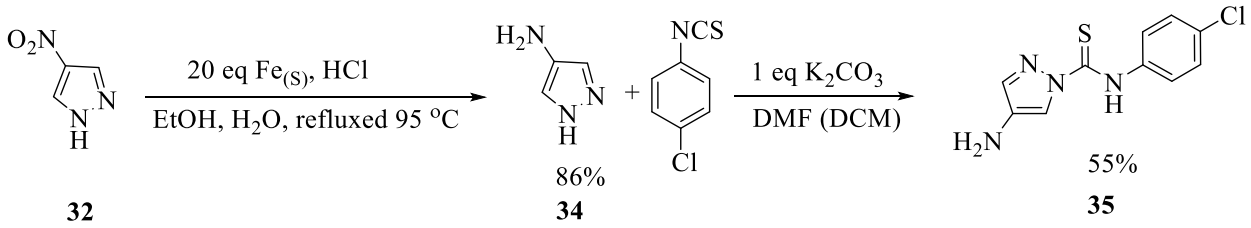

Scheme 2.9 Reduction of 4-nitropyrazole into 4-aminopyrazole and subsequent reaction with 4-chlorophenylisothiocyanate to synthesize compound 35.

The results summarized in Table 2.5 indicate that compounds **33** and **35** did not show antibacterial activity with Cu(I) against MSSA. In addition, compound **16** and **35**, both donate electron density toward pyrazole ring inductively but compound **35** was not active when compared to **16**.

Table 2.5 Minimum inhibitory concentrations values of thiosemicarbazones 33 and 35 after substituting -NO_2 and -NH_2 at the 4th carbon of the pyrazole ring.

Compound	MIC (μM)
33	Not active
35	Not active

As shown in the Scheme 2.10a resonance structures, pyrazole's 5C has a higher electron density via delocalization of the amine's free lone pair which leaves the pyridine like N untouched with respect electron delocalization. In a similar manner, as shown in Scheme 2.10b, pyrazole's pyridine-like N gets more electron density compared to other positions via delocalization of the amine's free lone pair. Therefore, this suggests that pyrazole's 2N and 3C positions play significant roles in the NNSN's antibacterial properties, which can be further enhanced by enriching the electron density by putting EDG at the 3C of the pyrazole.

Scheme 2.10 The Lewis resonance structures of 4-aminopyrazole and 3-aminopyrazole to show the delocalization of the nitrogen's lone pair to the pyrazole ring.

A methyl ester was installed at pyrazole's 3C in the next investigation in order to probe the effect of an EWG on pyrazole's 3C. In Scheme 2.11, 3-methylpyrazole was oxidized with potassium permanganate to generate pyrazole-3-carboxylic acid, **36**.[194] As esterification required the activation of the acid's hydroxyl group, thionyl chloride was used to convert the carboxylic acid into its corresponding acid chloride.[195] Methanol was used as the solvent for the esterification to acquire methyl 1H-pyrazole-3-carboxylate, **37**. The ester derivative was refluxed with 4-chlorophenyl isothiocyanate overnight to obtain compound **38**.

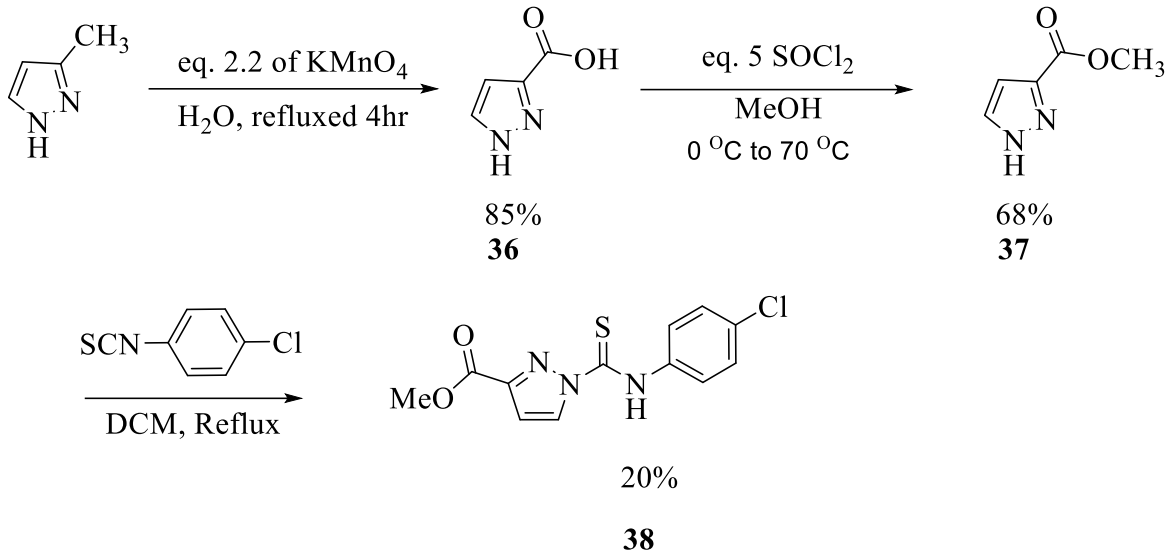

Scheme 2.11 Synthesis of compound 38. 3-methyl pyrazole was oxidized with potassium permanganate to obtain methyl 1H-pyrazole-3-carboxylate. Esterification was performed via the acid chloride.

No additional bases were employed for this nucleophilic attack as the EWG ester increased the acidity of the pyrazole's 1N-H. However, the overall yield percentage was 20% which could be further increased if an additional base was employed for this nucleophilic attack. According to the biological data, compound **38** showed a MIC of 5 µM against MSSA which was not significantly active compared to the compound with a EDG at the 3C. Up to this point, 3-amino pyrazole containing derivatives showed very promising antibacterial properties, but they tended to undergo structural isomerization. Thus, substitution of different EDGs at the 3C position is critical

to get further insight into the significance of EDGs towards the overall antibacterial properties of the NNSN compounds. Thus, I thought to substitute a benzyl ether functionality on the 3C position of the pyrazole as shown in Scheme 2.12.[196]

Methyl 3-methoxyacrylate and hydrazine hydrate were refluxed in MeOH for 2 hours to obtain compound **39**, 1H-pyrazole-3-ol. This reaction did not require any further work-up as **39** was present in 99% yield. Pyrazole's 1N was protected by acetylation with acetic anhydride in pyridine. The desired N-acetylated product **40** was obtained without further work-up. Benzyl bromide and compound **40** were reacted with anhydrous potassium carbonate to deliver the stable benzyl ether derivative, compound **41**. The acyl protecting group on 1N was removed with 10% NaOH to afford compound **42** which was then further reacted with 4-chlorophenyl isothiocyanate with potassium carbonate in DMF to form the desired compound **43**. ·

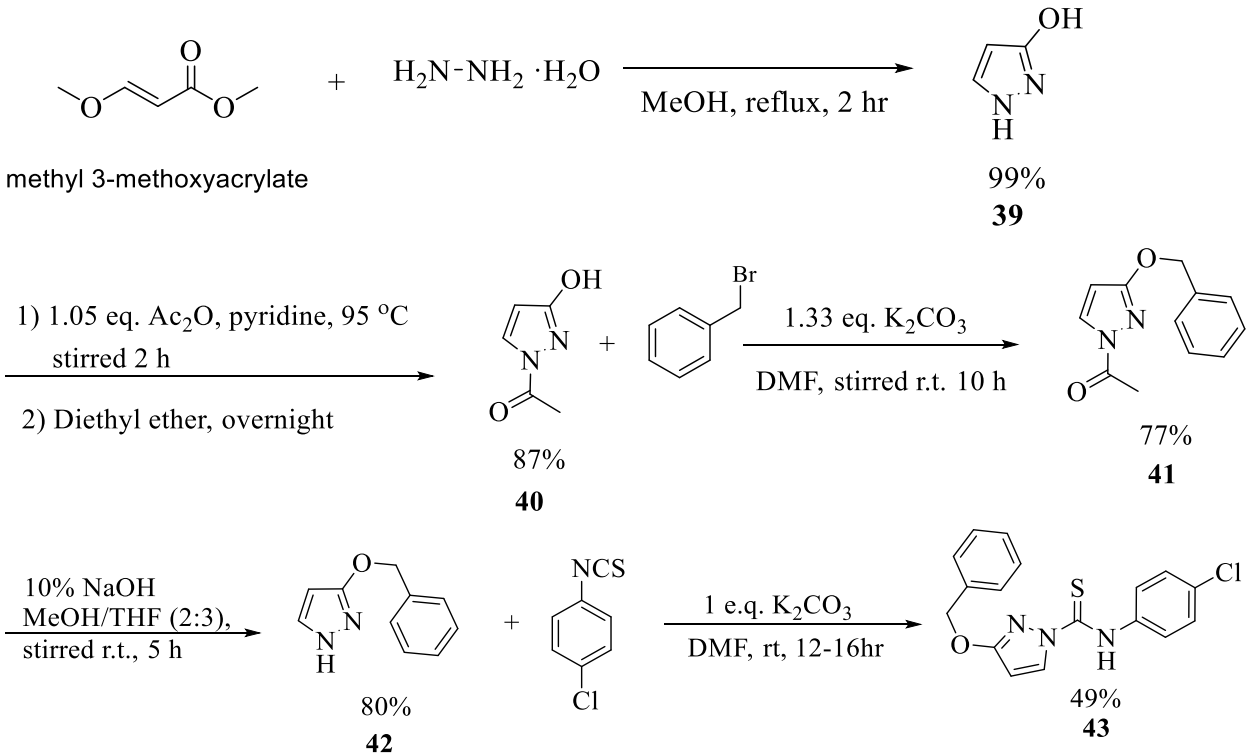

Scheme 2.12 Synthesis of compound 43.

Compound **43** showed significant antibacterial activity against MSSA as the MIC of 0.15 µM indicates. We will discuss the potential structure of Cu(I)-NNSN complex below. Unlike compound **16**, there was no isomerization noticed with compound **43,** and its antibacterial activity was maintained for a considerably longer period.

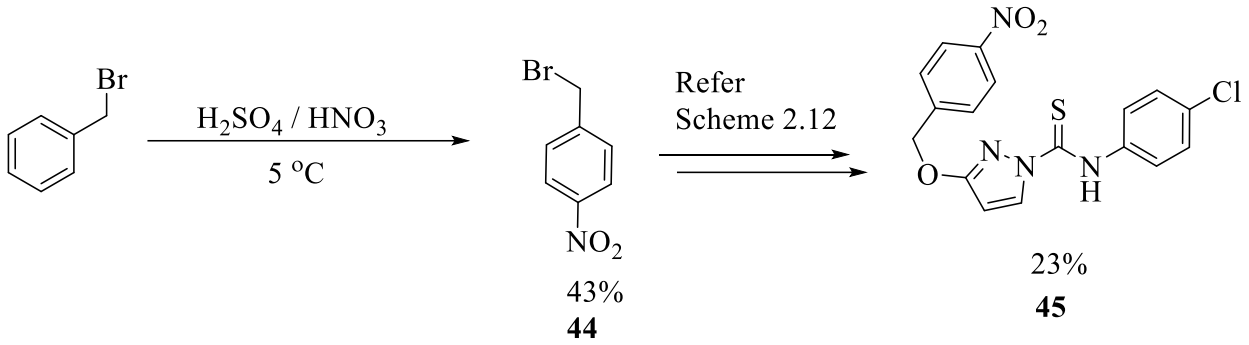

Scheme 2.13 Nitration of benzyl bromide to synthesize a nitrated benzyl ether derivative 45

Increased antibacterial activity of EDG substituents was further supported by adding a methyl group to the 3C of the pyrazole. The 3-methyl pyrazole substrate was inexpensive and readily available for purchasing. It was reacted with 4-chlorophenyl isothiocyanate in DCM at room temperature as shown in Scheme 2.14. The resulting solid product was tested for MSSA and it showed a MIC value of 0.625 µM. Therefore, it further provided evidence that EDGs at the 3C of the pyrazole are important.

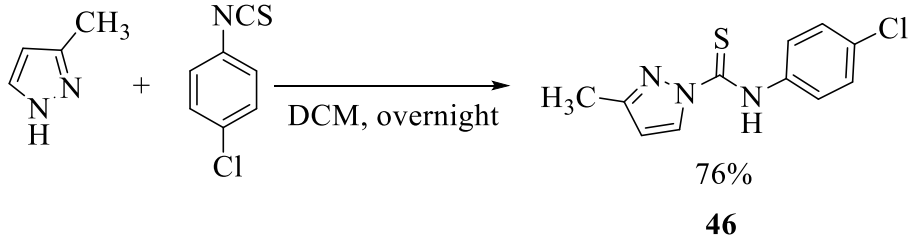

Scheme 2.14 Reaction of 3-methyl pyrazole and 4-chlorophenyl isothiocyanate.

2.3 Binding Constants and Hypothetical Binding Geometry of Cu(I)NNSN Compounds

2.3.1. Job Plots

Taking into account that the comparison with type-1 active centers of copper-containing enzymes suggests a distorted tetrahedral geometry (Figure 2.5) and starting from the mechanistic paradigm that only Cu(I) is available in activated phagosomes, 1:1, 1:2, and even 1:3 stoichiometries between a central Cu(I) cation and NNSN ligands could be possible. Therefore, Dr. Madumali Kalubowilage performed job plots (Figure 2.4) with Cu(I) and signature NNSN compounds in 2020 to elucidate the principal stoichiometry. Although this method can be challenging for complicated supramolecular assemblies, it is straightforward for simple 1:1, 1:2, and 1:3 complexes.[197]

Job plots are based on the observation that there is one optimal ratio between central metal cation and ligand at which a physical property P is maximal. For an example of a series of UV/VIS spectra obtained for compounds 15, 16, 20, 21, and 45, and CuBr see Figure 2.4 below. The units of the x-axis are expressed as mole fraction X of NNSN compound (A) and Cu(I) (B):

$$X_{NNSN} = \frac{[NNSN]}{[NNSN] + [Cu(I)]} = 1 - X_{Cu(I)}$$

The position of the (normalized) maximum of the UV/Vis absorption at a peak that occurs during NNSN/Cu(I) complexation is indicative of the stoichiometry of interaction. X_{NNSN} = 0.5 for 1:1 complexes, X_{NNSN} = 0.667 for 2:1 complexes (two NNSN compounds per one Cu(I) cation), X_{NNSN} = 0.75 for 3:1 complexes. Note that the position of the maximum at X_{NNSN} = 0.5 does not

distinguish between 1:1, 2:2, n:n complexes. However, 1:1 complexes show a linear increase/decrease, whereas higher order complexes display sloped curvatures.[197]

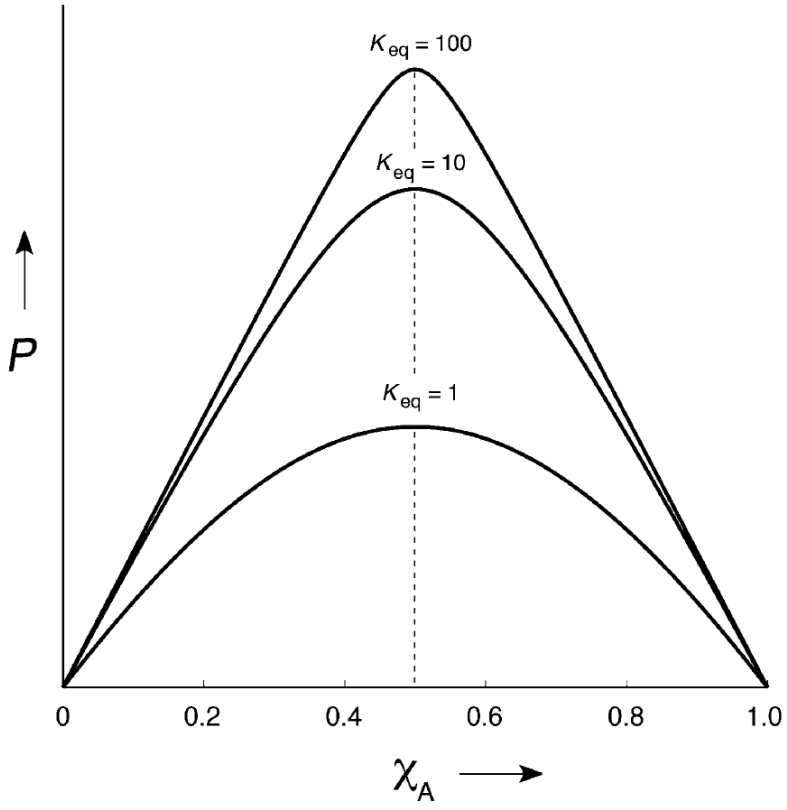

Figure 2.3 Job plots obtained for binary 1:1 combination. P: physical property of the formed binary complex. The units of the x-axis are expressed as mole fraction X of compound A (X_A). K_{eq}=1, K_{eq}=10, and K_{eq}=100: binding constants.

In Figure 2.4, a combined job plot for the complexation of CuBr with 5 NNSN compounds is shown. These results were obtained by Dr. Kalubowilage and indicated the principal binding stoichiometry of Cu(I)NNSN complexes. These results are unpublished to date. The normalized UV/Vis absorption at λ=280 nm of the complexes of Cu(I) and 10 NNSN are shown. All these compounds were synthesized in this thesis.

2.3.2. UV/Vis Measurements

All UV/Vis measurements were performed in HEPES buffer (5.5957 mL of HEPES in 1.0 L bidest. H_2O, pH = 7.2 adjusted with HCl). A stock solution of 0.00011 M Cuprous Bromide CuBr in methanol (1.578 mg in 100 mL MeOH) was prepared via sonication under argon. 0.00011M of the corresponding NNSN compound were dissolved in MeOH via sonication under argon as well. UV/Vis experiments were performed using a Varian Cary 100 UV/Vis spectrophotometer. All solutions consisted of 1800 μL HEPES buffer plus aliquots of Cu(I) and respective NNSN-compound (0.00011M each) in methanol to obtain X_{NNSN} = 0.1, 0.2, 0.4, 0.5, 0.6, 0.8, 0.9. The observed absorption increases at λ=280 nm were normalized to maximal increase = 1 to allow direct comparisons. Note that binding constants can be determined from Job Plots as well, but they are not regarded trustworthy in the literature.[197] Therefore, the Bossmann group has developed an independent procedure for measuring binding constants (see below).

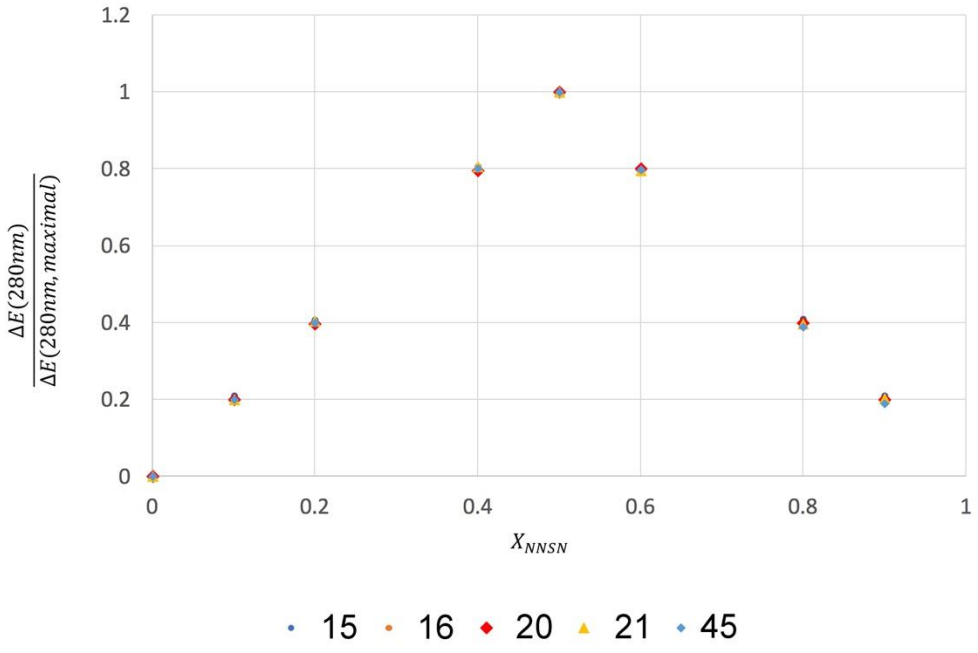

Figure 2.4 Normalized Job Plots of 1-(4-chlorophenyl)-3-(1H-pyrazol-3-yl)thiourea (15), 3-amino-N-(4-chlorophenyl)-1H-pyrazole-1-carbothioamide (16), 1-(4-chlorobenzyl)-3-(1-methyl-1H-pyrazol-3-yl)urea (20), N-(4-nitrophenyl)-1H-pyrazole-1-carbothioamide (21), and N-(4-chlorophenyl)-3-((4-nitrobenzyl)oxy)-1H-pyrazole-1-carbothioamide (45). Original data and data interpretation by Dr. Madumali Kalubowilage (2020). Experimental details are described above.

The data summarized in Figure 2.4 clearly indicates that 1:1 stoichiometry is preferred for a wide variety of Cu(I)-NNSN complexes. Note that this data contains structurally very different NNSN compounds. Based on this work, which also included numerous compounds that are not described here), the Bossmann group has assumed 1:1 stoichiometry for the determination of the binding constants of all Cu(I)-NNSN complexes. In chapter 1.10, I have identified the type 1 binding site of Cu(I/II) in copper-containing enzymes[107] as the most likely natural model environment for NNSN compounds. Type 1 binding sites are characterized by two histidine and a cysteine site that form a distorted tetrahedron around the central copper cation. In analogy to this model, I propose the following binding geometry (distorted tetrahedron) for Cu(I) by NNSN.

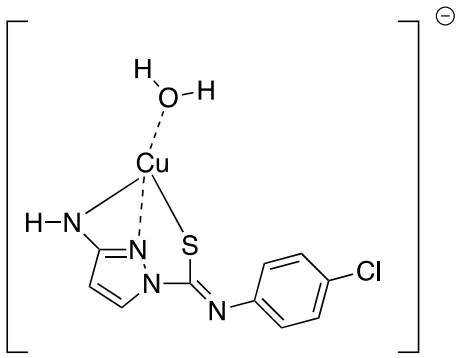

Figure 2.5 Proposed binding geometry (distorted tetrahedron) for Cu(I) at NNSN. The fourth coordination site is occupied either by water (shown) or by an anion in the HEPES buffer (chloride or bromide), which is less likely.

2.3.3 Binding Constants

The binding constants of the entire library of NNSN compounds that exists in the Bossmann group to date have been determined by Kayla Eschliman and Dr. Madumali Kalubowilage. In short, a HEPES buffer and a 0.00011 M CuBr solution in methanol were prepared (identical to the solutions discussed above)

The amount of NNSN must then be calculated according to the equation: $\frac{1\ x\ 10^{-3}\ moles}{1000\ mL}\ x\ 2\ mL\ x\ MW\left(\frac{g}{mole}\right) = Theoretical\ Mass\ Needed$. Once this amount has been weighed, it should be dissolved in 200 microliters of methanol and sonicated until fully dissolved. Add 1800 microliters of HEPES buffer. Once these solutions have been prepared, then a concentration gradient was performed, and UV/Vis absorption spectra were recorded. The following solutions were analyzed:

1: 2.4 mL CuBr stock solution + 0.6 mL of HEPES buffer
2: 2.4 mL CuBr stock solution + 525 µl of HEPES buffer + 75 µL NNSN stock solution
3: 2.4 mL CuBr stock solution + 450 µl of HEPES buffer + 150 µL NNSN stock solution
4: 2.4 mL CuBr stock solution + 375 µl of HEPES buffer + 225 µL NNSN stock solution
5: 2.4 mL CuBr stock solution + 300 µl of HEPES buffer + 300 µL NNSN stock solution
6: 2.4 mL CuBr stock solution + 150 µl of HEPES buffer + 450µL NNSN stock solution

The resulting UV/Vis spectra are summarized in Figure 2.6.

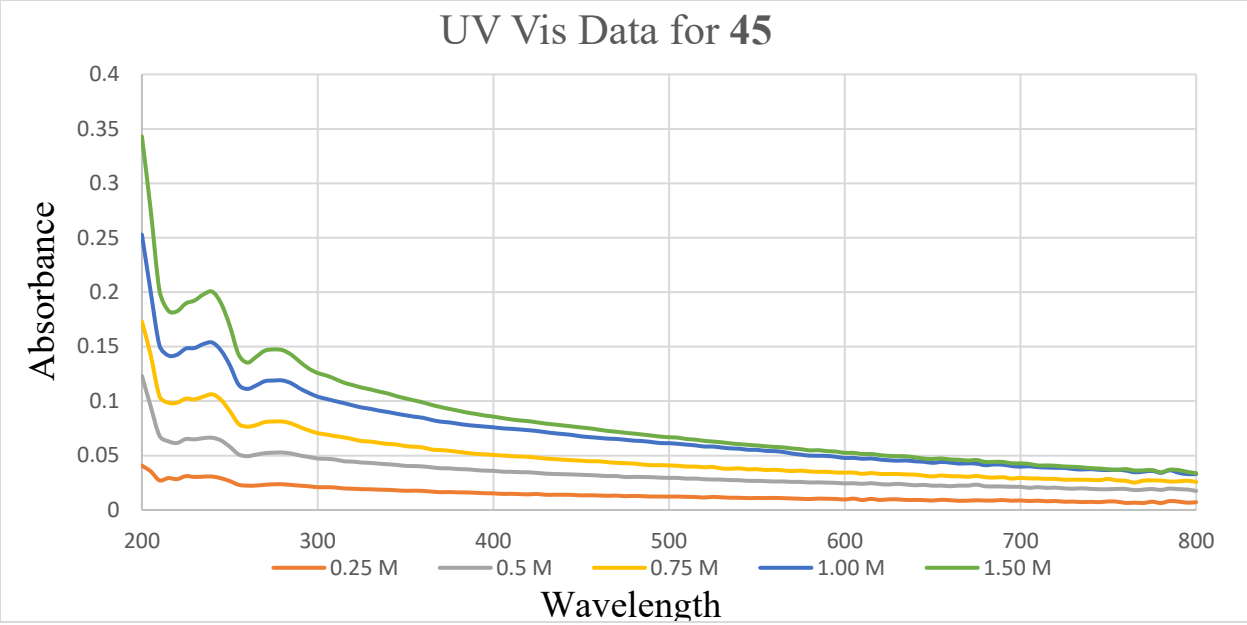

Figure 2.6 UV/Vis titration experiments of N-(4-chlorophenyl)-3-((4-nitrobenzyl)oxy)-1H-pyrazole-1-carbothioamide (45) with CuBr. Experimental details are described above. A solution of CuBr in the absence of NNSN compound was used as blank.

The observed differences in UV/Vis absorptions in the peak regions (224nm, 240nm, 280 nm) and at 400nm vs. NNSN compound concentration were written into an Excel sheet and then run on the UV 1:1 Bindfit program from Supramolecular.com. If the run is successful, then an optimized value is generated that is considered the Copper Binding Constant for that NNSN compound.

Table 2.6 summarized the binding constants that were obtained for the NNSN compounds synthesized here:

Table 2.6 Copper(I)-binding Constants of Compounds with NNSN-motif According to Fits Obtained with Bindfit Assuming 1:1 Stoichiometry.

Compound	Structure	Binding Constant with CuBr K_B [M^{-1}]	Minimum Inhibitory Concentration (MIC) against S. A. Newman (μM)
15	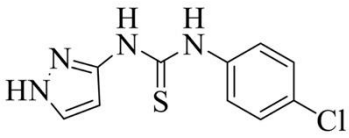	51,000	1.25
16	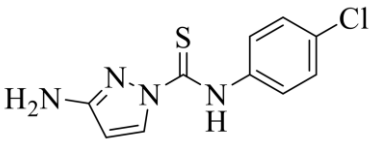	53,200	0.07
17	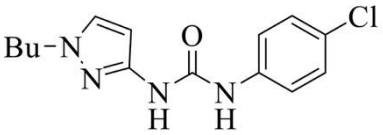	< 100	> 1,000
18	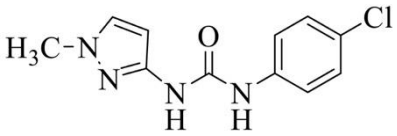	< 100	> 1,000
19	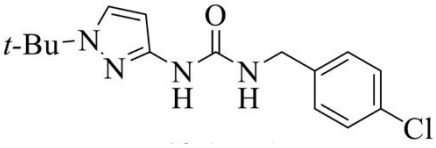	< 100	> 1,000
20	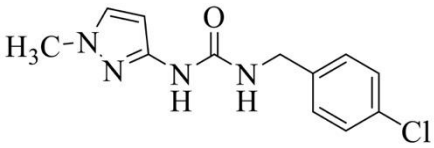	< 100	> 1,000
21	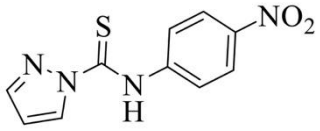	2,450	10

22	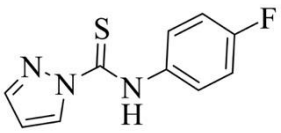	1,250	> 10
23	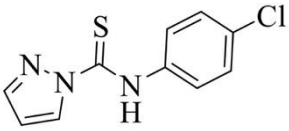	2,100	1.25
24	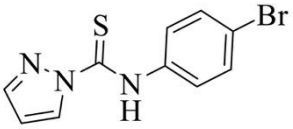	2,350	5.0
25	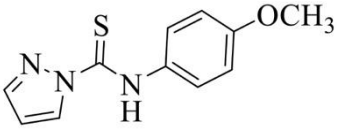	550	> 10
26	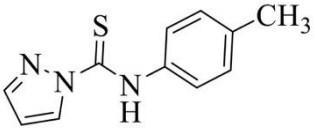	825	> 10
27	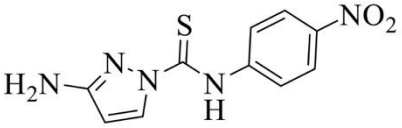	74,000	0.3
28	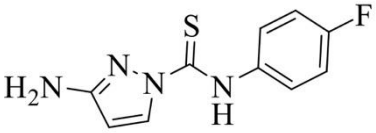	26,300	10
29	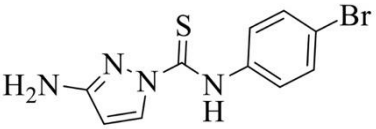	72,400	1.25
30	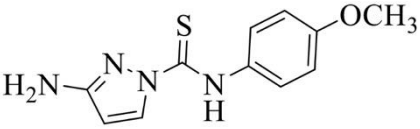	7,400	10

31	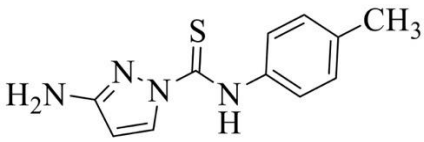	11,050	2.5
33	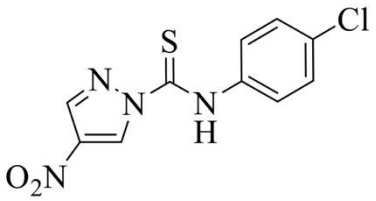	5,200	> 500
35	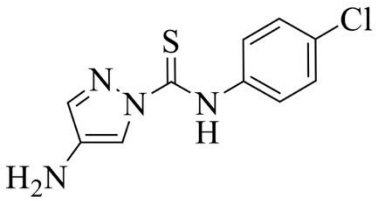	17,400	> 500
38	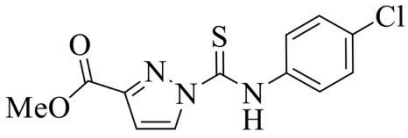	800	5
43	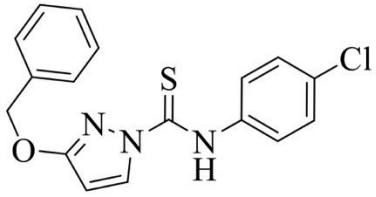	25,700	0.15
45	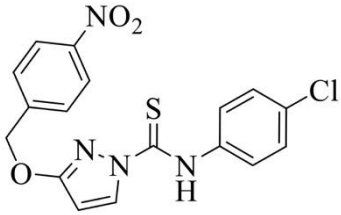	11,500	10
46	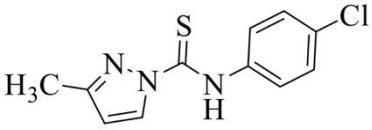	54,000	0.625

The determination of the minimum inhibitory concentrations was performed by Dr. Alex Dalecki in the groups of Prof. Dr. Wolschendorf (2014-2018) and Prof. Dr. Olaf Kutsch (2018-2021) in the Department of Medicine at the University of Alabama at Birmingham (UAB). The procedure is described in Appendix A.

2.3.4 Linear Free-Energy Relationship Analysis of the Observed Binding Constants

To understand the observed binding behavior of NNSN and Cu(I) at least semi-quantitatively, a Hammett analysis of the obtained data was performed. The Hammett equation that was published in 1937 by Louis Plack Hammett[198] is one of the most widely used quantitative structure-activity relationships (QSAR) in the literature.[199] The Hammett methodology can discern principle organic reaction mechanisms in aromatic systems.[199] It is noteworthy that a Hammett analysis does not take steric factors into account.[199] Principally, this is possible by using the Taft's equation.[199] However, for the compounds with NNSN motif investigated here, Hammett methodology does suffice, because all compounds show a high degree of structural similarity.
Although the Hammett methodology has been frequently criticized as too empirical, it permits the straightforward elucidation of electronic contributions to organic reaction mechanisms.[199] It is based on the paradigm that the "change of free energy of activation is proportional to the change in Gibbs free energy".[200] This is observed in aromatic organic compounds with differing substituents in virtually any organic reaction.[199]

The basic Hammett equation relates the equilibrium constant K for a reaction of an aromatic compound with substituent R with the reaction rates:

$$log\frac{K}{K_0} = log\frac{k}{k_0}$$

K: equilibrium constant (of the complexation of Cu(I) with an NNSN compound with substituent R in a defined position (here: para)), K_0: equilibrium constant for the reference compound (R = H); k: reaction rate of the aromatic compound (NNSN compound) featuring the substituent R with

Cu(I), k_0: reaction rate of the aromatic compound (NNSN compound) featuring the substituent R = H with Cu(I).[198,199,201]

The **substituent constant** σ (Greek: sigma) (Greek: rho) If ρ is positive, a negative charge is formed during the rate-determining step of the reaction, and vice versa. Electron withdrawing substituents can decrease a negative charge built-up, thus accelerating the reaction. Electron donating substituents can decrease a positive charge built-up, which again accelerates the reaction. However, electron withdrawing substituents increase the positive charge build-up, thus decelerating this type of reaction, as do electron donating substituents with a reaction of negative charge build-up.

There are examples of Hammett plots, which do not follow a straight line for all substituents but exhibit an **inflection point**.[199,202] Any deviation from a straight line is interpreted as a change of reaction mechanism. For instance, an increased charge-build up in a transition state can open a bifurcated reaction pathway, depending on the substituents.[202] Here, a second reaction mechanism becomes increasingly competitive, until it finally takes over. It should be noted that the deviations from straight Hammett plots observed in this thesis occur most likely from the chemical instability of NNSN compounds with nitro groups in the presence of Cu(I), or the occurrence of a second binding site due to the presence of a nitro group.

Table 2.7 Selected Hammett substituent constants for para and meta substitutes benzene rings[198,199,201]

Substituent		
Dimethylamino	-0.83	-0.221
Amino	-0.66	-0.161
Butylamino	-0.51	-0.34
Hydroxy	-0.37	+0.12
Methoxy	-0.268	+0.115
Ethoxy	-0.25	+0.015

Methyl	-0.17	-0.069
Trimethylsilyl	-0.07	-0.04
None (Hydrogen)	0.00	0.00
Fluoro	+0.062	+0.337
Chloro	+0.227	+0.373
Bromo	+0.232	+0.393
Iodo	+0.276	+0.353
Ethoxycarbonyl	+0.45	+0.37
Trifluoromethyl	+0.54	+0.43
Cyano	+0.66	+0.56
Nitro	+0.778	+0.710

In order to understand the observed binding behavior of NNSN and Cu(I) at least semi-quantitatively, I performed a Hammett analysis of the obtained complexation constants of Cu(I) with a series of NNSN complexes. By applying the Hammett formalism described above, I have attempted to discover the mechanism of Cu(I) binding to compounds with NNSN motif by plotting the decadic logarithm of their binding constants versus the Hammett substituent constants for para-substituted phenyl derivatives.[201]

The following text passage is from the third revision of my thesis. It utilizes the concepts discussed above.

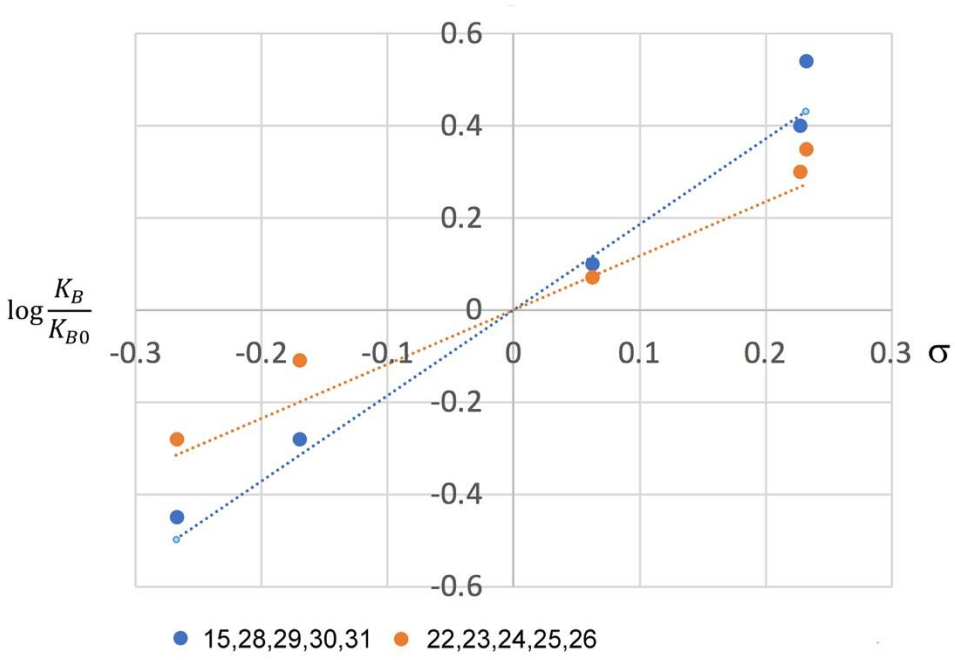

Figure 2.7 Hammett plots for NNSN compounds 15, 28, 29, 30, 31, and 22, 23, 24, 25, and 26. Both plots have are sufficiently linear r > 0.97.

The Hammett plot for the NNSN-compounds without substitution at the heterocyclic ring yields $\log K_B/K_{B0} = 1.1784\ \sigma$. Therefore, $\rho \approx +1.18$, which is indicative that a negative charge is formed during the reaction. Therefore, electron withdrawing substituents are able to accelerate the reaction and, at the same time, shift the equilibrium to Cu(I)-NNSN complex formation.

For the group of NNSN-compounds with an amine-group in 3-position of the pyrazole ring, the Hammett plot $\log K_B/K_{B0} = 1.8477\sigma$ proves that the negative charge-build-up is significantly stronger than in the group of unsubstituted NNSN compounds ($\rho \approx +1.8$). It should be noted that the complex formation equilibrium constants are significantly bigger when the pyrazole ring is substituted with an electron donating substituent.

Since both groups of NNSN compounds show a positive ρ, the negative charge is formed in a part of the molecule that both groups share. Based on this assumption, I have identified the thioketone

function in NNSN compounds. As already indicated in Figure 2.5, thioenolization is likely to occur before Cu(I) binding can take place, which will generate a mildly acidic -SH group. Most thiols have a pKa's around 5 to beyond 11.[203] Therefore, electron withdrawing effects will enhance -SH acidity under the pH conditions in activated phagosomes of M1-polarized macrophages (pH = 7 to 9).[203]

2.3.5 Is the Activity of NNSN Compounds Dependent on Their Activity to Form Copper(I)-Complexes?

The next step towards elucidating the mechanistic reasons behind the bacterial toxicity of NNSN compounds in the presence of copper(I) was to plot the MIC values against the well-defined strain *Staphylococcus aureus Newman*. The result is shown in Figure 2.8. Since the plot of K_B vs. MIC was clouded, I have plotted log K_B vs. MIC. From this data it can be deduced that a general trend can be observed. All compounds with low MICs have high copper(I)-binding constants. However, this data does not permit a meaningful Hammett correlation. The outliers are compounds **21**, **28**, and **30**. Nevertheless, since no compounds showed activity against the staphylococcus aureus strain S. A. Newman in the absence of copper, it can be concluded that copper(I) is required for activity and that a relatively high copper(I)-binding constant is generally favoring activity. Other conclusions could not be drawn because of the structural diversity of the NNSN compounds that were synthesized in this thesis.

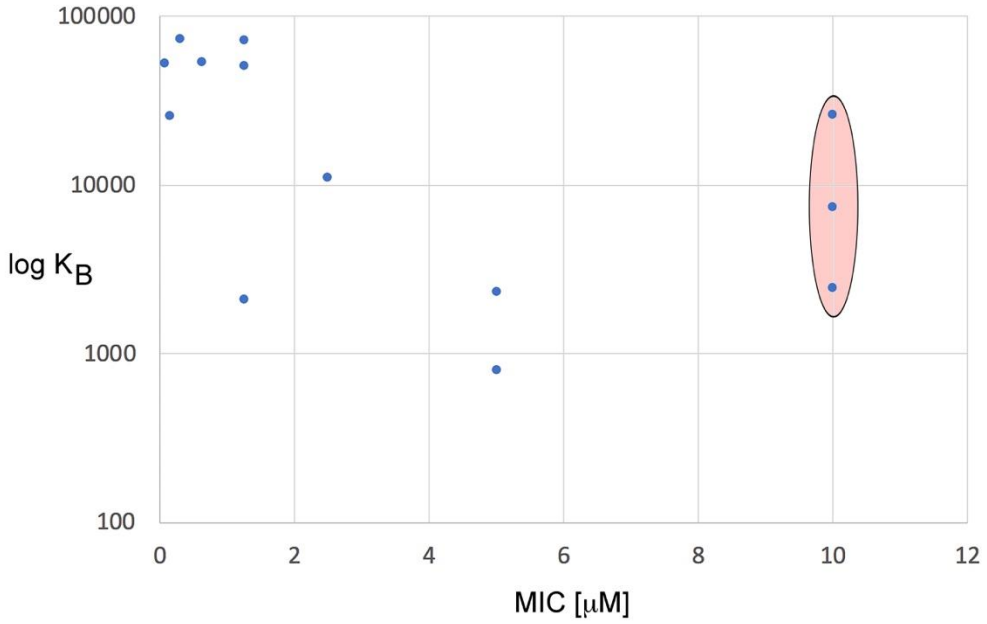

Figure 2.8 Plot of decadic logarithm of the binding constant K_B of Cu(I)NNSN complexes vs. Minimum Inhibitory Concentration (MIC) obtained for *S. aureus Newman*.

In chapter 1.6, I have established that the binding constants of Cu(I) by CTR1 and other Cu(I)-binding proteins, such as Atox1 (Antioxidant Protein 1) and ATP7B (ATPase Copper Transporting Beta) range from K_B's = 10^{14} to 10^{16} M^{-1}.[113] Compared to these extraordinarily high K_B's, the binding constants for Cu(I)-NNSN complexes range only from 10^2 to 10^5 M^{-1}. Therefore, it is absolutely impossible that NNSN compounds would be successful in extracting Cu(I) from mammalian copper storage proteins. Virtually the only place in a mammalian body where bio-available Cu(I) is found is in the activated phagosome where bacteria and viruses will be encapsulated. Although the reported concentrations of copper in activated phagosomes vary in the literature,[123] we can estimate 50 to 150 μmol (and beyond) in activated phagosomes.[123, 127] This means that there is sufficient Cu(I) in an activated phagosome to complex at least a fraction of NNSN compounds.

The relatively small binding constants of Cu(I)NNSN complexes make it not likely that this group of compounds can act as efficient Cu(I) shuttle through the membrane of Gram-positive bacteria.

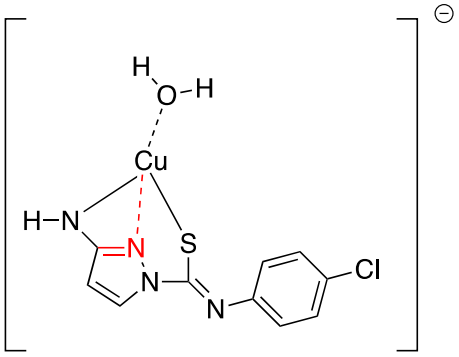

Scheme 2.15 Proposed binding geometry (distorted tetrahedron) for Cu(I) at NNSN. The Cu(+)-analog of an iminium cation is marked in red.

When analyzing the structure of the proposed Cu(I)-NNSN complex, one can discern the Cu(+)-analog of an iminium cation. Iminium cations are found in natural compounds with antibiotic properties, such as tyrosine phosphatase B inhibitors.[182] Iminium cations are also capable of acting as an ene component in Diels-Alder reactions with electron-rich aromatic amino acids (tyrosine, tryptophan, histidine, and cysteine),[183] and could undergo Michael-additions with cysteine, as well as participate in electron transfer-mediated reactions (ET). The latter reactions generate reactive oxygen species (ROS) and, consequently, oxidative stress (OS).[180, 181]

2.4 Summary

Studies exploring the use of thiosemicarbazone (NNSN) as drug candidates are currently underway with very promising results. NNSN molecules mainly consist of three structural regions. As mentioned in Figure 2.9, the NNSN core is vital to maintain the copper dependent antibacterial

properties. Moreover, pyrazole's 3C (R^1) substituents and the substituents at R^2 of the phenyl ring can adjust the antibacterial property based on their electron donating and electron withdrawing effects. Chlorine substitution at the R^2 position has so far showed the highest antibacterial activity among several other groups including NO_2, F, Br, CH_3 and -OCH_3. Likewise, antibacterial activity was considerably increased with electron donating substituents at pyrazole's 3C (R^1 position). Compounds **16**, **43** and **46** showed the highest activity in the molecular library. However, compound **16** was isomerized to its' structural isomer compound **15** when it was dissolved in polar solvents. Therefore, it is essential to further explore electron donating substituents that do not show any isomerization.

(a)

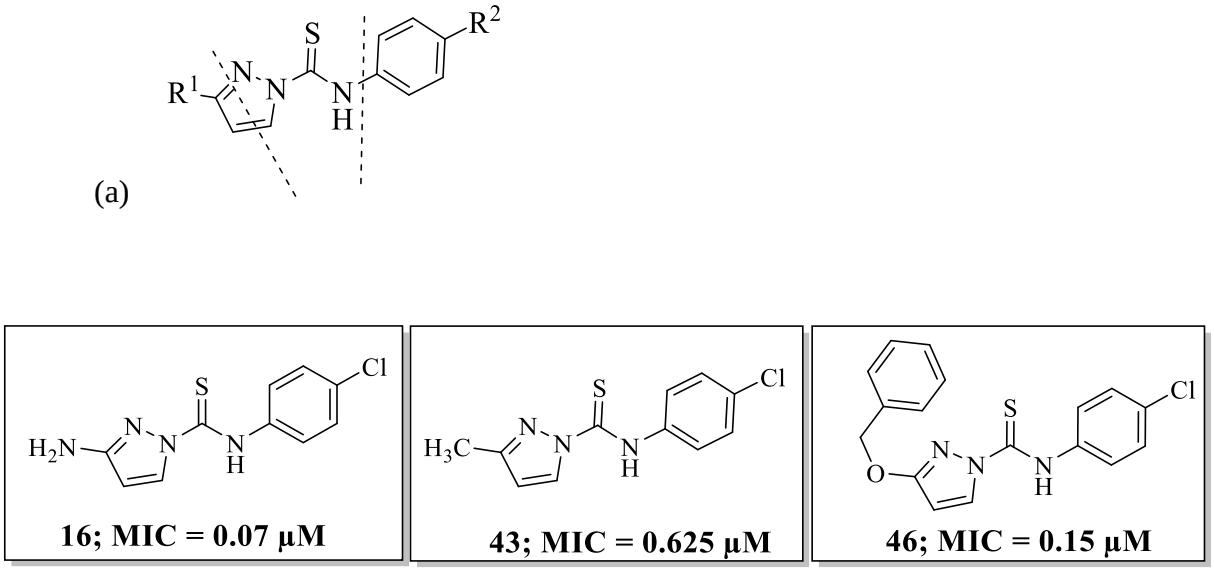

Figure 2.9 (a) NNSN compounds contain three structural features such as 3C substituted pyrazoles, a thionyl center and para substituted phenyl ring. (b) MIC values of compound 16, 43 and 46.

From the job plots, it was found that most likely NNSN complexes form with Cu(I) in a 1:1 molar ration. Thus this assumption was made to determine their binding constants. According to the literatures available in chapter 1.10, NNSN compounds tend to possess a Type 1 binding site of Cu (I/II) in natural model environment. In analogy to the Type 1 model (main ligands: two

histidines and a cysteine), NNSN molecules may show a distorted tetrahedral binding geometry. Online based, "Supramolecular.com" Bindfit program was used to determine the copper binding constants for NNSN compounds and the results showed that compounds with low MIC values tended to show higher binding constants.

In order to understand the observed binding actions of NNSNs and Cu(I), a Hammett analysis was conducted using the NNSN compounds' binding constants versus Hammett substituent constants for para-substituted phenyl derivatives. For this study, two sets of compounds were used, one set was with a pyrazole ring without any substitutions and the second set was with an amino group on the pyrazole ring. Based on the Hammett plots, both the sets of pyrazoles (unsubstituted and substituted) showed that ($\rho \approx + 1.18$ and $\rho \approx + 1.8$) negative charge is formed during Cu(I) binding. Therefore, the presence of electron withdrawing groups would be able to accelerate the reaction and at the same time, drive the reaction toward Cu(I)-NNSN complex formation. Moreover, these values implied that the complex formation equilibrium constants were significantly larger when the pyrazole ring was substituted with EDG. Based on the assumption, it was hypothesized that thio-enolization was likely to occur before Cu(I) binding could take place, which would generate a mildly acidic -SH group. Most thiols are fairly acidic with a pKa's in the range of 5 to beyond 11.[203] Thus, the substitution of EWGs on the phenyl ring could enhance the thiol's acidity. Furthermore, this deprotonation step appears to be at or near the rate-limiting step of Cu(I)-NNSN complex formation.

2.5 Working Principles of NNSN Compounds

2.5.1 Copper(I)-Binding Within Activated Phagosomes

As discussed in chapter 1.8.4, the pH of activated phagosomes in M1-polarized macrophages remains in the range of pH = 7 to 9 during the first 30 min. after engulfing bacteria.

During this "window of opportunity", Cu(I) binding to NNSN compounds occurs. According to the analysis of the Hammet plots discussed in chapter 2.33, the binding of Cu(I) is most likely preceded by the deprotonation of a thioenol that is formed from the thioketone by enolization. The pKa's of thiols vary from around 5 to beyond 11, depending on their structures.[203] We have selected prop-1-ene-2-thiol (pKa = 7.86[203]) as a model for the thioenols formed by NNSN's during the process of Cu(I) complex formation. Based on this comparison, NNSN compounds will be partly to fully deprotonized in the pH-window in activated phagosomes in M1-polarized macrophages. Furthermore, the average binding energy of the copper-sulfur bond is -258 kJ mol^{-1}.[204] Assuming that the formation of Cu@NNSN complexes is an equilibrium reaction (there is evidence from measuring the binding constants by means of UV/Vis titration), the Cu-S formation energy should be able to more than offset the presence of partially protonated thioenols at the beginning of the reaction.[205]

The next important question regarding the pharmacological activity of NNSN-compounds is, whether they can form copper(I)-complexes in sufficient concentrations within phagosomes. The simulations shown in Figure 2.12 were performed by using Supramolecular.org.[206] We were assuming a concentration of NNSN-compound of 1.0 x 10^{-6} mol L^{-1} (1 micromolar) within the activated phagosome. The concentration of Cu(I) was varied from 1 to 150 x 10^{-6} mol L^{-1}; and the binding constant K_B of Cu(I) to NNSN was set to 5,000 M L mol^{-1}(A), 10,000 M L mol^{-1}(B), and 50,000 M L mol^{-1}(C). The range of Cu(I) concentration was chosen based on elemental analyses within phagosomes.[159]

A: The calculated molefraction of Cu(I)NNSN complex with assumed binding constant K_B = 5,000 M L mol^{-1} reaches 0.4 at concentrations > 140 micromoles of Cu(I). K_B = 5,000 M L mol^{-1} can be

considered the lower bound for binding constants of Cu(I)NNSN complexes that show micromolar activity against *S. aureus* strains.

B: The calculated molefraction of Cu(I)NNSN complex with assumed binding constant K_B = 10,000 M L mol^{-1} reaches 0.5 at concentrations > 105 micromoles of Cu(I). This is the case for numerous NNSN compounds that are active in the low micromolar range.

C: The calculated molefraction of Cu(I)NNSN complex with assumed binding constant K_B = 50,000 M L mol^{-1} reaches 0.5 at concentrations > 20 micromoles of Cu(I) and 0.8 at concentrations > 80 micromoles of Cu(I). This is the case for the best NNSN compounds that are active in the sub-micromolar range.

These simulations clearly indicate that Cu(I)-binding within activated phagosomes is realistic. Due to the relative low binding constants of the NNSN-compounds, it is safe to assume that there will be competitive binders available, for instance proteins with cysteine, methionine, or lysine residues available at their surfaces. However, as shown in Figure 2.12, the calculated binding isotherms at each of the investigated binding constants only rise slowly with increasing copper(I) availability. This also means that they only decline slowly with decreasing copper(I) concentrations within the phagosome. In all three cases, the decrease of available copper(I) due to competitive binding is not a major problem.

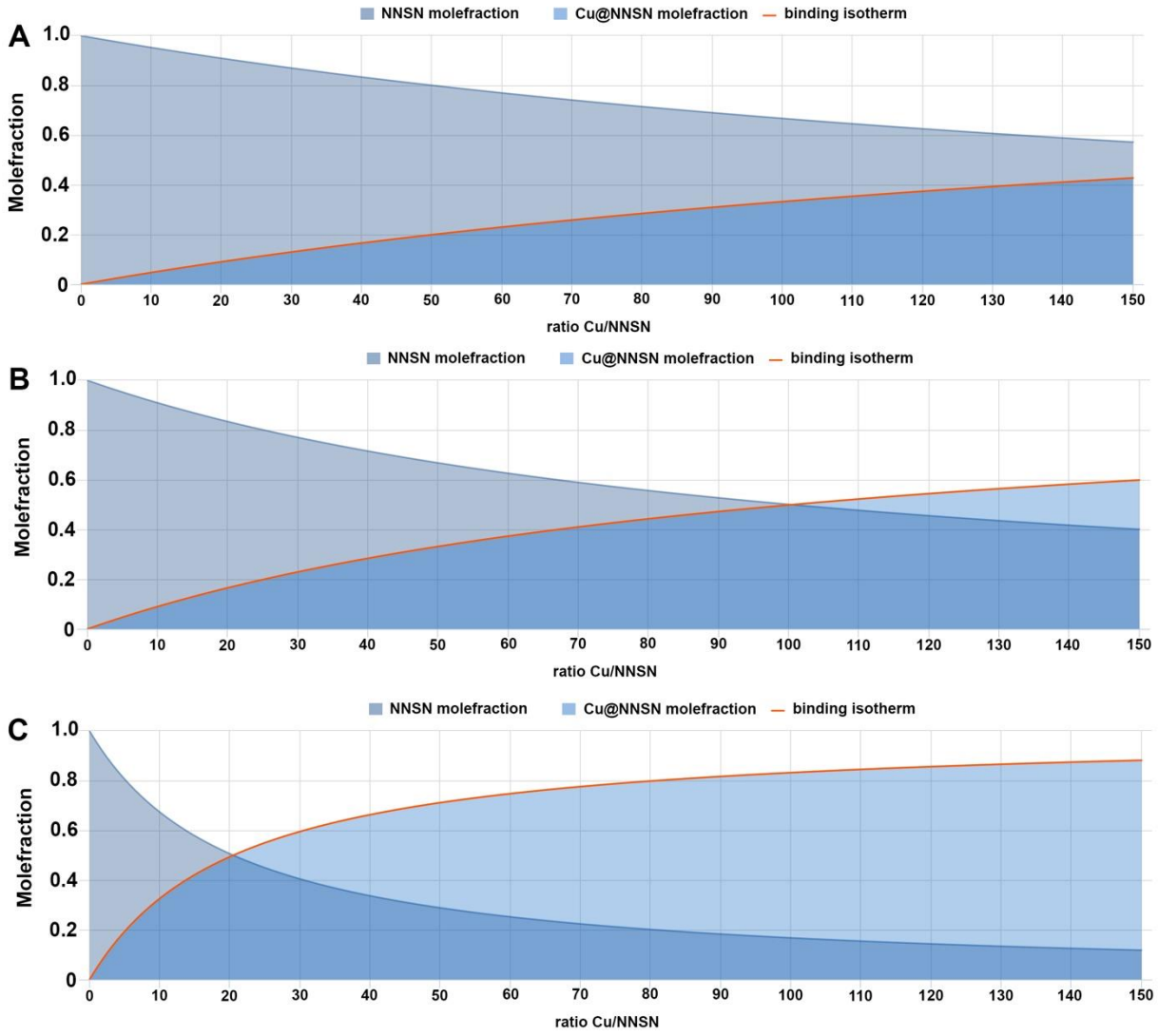

Figure 2.10 Simulated binding isotherms of NNSN compounds with Cu(I) under phagosome-like conditions. A: concentration (NNSN) = 1 x 10^{-6} mol L^{-1}; concentration Cu(I): variable from 1 to 150 x 10^{-6} mol L^{-1}; binding constant of Cu(I) to NNSN: 5,000 M L mol^{-1}; **B:** concentration (NNSN) = 1 x 10^{-6} mol L^{-1}; concentration Cu(I): variable from 1 to 150 x 10^{-6} mol L^{-1}; binding constant of Cu(I) to NNSN: 10,000 M L mol^{-1}; **C:** concentration (NNSN) = 1 x 10^{-6} mol L^{-1}; concentration Cu(I): variable from 1 to 150 x 10^{-6} mol L^{-1}; binding constant of Cu(I) to NNSN: 50,000 M L mol^{-1}. The simulations were performed with supramolecular.org.[206]

2.5.2 What Pharmacokinetic Properties Can We Anticipate for NNSN-Compounds?

The question, which remains at this point of the discussion is whether NNSN-Compounds are capable of diffusing through human cell membranes to reach the phagosomes prior to the uptake of bacteria? To assess bioavailability of NNSN compounds, we have use the web service

SwissADME,[207] which is able to determine the pharmacokinetic properties, druglike nature and medicinal chemistry friendliness of small molecules *in-silico*. SwissADME is based on references[208], [209],[210] and has been developed by the Molecular Modeling Group of the Swiss Institute of Bioinformatics in Lausanne. The following compounds have been evaluated: Compounds 16, 43, and 46 were synthesized in this thesis; the former lead compound has been published by Wolschendorf et al.[115]

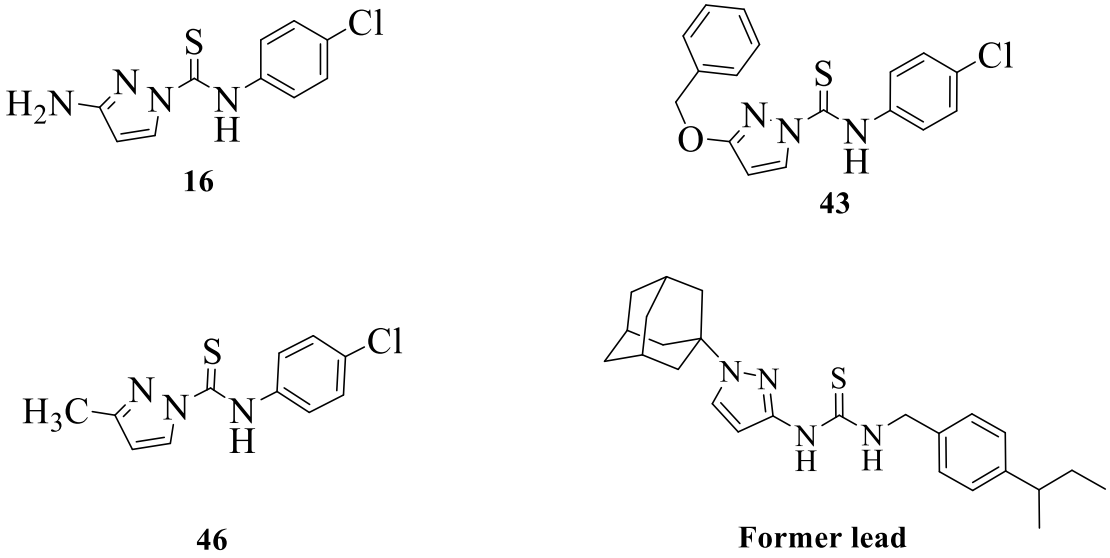

Figure 2.11 Most effective NNSN-compounds from this thesis and former lead compound.[115]

Table 2.8 Estimation of Human Gastrointestinal Absorption (HIB), Blood Brain Barrier Permeability (BBB), log P, and Solubility in Water of the NNSN-Compounds shown in Figure 2.13.[208,209,210]

Compound	HIA[a)]	BBB[b)]	LogP consensus	Solubility (mol L^{-1})[c)]
16	High	No	2.06	$6.07\ 10^{-4}$ mol
43	High	Yes	2.80	$6.04\ 10^{-4}$ mol
46	High	Yes	3.90	$1.06\ 10^{-5}$ mol
former lead	High	No	5.07	$1.18\ 10^{-6}$ mol

a) Passive human gastrointestinal absorption
b) Transfer through the blood brain barrier
c) Solubility in water

All four lead compounds show high gastrointestinal absorption. 43 and 46 are able to cross the blood-brain-barrier. All compounds feature a LogP consensus > 2.0 and at least four polar (nitrogen) atoms and have molecular weights smaller than 500. Therefore, it can be predicted that all four NNSN compounds can cross human cell membranes, including all cell organelles (mitochondria, nucleus, and especially endosomes/phagosomes).[208,209] Based on the assessment from SwissADME, NNSN-compounds can be delivered intravenously and will distribute throughout the human body. They will be activated only in activated phagosomes, because only there they will be able to react with sufficient quantities of available Cu(I). Since the bacteria will be taken up by the same phagosomes prior to the release of Cu(I), neither additional diffusion steps nor transport of Cu(I)-NNSN across membranes is required for antibacterial activity. Therefore, copper(I)-activation is more specific than any other approach to administering antibiotics to (gram-positive) bacteria.

2.6 Conclusions

Although, the mode of action of copper complexes of NNSN compounds is yet to be identified, the current results showed that NNSN compounds with lower MIC values feature higher

binding constants. Furthermore, the binding constants for Cu(I)-NNSN complexes range only from 10^2 to 10^5 M^{-1} which suggested that NNSN compounds would not be able extract Cu(I) from mammalian copper storage proteins. The following "milestones" regarding the reactivity of NNSN-compounds with copper(I) have been established in this thesis:

- NNSN-compounds are able to cross human cell membrane and to reach cell organelles, such as endosomes and phagosomes.
- Upon sensing the presence bacteria via detection of LPS (lipopolysaccharides), phagosomes are activated. They engulf the bacteria and increase the copper(I) content within the phagosomes. Note that the pH in early phagosomes of M1-polarized macrophages is in the range of 7 to 9, thus permitting available Cu(I) that can form complexes with NNSN-compounds in 1:1 stoichiometry.
- Although bacteria (e.g. *S. aureus*) feature a defense system against copper(I), the NNSN-compounds form copper(I)-complexes, which can diffuse through bacterial cell walls.
- The bacterial toxicity of Cu(I)NNSN compounds has to be high enough to impair bacterial efflux pumps. Note that the gram-positive bacterium *S. aureus* does not possess efflux pumps for Cu(I)NNSN, but only for Cu(I).
- The consequence of Cu(I)NNSN drug action is bactericidal action against several *S. aureus* strains, among them MRSA.
- The best compounds 16, 43, and 46 have activities against MSSA and MRSA in the nanomolar range.

These results showed very promising antibacterial properties which will serve as the foundation for future studies.

3. A Catalyst Free, Temperature Driven One Pot Synthesis of 1-adamantylhydrazine hydrochloride

3.1 The Importance of the Adamantyl Derivatives

According to Dr. Rachel Codd, School of Medical Sciences (Pharmacology) and Bosch Institute, University of Sydney, the value of the adamantyl group in drug design is multidimensional.[211] Most adamantyl bearing derivatives exhibit enhanced medicinal properties. Gerzon and co-workers had tested different lipophilic groups (n-C_4H_9, 1-adamantyl and cyclohexyl) at hypoglycemic sulfonylurea's side chain. They observed increased relative potencies, hypoglycemic activity and longer lasting activity of these compounds when the n-butyl group was replaced with 1-adamantyl.[212] Likewise, adamantyl was used in modification of anabolic steroids and nucleosides.[213] The main reason to use adamantyl modification is enhanced lipophilicity and stability of the drugs, so that it increases their pharmacokinetic properties.[213] Moreover, adamantyl derivatives are useful in material science applications also, for instance in the calibration of AFM tips.[214] Adamantyl rings consist of four tertiary and six secondary carbon centers and the tertiary carbon centers are more prone to functionalization than secondary carbons. However, the addition of complex functionalities into adamantane rings often requires catalytic systems, or high energy inputs to go over large energy barriers. Due to these reasons, some adamantyl derivatives are not commercially available to purchase and sometimes can be very expensive. Therefore, it is essential to focus on developing an energy efficient and cost-effective method for functionalizing the adamantyl group. In particular, our research needed an efficient and straightforward synthetic protocol for 1-adamantylhydrazine (Figure 3.1a) because it is a required precursor for the synthesis of 1-adamantyl substituted pyrazolyl thioureas (Figure 3.1b) with an NNSN motif.[132] These adamantyl substituted pyrazolyl thioureas have demonstrated copper

dependent antibacterial properties toward GP bacteria such as MRSA in activated phagosomes.[115,215] During literature studies, I realized that there are only a limited number of procedures available that describe the introduction of an adamantyl ring to pyrazole's 1N. Thus, this research is concerned with the development of a new synthetic approach for accessing 1-(adamantan-1-yl)-1H-pyrazol-3-amine.

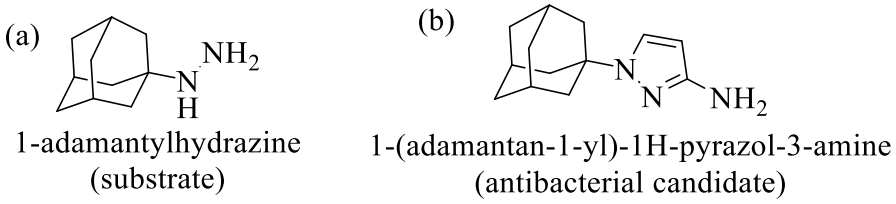

Figure 3.1 Structures of (a) 1-adamantylhydrazine and (b) 1-(adamantan-1-yl)-1H-pyrazol-3-amine.

3.2 Novel Synthetic Approach for 1-adamantylhydrazine

Adamantane's tertiary carbon centers are more prone to functionalization because the positive charge of the tertiary carbocation can be selectively stabilized by other bridgehead positions via second order hyperconjugation (blue color lobes) as shown in Figure 3.2a.[216] Another study revealed that the positive charge can be equally distributed to other bridge head tertiary carbons as shown in Figure 3.2b.[217] Moreover, structures I, II and III equally contribute to the resonance stabilization. The functionalization of adamantyl generally occurs via halogenation as a pre-initiation step followed by polar S_N1 substitution under electrophilic conditions.

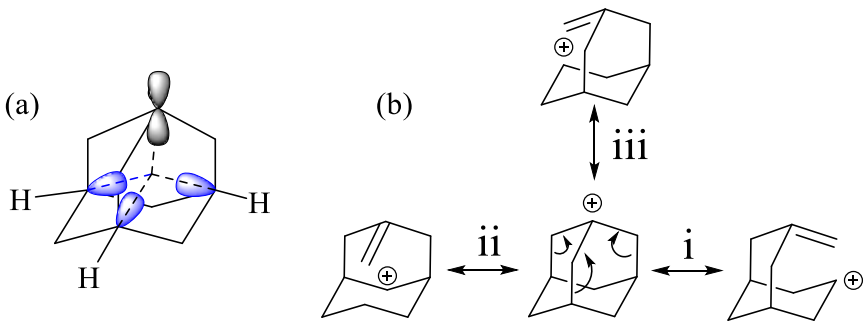

Figure 3.2 Stabilization of the empty p-orbital of the carbocation. (a) Black shaded empty p-orbitals can be stabilized by the blue shaded antibonding orbitals of other bridgehead C-H bonds. (b) Resonance stabilization of the positive charge on the top tertiary carbo cation to other bridge head positions.

Daeniker had used 1-aminoadamantane to synthesize 1-adamantylhydrazine in five steps.[79] However, this method was lengthy and overall yield was low.[218] In another study (Scheme 3.1), highly strained 1,3-dehydroadamantane was reacted with an excessive amount of 2-aminoethan-1-ol and 3-aminopropan-1-ol at 60-70 ˚C for 1 hour to obtain the O- and N-alkylated products.[219] However, the highly strained substrate 1,3-dehydroadamantane is expensive and not readily available for purchase.

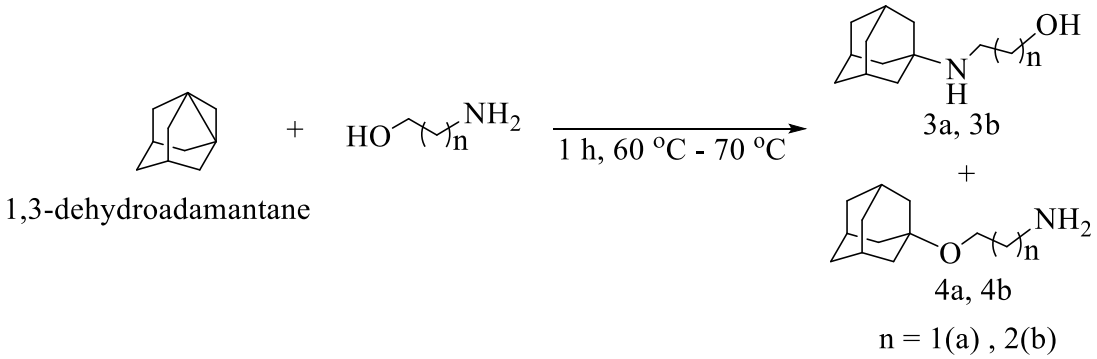

Scheme 3.1 The reaction of 1,3-dehydroadamantane and amino alcohols to obtain a mixture of O- and N- alkylated products.[219]

In 1968, Thomas and Shetty patented the synthesis of 1-adamantylhydrazine and its derivatives by reacting halogenated adamantane with anhydrous hydrazine under inert atmosphere and high heat.[220] Some of the drawbacks I encountered reproducing these results was the need for anhydrous hydrogen chloride, inefficient drying methods for accessing the anhydrous form and the presence of the target compound as well as a mixture of byproducts. Therefore, I modified the original synthetic approach by Thomas and Shetty. To probe the novel synthetic approach, 1-bromoadamantane was reacted with hydrazine under different reaction conditions (Table 3.1)

Table 3.1 Optimization of the Reaction Conditions

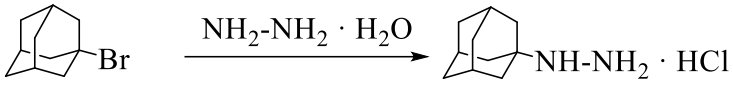

1-bromoadamantane 47

Entry	External temperature (ºC)	Internal temperature (ºC)	Base	Solvent	Time (h)	Yield %
1[a]	No heating	27-33	K_2CO_3 (1eq.)	DMF	5	0
2[a]	No heating	25-31	K_2CO_3 (1eq.)	DMF	overnight	0
3[b]	90 -100	82-95	No base	Excess hydrazine	5	0
4[b]	90 -100	82-93	No base	Excess hydrazine	overnight	Trace
5	125-135	110-115	No base	Excess hydrazine	5	42
6[c]	125-135	110-115	No base	Excess hydrazine	8 (12h)	83 (>88)

[a]1eq. of hydrazine monohydrate was used and an oil bath was not used for this step. Internal temperatures were taken occasionally. [b]Excess hydrazine monohydrate was used and played dual role in this step. Oil bath temperatures were set to 90 – 100 °C and internal temperatures were taken at the beginning and end of the reactions. [c]The reaction was carried out for 8 h, 10 h and 12 h and their yields were around 85%. Further optimization was not performed after 12 h.

This reaction was performed under Ar gas since 1-bromoadamantane is moisture, light and air sensitive. It is worth mentioning that the reaction apparatus was covered with aluminum foil to block additional light. Additionally, foil paper provided thermal insulation to the reaction vessel which helped to maintain a constant temperature inside. In contrast to the patent, use of anhydrous hydrazine was not cost effective as it plays dual roles in this reaction as the solvent and reactant. Thus, I employed hydrazine monohydrate in excessive amounts. However, 1-bromoadamantane did not readily dissolve in hydrazine monohydrate, since it is more lipophilic. In entry 1, a stoichiometric amount of NH_2-NH_2·H_2O (1 eq) and K_2CO_3 (1eq) were reacted with 1-

bromoadamantane in DMF without heating. However, no product formation was observed in entries 1 and 2. We discontinued the use of K_2CO_3 as hydrazine was basic enough for subsequent reactions (entry 3 and 4). Furthermore, excess of hydrazine monohydrate was employed as DMF was not used as the solvent in further attempts. Five hours were not enough to form the desired product in entry 3 but trace amounts of compound **47** were observed after reacting overnight in entry 4. It is worth noticing that low internal temperatures such as in entries 3 and 4, 1-bromoadamantane showed low solubility in hydrazine which may cause the traceable amounts of our desired product. In order to increase 1-bromoadamantane's solubility in hydrazine the reaction was refluxed at 125 – 135 $^{\circ}$C as stated in entries 5 and 6. In entries 5 and 6, 1-bromoadamanane was dissolved and the reaction mixture became clear light yellow color solution as shown in Figure 3.3a.

Figure 3.3b. The reaction was monitored by TLC and the starting material 1-bromoadamanane was not visible with UV light. Thus, phosphomolybdic acid (PMA) was used as the visualizing agent.

a)

b)

Figure 3.3 (a) 1-bromoadamanatane was not dissolved in hydrazine monohydrate. (b) 1-bromoadamantane was dissolved in hydrazine monohydrate as the internal temperature was elevated to 110 ˚C.

During the reflux, a white colored solid precipitate was observed at the middle region of the water jacketed condenser. Once the reaction was completed, the reaction mixture was cooled to room temperature which turned the crude mixture into a cloudy solution because of the adamantyl compound's poor solubility in polar solvents. Afterward, the crude mixture was charged with 45% (W/W) potassium hydroxide solution to remove unreacted hydrazine. Upon addition of potassium hydroxide, the previously cloudy mixture formed an opaque dispersion. The organic layer was then dried over anhydrous sodium sulfate whereas in the original patent, the drying agent that was used was anhydrous magnesium sulfate.[220] However, it is worth using anhydrous sodium sulfate for the drying step as 1-admantylhydrazine's nitrogens are basic enough to react with the magnesium sulfate. The addition of the drying agent turned the opaque dispersion into clear solution. The dried ether layer was then concentrated under vacuum to approximately a quarter of the solvent volume followed by acidifying the solution to pH 2 by adding concentrated hydrochloric acid. Upon acidification, the 1-adamantylhydrazine hydrochloride salt was precipitated out as a white solid shown in Figure 3.4a. This hydrochloride salt formation was essential for the next step as it was more stable than 1-adamantylhydrazine. Thomas and Shetty stated that this salt was further recrystallized using isopropanol. However, according to my studies, the recrystallization step was not required as it led to considerable loss of product due to its high solubility in isopropanol. Thus, a white solid was isolated by means of gravity filtration and dried under high vacuum to obtain >88% yield (with recrystallization ~53% yield).

a)  b) 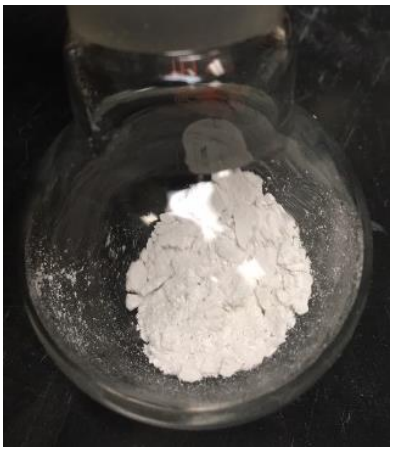

Figure 3.4 (a) White solid crashed out upon the addition of concentrated HCl. (b) Dried 1-adamantylhydrzine hydrochloride salt.

The purity of the product was determined by NMR spectroscopy and UPLC-MS. The melting point observed was 216-220 °C which did not fit with the literature value, 250-253 °C.[220] However, Thomas and Shetty did not use any spectroscopic date to evaluate their product's purity. To summarize, we successfully synthesized the 1-adamantylhydrazine with this novel approach with >88% yield and the purity of the compound was confirmed with the use of NMR spectroscopy and UPLC-MS.

3.3 Synthesis of 1-(adamantan-1-yl)-1H-pyrazol-3-amine (48)

Our efforts were then directed to checking the synthetic route towards antibacterial candidate 1-(adamantan-1-yl)-1H-pyrazol-3-amine. Dionisia *et al.* mixed equimolar amounts of 1-aminopyrazole and 1-bromoadamantane together and heated the reaction at 160-170 °C to introduce adamantyl to 1NH position of the pyrazole (Scheme 3.2).[221] However, they obtained three different products including 1-(adamantan-1-yl)-1H-pyrazol-3-amine with 15% yield.[221] Looking at the products, it is clear that the elevated temperature facilitated all the nucleophilic centers to attack the 1-bromoadamantane in a non-regioselective manner followed by the subsequent isomerization to deliver all three compounds. Therefore, I wanted to investigate methods to access the 1N substituted 3-aminopyrazlole.

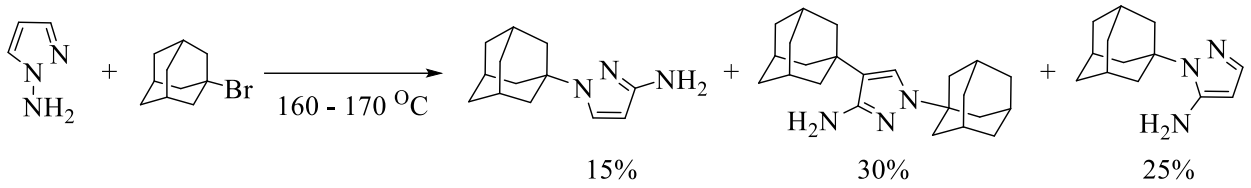

Scheme 3.2 Previous synthetic approach to synthesize 1-(adamantan-1-yl)-1H-pyrazol-3-amine.

Based on my previous experience, 2-chloroacrylonirile can be reacted with any hydrazine derivative to obtain the corresponding 3-aminopyrazole derivatives. With this knowledge, previously synthesized 1-adamantylhydrazine (**47**) was reacted with 2-chloroacrylonitrile in the presence of additive K_2CO_3/ $NaHCO_3$ (1:2 molar ratio) as referenced in the previously published work.[188]

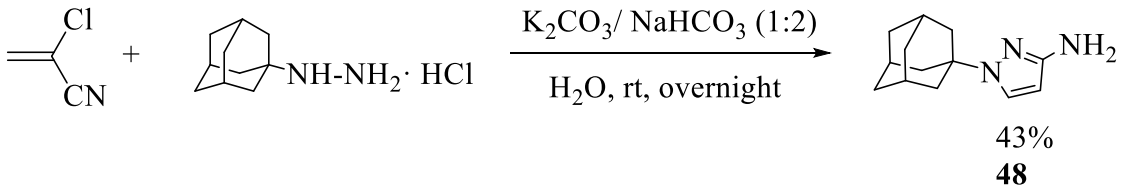

Scheme 3.3 Synthesis of 1-(adamantan-1-yl)-1H-pyrazol-3-amine.

However, most of the pyrazole products were lost during the work up process as they tend to partition in the polar water layer. The original publication did not state any improvements to avoid this product loss. Therefore, I employed a continuous extraction method to increase the partition of pyrazolic derivative in the organic layer by which the overall yield obtained was 43%. In contrast to the highly strained 1,3-dehydroadamantane, our novel approach is economically more feasible and more sustainable.

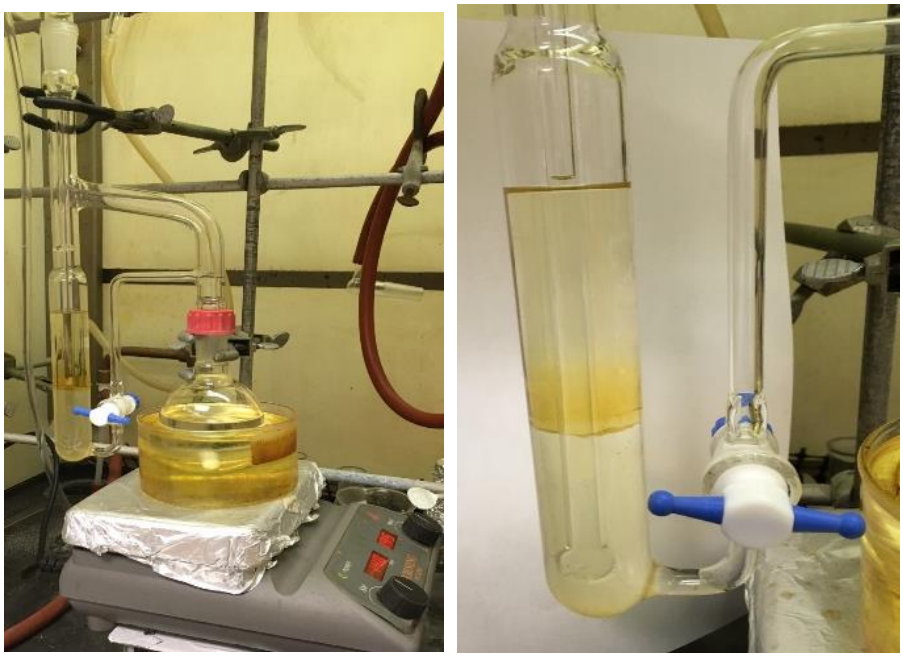

Figure 3.5 The continuous extraction apparatus. Right side- Extraction of pyrazole derivatives from aqueous layer to Ethyl acetate (Top-EtOAc, Bottom Aq).

In conclusion, I have developed a catalyst and solvent free temperature driven methodology to synthesize 1-adamantylhydrazine, which otherwise requires multiple steps for access in synthetic quantities. The reaction occurred by a nucleophilic substitution reaction to introduce a hydrazine moiety with considerably higher yield. The use of a continuous extraction apparatus enabled an increase in the overall yield of 1-(adamantan-1-yl)-1H-pyrazol-3-amine. This allowed the further analysis of the medicinal properties of adamantyl bearing pyrazole derivatives.

4. Other Structural Approaches

As mentioned in chapter 1.10, amino acids containing S and N atoms tend to bind with copper metal ions predominantly. Based on this finding, the addition of a secondary "S" atom to NNSN compounds may increase the antibacterial activity as it enables multiple sulfur-based coordination sites for the Cu(I) ion center. In order to test this paradigm, I designed a new compound with two NNSN moieties by reacting a bis-pyrazole substrate with the desired isothiocyanate derivative. The synthesis of the bis-pyrazole substrate was initiated by forming 4-bromopyrazole **49** using the previously reported procedure as shown in Scheme 4.1.[222]

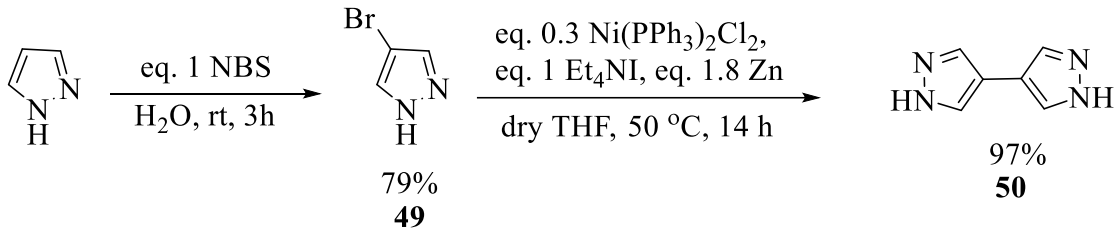

Scheme 4.1 Synthesis of 4,4'-bipyrazolyl (50) via 4-bromopyrazole (49).

Bromination of pyrazole's 4C was easily performed under very mild conditions using distilled water and room temperature. Pyrazole's nucleophilicity and reactivity of NBS greatly affected this benign bromination. Among the three C atoms of the pyrazole, most of the electron density resides at 4C so the regioselectivity of the electrophilic aromatic substitution was high However, after the desired reaction time, there were two spots visible on the crude TLC. The spot at $R_f = 0.52$ represented the desired product and the spot $R_f = 0.15$ showed the presence of the byproduct succinimide. This was further proved by performing the ^{1}H-NMR for the crude sample. A previously reported for the homo-coupling of two 4-bromopyrazoles utilized a Ni catalyst, Et_4NI and Zn dust under anhydrous reaction conditions.[223] In contrast to Pd catalysts, the use of a Ni complex in this homo-coupling reaction was very cost effective. The bis-pyrazole compound **50**

was reacted with 2 equivalents of 4-chloroisothiocyante to form compound **51**, which possessed two NNSN moieties (Scheme 4.2). Overall, the molecule is symmetric, as was observed in the ^{1}H-NMR spectrum. Compound **51**'s bacterial study is still being processed at the University of Alabama. Based on the *in-vitro* bacterial study, it may be worth introducing different isothiocyanates to bis-pyrazolic compound **50**.

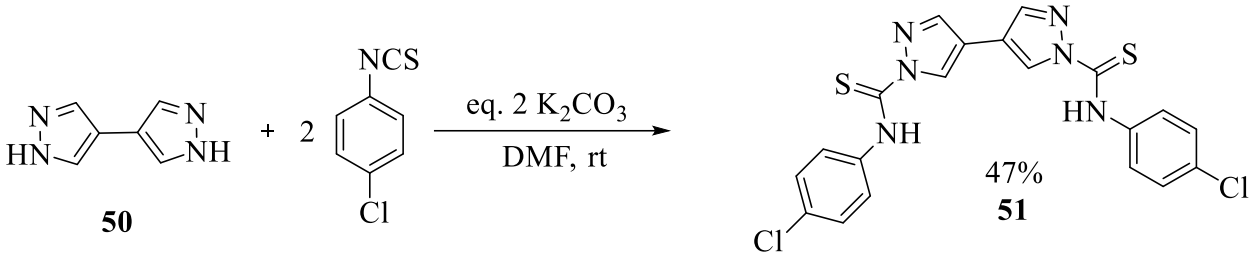

Scheme 4.2 Synthesis of bis-pyrazolic NNSN compound 51

As 4-bromopyrazole was successfully formed, it could be worth reacting this brominated pyrazole with 4-chlorophenyl isothiocyanate. Hence compound **49** was reacted with 4-chlorophenyl isothiocyanate in DMF with 1 equivalent of K_2CO_3. The complex of compound **52** and copper showed MIC values of 10 µM against MSSA and it further proved that 4C substitution does not significant influence NNSN antibacterial activity.

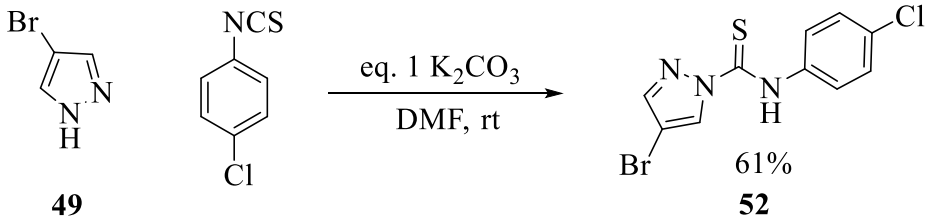

Scheme 4.3 Reaction between 4-bromo pyrazole (49) and 4-chloroisothiocyanate.

All the NNSN compounds consisted of three major structural motifs including a thionyl center, a pyrazole ring and a phenyl ring. Synthesizing different isothiocyanates could be beneficial

for our SAR studies. In addition, working on two sides in parallel may reveal a broader picture in a shorter period of time. In chapter 2, it is very clear that chlorine substitution at para position of the phenyl ring significantly influenced the NNSN's antibacterial properties. However, it is still worth trying some substituents at ortho position as it is very close to the thionyl center. In this case, we were inspired to investigate the steric hindrance that would occur with ortho substitutions. Therefore, I used the two-step approach of a modified Kaluza isothiocyanate synthesis to obtain the corresponding thiosemicarbazone from 2,6-dimethyl aniline as shown Scheme 4.4.[224] In the second step, cyanuric chloride was used as the desulfurylation reagent, and the resulting by-product 1,3,5-triazine-2,4,6-trithiol tended to form an emulsion during the work up. However, this emulsion diminished over the time and the rest of the emulsion was adsorbed on to anhydrous Na_2SO_4 during the drying step. Moreover, the low yield could be attributed to the formation of unwanted emulsion layer during the work up.

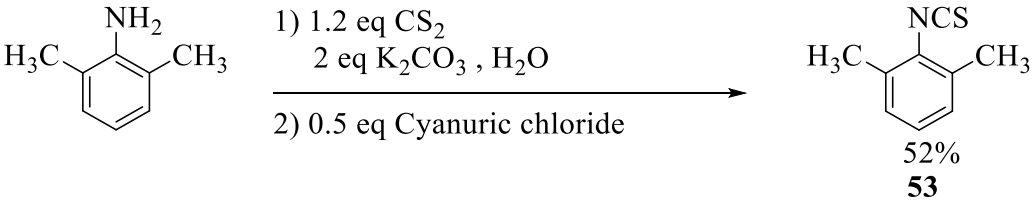

Scheme 4.4 Synthesis of 2,6-di methylphenyl isothiocyanate.

The synthesized compound 2,6-dimethylphenyl isothiocyanate **53** was reacted with different pyrazole-derivatives to obtain new NNSN derivatives **54**-**57**. As usual, the reaction times for the following compounds, **54**-**57,** were about 20 - 22 h (overnight reactions). Since 3-aminopyrazole derivatives are not stable in polar solvents, they were to reacted with isothiocyanate **53**. In order to determine the antibacterial properties of compound **53** exclusively, it was worth reacting unsubstituted pyrazole with **53** (entry 1, Table 4.1). Compound **54** showed significant

antibacterial properties (0.6 µM) against GP MSSA. Similarly compound **55** with methyl group substitution at pyrazole's 3C also showed the same MIC value of 0.6 µM against GP MSSA. These results suggested that modifications on the phenyl rings can adjust the antibacterial properties of the NNSN complexes. I then wanted to analyze the effects of the new isothiocyanate derivative, **53,** on the pyrazole with a 4C substitution. Hence, **53** was reacted with 4-bromo pyrazole **49** to obtain compound **56**. Compound **56** was submitted for the *in-vitro* biological studies. As discussed in the chapter 2 conclusion section, compound **46** was the most active compound against MSSA, which possessed a benzyl ether moiety at 3C of the pyrazole. In order to observe the benzyl ether's effect on the overall antibacterial property of compound **53**, compound **42** was reacted with **53** in DMF to give compound **57**. Compound **57** was also submitted for its biological studies.

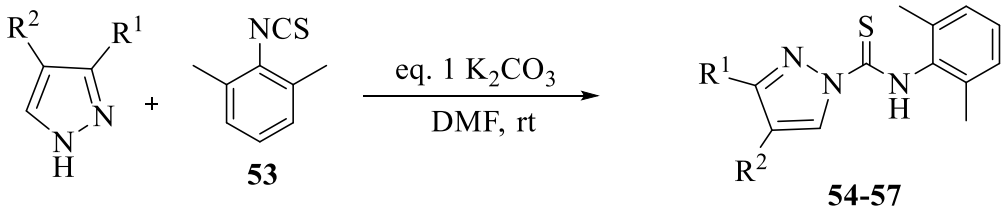

Table 4.1 Synthesizing of 2,6-di methylphenyl containing NNSN compounds 54-57.

Entry	Compound	R^1	R^2	Yield (100%)	MIC (µM)
1	54	H	H	74	0.6
2	55	$-CH_3$	H	48	0.6
3	56	H	-Br	26	TBD
4	57	-O-Bn	H	42	TBD

5. Future Studies

Efforts toward identifying lead compounds are proceeding with great success. Up to this moment, ED substituents at pyrazole's 3C increase the antibacterial activities of compounds with NNSN motif. It is worth mentioning that pyrazole's pyridine-like nitrogen could be involved in the complexation of Cu(I) ions besides the thiolate ligands of the NNSN moiety. It is apparent that more electron density should be directed toward the pyridine like nitrogen and the sulfur atom in order to obtain effective complexations, which can be achieved by substituting pyrazole's 3C with electron donating heterocycles. However, the results showed that a primary or secondary amine would not be feasible as it can drive structural isomerization. Therefore, pyrazole's 3C can be substituted with tertiary amine groups such as alkyl amines, cyclic amines and aryl amines as shown in Scheme 5.1. As proposed in chapter 1, the presence of additional nitrogen moieties could participate in copper bindings events and stabilize it's distorted tetrahedral geometry.

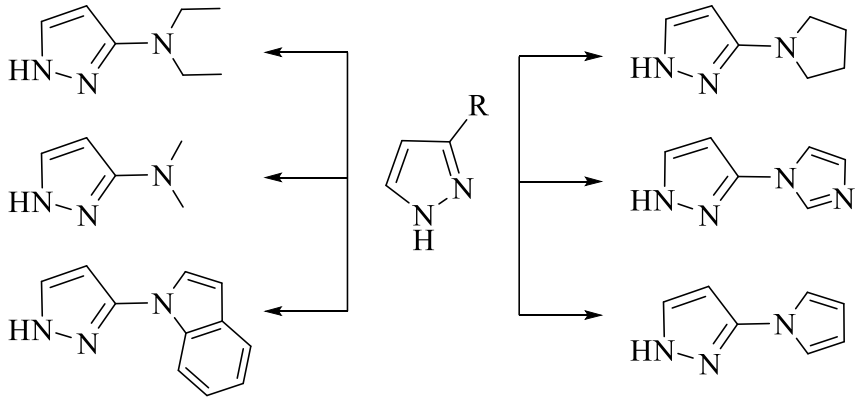

Scheme 5.1 Possible nitrogen containing substituents to pyrazole's 3rd carbon.

As mentioned in chapter 2.4, it is apparent that amine groups at the 3C of the pyrazole may be involved in copper binding, which could provide a distorted tetrahedral geometry. Moreover Table 1.3 showed that cysteine and methionine also may complex Cu(I) in this geometry. Thus, the introduction of sulfur containing moieties to NNSN compounds may enhance

their binding efficacy. So far X has been an amine, alkyl and an ether (benzyl ether). All of these groups increased the antibacterial properties of NNSN's. However, in order to sustain the distorted tetrahedral geometry, "Y" could consist of an additional nitrogen or sulfur donor. Moreover, it is important to have the flexibility to move around the copper(I) ion. Therefore, we could easily achieve this by placing aliphatic R^1 spacer between the X and Y moieties (Figure 5.1). In chapter 2.5, we have postulated that the rate limiting step could be the deprotonation of the -SH, whichwas enhanced by electron withdrawing effects. Therefore, it is electronically vital to substitute EWG at the S1and S2 positions. This can be easily accomplished by substituting carbonyl functionalites in these positions. Additionally, the Z group can be any nitrogen or sulfur containing moieties as mentioned in Figure 5.1. Moreover, multi-denticity could increase the chelating effects of NNSN compounds, which may eventually form more stable and potentially more toxic copper(I) complexes. This is based on the paradigm that increasing the Cu(I) binding constant will increase the toxicity of Cu(I)-NNSN complexes. However, it should be noted that the Cu(I) binding constant is only one of the parameters that may lead to increased efficacy against MRSA.

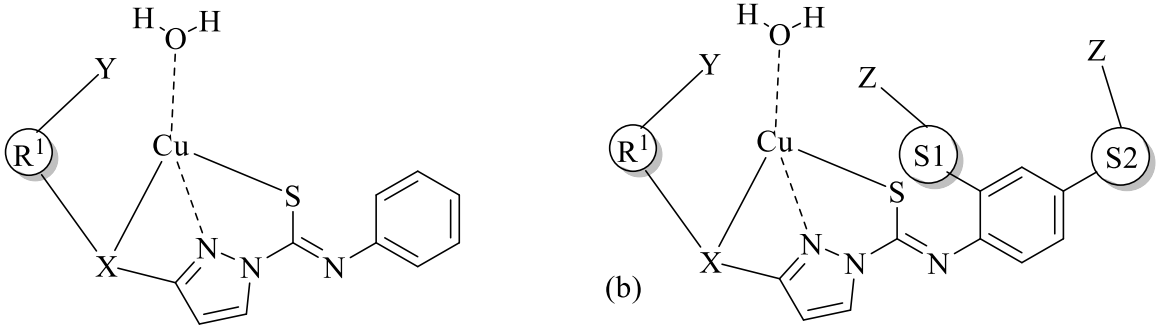

Figure 5.1 Designing multi-dentate NNSN compounds.

Another important aspect that I need to address is obtaining the crystal structure of Cu-NNSN complexes. Up to this moment, slow evaporation and vapor diffusion methods were used to crystallize the Cu-NNSN complexes. But those complexes grew as crystal needles or gave

brown precipitates, which were not able to be used for single crystal x-ray crystallography. So far Cu(I) salts such as CuBr and CuI were used to complex with NNSN. It was apparent that under aerobic conditions, Cu(I) ions tend to become oxidized to the most stable valence state of Cu(II), which could be the reason for the observation of a brown precipitate. It is essential to discover a possible way to obtain a single crystal to determine the absolute binding geometry. With the technical difficulties in acquiring single crystal of Cu-NNSN complexes, it is worth using Electron paramagnetic resonance (EPR) spectroscopy.[173] Overall, EPR data can be useful to determine the accuracy of our hypothesis on proposed "distorted tetrahedral" binding geometry. However, EPR will only work with Cu(II), which is paramagnetic. Cu(I) cannot be detected by means of EPR. However, if one-electron-redox chemistry is involved in the activation of NNSN compounds upon copper(I)-binding, EPR will be able to detect the organic radicals.[225]

Another possible area that we can improve in this research is modifying the NNSN compounds against GN bacteria species because there are several studies demonstrating that Cu(II)-bis(thiosemicarbazone) complexes show antibacterial properties against GN bacteria such as *N. gonorrhoeae* [226] and *mycobacterium tuberculosis*.[131] Another rising area of interest for copper complexes is using copper-thiosemicarbazone complexes as chemotherapeutic agents as they show anticancer properties. In addition, there are numerous investigations showing the cytotoxicity of Cu-thiosemicarbazone (2-pyridine derivatives and bis-thiosemicarbazone) complexes against cancer lines including human liver, cervical, breast, prostate and ovarian cancer cell lines.[227, 228] For this purpose, in-vitro experiments with murine and human cancer cell cultures could be performed. The cancer cells will be grown in their respective substrates in the presence of 50 micromoles of Cu(I) (via RMPI-reduction of Cu(II)), washed once they reached confluence, and then treated with varying concentrations of NNSN compound in 95% PBS buffer / 5% DMSO.

Cell viabilities will be determined by means of an MTT assay using 95% PBS buffer / 5% DMSO treated cells as control.[229]

Our research into NNSN compounds is still in its exploratory stages. I focused on structural analysis to find possible leads. The outcome of my research yielded NNSN compounds that displayed exceptionally encouraging antibacterial properties. Although there are many publications accessible on copper complexes with antibacterial properties, very limited data is available on their mode of actions. Therefore, studying the modes of actions of Cu-NNSN complexes can be beneficial for many researchers who pursue on novel drug designing studies with copper complexes. The best approach for finding potential drug targets is to perform RNA sequencing of mammalian cells and bacteria to perform a competitive kinase screening and profiling and assay that has become recently available.[230], [231] This technique is becoming routine in basically all laboratories concerned with biological research. Here, we propose to perform single cell-based assays that able to demonstrate the (epi)genetic range in each sample of pathogenetic bacteria.

6. References

(1) Kato, C.; Li, L.; Nogi, Y.; Nakamura, Y.; Tamaoka, J.; Horikoshi, K. Extremely Barophilic Bacteria Isolated from the Mariana Trench, Challenger Deep, at a Depth of 11,000 Meters. *Appl. Environ. Microbiol.* **1998**, *64* (4), 1510 LP – 1513. https://doi.org/10.1128/AEM.64.4.1510-1513.1998.

(2) Danovaro, R.; Canals, M.; Tangherlini, M.; Dell'Anno, A.; Gambi, C.; Lastras, G.; Amblas, D.; Sanchez-Vidal, A.; Frigola, J.; Calafat, A. M.; Pedrosa-Pàmies, R.; Rivera, J.; Rayo, X.; Corinaldesi, C. A Submarine Volcanic Eruption Leads to a Novel Microbial Habitat. *Nat. Ecol. Evol.* **2017**, *1* (6), 144. https://doi.org/10.1038/s41559-017-0144.

(3) Guarner, F.; Malagelada, J.-R. Gut Flora in Health and Disease. *Lancet (London, England)* **2003**, *361* (9356), 512–519. https://doi.org/10.1016/S0140-6736(03)12489-0.

(4) Clark, F. E. Notes on Types of Bacteria Associated with Plant Roots. *Trans. Kansas Acad. Sci.* **1940**, *43*, 75–84. https://doi.org/10.2307/3625499.

(5) Peterson, J. W. Chapter 7 Bacterial Pathogenesis. In *Medical Microbiology. 4th edition*; S, B., Ed.; University of Texas Medical Branch at Galveston, Galveston (TX), 1996.

(6) *What You Need to Know About Infectious Disease*; 2011. https://doi.org/10.17226/13006.

(7) Hill, D. A.; Artis, D. Intestinal Bacteria and the Regulation of Immune Cell Homeostasis. *Annu. Rev. Immunol.* **2010**, *28*, 623–667. https://doi.org/10.1146/annurev-immunol-030409-101330.

(8) Zhang, Y.-J.; Li, S.; Gan, R.-Y.; Zhou, T.; Xu, D.-P.; Li, H.-B. Impacts of Gut Bacteria on Human Health and Diseases. *Int. J. Mol. Sci.* **2015**, *16* (4), 7493–7519.

https://doi.org/10.3390/ijms16047493.

(9) Rastogi, M.; Nandal, M.; Khosla, B. Microbes as Vital Additives for Solid Waste Composting. *Heliyon* **2020**, *6* (2), e03343. https://doi.org/10.1016/j.heliyon.2020.e03343.

(10) Fischbach, M. A. Antibiotics from Microbes: Converging to Kill. *Curr. Opin. Microbiol.* **2009**, *12* (5), 520–527. https://doi.org/10.1016/j.mib.2009.07.002.

(11) Auer, G. K.; Weibel, D. B. Bacterial Cell Mechanics. *Biochemistry* **2017**, *56* (29), 3710–3724. https://doi.org/10.1021/acs.biochem.7b00346.

(12) de Kraker, M. E. A.; Stewardson, A. J.; Harbarth, S. Will 10 Million People Die a Year Due to Antimicrobial Resistance by 2050? *PLoS Med.* **2016**, *13* (11), e1002184–e1002184. https://doi.org/10.1371/journal.pmed.1002184.

(13) Neill, J. O. '. Antimicrobial Resistance: Tackling a Crisis for the Health and Wealth of Nations The Review on Antimicrobial Resistance Chaired. **2014**, No. December.

(14) Biggest Threats and Data https://www.cdc.gov/drugresistance/biggest-threats.html.

(15) Gupta, V.; Datta, P. Next-Generation Strategy for Treating Drug Resistant Bacteria: Antibiotic Hybrids. *Indian J. Med. Res.* **2019**, *149* (2), 97–106. https://doi.org/10.4103/ijmr.IJMR_755_18.

(16) Miller, S. I. Antibiotic Resistance and Regulation of the Gram-Negative Bacterial Outer Membrane Barrier by Host Innate Immune Molecules. *MBio* **2016**, *7* (5). https://doi.org/10.1128/mBio.01541-16.

(17) Alana Biggers. Gram-Positive Bacteria Explained in Simple Terms https://www.healthline.com/health/gram-positive.

(18) U.S. and World Population Clock.

(19) Methicillin-resistant Staphylococcus aureus (MRSA) https://www.cdc.gov/MRSA/.

(20) Appelbaum, P. C. 2012 and beyond: Potential for the Start of a Second Pre-Antibiotic Era? *J. Antimicrob. Chemother.* **2012**, *67* (9), 2062–2068. https://doi.org/10.1093/jac/dks213.

(21) Fair, R. J.; Tor, Y. Antibiotics and Bacterial Resistance in the 21st Century. *Perspect. Medicin. Chem.* **2014**, *6*, 25–64. https://doi.org/10.4137/PMC.S14459.

(22) No Title http://www.cdc.gov/media/releases/2011/f0407_antimicrobialresistance.pdf.

(23) Projan, S. J. Why Is Big Pharma Getting out of Antibacterial Drug Discovery? *Curr. Opin. Microbiol.* **2003**, *6* (5), 427–430. https://doi.org/10.1016/j.mib.2003.08.003.

(24) Power, E. Impact of Antibiotic Restrictions: The Pharmaceutical Perspective. *Clin. Microbiol. Infect. Off. Publ. Eur. Soc. Clin. Microbiol. Infect. Dis.* **2006**, *12 Suppl 5*, 25–34. https://doi.org/10.1111/j.1469-0691.2006.01528.x.

(25) R., P. S. Humans as the World's Greatest Evolutionary Force. *Science (80-.).* **2001**, *293* (5536), 1786–1790. https://doi.org/10.1126/science.293.5536.1786.

(26) Von Döhren, H. Antibiotics: Actions, Origins, Resistance, by C. Walsh. 2003. Washington, DC: ASM Press. 345 Pp. $99.95 (Hardcover). *Protein Sci.* **2004**, *13* (11), 3059–3060. https://doi.org/https://doi.org/10.1110/ps.041032204.

(27) Kluytmans, J.; van Belkum, A.; Verbrugh, H. Nasal Carriage of Staphylococcus Aureus: Epidemiology, Underlying Mechanisms, and Associated Risks. *Clin. Microbiol. Rev.* **1997**, *10* (3), 505–520. https://doi.org/10.1128/CMR.10.3.505.

(28) Costerton, J. W.; Stewart, P. S.; Greenberg, E. P. Bacterial Biofilms: A Common Cause of Persistent Infections. *Science* **1999**, *284* (5418), 1318–1322. https://doi.org/10.1126/science.284.5418.1318.

(29) Turner, N. A.; Sharma-Kuinkel, B. K.; Maskarinec, S. A.; Eichenberger, E. M.; Shah, P.

P.; Carugati, M.; Holland, T. L.; Fowler, V. G. Methicillin-Resistant Staphylococcus Aureus: An Overview of Basic and Clinical Research. *Nat. Rev. Microbiol.* **2019**, *17* (4), 203–218. https://doi.org/10.1038/s41579-018-0147-4.

(30) Fischbach, M. A.; Walsh, C. T. Antibiotics for Emerging Pathogens. *Science* **2009**, *325* (5944), 1089–1093. https://doi.org/10.1126/science.1176667.

(31) Boucher, H. W.; Talbot, G. H.; Bradley, J. S.; Edwards, J. E.; Gilbert, D.; Rice, L. B.; Scheld, M.; Spellberg, B.; Bartlett, J. Bad Bugs, No Drugs: No ESKAPE! An Update from the Infectious Diseases Society of America. *Clin. Infect. Dis. an Off. Publ. Infect. Dis. Soc. Am.* **2009**, *48* (1), 1–12. https://doi.org/10.1086/595011.

(32) Smith, A. Bacterial Resistance to Antibiotics. *Hugo and Russell's Pharmaceutical Microbiology*. January 1, 2004, pp 220–232. https://doi.org/https://doi.org/10.1002/9780470988329.ch13.

(33) Xian-Zhi, L.; Patrick, P.; Hiroshi, N. The Challenge of Efflux-Mediated Antibiotic Resistance in Gram-Negative Bacteria. *Clin. Microbiol. Rev.* **2015**, *28* (2), 337–418. https://doi.org/10.1128/CMR.00117-14.

(34) Arias, C. A.; Murray, B. E. Antibiotic-Resistant Bugs in the 21st Century — A Clinical Super-Challenge. *N. Engl. J. Med.* **2009**, *360* (5), 439–443. https://doi.org/10.1056/NEJMp0804651.

(35) Kumarasamy, K. K.; Toleman, M. A.; Walsh, T. R.; Bagaria, J.; Butt, F.; Balakrishnan, R.; Chaudhary, U.; Doumith, M.; Giske, C. G.; Irfan, S.; Krishnan, P.; Kumar, A. V; Maharjan, S.; Mushtaq, S.; Noorie, T.; Paterson, D. L.; Pearson, A.; Perry, C.; Pike, R.; Rao, B.; Ray, U.; Sarma, J. B.; Sharma, M.; Sheridan, E.; Thirunarayan, M. A.; Turton, J.; Upadhyay, S.; Warner, M.; Welfare, W.; Livermore, D. M.; Woodford, N. Emergence of a

New Antibiotic Resistance Mechanism in India, Pakistan, and the UK: A Molecular, Biological, and Epidemiological Study. *Lancet. Infect. Dis.* **2010**, *10* (9), 597–602. https://doi.org/10.1016/S1473-3099(10)70143-2.

(36) Silhavy, T. J.; Kahne, D.; Walker, S. The Bacterial Cell Envelope. *Cold Spring Harb. Perspect. Biol.* **2010**, *2* (5), a000414. https://doi.org/10.1101/cshperspect.a000414.

(37) BOYAN B. B.,Brown, N. M. Bacterial Resistance to Antibiotics: From Molecules to Man; 2019; pp 201–238.

(38) Sankaran, K.; Wu, H. C. Lipid Modification of Bacterial Prolipoprotein. Transfer of Diacylglyceryl Moiety from Phosphatidylglycerol. *J. Biol. Chem.* **1994**, *269* (31), 19701–19706.

(39) Vollmer, W. Structural Variation in the Glycan Strands of Bacterial Peptidoglycan. *FEMS Microbiol. Rev.* **2008**, *32* (2), 287–306. https://doi.org/10.1111/j.1574-6976.2007.00088.x.

(40) Vollmer, W.; Blanot, D.; De Pedro, M. A. Peptidoglycan Structure and Architecture. *FEMS Microbiol. Rev.* **2008**, *32* (2), 149–167. https://doi.org/10.1111/j.1574-6976.2007.00094.x.

(41) Braun, V. Covalent Lipoprotein from the Outer Membrane of Escherichia Coli. *Biochim. Biophys. Acta* **1975**, *415* (3), 335–377. https://doi.org/10.1016/0304-4157(75)90013-1.

(42) de Duve, C.; Wattiaux, R. Functions of Lysosomes. *Annu. Rev. Physiol.* **1966**, *28* (1), 435–492. https://doi.org/10.1146/annurev.ph.28.030166.002251.

(43) W., M. C.; Anja, N.; Nicola, R.; Colin, R. Diffusion of Green Fluorescent Protein in Three Cell Environments in Escherichia Coli. *J. Bacteriol.* **2006**, *188* (10), 3442–3448. https://doi.org/10.1128/JB.188.10.3442-3448.2006.

(44) Neuhaus, F. C.; Baddiley, J. A Continuum of Anionic Charge: Structures and Functions of

D-Alanyl-Teichoic Acids in Gram-Positive Bacteria. *Microbiol. Mol. Biol. Rev.* **2003**, *67* (4), 686–723. https://doi.org/10.1128/MMBR.67.4.686-723.2003.

(45) Dramsi, S.; Magnet, S.; Davison, S.; Arthur, M. Covalent Attachment of Proteins to Peptidoglycan. *FEMS Microbiol. Rev.* **2008**, *32* (2), 307–320. https://doi.org/10.1111/j.1574-6976.2008.00102.x.

(46) Scott, J. R.; Barnett, T. C. Surface Proteins of Gram-Positive Bacteria and How They Get There. *Annu. Rev. Microbiol.* **2006**, *60*, 397–423. https://doi.org/10.1146/annurev.micro.60.080805.142256.

(47) Rohrer, S.; Berger-Bächi, B. FemABX Peptidyl Transferases: A Link between Branched-Chain Cell Wall Peptide Formation and Beta-Lactam Resistance in Gram-Positive Cocci. *Antimicrob. Agents Chemother.* **2003**, *47* (3), 837–846. https://doi.org/10.1128/AAC.47.3.837-846.2003.

(48) Pratt, R. F. Substrate Specificity of Bacterial DD-Peptidases (Penicillin-Binding Proteins). *Cell. Mol. Life Sci.* **2008**, *65* (14), 2138–2155. https://doi.org/10.1007/s00018-008-7591-7.

(49) Sauvage, E.; Kerff, F.; Terrak, M.; Ayala, J. A.; Charlier, P. The Penicillin-Binding Proteins: Structure and Role in Peptidoglycan Biosynthesis. *FEMS Microbiol. Rev.* **2008**, *32* (2), 234–258. https://doi.org/10.1111/j.1574-6976.2008.00105.x.

(50) Clarke, S. R.; Foster, S. J. Surface Adhesins of Staphylococcus Aureus. *Adv. Microb. Physiol.* **2006**, *51*, 187–224. https://doi.org/10.1016/S0065-2911(06)51004-5.

(51) Lewis, K. Platforms for Antibiotic Discovery. *Nat. Rev. Drug Discov.* **2013**, *12* (5), 371–387. https://doi.org/10.1038/nrd3975.

(52) Saier, M. H. J.; Reddy, V. S.; Tamang, D. G.; Västermark, A. The Transporter Classification Database. *Nucleic Acids Res.* **2014**, *42* (Database issue), D251-8.

https://doi.org/10.1093/nar/gkt1097.

(53) Lin, H. T.; Bavro, V. N.; Barrera, N. P.; Frankish, H. M.; Velamakanni, S.; van Veen, H. W.; Robinson, C. V; Borges-Walmsley, M. I.; Walmsley, A. R. MacB ABC Transporter Is a Dimer Whose ATPase Activity and Macrolide-Binding Capacity Are Regulated by the Membrane Fusion Protein MacA. *J. Biol. Chem.* **2009**, *284* (2), 1145–1154. https://doi.org/10.1074/jbc.M806964200.

(54) Yin, Y.; He, X.; Szewczyk, P.; Nguyen, T.; Chang, G. Structure of the Multidrug Transporter EmrD from Escherichia Coli. *Science* **2006**, *312* (5774), 741–744. https://doi.org/10.1126/science.1125629.

(55) Law, C. J.; Maloney, P. C.; Wang, D.-N. Ins and Outs of Major Facilitator Superfamily Antiporters. *Annu. Rev. Microbiol.* **2008**, *62*, 289–305. https://doi.org/10.1146/annurev.micro.61.080706.093329.

(56) Dastvan, R.; Fischer, A. W.; Mishra, S.; Meiler, J.; Mchaourab, H. S. Protonation-Dependent Conformational Dynamics of the Multidrug Transporter EmrE. *Proc. Natl. Acad. Sci.* **2016**, *113* (5), 1220 LP – 1225. https://doi.org/10.1073/pnas.1520431113.

(57) Gayen, A.; Leninger, M.; Traaseth, N. J. Protonation of a Glutamate Residue Modulates the Dynamics of the Drug Transporter EmrE. *Nat. Chem. Biol.* **2016**, *12* (3), 141–145. https://doi.org/10.1038/nchembio.1999.

(58) Bay, D. C.; Budiman, R. A.; Nieh, M.-P.; Turner, R. J. Multimeric Forms of the Small Multidrug Resistance Protein EmrE in Anionic Detergent. *Biochim. Biophys. Acta* **2010**, *1798* (3), 526–535. https://doi.org/10.1016/j.bbamem.2009.12.017.

(59) He, X.; Szewczyk, P.; Karyakin, A.; Evin, M.; Hong, W.-X.; Zhang, Q.; Chang, G. Structure of a Cation-Bound Multidrug and Toxic Compound Extrusion Transporter.

Nature **2010**, *467* (7318), 991–994. https://doi.org/10.1038/nature09408.

(60) Lu, M. Structures of Multidrug and Toxic Compound Extrusion Transporters and Their Mechanistic Implications. *Channels (Austin).* **2016**, *10* (2), 88–100. https://doi.org/10.1080/19336950.2015.1106654.

(61) Blair, J. M. A.; Webber, M. A.; Baylay, A. J.; Ogbolu, D. O.; Piddock, L. J. V. Molecular Mechanisms of Antibiotic Resistance. *Nat. Rev. Microbiol.* **2015**, *13* (1), 42–51. https://doi.org/10.1038/nrmicro3380.

(62) Murakami, S.; Nakashima, R.; Yamashita, E.; Yamaguchi, A. Crystal Structure of Bacterial Multidrug Efflux Transporter AcrB. *Nature* **2002**, *419* (6907), 587–593. https://doi.org/10.1038/nature01050.

(63) Takatsuka, Y.; Nikaido, H. Covalently Linked Trimer of the AcrB Multidrug Efflux Pump Provides Support for the Functional Rotating Mechanism. *J. Bacteriol.* **2009**, *191* (6), 1729–1737. https://doi.org/10.1128/JB.01441-08.

(64) Murakami, S.; Nakashima, R.; Yamashita, E.; Matsumoto, T.; Yamaguchi, A. Crystal Structures of a Multidrug Transporter Reveal a Functionally Rotating Mechanism. *Nature* **2006**, *443* (7108), 173–179. https://doi.org/10.1038/nature05076.

(65) A., S. M.; André, S.; Thomas, E.; François, V.; Kay, D.; M., P. K. Structural Asymmetry of AcrB Trimer Suggests a Peristaltic Pump Mechanism. *Science (80-.).* **2006**, *313* (5791), 1295–1298. https://doi.org/10.1126/science.1131542.

(66) Hassan, K. A.; Elbourne, L. D. H.; Li, L.; Gamage, H. K. A. H.; Liu, Q.; Jackson, S. M.; Sharples, D.; Kolstø, A.-B.; Henderson, P. J. F.; Paulsen, I. T. An Ace up Their Sleeve: A Transcriptomic Approach Exposes the AceI Efflux Protein of Acinetobacter Baumannii and Reveals the Drug Efflux Potential Hidden in Many Microbial Pathogens. *Front.*

Microbiol. **2015**, *6*, 333. https://doi.org/10.3389/fmicb.2015.00333.

(67) A., H. K.; Qi, L.; F., H. P. J.; T., P. I.; Karen, B. Homologs of the Acinetobacter Baumannii AceI Transporter Represent a New Family of Bacterial Multidrug Efflux Systems. *MBio* **2021**, *6* (1), e01982-14. https://doi.org/10.1128/mBio.01982-14.

(68) L., S. L. Challenges of Antibacterial Discovery. *Clin. Microbiol. Rev.* **2011**, *24* (1), 71–109. https://doi.org/10.1128/CMR.00030-10.

(69) Newman, D. J.; Cragg, G. M. Natural Products as Sources of New Drugs over the Last 25 Years. *J. Nat. Prod.* **2007**, *70* (3), 461–477. https://doi.org/10.1021/np068054v.

(70) Dalecki, A. G.; Malalasekera, A. P.; Schaaf, K.; Kutsch, O.; Bossmann, S. H.; Wolschendorf, F. Combinatorial Phenotypic Screen Uncovers Unrecognized Family of Extended Thiourea Inhibitors with Copper-Dependent Anti-Staphylococcal Activity. *Metallomics* **2016**, *8* (4), 412–421. https://doi.org/10.1039/c6mt00003g.

(71) Azevedo-Barbosa, H.; Dias, D. F.; Franco, L. L.; Hawkes, J. A.; Carvalho, D. T. From Antibacterial to Antitumour Agents: A Brief Review on The Chemical and Medicinal Aspects of Sulfonamides. *Mini Rev. Med. Chem.* **2020**, *20* (19), 2052–2066. https://doi.org/10.2174/1389557520666200905125738.

(72) Markowitz, N.; Quinn, E. L.; Saravolatz, L. D. Trimethoprim-Sulfamethoxazole Compared with Vancomycin for the Treatment of Staphylococcus Aureus Infection. *Ann. Intern. Med.* **1992**, *117* (5), 390–398. https://doi.org/10.7326/0003-4819-117-5-390.

(73) Bonomo, R. A.; Szabo, D. Mechanisms of Multidrug Resistance in Acinetobacter Species and Pseudomonas Aeruginosa. *Clin. Infect. Dis. an Off. Publ. Infect. Dis. Soc. Am.* **2006**, *43 Suppl 2*, S49-56. https://doi.org/10.1086/504477.

(74) Collignon, P. J.; Conly, J. M.; Andremont, A.; McEwen, S. A.; Aidara-Kane, A.; Agerso,

Y.; Andremont, A.; Collignon, P.; Conly, J.; Dang Ninh, T.; Donado-Godoy, P.; Fedorka-Cray, P.; Fernandez, H.; Galas, M.; Irwin, R.; Karp, B.; Matar, G.; McDermott, P.; McEwen, S.; Mitema, E.; Reid-Smith, R.; Scott, H. M.; Singh, R.; DeWaal, C. S.; Stelling, J.; Toleman, M.; Watanabe, H.; Woo, G.-J. World Health Organization Ranking of Antimicrobials According to Their Importance in Human Medicine: A Critical Step for Developing Risk Management Strategies to Control Antimicrobial Resistance From Food Animal Production. *Clin. Infect. Dis. an Off. Publ. Infect. Dis. Soc. Am.* **2016**, *63* (8), 1087–1093. https://doi.org/10.1093/cid/ciw475.

(75) Tomasz, A. The Mechanism of the Irreversible Antimicrobial Effects of Penicillins: How the Beta-Lactam Antibiotics Kill and Lyse Bacteria. *Annu. Rev. Microbiol.* **1979**, *33*, 113–137. https://doi.org/10.1146/annurev.mi.33.100179.000553.

(76) Challis, G. L. Genome Mining for Novel Natural Product Discovery. *J. Med. Chem.* **2008**, *51* (9), 2618–2628. https://doi.org/10.1021/jm700948z.

(77) Torres, J. A.; Villegas, M. V.; Quinn, J. P. Current Concepts in Antibiotic-Resistant Gram-Negative Bacteria. *Expert Rev. Anti. Infect. Ther.* **2007**, *5* (5), 833–843. https://doi.org/10.1586/14787210.5.5.833.

(78) Chastre, J.; Wunderink, R.; Prokocimer, P.; Lee, M.; Kaniga, K.; Friedland, I. Efficacy and Safety of Intravenous Infusion of Doripenem versus Imipenem in Ventilator-Associated Pneumonia: A Multicenter, Randomized Study. *Crit. Care Med.* **2008**, *36* (4), 1089–1096. https://doi.org/10.1097/CCM.0b013e3181691b99.

(79) Pankey, G. A.; Sabath, L. D. Clinical Relevance of Bacteriostatic versus Bactericidal Mechanisms of Action in the Treatment of Gram-Positive Bacterial Infections. *Clin. Infect. Dis.* **2004**, *38* (6), 864–870. https://doi.org/10.1086/381972.

(80) Falagas, M. E.; Kopterides, P. Old Antibiotics for Infections in Critically Ill Patients. *Curr. Opin. Crit. Care* **2007**, *13* (5), 592–597. https://doi.org/10.1097/MCC.0b013e32827851d7.

(81) Kehrenberg, C.; Schwarz, S.; Jacobsen, L.; Hansen, L. H.; Vester, B. A New Mechanism for Chloramphenicol, Florfenicol and Clindamycin Resistance: Methylation of 23S Ribosomal RNA at A2503. *Mol. Microbiol.* **2005**, *57* (4), 1064–1073. https://doi.org/10.1111/j.1365-2958.2005.04754.x.

(82) Chesneau, O.; Tsvetkova, K.; Courvalin, P. Resistance Phenotypes Conferred by Macrolide Phosphotransferases. *FEMS Microbiol. Lett.* **2007**, *269* (2), 317–322. https://doi.org/10.1111/j.1574-6968.2007.00643.x.

(83) Moore, R. A.; DeShazer, D.; Reckseidler, S.; Weissman, A.; Woods, D. E. Efflux-Mediated Aminoglycoside and Macrolide Resistance in Burkholderia Pseudomallei. *Antimicrob. Agents Chemother.* **1999**, *43* (3), 465–470. https://doi.org/10.1128/AAC.43.3.465.

(84) Roberts, M. C. Update on Acquired Tetracycline Resistance Genes. *FEMS Microbiol. Lett.* **2005**, *245* (2), 195–203. https://doi.org/10.1016/j.femsle.2005.02.034.

(85) No Title https://www.accessdata.fda.gov/scripts/cder/daf/index.cfm.

(86) Y., P. A.; Jennifer, A.; L., P. D. Tigecycline Efflux as a Mechanism for Nonsusceptibility in Acinetobacter Baumannii. *Antimicrob. Agents Chemother.* **2007**, *51* (6), 2065–2069. https://doi.org/10.1128/AAC.01198-06.

(87) Cetinkaya, Y.; Falk, P.; Mayhall, C. G. Vancomycin-Resistant Enterococci. *Clin. Microbiol. Rev.* **2000**, *13* (4), 686–707. https://doi.org/10.1128/CMR.13.4.686.

(88) Shaw, J. P.; Seroogy, J.; Kaniga, K.; Higgins, D. L.; Kitt, M.; Barriere, S.

Pharmacokinetics, Serum Inhibitory and Bactericidal Activity, and Safety of Telavancin in Healthy Subjects. *Antimicrob. Agents Chemother.* **2005**, *49* (1), 195–201. https://doi.org/10.1128/AAC.49.1.195-201.2005.

(89) Urgaonkar, S.; La Pierre, H. S.; Meir, I.; Lund, H.; RayChaudhuri, D.; Shaw, J. T. Synthesis of Antimicrobial Natural Products Targeting FtsZ: (+/-)-Dichamanetin and (+/-)-2’ ’ “-Hydroxy-5” ’-Benzylisouvarinol-B. *Org. Lett.* **2005**, *7* (25), 5609–5612. https://doi.org/10.1021/ol052269z.

(90) Tsiodras, S.; Gold, H. S.; Sakoulas, G.; Eliopoulos, G. M.; Wennersten, C.; Venkataraman, L.; Moellering, R. C.; Ferraro, M. J. Linezolid Resistance in a Clinical Isolate of Staphylococcus Aureus. *Lancet (London, England)*. England July 2001, pp 207–208. https://doi.org/10.1016/S0140-6736(01)05410-1.

(91) Bertsche, U.; Yang, S.-J.; Kuehner, D.; Wanner, S.; Mishra, N. N.; Roth, T.; Nega, M.; Schneider, A.; Mayer, C.; Grau, T.; Bayer, A. S.; Weidenmaier, C. Increased Cell Wall Teichoic Acid Production and D-Alanylation Are Common Phenotypes among Daptomycin-Resistant Methicillin-Resistant Staphylococcus Aureus (MRSA) Clinical Isolates. *PLoS One* **2013**, *8* (6), e67398. https://doi.org/10.1371/journal.pone.0067398.

(92) Lawrence, L.; Danese, P.; DeVito, J.; Franceschi, F.; Sutcliffe, J. In Vitro Activities of the Rx-01 Oxazolidinones against Hospital and Community Pathogens. *Antimicrob. Agents Chemother.* **2008**, *52* (5), 1653–1662. https://doi.org/10.1128/AAC.01383-07.

(93) Kohanski, M. A.; Dwyer, D. J.; Collins, J. J. How Antibiotics Kill Bacteria: From Targets to Networks. *Nat. Rev. Microbiol.* **2010**, *8* (6), 423–435. https://doi.org/10.1038/nrmicro2333.

(94) Li, J.; Nation, R. L.; Milne, R. W.; Turnidge, J. D.; Coulthard, K. Evaluation of Colistin as

an Agent against Multi-Resistant Gram-Negative Bacteria. *Int. J. Antimicrob. Agents* **2005**, *25* (1), 11–25. https://doi.org/10.1016/j.ijantimicag.2004.10.001.

(95) Rastogi, N.; Potar, M. C.; David, H. L. Antimycobacterial Spectrum of Colistin (Polymixin E). *Ann. Inst. Pasteur. Microbiol.* **1986**, *137A* (1), 45–53. https://doi.org/10.1016/s0769-2609(86)80004-7.

(96) Long, K. S.; Poehlsgaard, J.; Kehrenberg, C.; Schwarz, S.; Vester, B. The Cfr RRNA Methyltransferase Confers Resistance to Phenicols, Lincosamides, Oxazolidinones, Pleuromutilins, and Streptogramin A Antibiotics. *Antimicrob. Agents Chemother.* **2006**, *50* (7), 2500–2505. https://doi.org/10.1128/AAC.00131-06.

(97) Andries, K.; Verhasselt, P.; Guillemont, J.; Göhlmann, H. W. H.; Neefs, J.-M.; Winkler, H.; Van Gestel, J.; Timmerman, P.; Zhu, M.; Lee, E.; Williams, P.; de Chaffoy, D.; Huitric, E.; Hoffner, S.; Cambau, E.; Truffot-Pernot, C.; Lounis, N.; Jarlier, V. A Diarylquinoline Drug Active on the ATP Synthase of Mycobacterium Tuberculosis. *Science* **2005**, *307* (5707), 223–227. https://doi.org/10.1126/science.1106753.

(98) Choo, E. J.; Chambers, H. F. Treatment of Methicillin-Resistant Staphylococcus Aureus Bacteremia. *Infect. Chemother.* **2016**, *48* (4), 267–273. https://doi.org/10.3947/ic.2016.48.4.267.

(99) How much copper has been found in the world https://www.usgs.gov/faqs/how-much-copper-has-been-found-world?qt-news_science_products=0#qt-news_science_products.

(100) The Bronze Age Timeline https://www.softschools.com/viewTimeline.action?id=145.

(101) Gale, N. H.; Stos-Gale, Z. A. Bronze Age Copper Sources in the Mediterranean: A New Approach. *Science (80-.).* **1982**, *216* (4541), 11 LP – 19. https://doi.org/10.1126/science.216.4541.11.

(102) Bremner, I. Copper in Human Health https://www.copper.org/consumers/health/cu_health_uk.html.

(103) Bronze Age.

(104) Hansen, S.; Montero-Ruiz, I.; Rovira, S.; Steiniger, D.; Toderaş, M. The Earliest Lead Ore Processing in Europe. 5th Millennium BC Finds from Pietrele on the Lower Danube. *PLoS One* **2019**, *14* (4), e0214218–e0214218. https://doi.org/10.1371/journal.pone.0214218.

(105) Grass, G.; Rensing, C.; Solioz, M. Metallic Copper as an Antimicrobial Surface. *Appl. Environ. Microbiol.* **2011**, *77* (5), 1541–1547. https://doi.org/10.1128/AEM.02766-10.

(106) Festa, R. A.; Thiele, D. J. Copper: An Essential Metal in Biology Copper in Prokaryotes. *Festa RA, Thiele DJ. Copp. An Essent. Met. Biol. Curr. Biol.* **2011**, *21* (21), 877–883. https://doi.org/10.1016/j.cub.2011.09.040.Copper.

(107) Tishchenko, K. I.; Beloglazkina, E. K.; Mazhuga, A. G.; Zyk, N. V. Copper-Containing Enzymes: Site Types and Low-Molecular-Weight Model Compounds. *Rev. J. Chem.* **2016**, *6* (1), 49–82. https://doi.org/10.1134/S2079978016010027.

(108) Tabti, R.; Tounsi, N.; Gaiddon, C.; Bentouhami, E.; Desaubry, L. Progress in Copper Complexes as Anticancer Agents. *Med. Chem. (Los. Angeles).* **2017**, *07* (05), 875–879. https://doi.org/10.4172/2161-0444.1000445.

(109) Rajalakshmi, S.; Fathima, A.; Rao, J. R.; Nair, B. U. Antibacterial Activity of Copper(Ii) Complexes against Staphylococcus Aureus. *RSC Adv.* **2014**, *4* (60), 32004–32012. https://doi.org/10.1039/C4RA03241A.

(110) Dorotíková, S.; Kožíšková, J.; Malček, M.; Jomová, K.; Herich, P.; Plevová, K.; Briestenská, K.; Chalupková, A.; Mistríková, J.; Milata, V.; Dvoranová, D.; Bučinský, L.

Copper(II) Complexes with New Fluoroquinolones: Synthesis, Structure, Spectroscopic and Theoretical Study, DNA Damage, Cytotoxicity and Antiviral Activity. *J. Inorg. Biochem.* **2015**, *150*, 160–173. https://doi.org/10.1016/j.jinorgbio.2015.06.017.

(111) n, Eunsung Mouradian, M. M. 基因的改变NIH Public Access. *Bone* **2008**, *23* (1), 1–7.

(112) Mandal, T.; Kar, S.; Maji, S.; Sen, S.; Gupta, A. Structural and Functional Diversity Among the Members of CTR, the Membrane Copper Transporter Family. *J. Membr. Biol.* **2020**, *253* (5), 459–468. https://doi.org/10.1007/s00232-020-00139-w.

(113) Kahra, D.; Kovermann, M.; Wittung-Stafshede, P. The C-Terminus of Human Copper Importer Ctr1 Acts as a Binding Site and Transfers Copper to Atox1. *Biophys. J.* **2016**, *110* (1), 95–102. https://doi.org/10.1016/j.bpj.2015.11.016.

(114) Haeili, M.; Moore, C.; Davis, C. J. C.; Cochran, J. B.; Shah, S.; Shrestha, T. B.; Zhang, Y.; Bossmann, S. H.; Benjamin, W. H.; Kutsch, O.; Wolschendorf, F. Copper Complexation Screen Reveals Compounds with Potent Antibiotic Properties against Methicillin-Resistant <Span Class="Named-Content Genus-Species" Id="Named-Content-1">Staphylococcus Aureus</Span> *Antimicrob. Agents Chemother.* **2014**, *58* (7), 3727 LP – 3736. https://doi.org/10.1128/AAC.02316-13.

(115) Dalecki, A. G.; Malalasekera, A. P.; Schaaf, K.; Kutsch, O.; Bossmann, S. H.; Wolschendorf, F. Combinatorial Phenotypic Screen Uncovers Unrecognized Family of Extended Thiourea Inhibitors with Copper-Dependent Anti-Staphylococcal Activity. *Metallomics* **2016**, *8* (4), 412–421. https://doi.org/10.1039/C6MT00003G.

(116) Borkow, G.; Gabbay, J. Copper as a Biocidal Tool. *Curr. Med. Chem.* **2005**, *12* (18), 2163–2175. https://doi.org/10.2174/0929867054637617.

(117) Colin, M.; Klingelschmitt, F.; Charpentier, E.; Josse, J.; Kanagaratnam, L.; De Champs,

C.; Gangloff, S. C. Copper Alloy Touch Surfaces in Healthcare Facilities: An Effective Solution to Prevent Bacterial Spreading. *Mater. (Basel, Switzerland)* **2018**, *11* (12), 2479. https://doi.org/10.3390/ma11122479.

(118) Song, J.; Li, R.; Jiang, J. Copper Homeostasis in <I>Aspergillus Fumigatus</I>: Opportunities for Therapeutic Development. *Frontiers in microbiology*. The Key Laboratory of Biotechnology for Medicinal Plants of Jiangsu Province and School of Life Science, Jiangsu Normal University, Xuzhou, China. 2019, p 774. https://doi.org/10.3389/fmicb.2019.00774.

(119) Naseer, M.; Ramadan, R.; Xing, J.; Samak, N. A. Facile Green Synthesis of Copper Oxide Nanoparticles for the Eradication of Multidrug Resistant Klebsiella Pneumonia and Helicobacter Pylori Biofilms. *Int. Biodeterior. Biodegrad.* **2021**, *159* (February), 105201. https://doi.org/10.1016/j.ibiod.2021.105201.

(120) Lemishko, S. S.; Lemishko, A. S. Cu2+/Cu+ Redox Battery Utilizing Low-Potential External Heat for Recharge. *J. Phys. Chem. C* **2017**, *121* (6), 3234–3240. https://doi.org/10.1021/acs.jpcc.6b12317.

(121) Knight, J.; Caseldine, C.; Boykoff, M. T. Forum Review. *Geogr. J.* **2010**, *176* (3), 267–269. https://doi.org/10.1111/j.1475-4959.2010.00371.x.

(122) Popov, S.; Saphier, O.; Popov, M.; Shenker, M.; Entus, S.; Shotland, Y.; Saphier, M. Factors Enhancing the Antibacterial Effect of Monovalent Copper Ions. *Curr. Microbiol.* **2020**, *77* (3), 361–368. https://doi.org/10.1007/s00284-019-01794-6.

(123) Besold, A. N.; Culbertson, E. M.; Culotta, V. C. The Yin and Yang of Copper during Infection. *JBIC J. Biol. Inorg. Chem.* **2016**, *21* (2), 137–144. https://doi.org/10.1007/s00775-016-1335-1.

(124) Kehl-Fie, T. E.; Skaar, E. P. Nutritional Immunity beyond Iron: A Role for Manganese and Zinc. *Curr. Opin. Chem. Biol.* **2010**, *14* (2), 218–224. https://doi.org/https://doi.org/10.1016/j.cbpa.2009.11.008.

(125) White, C.; Lee, J.; Kambe, T.; Fritsche, K.; Petris, M. J. A Role for the ATP7A Copper-Transporting ATPase in Macrophage Bactericidal Activity. *J. Biol. Chem.* **2009**, *284* (49), 33949–33956. https://doi.org/10.1074/jbc.M109.070201.

(126) Achard, M. E. S.; Stafford, S. L.; Bokil, N. J.; Chartres, J.; Bernhardt, P. V; Schembri, M. A.; Sweet, M. J.; McEwan, A. G. Copper Redistribution in Murine Macrophages in Response to Salmonella Infection. *Biochem. J.* **2012**, *444* (1), 51–57. https://doi.org/10.1042/BJ20112180.

(127) Wagner, D.; Maser, J.; Lai, B.; Cai, Z.; Barry, C. E.; Höner zu Bentrup, K.; Russell, D. G.; Bermudez, L. E. Elemental Analysis of Mycobacterium Avium -, Mycobacterium Tuberculosis -, and Mycobacterium Smegmatis -Containing Phagosomes Indicates Pathogen-Induced Microenvironments within the Host Cell's Endosomal System . *J. Immunol.* **2005**, *174* (3), 1491–1500. https://doi.org/10.4049/jimmunol.174.3.1491.

(128) Pham, A. N.; Xing, G.; Miller, C. J.; Waite, T. D. Fenton-like Copper Redox Chemistry Revisited: Hydrogen Peroxide and Superoxide Mediation of Copper-Catalyzed Oxidant Production. *J. Catal.* **2013**, *301*, 54–64. https://doi.org/https://doi.org/10.1016/j.jcat.2013.01.025.

(129) Niederweis, M; Kutsch, O.; Wolschendorf, F. No Title, 2012.

(130) Somoskovi, A.; Parsons, L. M.; Salfinger, M. The Molecular Basis of Resistance to Isoniazid, Rifampin, and Pyrazinamide in Mycobacterium Tuberculosis. *Respir. Res.* **2001**, *2* (3), 164–168. https://doi.org/10.1186/rr54.

(131) Speer, A.; Shrestha, T. B.; Bossmann, S. H.; Basaraba, R. J.; Harber, G. J.; Michalek, S. M.; Niederweis, M.; Kutsch, O.; Wolschendorf, F. Copper-Boosting Compounds: A Novel Concept for Antimycobacterial Drug Discovery. *Antimicrob. Agents Chemother.* **2013**, *57* (2), 1089 LP – 1091. https://doi.org/10.1128/AAC.01781-12.

(132) Haeili, M.; Moore, C.; Davis, C. J. C.; Cochran, J. B.; Shah, S.; Shrestha, T. B.; Zhang, Y.; Bossmann, S. H.; Benjamin, W. H.; Kutsch, O.; Wolschendorf, F. Copper Complexation Screen Reveals Compounds with Potent Antibiotic Properties against Methicillin-Resistant Staphylococcus Aureus. *Antimicrob. Agents Chemother.* **2014**, *58* (7), 3727–3736. https://doi.org/10.1128/AAC.02316-13.

(133) Dalecki, A. G.; Wolschendorf, F. Development of a Web-Based Tool for Automated Processing and Cataloging of a Unique Combinatorial Drug Screen. *J. Microbiol. Methods* **2016**, *126*, 30–34. https://doi.org/10.1016/j.mimet.2016.04.013.

(134) Crawford, C. L.; Dalecki, A. G.; Narmore, W. T.; Hoff, J.; Hargett, A. A.; Renfrow, M. B.; Zhang, M.; Kalubowilage, M.; Bossmann, S. H.; Queern, S. L.; Lapi, S. E.; Hunter, R. N.; Bao, D.; Augelli-Szafran, C. E.; Kutsch, O.; Wolschendorf, F. Pyrazolopyrimidinones, a Novel Class of Copper-Dependent Bactericidal Antibiotics against Multi-Drug Resistant S. Aureus. *Metallomics* **2019**, *11* (4), 784–798. https://doi.org/10.1039/C8MT00316E.

(135) Dalecki, A. G.; Zorn, K. M.; Clark, A. M.; Ekins, S.; Narmore, W. T.; Tower, N.; Rasmussen, L.; Bostwick, R.; Kutsch, O.; Wolschendorf, F. High-Throughput Screening and Bayesian Machine Learning for Copper-Dependent Inhibitors of Staphylococcus Aureus†. *Metallomics* **2019**, *11* (3), 696–706. https://doi.org/10.1039/c8mt00342d.

(136) Crawford, C. L.; Dalecki, A. G.; Perez, M. D.; Schaaf, K.; Wolschendorf, F.; Kutsch, O. A Copper-Dependent Compound Restores Ampicillin Sensitivity in Multidrug-Resistant

Staphylococcus Aureus. *Sci. Rep.* **2020**, *10* (1), 8955. https://doi.org/10.1038/s41598-020-65978-y.

(137) Dalecki, A. G.; Crawford, C. L.; Wolschendorf, F. Copper and Antibiotics: Discovery, Modes of Action, and Opportunities for Medicinal Applications. *Adv. Microb. Physiol.* **2017**, *70*, 193–260. https://doi.org/10.1016/bs.ampbs.2017.01.007.

(138) Bossmann, S. H.; Kalubowilage, M.; Zhang, M.; Delpe-Acharige, A.; Eschliman, K.; Wolschendorf, F.; Kutsch, O.; Dalecki, A.; Narmore, W. Compounds with Copper- or Zinc-Activated Toxicity against Microbial Infection. WO2020061412A1, 2020.

(139) Udaya Kumar, A. H.; Kumara, K.; Harohally, N. V; Pampa, K. J.; Lokanath, N. K. Square Planar Trans-N2O2 Cu(II) Complex: Synthesis, Crystal Structure, Hirshfeld Surface, DFT, Antimicrobial and Docking Studies. *ChemistrySelect* **2021**, *6* (24), 6240–6255. https://doi.org/https://doi.org/10.1002/slct.202101149.

(140) Munzeiwa, W. A.; Oladipo, S. D.; Ibeji, C. U.; Mocktar, C.; Omondi, B. Copper(II)-N-Hydroxy-N,N'-Diarylformamidine Complexes: Synthesis, Crystal Structures, Antibacterial and Molecular Docking Studies. *J. Inorg. Biochem.* **2021**, *225*, 111600. https://doi.org/10.1016/j.jinorgbio.2021.111600.

(141) Hema, M. K.; Karthik, C. S.; Mahesha; Pampa, K. J.; Mallu, P.; Lokanath, N. K. 4,4,4-Trifluoro-1-Phenylbutane-1,3-Dione Metal [Cu(II) and Ni(II)] Complexes as an Superlative Antibacterial Agent against MRSA: Synthesis, Structural Quantum-Chemical and Molecular Docking Studies. *J. Mol. Struct.* **2021**, *1243*, 130774. https://doi.org/https://doi.org/10.1016/j.molstruc.2021.130774.

(142) Touj, N.; Nasr, I. S. Al; Koko, W. S.; Khan, T. A.; Özdemir, I.; Yasar, S.; Mansour, L.; Alresheedi, F.; Hamdi, N. Anticancer, Antimicrobial and Antiparasitical Activities of

Copper(I) Complexes Based on N-Heterocyclic Carbene (NHC) Ligands Bearing Aryl Substituents. *J. Coord. Chem.* **2020**, *73* (20–22), 2889–2905. https://doi.org/10.1080/00958972.2020.1836359.

(143) Ghorab, M. M.; Alqahtani, A. S.; Soliman, A. M.; Askar, A. A. Novel N-(Substituted) Thioacetamide Quinazolinone Benzenesulfonamides as Antimicrobial Agents. *Int. J. Nanomedicine* **2020**, *15*, 3161–3180. https://doi.org/10.2147/IJN.S241433.

(144) Barrett, S.; Delaney, S.; Kavanagh, K.; Montagner, D. Evaluation of in Vitro and in Vivo Antibacterial Activity of Novel Cu(II)-Steroid Complexes. *Inorganica Chim. Acta* **2018**, *479*, 261–265. https://doi.org/https://doi.org/10.1016/j.ica.2018.04.054.

(145) Gwon, K.; Kim, Y.; Cho, H.; Lee, S.; Yang, S.-H.; Kim, S.-J.; Lee, D. N. Robust Copper Metal–Organic Framework-Embedded Polysiloxanes for Biomedical Applications: Its Antibacterial Effects on MRSA and In Vitro Cytotoxicity. *Nanomaterials* . 2021. https://doi.org/10.3390/nano11030719.

(146) Jo, J. H.; Kim, H.-C.; Huh, S.; Kim, Y.; Lee, D. N. Antibacterial Activities of Cu-MOFs Containing Glutarates and Bipyridyl Ligands. *Dalt. Trans.* **2019**, *48* (23), 8084–8093. https://doi.org/10.1039/C9DT00791A.

(147) Ren, G.; Hu, D.; Cheng, E. W. C.; Vargas-Reus, M. A.; Reip, P.; Allaker, R. P. Characterisation of Copper Oxide Nanoparticles for Antimicrobial Applications. *Int. J. Antimicrob. Agents* **2009**, *33* (6), 587–590. https://doi.org/https://doi.org/10.1016/j.ijantimicag.2008.12.004.

(148) Niaz, N.; Bano, A.; Fasim, F.; Kausar, R.; Khan, B. A.; Zafar, N.; Khan, S.; Uzair, B. Synthesis, Characterization and Evaluation of Antibacterial Activity of Copper Oxide Nanoparticles against Clinical Strains of Staphylococcus Aureus. *Pak. J. Pharm. Sci.*

2018, *31* (4(Supplementary)), 1549–1553.

(149) Zhang, L.; Lou, J.; Zhang, W.; Wu, C.; Jin, Z. Bacteria Killing in ICU Associated Infections: Antibacterial Nanosheets as Disinfectant. *RSC Adv.* **2018**, *8* (1), 278–283. https://doi.org/10.1039/C7RA12148B.

(150) Kondranova, A. M.; Lozhkomoev, A. S.; Kazantsev, S. O.; Pervikov, A. V. Synthesis and Antimicrobical Activity of Composite Oxides Nanoparticles Based on ZnO. *IOP Conf. Ser. Mater. Sci. Eng.* **2019**, *684* (1), 1–7. https://doi.org/10.1088/1757-899X/684/1/012012.

(151) Balcucho, J.; Narváez, D. M.; Castro-Mayorga, J. L. Antimicrobial and Biocompatible Polycaprolactone and Copper Oxide Nanoparticle Wound Dressings against Methicillin-Resistant Staphylococcus Aureus. *Nanomaterials* . 2020. https://doi.org/10.3390/nano10091692.

(152) Zhen, X.; Chudal, L.; Pandey, N. K.; Phan, J.; Ran, X.; Amador, E.; Huang, X.; Johnson, O.; Ran, Y.; Chen, W.; Hamblin, M. R.; Huang, L. A Powerful Combination of Copper-Cysteamine Nanoparticles with Potassium Iodide for Bacterial Destruction. *Mater. Sci. Eng. C* **2020**, *110*, 110659. https://doi.org/https://doi.org/10.1016/j.msec.2020.110659.

(153) Kannan, S.; Solomon, A.; Krishnamoorthy, G.; Marudhamuthu, M. Liposome Encapsulated Surfactant Abetted Copper Nanoparticles Alleviates Biofilm Mediated Virulence in Pathogenic Pseudomonas Aeruginosa and MRSA. *Sci. Rep.* **2021**, *11* (1), 1102. https://doi.org/10.1038/s41598-020-79976-7.

(154) Saporito-Magriñá, C. M.; Musacco-Sebio, R. N.; Andrieux, G.; Kook, L.; Orrego, M. T.; Tuttolomondo, M. V.; Desimone, M. F.; Boerries, M.; Borner, C.; Repetto, M. G. Copper-Induced Cell Death and the Protective Role of Glutathione: The Implication of Impaired

Protein Folding Rather than Oxidative Stress. *Metallomics* **2018**, *10* (12), 1743–1754. https://doi.org/10.1039/c8mt00182k.

(155) Lutsenko, S. Human Copper Homeostasis: A Network of Interconnected Pathways. *Curr. Opin. Chem. Biol.* **2010**, *14* (2), 211–217. https://doi.org/10.1016/j.cbpa.2010.01.003.

(156) Solioz, M.; Abicht, H. K.; Mermod, M.; Mancini, S. Response of Gram-Positive Bacteria to Copper Stress. *J. Biol. Inorg. Chem. JBIC a Publ. Soc. Biol. Inorg. Chem.* **2010**, *15* (1), 3–14. https://doi.org/10.1007/s00775-009-0588-3.

(157) Besold, A. N.; Culbertson, E. M.; Cullota, V. C. The Yin and Yang of Copper During Infection Angelique. *J Biol Inorg Chem.* **2016**, *21(2)* (1), 137–144. https://doi.org/10.1007/s00775-016-1335-1.The.

(158) Monteith, A. J.; Skaar, E. P. The Impact of Metal Availability on Immune Function during Infection. *Trends Endocrinol. Metab.* **2021**, *32* (11), 916–928. https://doi.org/10.1016/j.tem.2021.08.004.

(159) Wagner, D.; Maser, J.; Lai, B.; Cai, Z.; Barry, C. E. 3rd; Höner Zu Bentrup, K.; Russell, D. G.; Bermudez, L. E. Elemental Analysis of Mycobacterium Avium-, Mycobacterium Tuberculosis-, and Mycobacterium Smegmatis-Containing Phagosomes Indicates Pathogen-Induced Microenvironments within the Host Cell's Endosomal System. *J. Immunol.* **2005**, *174* (3), 1491–1500. https://doi.org/10.4049/jimmunol.174.3.1491.

(160) Peters, K.; Pazos, M.; Edoo, Z.; Hugonnet, J.-E.; Martorana, A. M.; Polissi, A.; VanNieuwenhze, M. S.; Arthur, M.; Vollmer, W. Copper Inhibits Peptidoglycan LD-Transpeptidases Suppressing β-Lactam Resistance Due to Bypass of Penicillin-Binding Proteins. *Proc. Natl. Acad. Sci. U. S. A.* **2018**, *115* (42), 10786–10791. https://doi.org/10.1073/pnas.1809285115.

(161) Rosario-Cruz, Z.; Eletsky, A.; Daigham, N. S.; Al-Tameemi, H.; Swapna, G. V. T.; Kahn, P. C.; Szyperski, T.; Montelione, G. T.; Boyd, J. M. The CopBL Operon Protects Staphylococcus Aureus from Copper Toxicity: CopL Is an Extracellular Membrane-Associated Copper-Binding Protein. *J. Biol. Chem.* **2019**, *294* (11), 4027–4044. https://doi.org/10.1074/jbc.RA118.004723.

(162) Shoshan, M. S.; Tshuva, E. Y. The MXCXXC Class of Metallochaperone Proteins: Model Studies. *Chem. Soc. Rev.* **2011**, *40* (11), 5282–5292. https://doi.org/10.1039/C1CS15086C.

(163) Canton, J.; Khezri, R.; Glogauer, M.; Grinstein, S. Contrasting Phagosome PH Regulation and Maturation in Human M1 and M2 Macrophages. *Mol. Biol. Cell* **2014**, *25* (21), 3330–3341. https://doi.org/10.1091/mbc.E14-05-0967.

(164) Galli, S. J.; Borregaard, N.; Wynn, T. A. Phenotypic and Functional Plasticity of Cells of Innate Immunity: Macrophages, Mast Cells and Neutrophils. *Nat. Immunol.* **2011**, *12* (11), 1035–1044. https://doi.org/10.1038/ni.2109.

(165) Namiecińska, E.; Sobiesiak, M.; Małecka, M.; Guga, P.; Budzisz*, B. R. and E. Antimicrobial and Structural Properties of Metal Ions Complexes with Thiosemicarbazide Motif and Related Heterocyclic Compounds. *Current Medicinal Chemistry*. 2019, pp 664–693. https://doi.org/http://dx.doi.org/10.2174/0929867325666180228164656.

(166) Thanh, N. D.; Duc, H. T.; Duyen, V. T.; Tuong, P. M.; Quoc, N. Synthesis and Antibacterial and Antifungal Activities of N-(Tetra-O-Acetyl-β-d-Glucopyranosyl)Thiosemicarbazones of Substituted 4-Formylsydnones. *Chem. Cent. J.* **2015**, *9* (1), 1–14. https://doi.org/10.1186/s13065-015-0138-8.

(167) Banerjee, D.; Yogeeswari, P.; Bhat, P.; Thomas, A.; Srividya, M.; Sriram, D. Novel

Isatinyl Thiosemicarbazones Derivatives as Potential Molecule to Combat HIV-TB Co-Infection. *Eur. J. Med. Chem.* **2011**, *46* (1), 106–121. https://doi.org/https://doi.org/10.1016/j.ejmech.2010.10.020.

(168) de Oliveira, R. B.; de Souza-Fagundes, E. M.; Soares, R. P. P.; Andrade, A. A.; Krettli, A. U.; Zani, C. L. Synthesis and Antimalarial Activity of Semicarbazone and Thiosemicarbazone Derivatives. *Eur. J. Med. Chem.* **2008**, *43* (9), 1983–1988. https://doi.org/https://doi.org/10.1016/j.ejmech.2007.11.012.

(169) Rogolino, D.; Gatti, A.; Carcelli, M.; Pelosi, G.; Bisceglie, F.; Restivo, F. M.; Degola, F.; Buschini, A.; Montalbano, S.; Feretti, D.; Zani, C. Thiosemicarbazone Scaffold for the Design of Antifungal and Antiaflatoxigenic Agents: Evaluation of Ligands and Related Copper Complexes. *Sci. Rep.* **2017**, *7* (1), 11214. https://doi.org/10.1038/s41598-017-11716-w.

(170) Mrozek-Wilczkiewicz, A.; Malarz, K.; Rejmund, M.; Polanski, J.; Musiol, R. Anticancer Activity of the Thiosemicarbazones That Are Based on Di-2-Pyridine Ketone and Quinoline Moiety. *Eur. J. Med. Chem.* **2019**, *171*, 180–194. https://doi.org/https://doi.org/10.1016/j.ejmech.2019.03.027.

(171) Gambinob, H. B. and D. The Wide Pharmacological Versatility of Semicarbazones, Thiosemicarbazones and Their Metal Complexes. *Mini-Reviews in Medicinal Chemistry*. 2004, pp 31–39. https://doi.org/http://dx.doi.org/10.2174/1389557043487484.

(172) Ohui, K.; Afanasenko, E.; Bacher, F.; Ting, R. L. X.; Zafar, A.; Blanco-Cabra, N.; Torrents, E.; Dömötör, O.; May, N. V; Darvasiova, D.; Enyedy, É. A.; Popović-Bijelić, A.; Reynisson, J.; Rapta, P.; Babak, M. V; Pastorin, G.; Arion, V. B. New Water-Soluble Copper(II) Complexes with Morpholine–Thiosemicarbazone Hybrids: Insights into the

Anticancer and Antibacterial Mode of Action. *J. Med. Chem.* **2019**, *62* (2), 512–530. https://doi.org/10.1021/acs.jmedchem.8b01031.

(173) Pahontu, E.; Julea, F.; Rosu, T.; Purcarea, V.; Chumakov, Y.; Petrenco, P.; Gulea, A. Antibacterial, Antifungal and in Vitro Antileukaemia Activity of Metal Complexes with Thiosemicarbazones. *J. Cell. Mol. Med.* **2015**, *19* (4), 865–878. https://doi.org/10.1111/jcmm.12508.

(174) Zeglis, B. M.; Divilov, V.; Lewis, J. S. Role of Metalation in the Topoisomerase IIα Inhibition and Antiproliferation Activity of a Series of α-Heterocyclic-N 4-Substituted Thiosemicarbazones and Their Cu(II) Complexes. *J. Med. Chem.* **2011**, *54* (7), 2391–2398. https://doi.org/10.1021/jm101532u.

(175) Mahendiran, D.; Amuthakala, S.; Bhuvanesh, N. S. P.; Kumar, R. S.; Rahiman, A. K. Copper Complexes as Prospective Anticancer Agents:: In Vitro and in Vivo Evaluation, Selective Targeting of Cancer Cells by DNA Damage and S Phase Arrest. *RSC Adv.* **2018**, *8* (30), 16973–16990. https://doi.org/10.1039/c8ra00954f.

(176) Liu, H.; Yang, W.; Zhou, W.; Xu, Y.; Xie, J.; Li, M. Crystal Structures and Antimicrobial Activities of Copper(II) Complexes of Fluorine-Containing Thioureido Ligands. *Inorganica Chim. Acta* **2013**, *405*, 387–394. https://doi.org/https://doi.org/10.1016/j.ica.2013.06.029.

(177) Helsel, M. E.; Franz, K. J. Pharmacological Activity of Metal Binding Agents That Alter Copper Bioavailability. *Dalton Trans.* **2015**, *44* (19), 8760–8770. https://doi.org/10.1039/c5dt00634a.

(178) Freedman, J. H.; Ciriolo, M. R.; Peisach, J. The Role of Glutathione in Copper Metabolism and Toxicity. *J. Biol. Chem.* **1989**, *264* (10), 5598–5605.

(179) Chauhan, A.; Kumar, M.; Kumar, A.; Kanchan, K. Comprehensive Review on Mechanism of Action, Resistance and Evolution of Antimycobacterial Drugs. *Life Sci.* **2021**, *274*, 119301. https://doi.org/10.1016/j.lfs.2021.119301.

(180) Kovacic, P.; Somanathan, R. Toxicity of Imine–Iminium Dyes and Pigments: Electron Transfer, Radicals, Oxidative Stress and Other Physiological Effects. *J. Appl. Toxicol.* **2014**, *34* (8), 825–834. https://doi.org/https://doi.org/10.1002/jat.3005.

(181) Kovacic, P.; Somanathan, R. New Developments in the Mechanism of Drug Action and Toxicity of Conjugated. **2014**, No. July, 583–597.

(182) Thanh, N. D.; Hai, D. S.; Ha, N. T. T.; Tung, D. T.; Le, C. T.; Van, H. T. K.; Toan, V. N.; Toan, D. N.; Dang, L. H. Synthesis, Biological Evaluation and Molecular Docking Study of 1,2,3-1H-Triazoles Having 4H-Pyrano[2,3-d]Pyrimidine as Potential Mycobacterium Tuberculosis Protein Tyrosine Phosphatase B Inhibitors. *Bioorg. Med. Chem. Lett.* **2019**, *29* (2), 164–171. https://doi.org/https://doi.org/10.1016/j.bmcl.2018.12.009.

(183) Freeman, J. L.; Li, F. F.; Furkert, D. P.; Brimble, M. A. Synthetic Studies towards Spirocyclic Imine Marine Toxins Using N -Acyl Iminium Ions as Dienophiles in Diels-Alder Reactions. *Synlett* **2020**, *31* (7), 657–671. https://doi.org/10.1055/s-0039-1691593.

(184) Davies, W. L.; Grunert, R. R.; Haff, R. F.; McGahen, J. W.; Neumayer, E. M.; Paulshock, M.; Watts, J. C.; Wood, T. R.; Hermann, E. C.; Hoffmann, C. E. Antiviral Activity of 1-Adamantanamine (Amantadine). *Science (80-.).* **1964**, *144* (3620), 862 LP – 863. https://doi.org/10.1126/science.144.3620.862.

(185) Khaziev, R.; Shtyrlin, N.; Pavelyev, R.; Nigmatullin, R.; Gabbasova, R.; Grishaev, D.; Shtro, A.; Galochkina, A.; Nikolaeva, Y.; Vinogradova, T.; Manicheva, O.; Dogonadze, M.; Gnezdilov, O.; Sokolovich, E.; Yablonskiy, P.; Shtyrlin*, K. B. and Y. Synthesis and

Antimicrobial Activity of Adamantyl Substituted Pyridoxine Derivatives. *Letters in Drug Design & Discovery*. 2019, pp 1360–1369. https://doi.org/http://dx.doi.org/10.2174/1570180816666190911150705.

(186) Kukushkin, M. E.; Skvortsov, D. A.; Kalinina, M. A.; Tafeenko, V. A.; Burmistrov, V. V; Butov, G. M.; Zyk, N. V; Majouga, A. G.; Beloglazkina, E. K. Synthesis and Cytotoxicity of Novel Oxindoles Dispiro Derivatives with Thiohydantoin and Adamantane Fragments. *Beilstein Arch.* **2019**.

(187) Augeri, D. J.; Robl, J. A.; Betebenner, D. A.; Magnin, D. R.; Khanna, A.; Robertson, J. G.; Wang, A.; Simpkins, L. M.; Taunk, P.; Huang, Q.; Han, S.-P.; Abboa-Offei, B.; Cap, M.; Xin, L.; Tao, L.; Tozzo, E.; Welzel, G. E.; Egan, D. M.; Marcinkeviciene, J.; Chang, S. Y.; Biller, S. A.; Kirby, M. S.; Parker, R. A.; Hamann, L. G. Discovery and Preclinical Profile of Saxagliptin (BMS-477118): A Highly Potent, Long-Acting, Orally Active Dipeptidyl Peptidase IV Inhibitor for the Treatment of Type 2 Diabetes. *J. Med. Chem.* **2005**, *48* (15), 5025–5037. https://doi.org/10.1021/jm050261p.

(188) Ji, N.; Meredith, E.; Liu, D.; Adams, C. M.; Artman, G. D.; Jendza, K. C.; Ma, F.; Mainolfi, N.; Powers, J. J.; Zhang, C. Syntheses of 1-Substituted-3-Aminopyrazoles. *Tetrahedron Lett.* **2010**, *51* (52), 6799–6801. https://doi.org/https://doi.org/10.1016/j.tetlet.2010.10.073.

(189) Sivasankar, C.; Sadhukhan, N.; Bera, J. K.; Samuelson, A. G. Is Copper(i) Hard or Soft? A Density Functional Study of Mixed Ligand Complexes. *New J. Chem.* **2007**, *31* (3), 385–393. https://doi.org/10.1039/B618494B.

(190) Gentry, C. L.; Egleton, R. D.; Gillespie, T.; Abbruscato, T. J.; Bechowski, H. B.; Hruby, V. J.; Davis, T. P. The Effect of Halogenation on Blood-Brain Barrier Permeability of a

Novel Peptide Drug. *Peptides* **1999**, *20* (10), 1229–1238. https://doi.org/10.1016/S0196-9781(99)00127-8.

(191) Molchanova, N.; Nielsen, J. E.; Sørensen, K. B.; Prabhala, B. K.; Hansen, P. R.; Lund, R.; Barron, A. E.; Jenssen, H. Halogenation as a Tool to Tune Antimicrobial Activity of Peptoids. *Sci. Rep.* **2020**, *10* (1), 1–10. https://doi.org/10.1038/s41598-020-71771-8.

(192) Secrieru, A.; O'Neill, P. M.; Cristiano, M. L. S. Revisiting the Structure and Chemistry of 3(5)-Substituted Pyrazoles. *Molecules* **2019**, *25* (1), 42. https://doi.org/10.3390/molecules25010042.

(193) Merlic, C. A.; Motamed, S.; Quinn, B. Structure Determination and Synthesis of Fluoro Nissl Green: An RNA-Binding Fluorochrome. *J. Org. Chem.* **1995**, *60* (11), 3365–3369. https://doi.org/10.1021/jo00116a020.

(194) Moriyama, K.; Suzuki, T.; Negishi, K.; Graci, J. D.; Thompson, C. N.; Cameron, C. E.; Watanabe, M. Effects of Introduction of Hydrophobic Group on Ribavirin Base on Mutation Induction and Anti-RNA Viral Activity. *J. Med. Chem.* **2008**, *51* (1), 159–166. https://doi.org/10.1021/jm7009952.

(195) Yuan, X.; Wu, H.; Bu, H.; Zheng, P.; Zhou, J.; Zhang, H. Design, Synthesis and Biological Evaluation of Pyridone–Aminal Derivatives as MNK1/2 Inhibitors. *Bioorganic Med. Chem.* **2019**, *27* (7), 1211–1225. https://doi.org/10.1016/j.bmc.2019.02.007.

(196) Huang, H.; Si, P.; Wang, L.; Xu, Y.; Xu, X.; Zhu, J.; Jiang, H.; Li, W.; Chen, L.; Li, J. Design, Synthesis, and Biological Evaluation of Novel Nonsteroidal Farnesoid X Receptor (FXR) Antagonists: Molecular Basis of FXR Antagonism. *ChemMedChem* **2015**, *10* (7), 1184–1199. https://doi.org/https://doi.org/10.1002/cmdc.201500136.

(197) Renny, J. S.; Tomasevich, L. L.; Tallmadge, E. H.; Collum, D. B. Method of Continuous

Variations: Applications of Job Plots to the Study of Molecular Associations in Organometallic Chemistry. *Angew. Chemie Int. Ed.* **2013**, *52* (46), 11998–12013. https://doi.org/https://doi.org/10.1002/anie.201304157.

(198) Hammett, L. P. The Effect of Structure upon the Reactions of Organic Compounds. Benzene Derivatives. *J. Am. Chem. Soc.* **1937**, *59* (1), 96–103. https://doi.org/10.1021/ja01280a022.

(199) Hansch, C.; Leo, A.; Taft, R. W. A Survey of Hammett Substituent Constants and Resonance and Field Parameters. *Chem. Rev.* **1991**, *91* (2), 165–195. https://doi.org/10.1021/cr00002a004.

(200) Carey, Francis A., R. J. S. *Advanced Organic Chemistry Part A: Structure and Mechanisms*; Springer, Boston, MA, 2007.

(201) Chapman, N.B., Shorter, J. *Advances in Linear Free Energy Relationships*; Springer, Boston, MA, 1972.

(202) Katori, T.; Itoh, S.; Sato, M.; Yamataka, H. Reaction Pathways and Possible Path Bifurcation for the Schmidt Reaction. *J. Am. Chem. Soc.* **2010**, *132* (10), 3413–3422. https://doi.org/10.1021/ja908899u.

(203) Thapa, B.; Schlegel, H. B. Density Functional Theory Calculation of PKa's of Thiols in Aqueous Solution Using Explicit Water Molecules and the Polarizable Continuum Model. *J. Phys. Chem. A* **2016**, *120* (28), 5726–5735. https://doi.org/10.1021/acs.jpca.6b05040.

(204) Cottrell T.L. *The Strengths of Chemical Bonds*; London : Butterworths, 1958.

(205) Gapsys, V.; Michielssens, S.; Peters, J. H.; de Groot, B. L.; Leonov, H. Calculation of Binding Free Energies. *Methods Mol. Biol.* **2015**, *1215*, 173–209. https://doi.org/10.1007/978-1-4939-1465-4_9.

(206) supramolecular.org http://app.supramolecular.org/bindsim/.

(207) SwissADME http://www.swissadme.ch/index.php.

(208) Daina, A.; Michielin, O.; Zoete, V. SwissADME: A Free Web Tool to Evaluate Pharmacokinetics, Drug-Likeness and Medicinal Chemistry Friendliness of Small Molecules. *Sci. Rep.* **2017**, *7* (1), 42717. https://doi.org/10.1038/srep42717.

(209) Daina, A.; Michielin, O.; Zoete, V. ILOGP: A Simple, Robust, and Efficient Description of n-Octanol/Water Partition Coefficient for Drug Design Using the GB/SA Approach. *J. Chem. Inf. Model.* **2014**, *54* (12), 3284–3301. https://doi.org/10.1021/ci500467k.

(210) Daina, A.; Zoete, V. A BOILED-Egg To Predict Gastrointestinal Absorption and Brain Penetration of Small Molecules. *ChemMedChem* **2016**, *11* (11), 1117–1121. https://doi.org/10.1002/cmdc.201600182.

(211) Liu, J.; Obando, D.; Liao, V.; Lifa, T.; Codd, R. The Many Faces of the Adamantyl Group in Drug Design. *Eur. J. Med. Chem.* **2011**, *46* (6), 1949–1963. https://doi.org/10.1016/j.ejmech.2011.01.047.

(212) GERZON, K.; KRUMKALNS, E. V; BRINDLE, R. L.; MARSHALL, F. J.; ROOT, M. A. THE ADAMANTYL GROUP IN MEDICINAL AGENTS. I. HYPOGLYCEMIC N-ARYLSULFONYL-N’ -ADAMANTYLUREAS. *J. Med. Chem.* **1963**, *6*, 760–763. https://doi.org/10.1021/jm00342a029.

(213) Wanka, L.; Iqbal, K.; Schreiner, P. R. The Lipophilic Bullet Hits the Targets: Medicinal Chemistry of Adamantane Derivatives. *Chem. Rev.* **2013**, *113* (5), 3516–3604. https://doi.org/10.1021/cr100264t.

(214) Li, Q.; Jin, C.; Petukhov, P. A.; Rukavishnikov, A. V; Zaikova, T. O.; Phadke, A.; LaMunyon, D. H.; Lee, M. D.; Keana, J. F. W. Synthesis of Well-Defined Tower-Shaped

1,3,5-Trisubstituted Adamantanes Incorporating a Macrocyclic Trilactam Ring System. *J. Org. Chem.* **2004**, *69* (4), 1010–1019. https://doi.org/10.1021/jo035640+.

(215) Wolschendorf, F.; Ackart, D.; Shrestha, T. B.; Hascall-Dove, L.; Nolan, S.; Lamichhane, G.; Wang, Y.; Bossmann, S. H.; Basaraba, R. J.; Niederweis, M. Copper Resistance Is Essential for Virulence of Mycobacterium Tuberculosis. *Proc. Natl. Acad. Sci. U. S. A.* **2011**, *108* (4), 1621–1626. https://doi.org/10.1073/pnas.1009261108.

(216) Olah, G. A.; Surya Prakash, G. K.; Shih, J. G.; Krishnamurthy, V. V.; Mateescu, G. D.; Liang, G.; Sipos, G.; Buss, V.; Gund, T. M.; Ragué Schleyer, P. V. Bridgehead Adamantyl, Diamantyl, and Related Cations and Dications. *J. Am. Chem. Soc.* **1985**, *107* (9), 2764–2772. https://doi.org/10.1021/ja00295a032.

(217) Sunko, D.; Hiršl-Starčević, S.; Pollack, S.; Hehre, W. Hyperconjugation and Homohyperconjugation in the 1-Adamantyl Cation. Qualitative Models for γ-Deuterium Isotope Effects. *J. Am. Chem. Soc.* **1979**, *101* (21), 6163–6170. https://doi.org/10.1021/ja00515a002.

(218) Daeniker, H. U. 1-Hydrazinoadamantan. *Helv. Chim. Acta* **1967**, *50* (7), 2008–2010. https://doi.org/10.1002/hlca.19670500733.

(219) Butov, G. M.; Mokhov, V. M. Chemical Transformations of Tetracyclo[3.3.1.13,7.01,3]Decane (1,3-Dehydroadamantane): VII. Reaction of 1,3-Dehydroadamantane with Alkanediols and Amino Alcohols. *Russ. J. Org. Chem.* **2018**, *54* (12), 1760–1763.

(220) T. Thomas; B. Shetty. Preparation of Hydrazinoadamantane Compounds, 1968.

(221) Sam, D.; Claramunt, R. M.; Elguero, J. Rearreagement of 1 -Amino- and 1 -Alkylamino-Pyrazoles to 5-Aminopyrazoles. **1990**, No. 2, 244–245.

(222) Zhao, Z.; Wang, Z. Halogenation of Pyrazoles Using N-Halosuccinimides in CCl4 and in Water. *Synth. Commun.* **2007**, *37* (1), 137–147. https://doi.org/10.1080/00397910600978549.

(223) Rajalakshmanan, E.; Alexander, V. Synthesis of Dimethylbipyridines by the Reductive Coupling of 2-Halomethylpyridines with Nickel Catalyst. *Synth. Commun.* **2005**, *35* (6), 891–895. https://doi.org/10.1081/SCC-200051056.

(224) Sun, N.; Li, B.; Shao, J.; Mo, W.; Hu, B.; Shen, Z.; Hu, X. A General and Facile One-Pot Process of Isothiocyanates from Amines under Aqueous Conditions. *Beilstein J. Org. Chem.* **2012**, *8*, 61–70.

(225) Ottaviani, M. F.; Bossmann, S.; Turro, N. J.; Tomalia, D. A. Characterization of Starburst Dendrimers by the EPR Technique. 1. Copper Complexes in Water Solution. *J. Am. Chem. Soc.* **1994**, *116* (2), 661–671. https://doi.org/10.1021/ja00081a029.

(226) Djoko, K. Y.; Goytia, M. M.; Donnelly, P. S.; Schembri, M. A.; Shafer, W. M.; McEwan, A. G. Copper(II)-Bis(Thiosemicarbazonato) Complexes as Antibacterial Agents: Insights into Their Mode of Action and Potential as Therapeutics. *Antimicrob. Agents Chemother.* **2015**, *59* (10), 6444 LP – 6453. https://doi.org/10.1128/AAC.01289-15.

(227) Deng, J.; Yu, P.; Zhang, Z.; Wang, J.; Cai, J.; Wu, N.; Sun, H.; Liang, H.; Yang, F. Designing Anticancer Copper(II) Complexes by Optimizing 2-Pyridine-Thiosemicarbazone Ligands. *Eur. J. Med. Chem.* **2018**, *158*, 442–452. https://doi.org/https://doi.org/10.1016/j.ejmech.2018.09.020.

(228) Palanimuthu, D.; Shinde, S. V.; Somasundaram, K.; Samuelson, A. G. In Vitro and in Vivo Anticancer Activity of Copper Bis(Thiosemicarbazone) Complexes. *J. Med. Chem.* **2013**, *56* (3), 722–734. https://doi.org/10.1021/jm300938r.

(229) van Meerloo, J.; Kaspers, G. J. L.; Cloos, J. Cell Sensitivity Assays: The MTT Assay. *Methods Mol. Biol.* **2011**, *731*, 237–245. https://doi.org/10.1007/978-1-61779-080-5_20.

(230) Stark, R.; Grzelak, M.; Hadfield, J. RNA Sequencing: The Teenage Years. *Nat. Rev. Genet.* **2019**, *20* (11), 631–656. https://doi.org/10.1038/s41576-019-0150-2.

(231) Kinase Screening & Profiling Services https://www.discoverx.com/services/drug-discovery-development-services/kinase-profiling.

(232) Baba, T.; Bae, T.; Schneewind, O.; Takeuchi, F.; Hiramatsu, K. Genome Sequence of <Em>Staphylococcus Aureus</Em> Strain Newman and Comparative Analysis of Staphylococcal Genomes: Polymorphism and Evolution of Two Major Pathogenicity Islands. *J. Bacteriol.* **2008**, *190* (1), 300 LP – 310. https://doi.org/10.1128/JB.01000-07.

(233) Nigst, T. A.; Antipova, A.; Mayr, H. Nucleophilic Reactivities of Hydrazines and Amines: The Futile Search for the α-Effect in Hydrazine Reactivities. *J. Org. Chem.* **2012**, *77* (18), 8142–8155. https://doi.org/10.1021/jo301497g.

(234) Giller, S. A.; Eremeev, A. V; Kalvin'sh, I. Y.; Liepin'sh, É. É.; Tikhomirov, D. A. Reaction of α-Chloroacrylonitrile with Hydrazines. *Chem. Heterocycl. Compd.* **1975**, *11* (2), 212–214. https://doi.org/10.1007/BF00471402.

(235) Ege, G.; Franz, H. Aminopyrazoles. III (1). Novel "One-Flask" Preparation of 1-Phenylpyrazol-3-Amine. *Journal of Heterocyclic Chemistry*. 1982, pp 1265–1266.

7. Procedures and spectroscopic data

General Methods

Unless otherwise noted, all commercial reagents and solvents were purchased with the highest purity grade from Fisher Scientific Inc. Para-substituted isothiocyanato benzene derivatives, 4-chlorophenyl-isothiocyanate, 4-chlorobenzyl-isothiocyanate, 4-chlorobenzyl-isocyanate, 1H-pyrazole, 1H-pyrazol-3-amine, 1-methyl-1H-pyrazol-3-amine were purchased from Aldrich and used without further purification. They were used without further purification unless specified. N,N-Dimethylformamide (DMF), Dichloromethane (Methylene Dichloride; DCM) and Tetrahydrofuran (THF) were distilled or purchased in high purity and anhydrous condition. All reactions were carried out under an argon or nitrogen atmosphere with analytical grade or dry solvents, unless otherwise noted. Reactions were monitored by thin-layer chromatography (TLC) on Silica XHL TLC Plates, w/UV254, glass backed, 250um. The visualization was done using UV light (shortwave length 254 nm), aniline, phosphomolybdic Acid (PMA) and iodine chamber. Silica gel (200–300 meshes) from Sorbtech was used for column chromatography. All the reagents and synthesized products were stored with flushed Ar environment. The synthesized compounds were stored in -10 to -20 ^{O}C freezer compartment. However, they are stable for room temperature also. Nuclear magnetic resonance (NMR) spectra were recorded on a Varian Unity plus and Bruker-Ascend spectrometer for 1H (400 MHz or 600 MHz) and 13C (101 MHz or 151 (MHz) in deuterated chloroform ($CDCl_3$) and DMSO- d_6 unless otherwise indicated. Infrared spectra were recorded with a Nicolet 380 FT-IR. HRMS (+ESI-TOF) measurements were performed using an LCT Premier instrument. HRMS (+ESI-TOF) measurements were performed using an LCT Premier instrument. Additional mass spectra were obtained with Waters Acquity UPLC TQD . Melting points were observed with Mel-Temp 1001D.

1-(tert-butyl)-1H-pyrazol-3-amine (10)

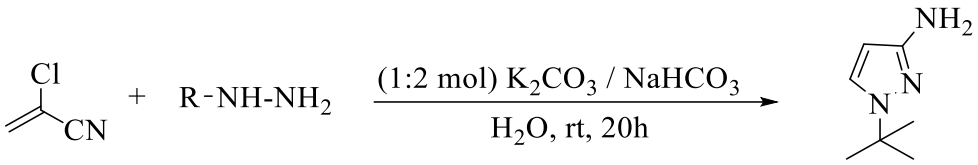

71%

10

A solution of 1.54 g (12.40 mmol, 1 equiv.) tert-butylhydrazine hydrochloride in 30 mL of distilled water was cooled to 0 °C. Then, 1.71 g (12.40mmol, 1 equiv.) K_2CO_3 and 2.08 g (24.80 mmol, 2 equiv.) $NaHCO_3$ was added sequentially. The reaction mixture was kept stirring at 0 °C for 2 hours until the resulting solution was clear and colorless. 2-Chloroacrylonitrile was added at 0 °C. Allowed it to warm to rt and kept stirring at rt for 12 hr. After 12 hr stirring, the reaction solution turned out to be light yellow. The resulting reaction solution was extracted with ethyl acetate. Combined organic layers were washed with brine, dried over anhydrous $NaSO_4$, concentrated to dryness and column chromatographed on silica gel using a gradient mixture of CH_2Cl_2 and MeOH as eluent to give 71% of compound **10** as a brown solid. ^{1}H NMR (400 MHz, DMSO-d_6) δ 11.01 (d, J = 27.7 Hz, 1H), 5.15 (d, 1H), 4.31 (s, 2H), 1.16 (s, 9H).^{13}C NMR (101 MHz, Chloroform-d) δ 136.82, 127.07, 94.35, 92.27, 29.82 (3C).

^{1}H NMR of compound 10

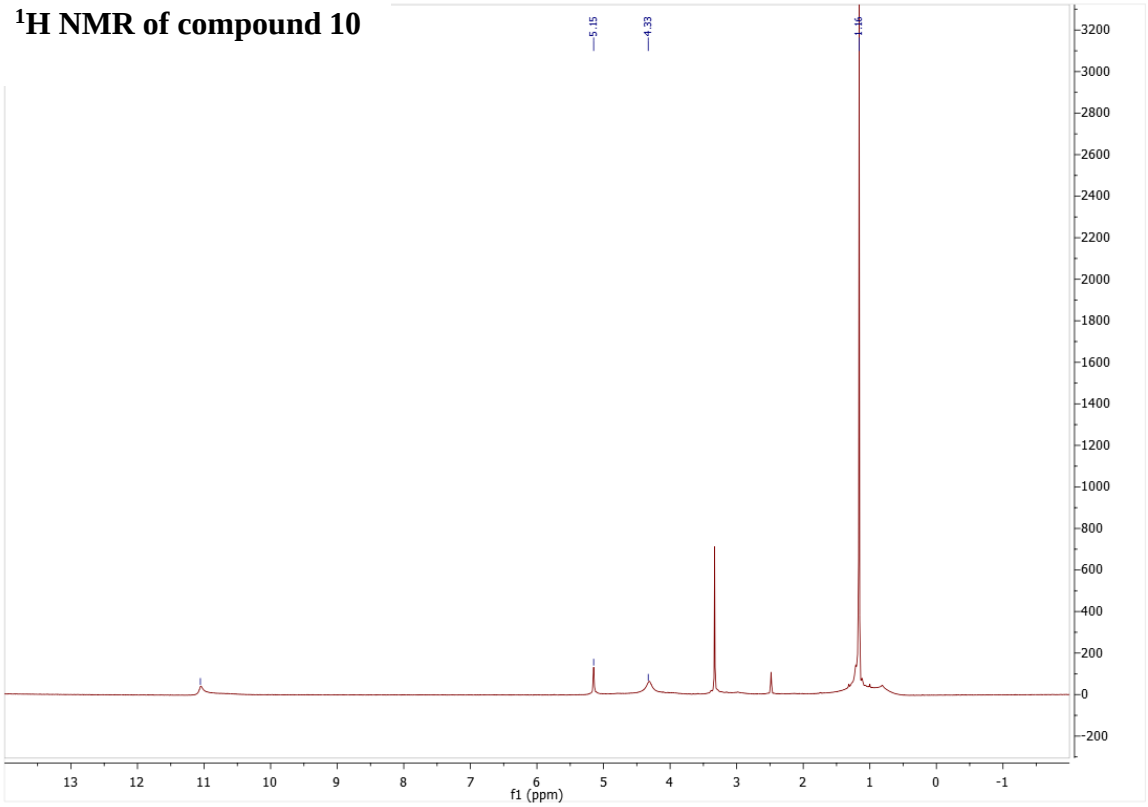

^{13}C NMR of compound 10

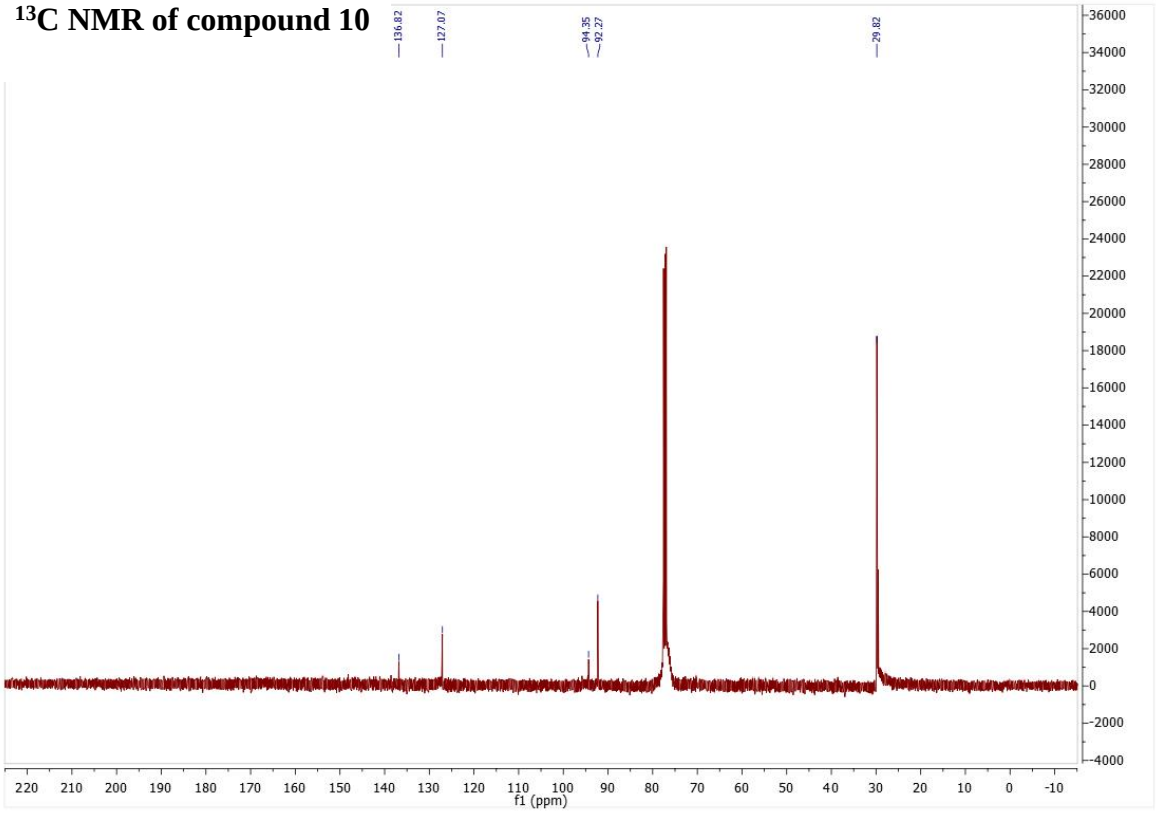

1-methyl-1H-pyrazol-3-amine (11)

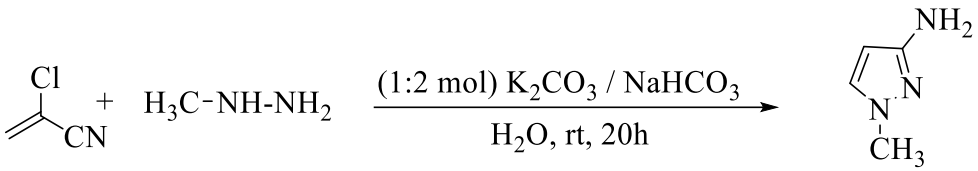

65%

11

A solution of 469 Mg (10.18 mmol, 1 equiv.) methylhydrazine hydrochloride in 30 mL of distilled water was cooled to 0 °C. Then, 1.31 g (10.18 mmol, 1 equiv.) K_2CO_3 and 1.72 g (20.5 mmol, 2 equiv.) $NaHCO_3$ was added sequentially. The reaction mixture was kept stirring at 0 °C for 2 hours until the resulting solution was clear and colorless. 2-Chloroacrylonitrile (885 mg, 10.18 mmol) was added at 0 °C. It was then allowed to warm to rt and kept stirring for 12 hr. After 12 hr stirring, reaction solution was an orange color. The resulting reaction solution was extracted with ethyl acetate. Combined organic layers were washed with brine, dried over anhydrous $NaSO_4$, concentrated to dryness and column chromatographed on silica gel using a gradient mixture of CH_2Cl_2 and MeOH as eluent to give 65% of compound **11** as a brown semi-solid. ^{1}H NMR (400 MHz, DMSO-d_6) δ 7.21 (d, J = 2.2 Hz, 1H), 5.32 (d, J = 2.2 Hz, 1H), 4.46 (bs, 2H), 3.53 (s, 3H). ^{13}C NMR (101 MHz, DMSO-d_6) δ 155.92, 131.51, 92.25, 38.44.

^{1}H NMR of compound 11

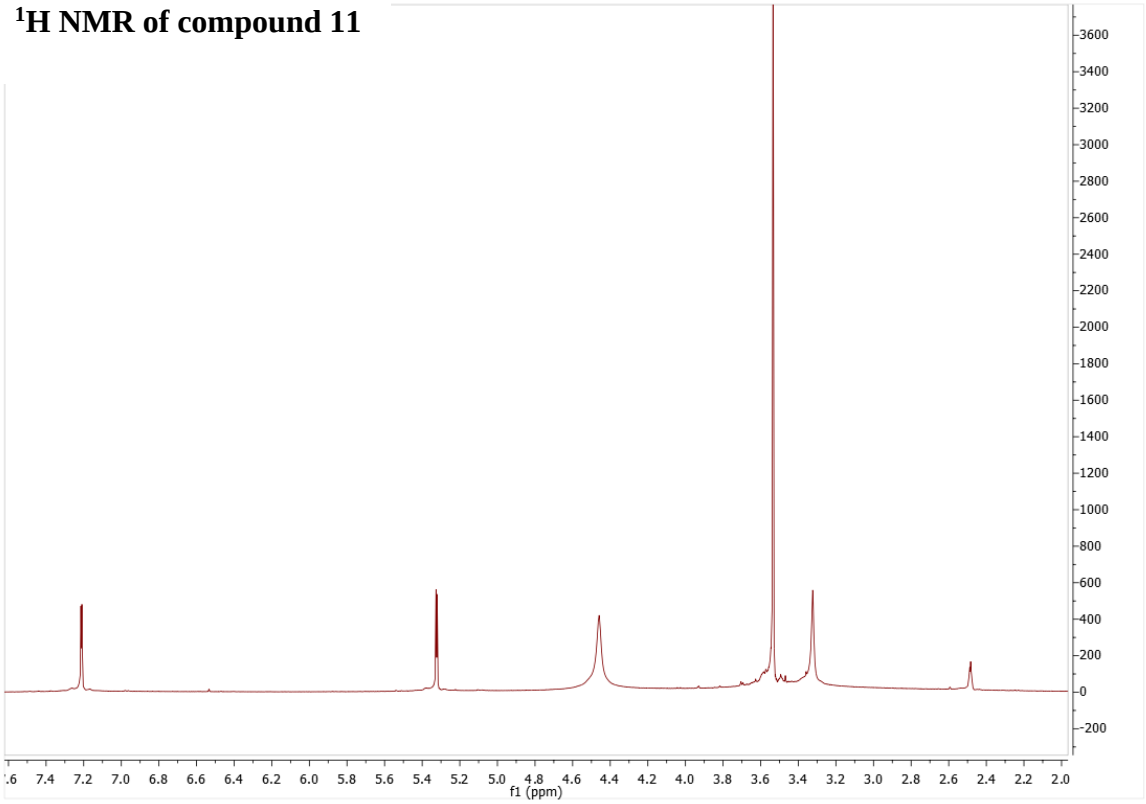

^{13}C NMR of compound 11

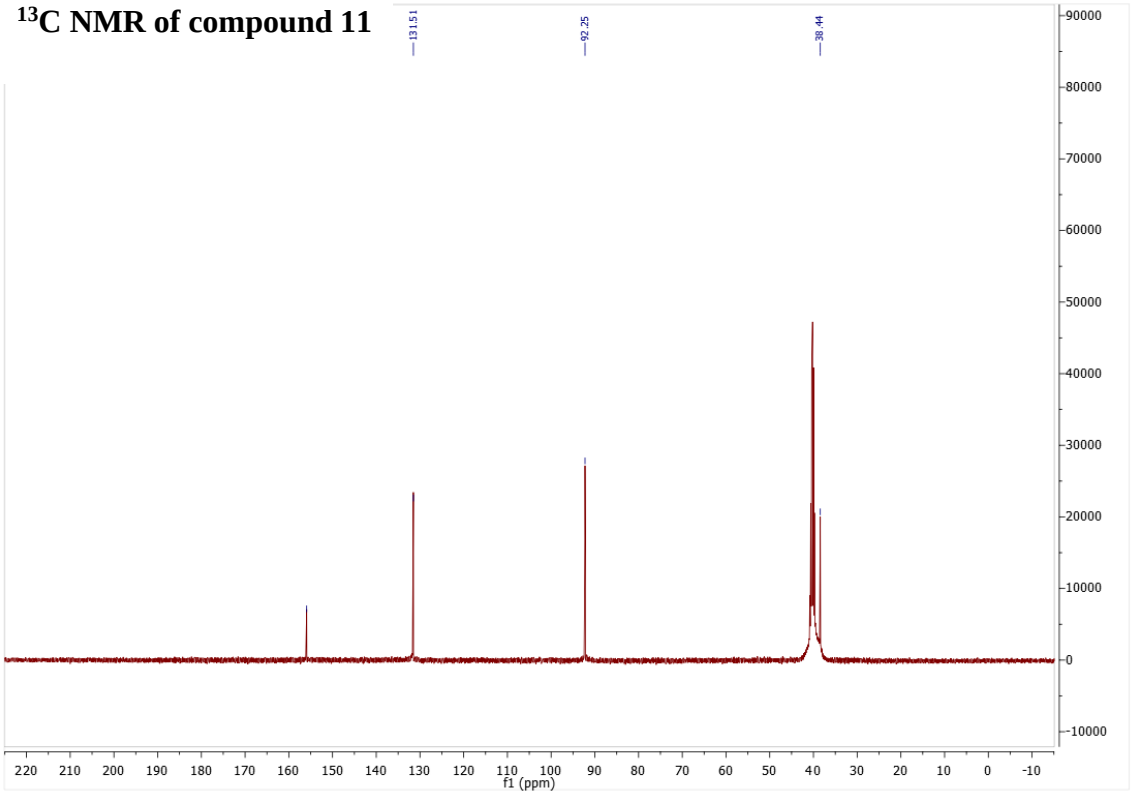

1-(4-chlorophenyl)-3-(1H-pyrazol-3-yl)thiourea (15) and 3-amino-N-(4-chlorophenyl)-1H-pyrazole-1-carbothioamide (16)

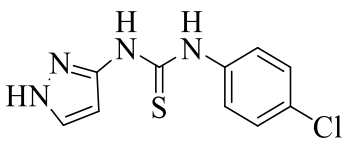

15 (35%)

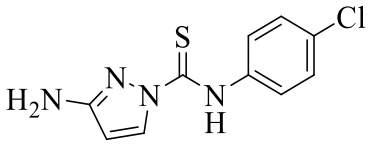

16 (55%)

1H-pyrazol-3-amine (1 g, 12.04 mmol) was dissolved in DCM and stirred in a 100 mL round bottom flask. 4-Chlorophenyl isothiocyanate (2.04 g, 12.04 mmol) was dissolved in DCM separately and added to the stirring reaction dropwise. The reaction was then stirred for 20 hours at room temperature. The reaction was monitored by TLC (50% EtOAc/hexanes). **16** shows R_f= 0.75 and **15** shows R_f= 0.45. All volatile components were evaporated under vacuum and the resulting crude product was purified by flash column chromatography (100% hexanes to 25% EtOAc/ hexanes) to afford 55% yield of **16** white color and 35% yield of **15** off-white color solids.

15: ^{1}H NMR (600 MHz, DMSO-d_6) δ 12.70 (s, 1H), 11.78 (s, 1H), 10.83 (s, 1H), 7.76 (S, 1H), 7.68 (d, 2H), 7.44 (d, 2H), 6.04 (s, 1H). ^{13}C NMR (151 MHz, DMSO-d_6) δ 176.74, 149.74, 138.41, 130.20, 129.57, 128.86, 126.27, 94.81. FTIR, cm^{-1}: 3361 (-NH-), 3060 (C-H aromatic), 1577 (aromatic C=C), 1524 (aromatic C=N), 1258 (C=S), 754 (aromatic C-Cl). HRMS (+ESI-TOF) m/z: [M^+] calcd for $C_{10}H_9ClN_4S$ 252.0236; found 252.0236

16: ^{1}H NMR (400 MHz, DMSO-d_6) δ 10.98 (d, 1H), 8.41 (s, 1H), 7.67 (d, 2H), 7.44 (d, 2H), 5.98 (s, 1H), 5.71 (d, 2H). ^{13}C NMR (151 MHz, DMSO-d_6) δ 176.30, 149.26, 137.93, 129.68, 129.08, 128.35, 125.75, 94.31. FTIR, cm^{-1}: 3471, 3460 (-NH_2), 3305 (-NH-), 3060-3005 (C-H aromatic), 2960, 2920 (CH pyrazole), 1610, 1588(aromatic C=C), 1516 (aromatic C=N), 1242 (C=S), 640 (aromatic C-Cl). HRMS (+ESI-TOF) m/z: [M^+] calcd for $C_{10}H_9ClN_4S$ 252.0236; found 252.0234.

^{1}H NMR of compound 15

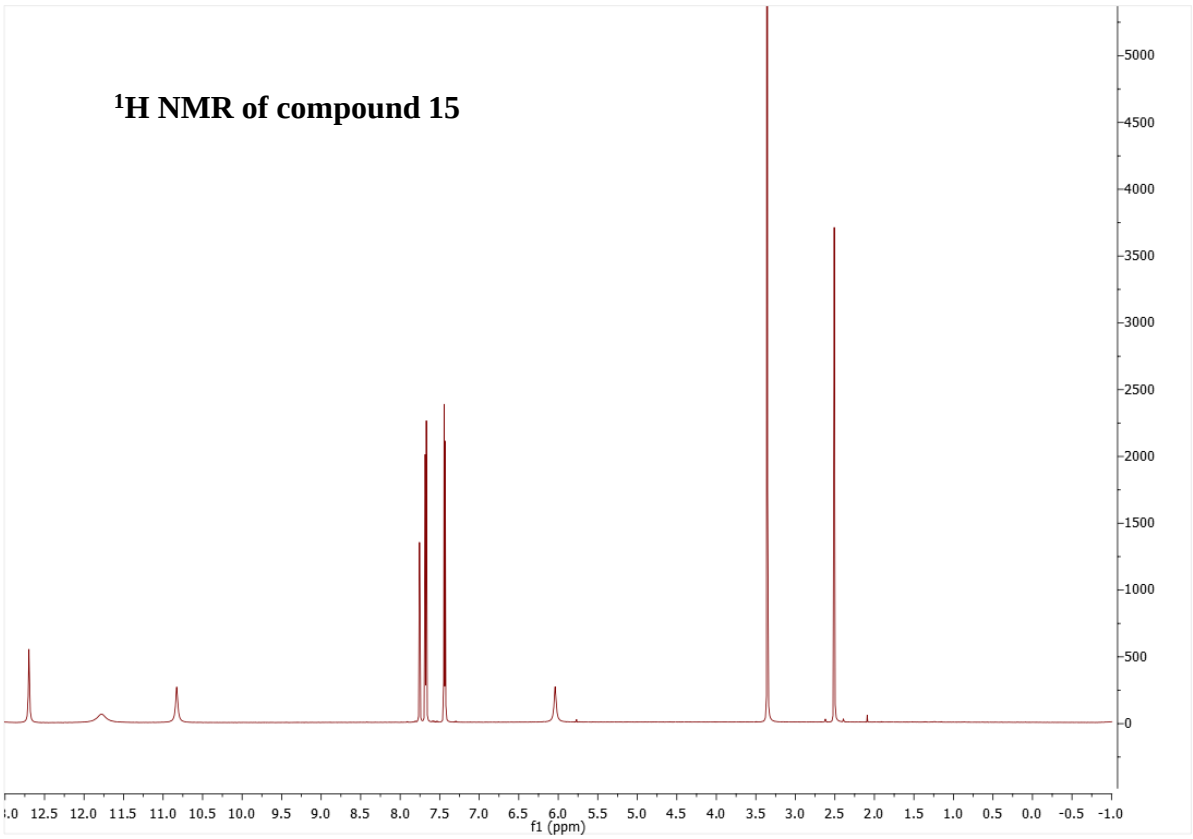

^{13}C NMR of compound 15

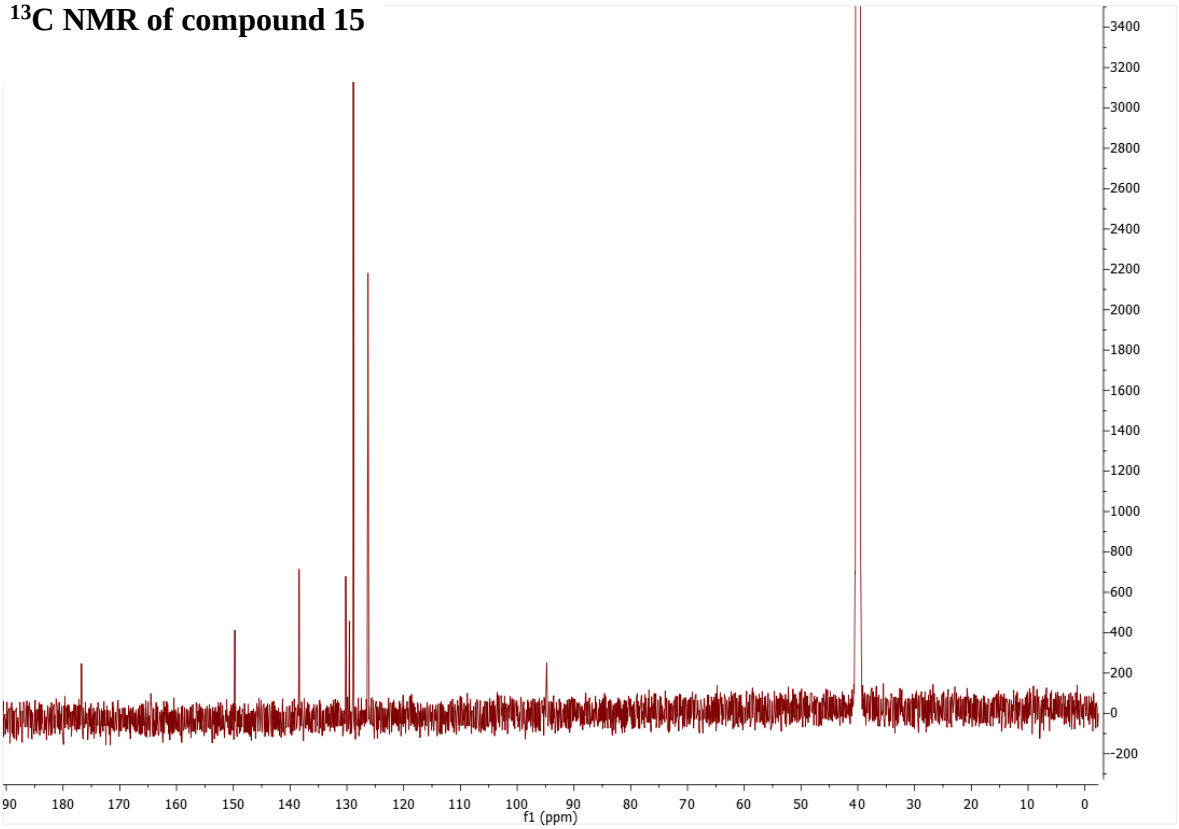

HRMS of compound 15

Monoisotopic Mass: 252.0230962

Found: 252.0236

Chemical Formula: $C_{10}H_9Cl_1N_4S_1$

M+

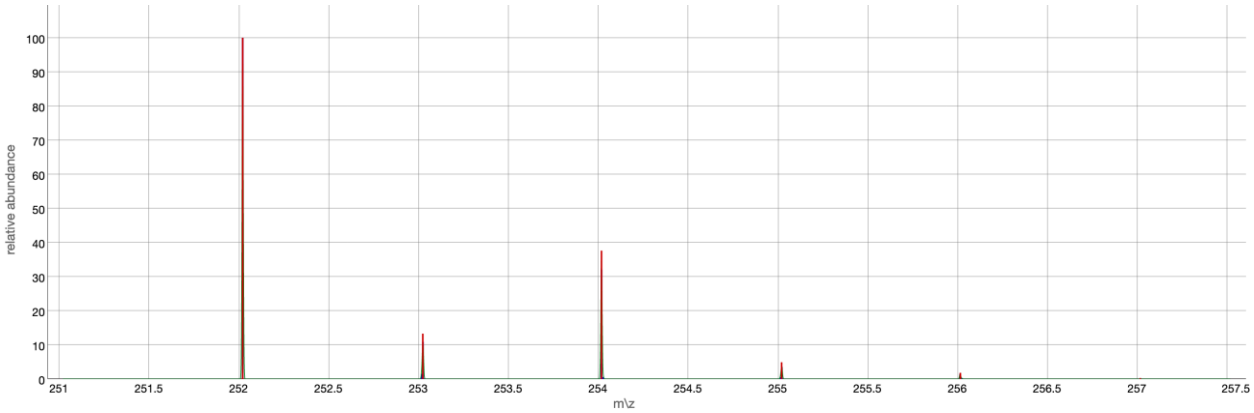

^{1}H NMR of compound 16

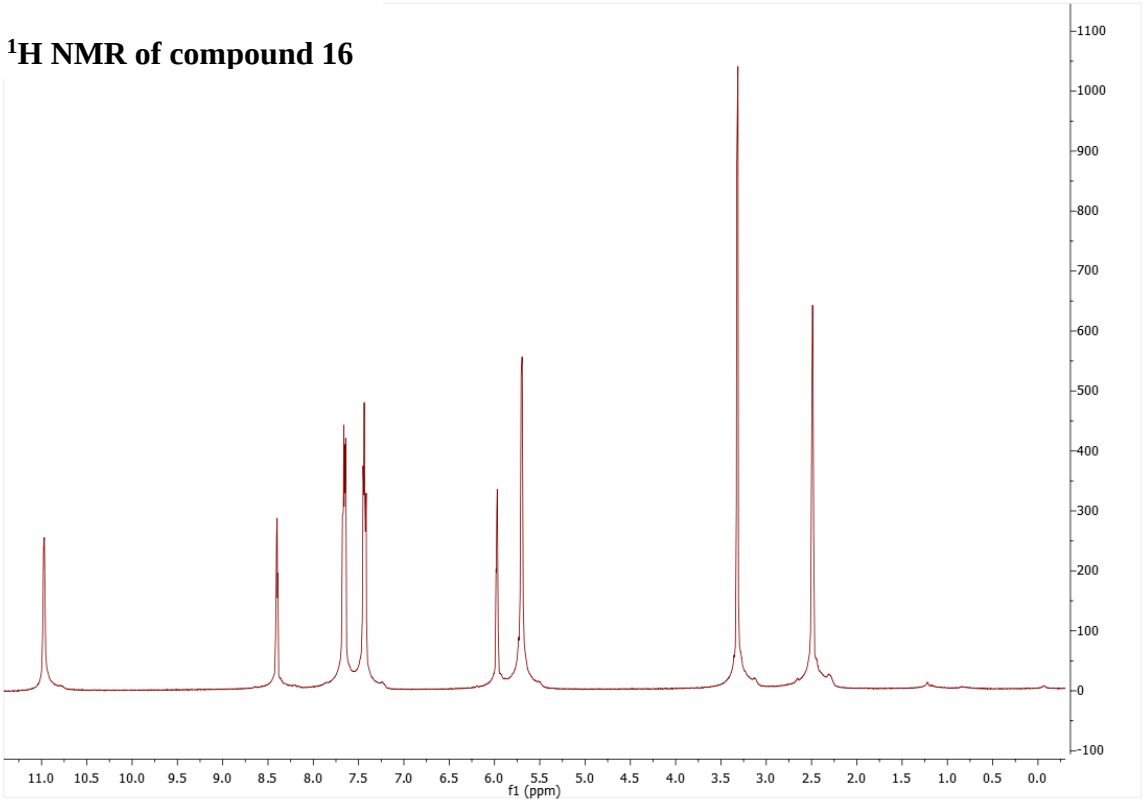

^{13}C NMR of compound 16

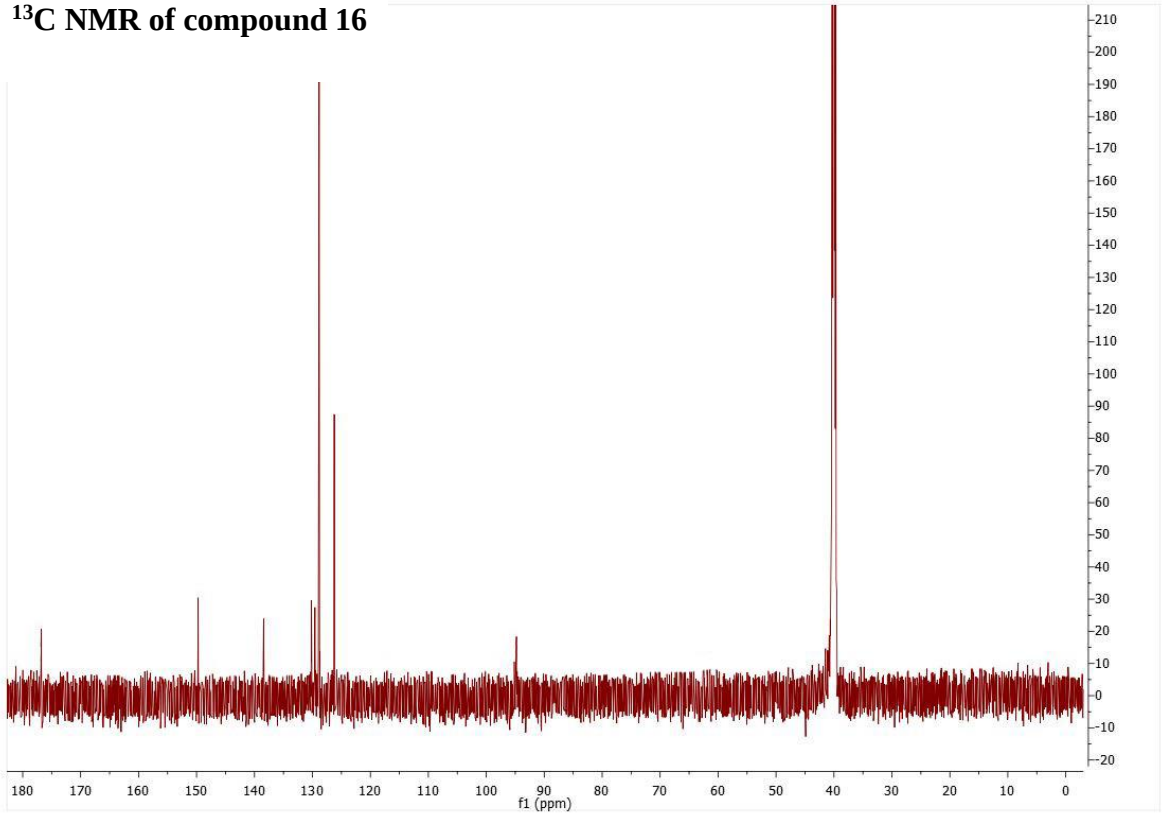

HRMS of compound **16**
Monoisotopic Mass: 252.0230962
Found: 252.0234
Chemical Formula: $C_{10}H_9Cl_1N_4S_1$
M+

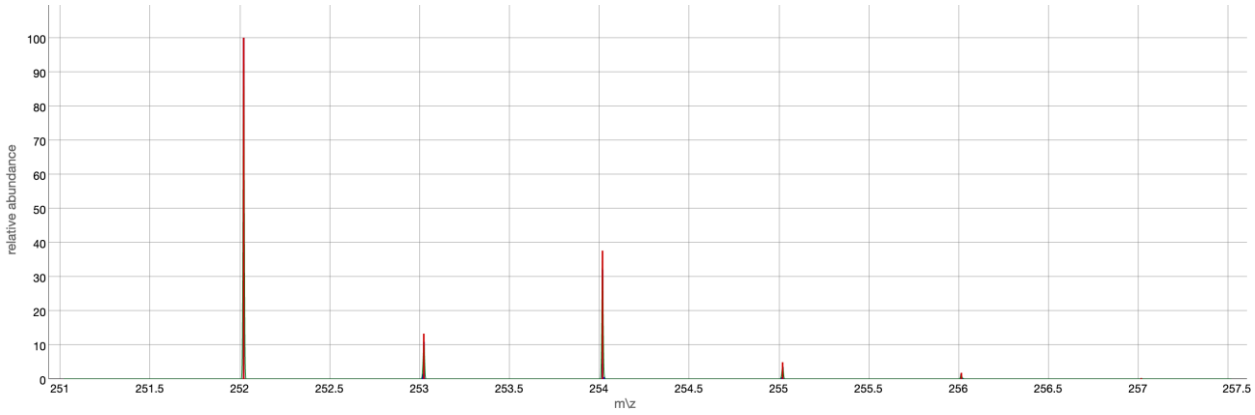

1-(1-(tert-butyl)-1H-pyrazol-3-yl)-3-(4-chlorophenyl)urea (17)

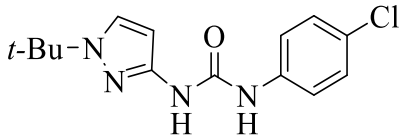

17 (68%)

1-(tert-butyl)-1H-pyrazol-3-amine (250 mg, 2.6 mmol) was dissolved in DCM and stirred in a 100 mL round bottom flask. 4-chlorophenyl isocyanate (395 mg, 2.6 mmol, 1 eq) dissolved in DCM was added to the reaction dropwise, stirred for 5 min at r.t and refluxed at 60 °C for 16 hours. The reaction was monitored by TLC (25% EtOAc/hexanes). Volatile components were removed under vacuum and resulting solid precipitate was re-crystallized with MeOH. Retrieved off-white color solid, **17** (68%) was oven dried. ^{1}H NMR (600 MHz, DMSO-d_6) δ 9.15 (s, NH), 7.67 (d, J = 2.4 Hz, 1H), 7.48 (m, 2H), 7.33 (m, 2H), 6.17 (s, 1H), 1.49 (s, 9H). ^{13}C NMR (151 MHz, DMSO-d_6) δ 152.31, 147.36, 139.02, 129.14, 127.63, 125.84, 120.08, 94.82, 58.01, 29.72. FTIR, cm^{-1}: 3245 (-NH-), 2974 (C-H aliphatic), 1538 (aromatic C=C), 1481 (aromatic C=N), 1686 (C=O), 734 (aromatic C-Cl). HRMS (+ESI-TOF) m/z: [M^{+}] calcd for $C_{14}H_{17}ClN_4O$ 292.1091; found 292.1093.

^{1}H NMR of compound 17

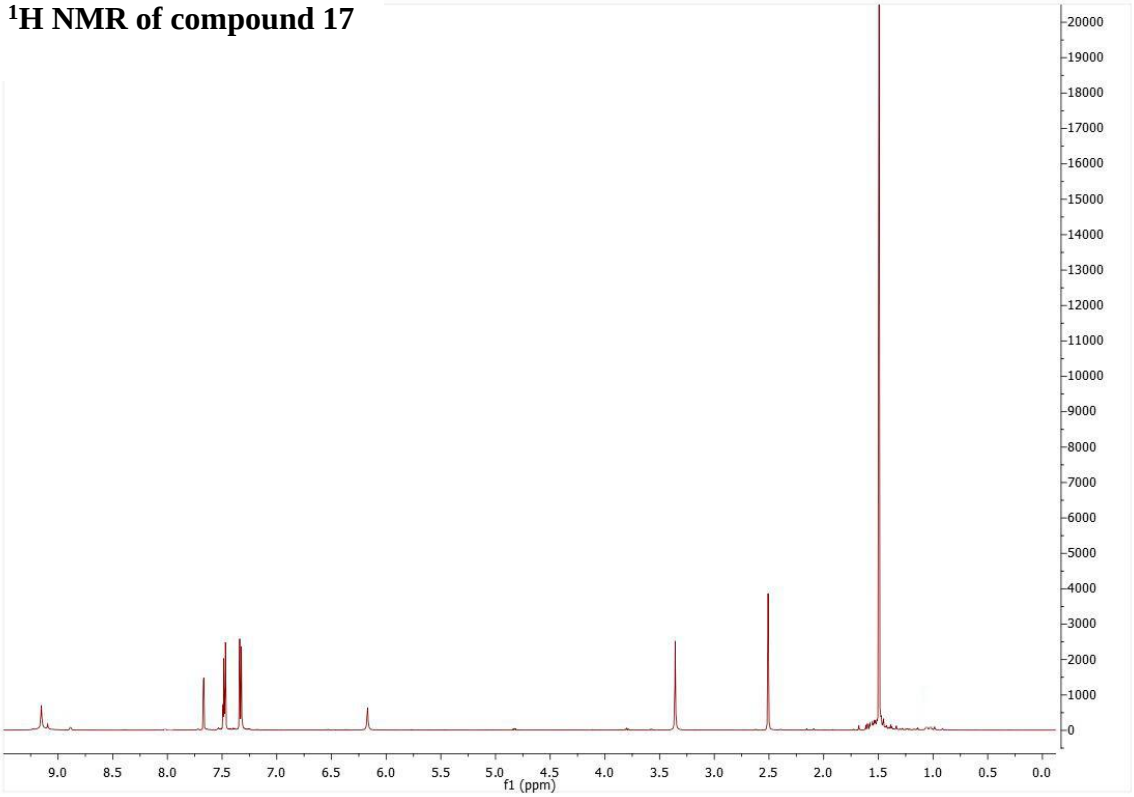

^{13}C NMR of compound 17

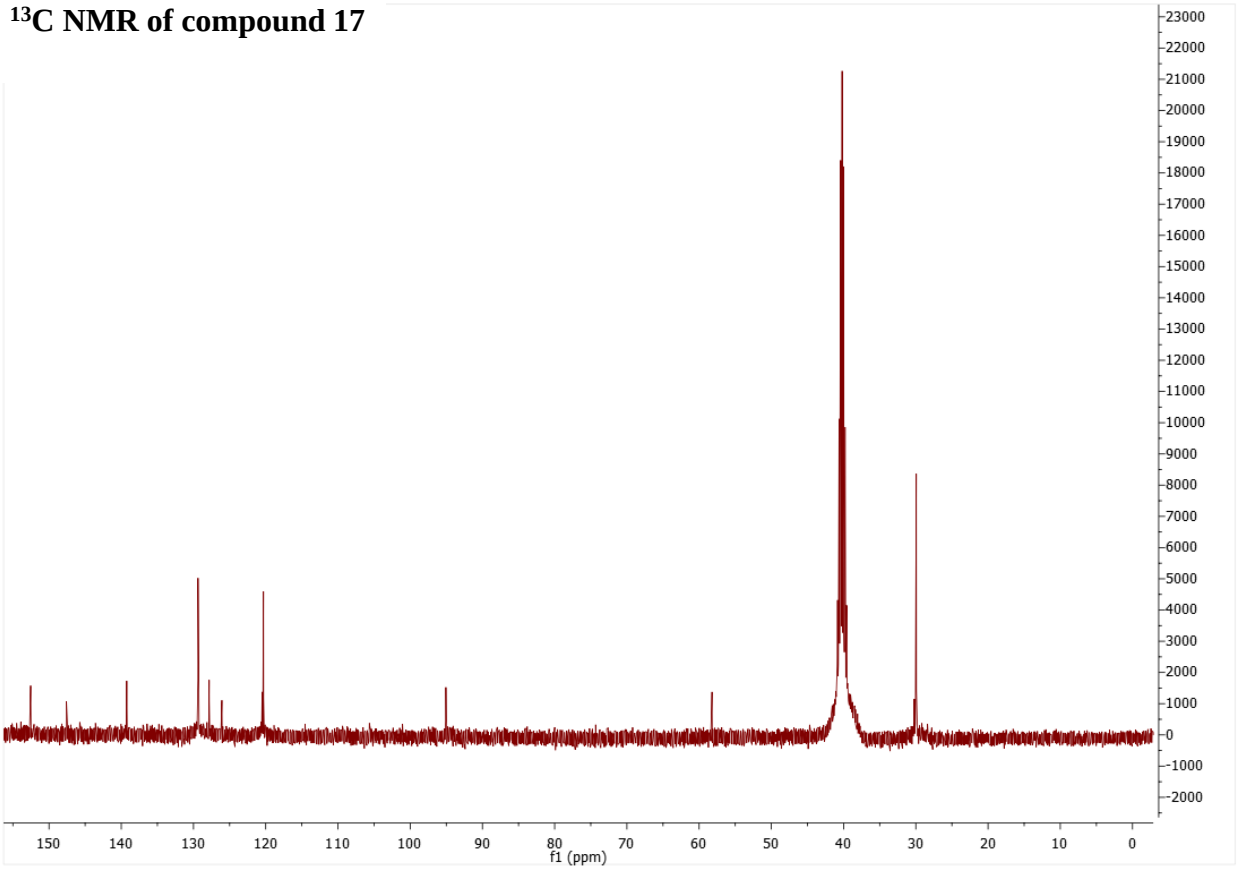

HRMS of compound **17**
Monoisotopic Mass: 292.1085403
Found: 292.1093
Chemical Formula: $C_{14}H_{17}Cl_1N_4O_1$
M+

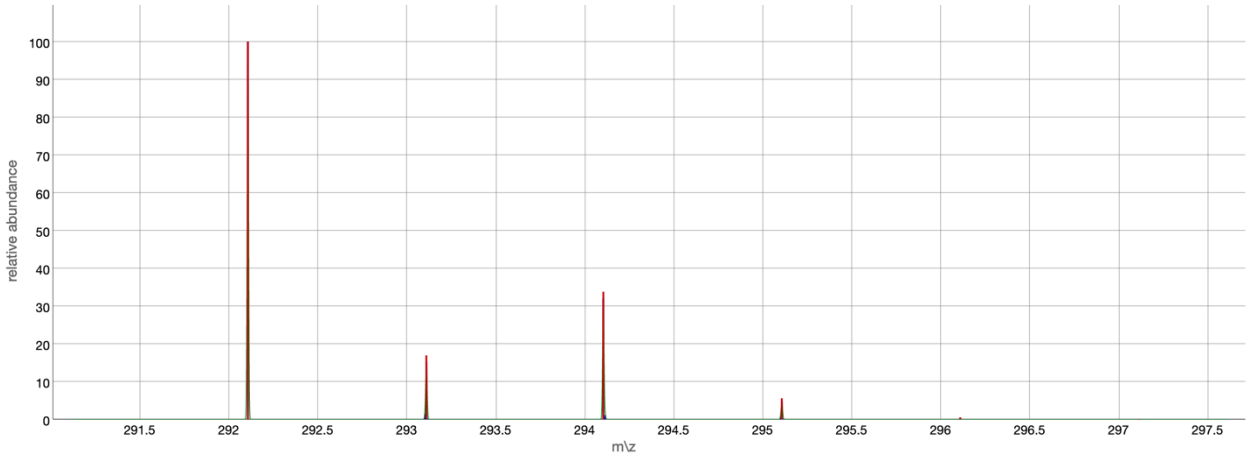

1-(4-chlorophenyl)-3-(1-methyl-1H-pyrazol-3-yl) (18)

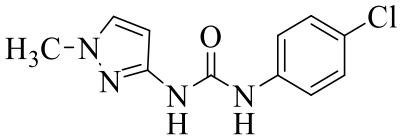

18 (61%)

1-methyl-1H-pyrazol-3-amine (250 mg, 2.6 mmol) was dissolved in DCM and stirred in a 100 mL round bottom flask. 4-chlorophenyl isocyanate (395 mg, 2.6 mmol, 1 eq) dissolved in DCM was added to the reaction dropwise, stirred for 5 min at r.t and refluxed at 60 $^{\circ}$C for 16 hours. The reaction was monitored by TLC (25% EtOAc/hexanes). Volatile components were removed under vacuum and resulting solid precipitate was re-crystallized with MeOH. Retrieved white color solid, **18** (61%) was oven dried. ^{1}H NMR (600 MHz, DMSO-d_6) δ 9.90 (S, NH), 8.78 (s, NH), 7.79 (d, J = 2.3 Hz, 1H), 7.48 (d, J = 8.9 Hz, 2H), 7.33 (d, J = 8.8 Hz, 2H), 6.27 (d, J = 2.3 Hz, 1H), 3.88 (s, 3H). ^{13}C NMR (151 MHz, DMSO-d_6) δ 154.81, 150.21, 139.02, 133.25, 129.11, 125.94, 120.42, 95.27, CH_3 overlapped with DMSO-d_6. FTIR, cm^{-1}: 3286 (-NH-), 1555 (aromatic C=C), 1486 (aromatic C=N), 1593 (C=O), 744 (aromatic C-Cl). HRMS (+ESI-TOF) m/z: [M^+] calcd for $C_{11}H_{11}ClN_4O$ 250.0621; found 250.0620.

^{1}H NMR of compound 18

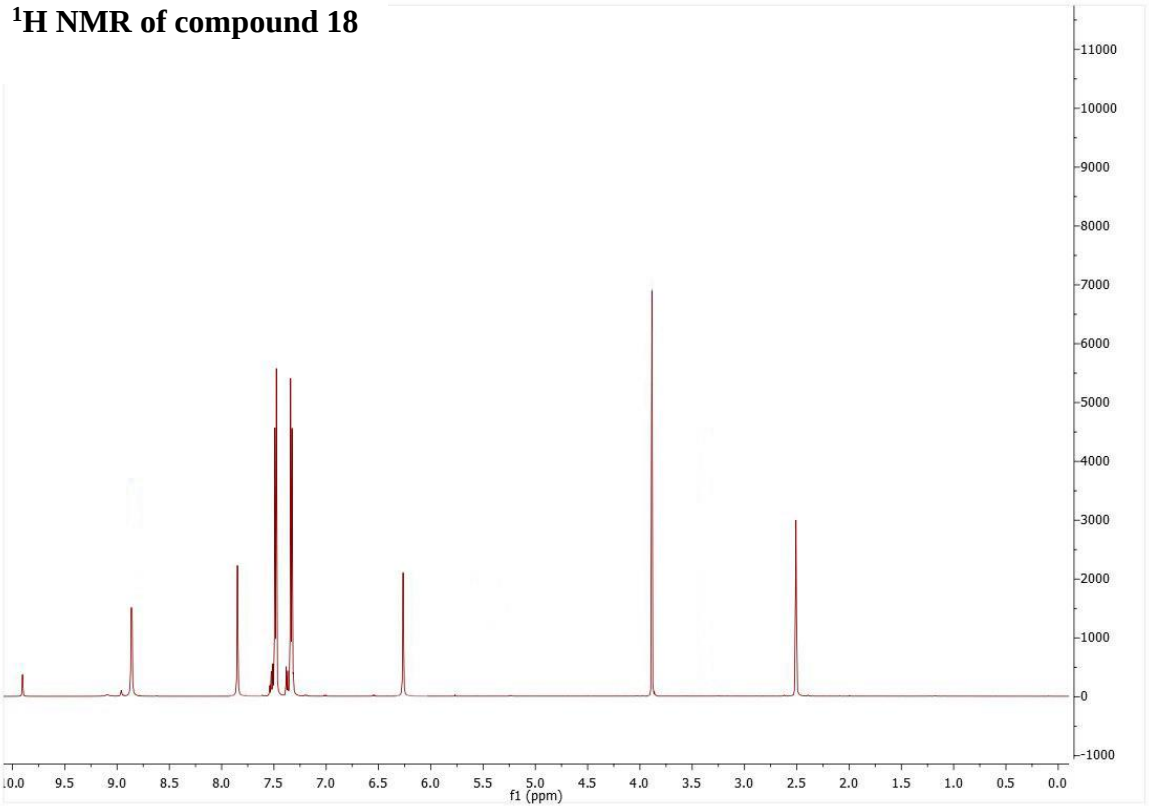

^{13}C NMR of compound 18

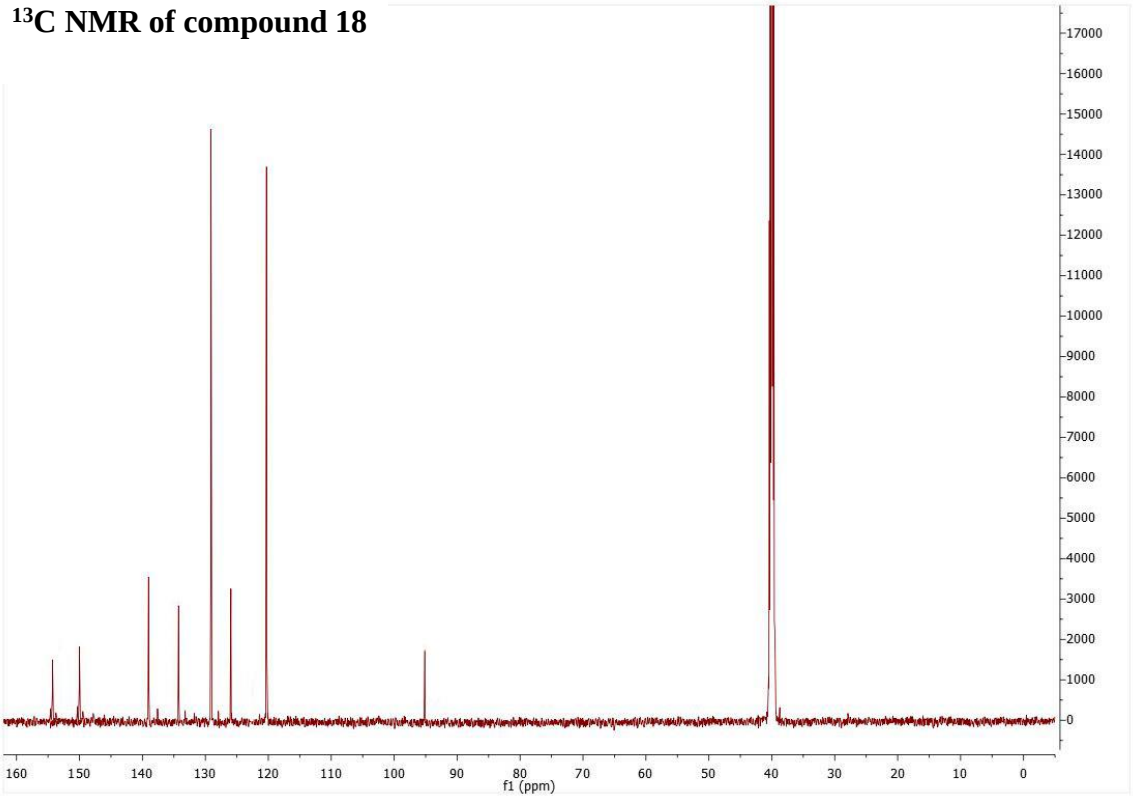

HRMS of compound **18**
Monoisotopic Mass: 250.0615901
Found: 250.0620
Chemical Formula: $C_{11}H_{11}ClN_4O$
M+

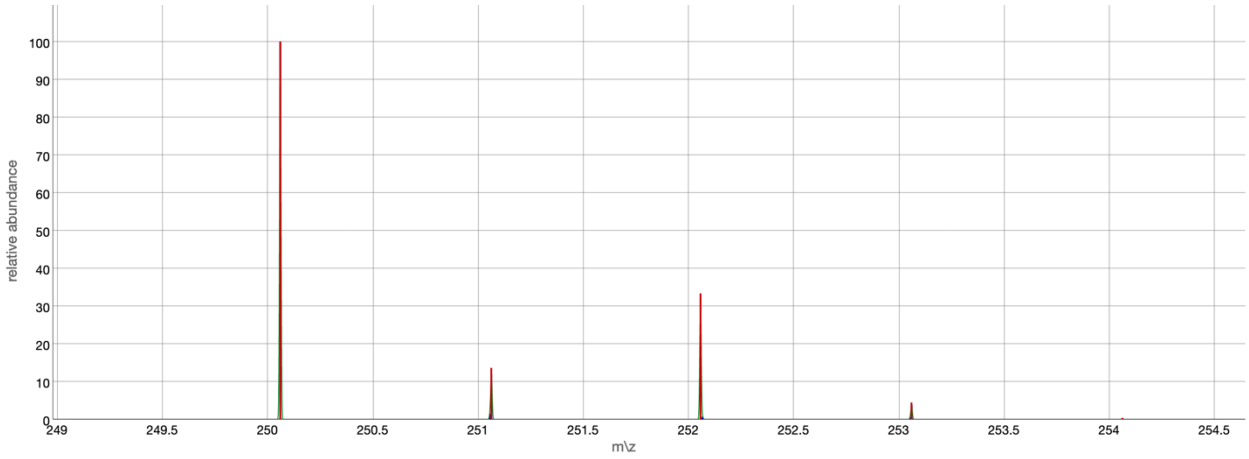

1-(1-(tert-butyl)-1H-pyrazol-3-yl)-3-(4-chlorobenzyl)urea (19)

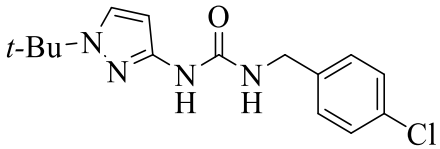

19 (68%)

1-(tert-butyl)-1H-pyrazol-3-amine (168 mg, 1.21 mmol) was dissolved in DCM and stirred in a 100 mL round bottom flask. 4-chlorobenzyl isocyanate (203 mg, 1.21 mmol, 1 eq) dissolved in DCM was added to the reaction dropwise, stirred for 5 min at r.t and refluxed at 60 °C for 16 hours. The reaction was monitored by TLC (25% EtOAc/hexanes). Volatile components were removed under vacuum and resulting solid precipitate was re-crystallized with MeOH. Retrieved white color solid, **19** (68%) was oven dried. ^{1}H NMR (400 MHz, DMSO-d_6) δ 9.58 (s, 1H), 7.21-7.37 (d, *J* 4H), 6.51 (s, 1H), 4.32 (s, 1H), 1.70 (s, 9H). ^{13}C NMR (151 MHz, DMSO-d_6) δ 158.23, 140.42, 135.37, 131.33, 129.41, 128.34, 126.14, 96.34, 55.10, 42.57, 29.47. FTIR, cm^{-1}: 3317 (-NH-), 2926 (C-H aliphatic), 1560 (aromatic C=C), 1491 (aromatic C=N), 1614 (C=O), 750 (aromatic C-Cl). HRMS (+ESI-TOF) m/z: [M^+] calcd for $C_{15}H_{19}ClN_4O$ 306.1247; found 306.1249.

^{1}H NMR of compound 19

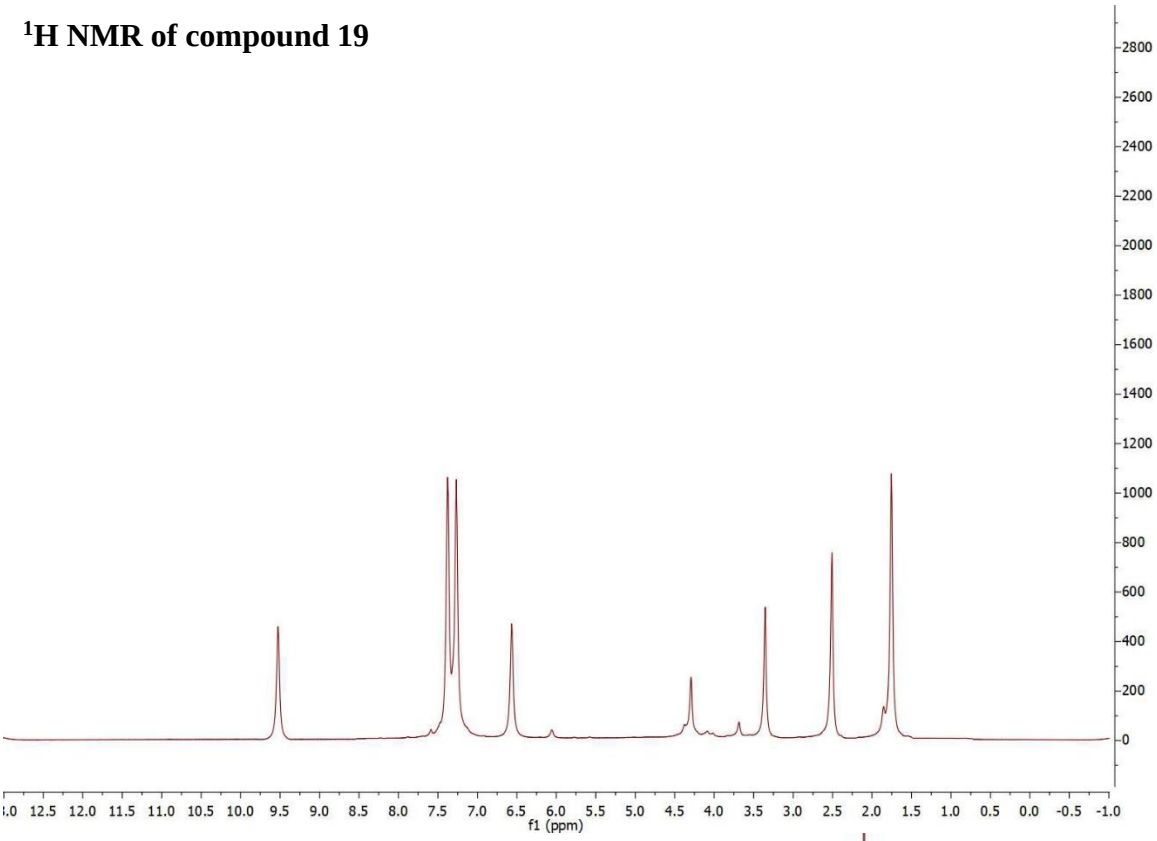

^{13}C NMR of compound 19

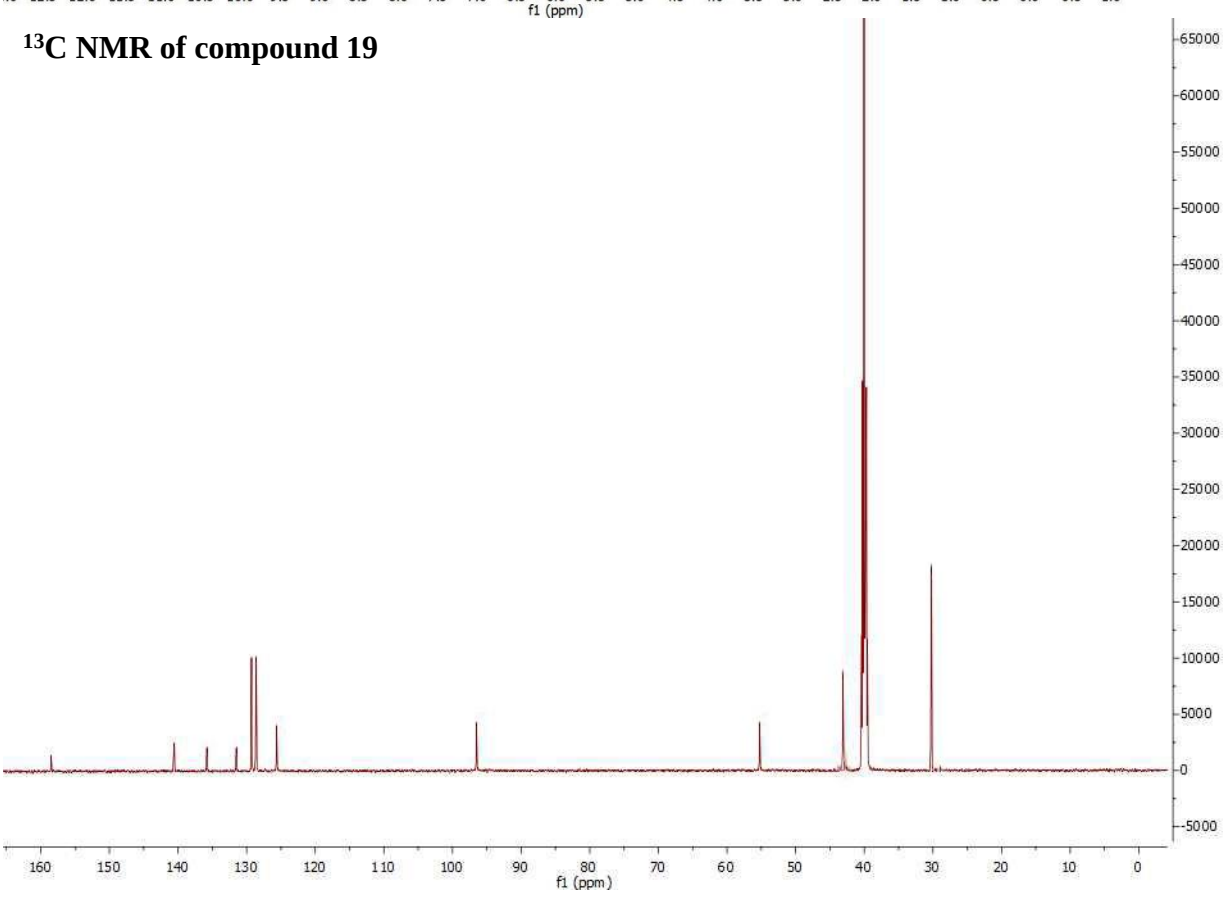

HRMS for compound **19**
Monoisotopic Mass: 306.1241904
Found: 306.1249
Chemical Formula: $C_{15}H_{19}ClN_4O$
M+

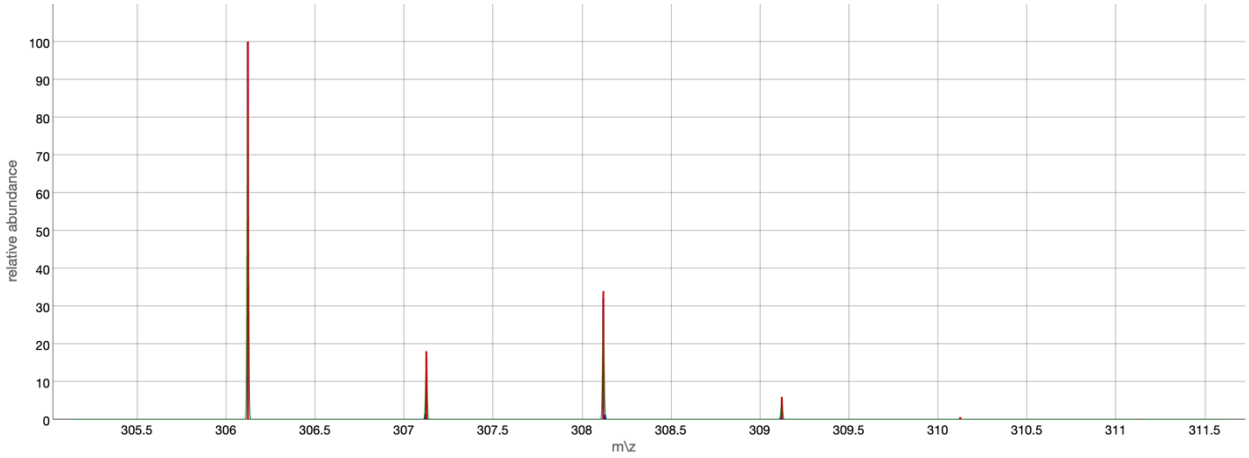

1-(4-chlorobenzyl)-3-(1-methyl-1H-pyrazol-3-yl)urea (20)

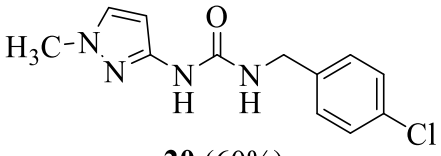

20 (60%)

1-methyl-1H-pyrazol-3-amine (92 mg, 0.95 mmol) was dissolved in DCM and stirred in a 100 mL round bottom flask. 4-chlorobenzyl isocyanate (159 mg, 0.95 mmol, 1 eq) dissolved in DCM was added to the reaction dropwise, stirred for 5 min at r.t and refluxed at 60 °C for 16 hours. The reaction was monitored by TLC (25% EtOAc/hexanes). Volatile components were removed under vacuum and resulting solid precipitate was re-crystallized with MeOH. Retrieved white color solid, **20** (60%) was oven dried. ^{1}H NMR (600 MHz, DMSO-d_6) δ 7.46 (s, 1H), 7.38 (m, 2H), 7.26 (m, 2H), 6.55 (t, J = 6.1 Hz, 1H), 4.21 (d, J = 6.1 Hz, 2H), 3.88 (s, 3H). ^{13}C NMR (151 MHz, DMSO-d_6) δ 158.18, 149.27, 140.52, 131.49, 130.35, 129.29, 128.61, 96.40, 42.74, CH_3 overlapped with DMSO-d_6. FTIR, cm^{-1}: 3225 (-NH-), 2911 (C-H aliphatic), 1563 (aromatic C=C), 1495 (aromatic C=N), 1608 (C=O), 757 (aromatic C-Cl). HRMS (+ESI-TOF) m/z: [M^+] calcd for $C_{12}H_{13}ClN_4O$ 264.0778; found 264.0777.

^{1}H NMR of compound 20

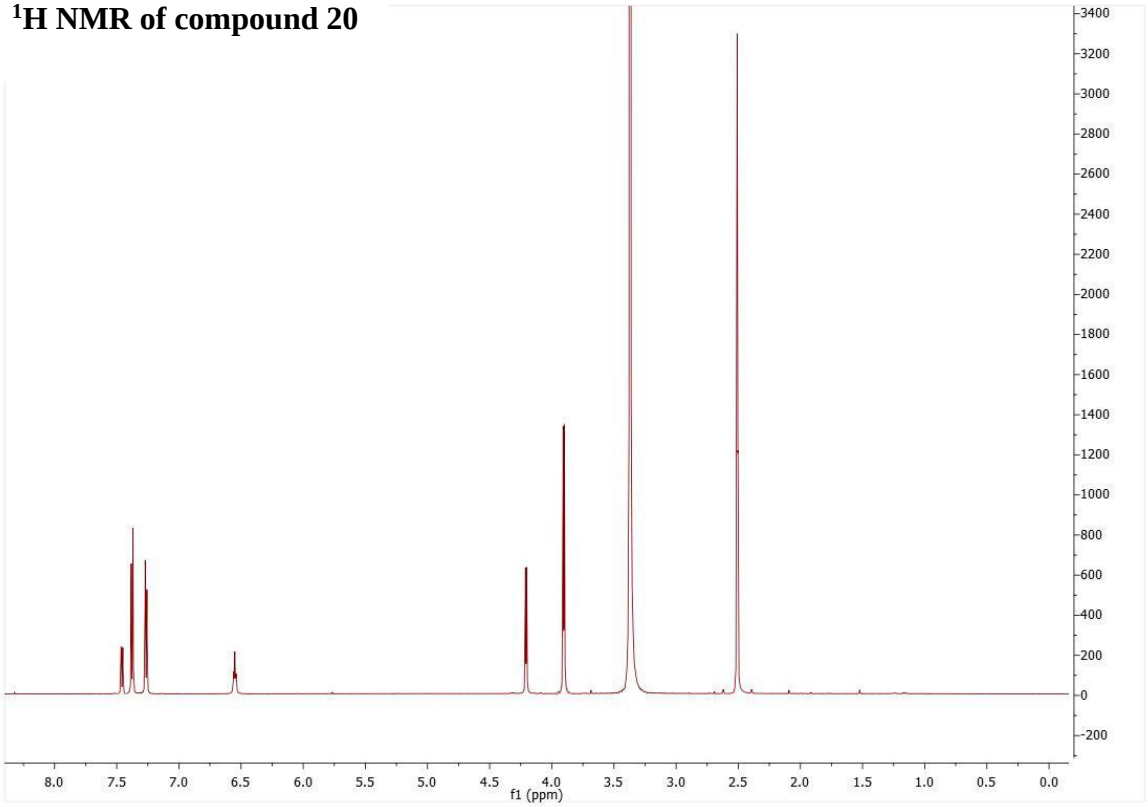

^{13}C NMR of compound 20

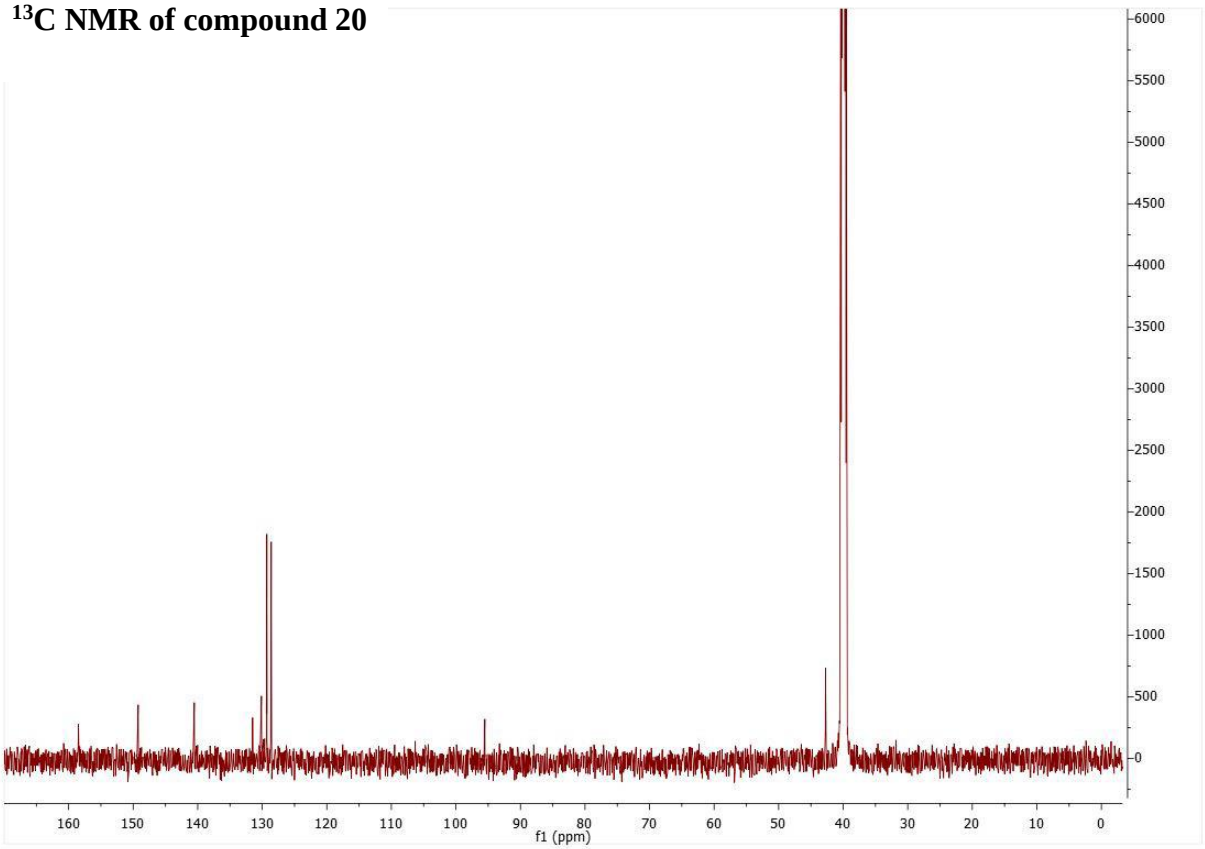

HRMS for compound **20**
Monoisotopic Mass: 264.0772402
Found: 264.0777
Chemical Formula: $C_{12}H_{13}ClN_4O$
M+

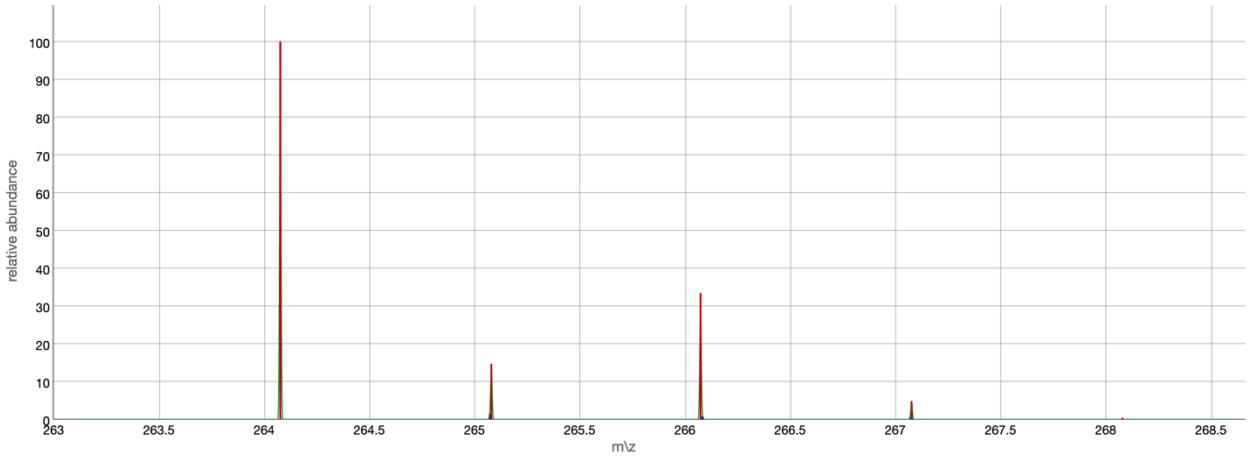

N-(4-nitrophenyl)-1H-pyrazole-1-carbothioamide (21)

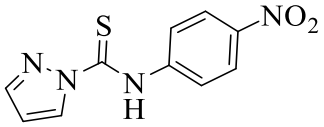

21 (65%)

Pyrazole (189 mg, 2.78 mmol) was dissolved in DCM and stirred in a 100 mL round bottom flask. 4-Nitrophenyl isothiocyanate (500 mg, 2.78 mmol, 1 eq) was dissolved in DCM separately and added to the stirring reaction dropwise. The reaction was then stirred vigorously for 20 hours at room temperature. The reaction was monitored by TLC (DCM/ methanol 20:1). All the volatile components were removed under vacuum and resulting yellow solid was re-crystallized with MeOH. Retrieved yellow color solid, **21** (65%) was oven-dried. ^{1}H NMR (400 MHz, DMSO-d_6) δ 8.77 (d, J = 2.9 Hz, 1H), 8.29 (t, 2H), 8.04 (d, 2H), 7.66 (d, 1H), 6.68 (t, 1H). ^{13}C NMR (101 MHz, DMSO-d_6) δ 144.43, 132.77, 127.95, 126.51, 126.01, 124.71, 111.28, 104.87. FTIR, cm^{-1}: 3254 (-NH-), 3125(C-H aromatic), 1605(aromatic C=C), 1593 (aromatic C=N), 1238 (C=S), 1501 and 1322 (N=O). HRMS (+ESI-TOF) m/z: [M^+] calcd for $C_{10}H_8N_4O_2S$ 248.0368; found 248.0366.

^{1}H NMR of compound 21

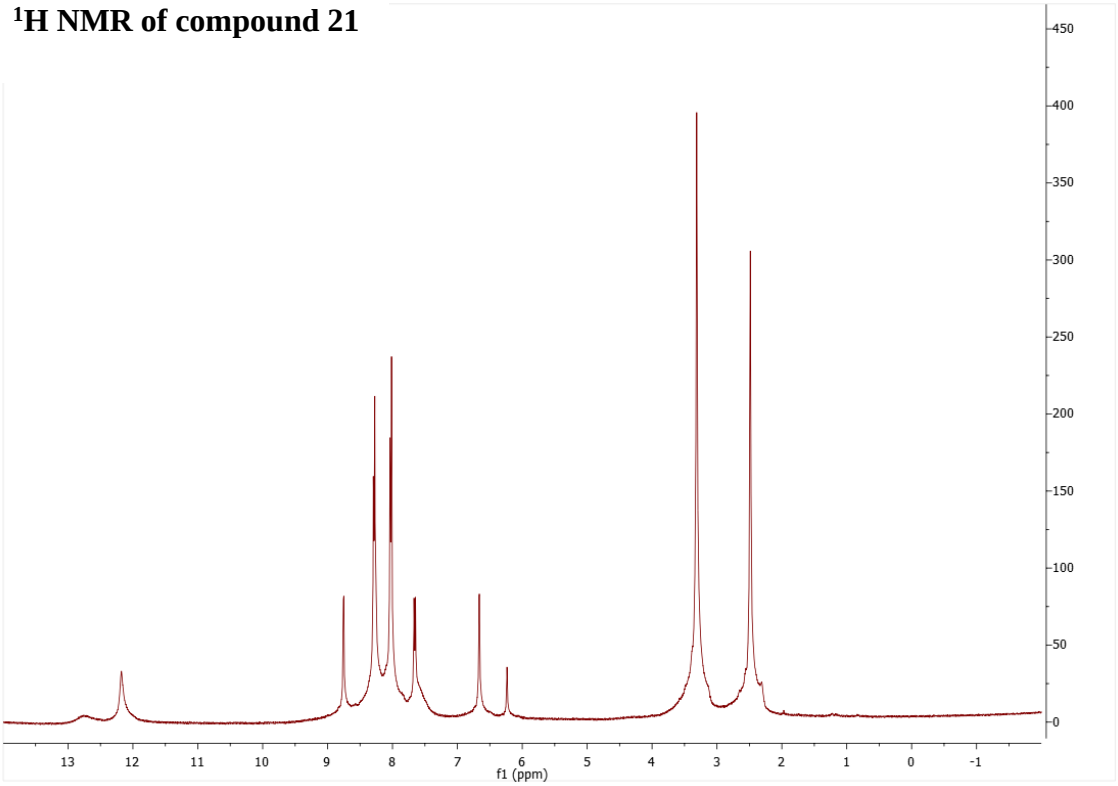

^{13}C NMR of compound 21

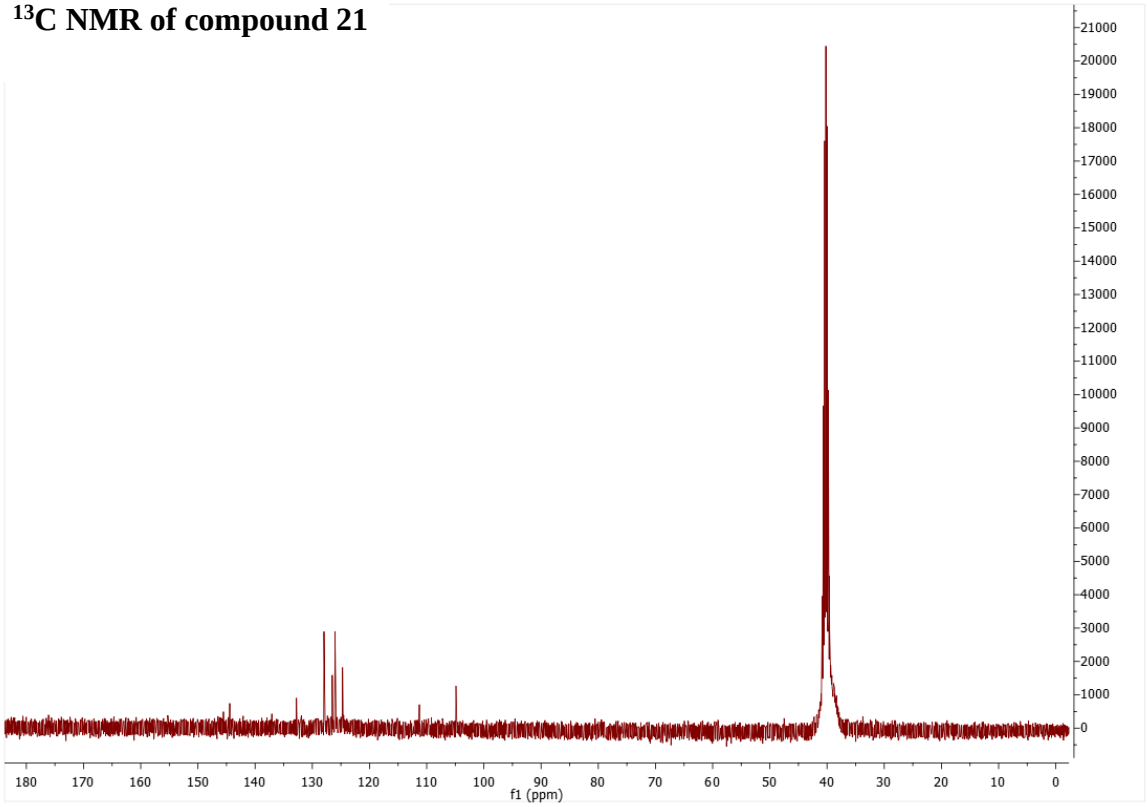

HRMS for compound **21**
Monoisotopic Mass: 248.0362477
Found: 248.0366
Chemical Formula: $C_{10}H_8N_4O_2S$
M+

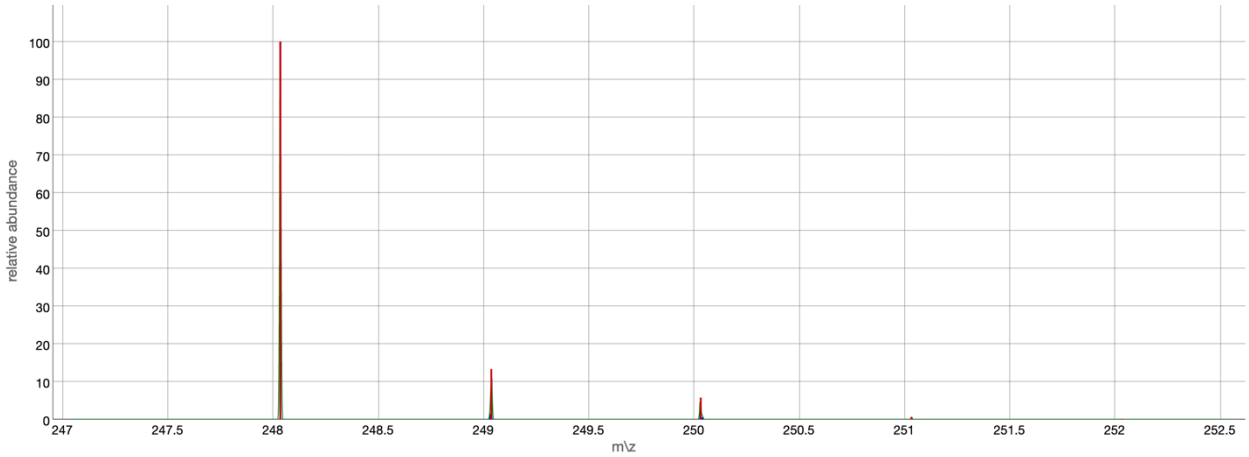

N-(4-fluorophenyl)-1H-pyrazole-1-carbothioamide (22)

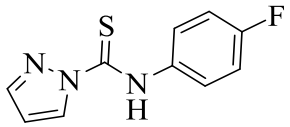

22 (55%)

1H-pyrazole (221 mg, 3.25 mmol) was dissolved in DMF and stirred in a 100 mL round bottom flask. K_2CO_3 (344 mg, 3.25 mmol, 1 eq) was placed in the reaction mixture and stirred vigorously for 1 hour at 50 °C. 4-Fluorophenyl isothiocyanate (500 mg, 3.25 mmol, 1 eq) was added and refluxed at 70 °C for 12 hours. The reaction was monitored by TLC (33% ethyl acetate: hexane). Sodium carbonate solid was filtered off by gravity filtration. THF was evaporated in *vacuum.* Resulting pale yellow solid was re-crystallized with minimum MeOH. Retrieved pale yellow color solid, **22** (55%) was oven dried. ^{1}H NMR (400 MHz, DMSO-d_6) δ 11.85 (s, 1H), 8.74 (s, 1H), 7.98 (s, 1H), 7.63 (d, 2H), 7.28 (d, J = 9.2 Hz, 2H), 6.63 (s, 1H). ^{13}C NMR (101 MHz, DMSO-d_6) δ 175.46, 144.06, 132.66, 128.91, 117.70, 116.09, 110.72, 104.89. FTIR, cm^{-1}: 3245 (-NH-), 3150 (C-H aromatic), 1608 (aromatic C=C), 1548 (aromatic C=N), 1291 (C=S), 1215 (aromatic C-F). HRMS (+ESI-TOF) m/z: [M^+] calcd for $C_{10}H_8FN_3S$ 221.0423; found 221.0421.

^{1}H NMR of compound 22

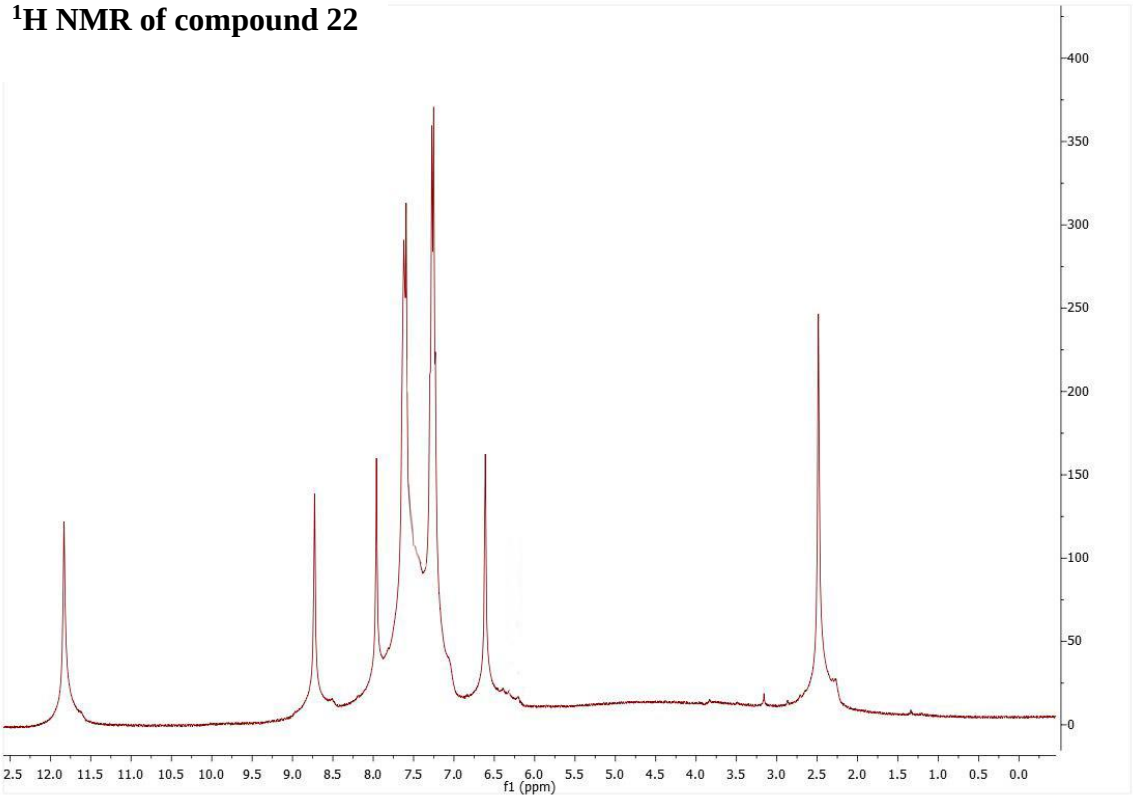

^{13}C NMR of compound 22

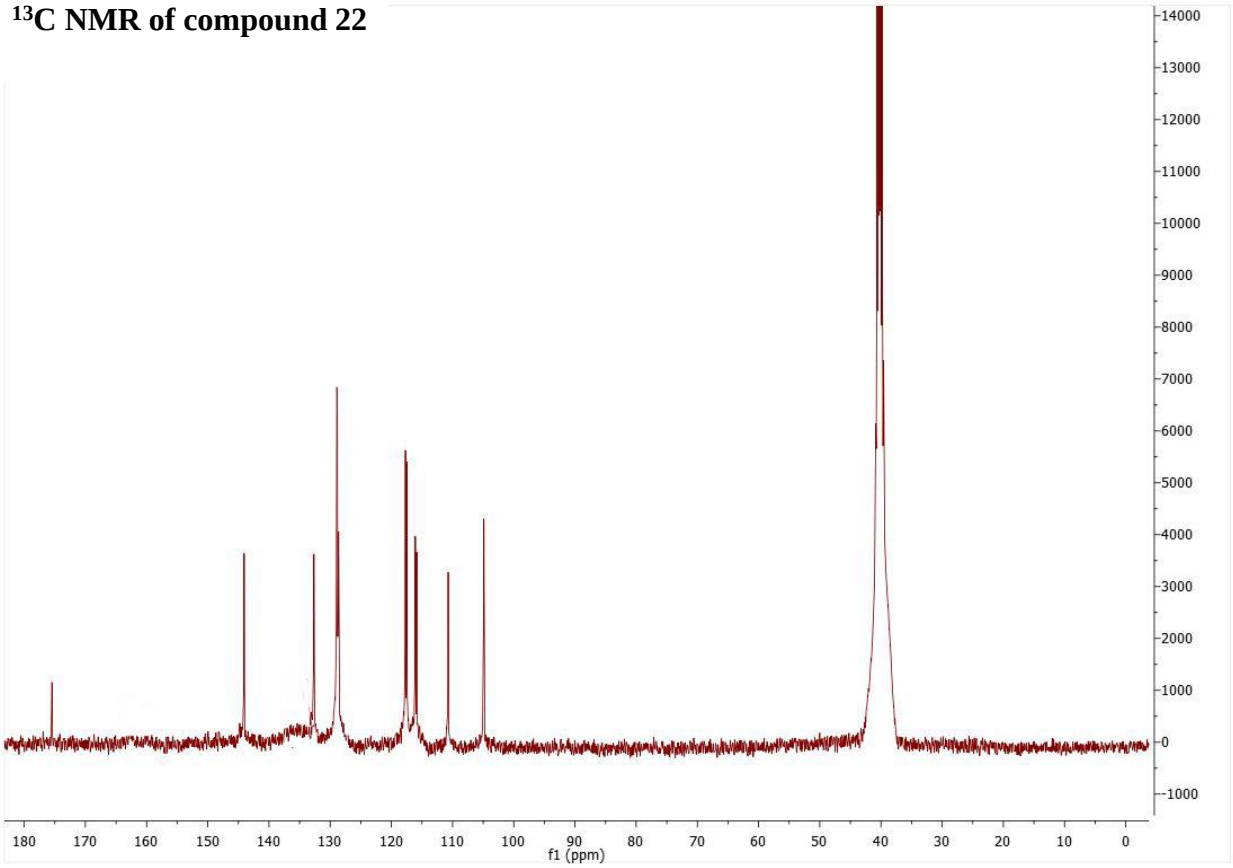

HRMS for compound **22**
Monoisotopic Mass: 221.0417476
Found: 221.0421
Chemical Formula: $C_{10}H_8FN_3S$
M+

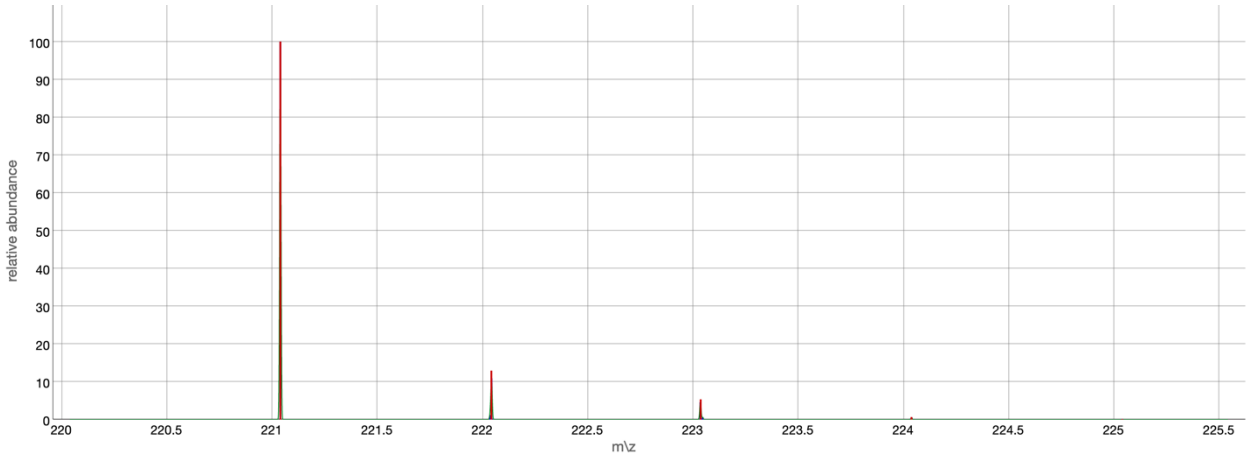

N-(4-chlorophenyl)-1H-pyrazole-1-carbothioamide (23)

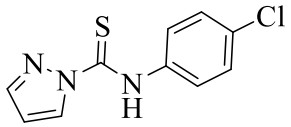

23 (62%)

1H-pyrazole (200 mg, 2.94 mmol) was dissolved in DMF and stirred in a 100 mL round bottom flask. Potassium carbonate (311 mg, 2.94 mmol, 1 eq) was placed in the reaction mixture and stirred vigorously. 4-chlorophenyl isothiocyanate (500 mg, 3.25 mmol, 1 eq) was added and continuously stirred for 15 hr at room temperature. The reaction was monitored by TLC (25% EtOAc/hexanes). Potassium carbonate solid was filtered off by gravity filtration. DMF was evaporated in *vacuum.* Resulting pale yellow solid was re-crystallized with minimum MeOH. Retrieved off-white-solid, **23** (62%) was oven-dried. ^{1}H NMR (400 MHz, DMSO-d_6) δ 8.77 (s, J = 2.6 Hz, 1H), 7.95 (d, 1H), 7.48 (d, 1H), 7.21 (d, 2H), 7.04 (d, 2H), 6.26 (s, J = 1.9 Hz, 1H). ^{13}C NMR (151 MHz, DMSO-d_6) δ 169.00, 162.79, 152.47, 140.03, 130.88, 127.91, 125.19, 105.34. FTIR, cm^{-1}: 3453 (-NH-), 3250 (C-H aromatic), 1645 (aromatic C=C), 1538 (aromatic C=N), 1236 (C=S), 762 (aromatic C-Cl). HRMS (+ESI-TOF) m/z: [M^+] calcd for $C_{10}H_8ClN_3S$ 237.0127; found 237.0124.

^{1}H NMR of compound 23

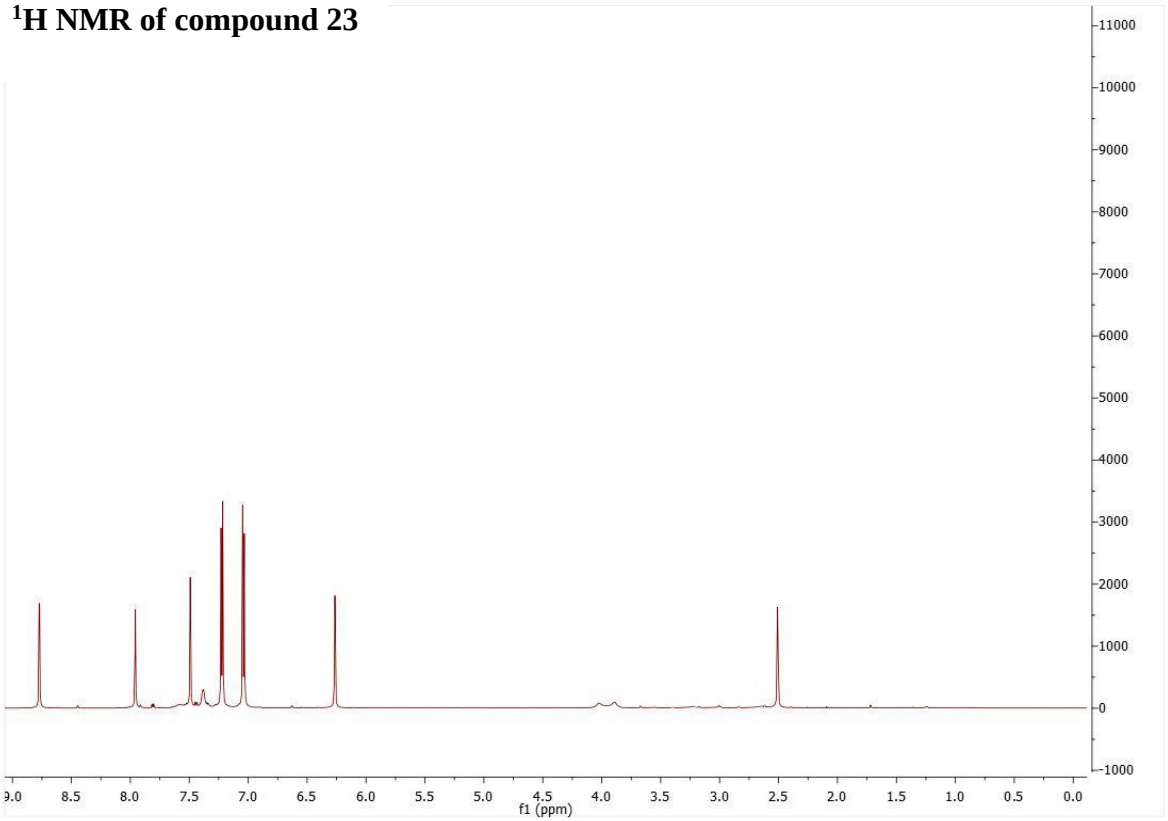

^{13}C NMR of compound 23

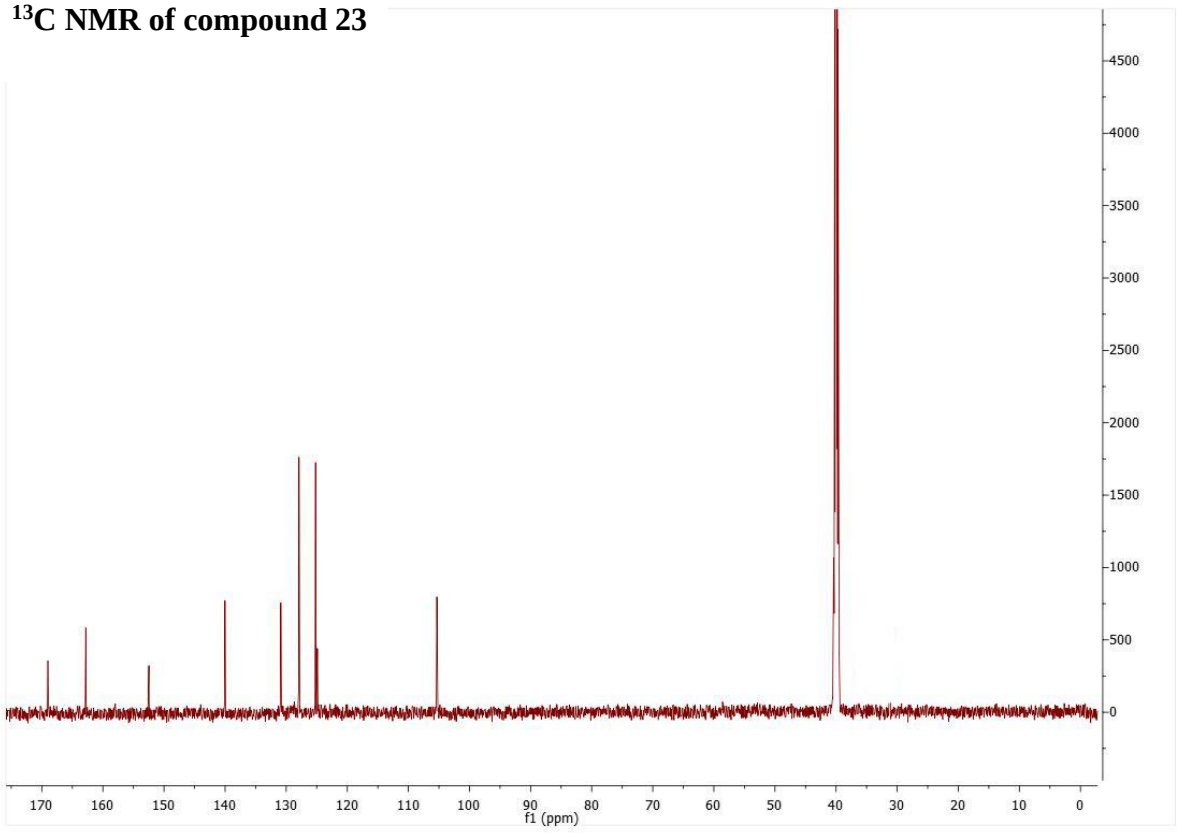

HRMS for compound **23**
Monoisotopic Mass: 237.0121971
Found: 237.0124
Chemical Formula: $C_{10}H_8ClN_3S$
M+

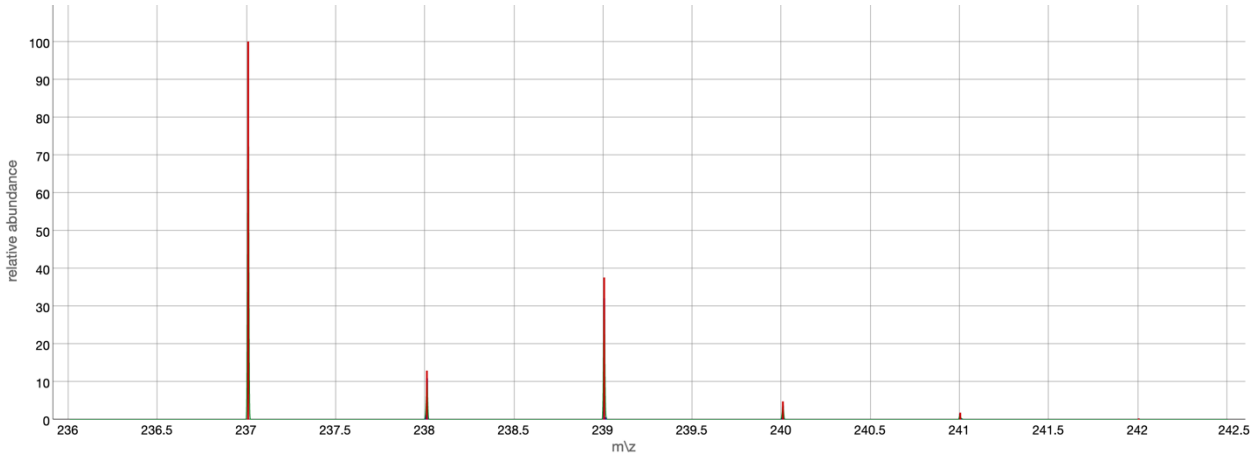

N-(4-bromophenyl)-1H-pyrazole-1-carbothioamide (24)

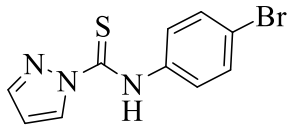

24 (60%)

A mixture of 1H-pyrazole (159 mg, 2.33 mmol) and 4-Bromophenyl isothiocyanate (500mg, 2.33 mmol) were mixed in DMF. Anhydrous potassium carbonate (248 mg, 2.33 mmol) was added to the reaction and stirred at room temperature for 20 hours. The reaction was monitored by TLC (33% EtOAc/hexanes). K_2CO_3 was filtered off by gravity filtration. DMF was distilled off under reduced pressure. Crude product was recrystallized with methanol washed with cold DCM to retrieve off-white solid product **24** (60%). ^{1}H NMR (400 MHz, DMSO-d_6) δ 8.73 (d, 1H), 7.93 (d, J = 14.6 Hz, 1H), 7.71 – 7.48 (m, 2H) Over lapped, 7.40 (d, 2H), 6.59 (d, 1H). ^{13}C NMR (101 MHz, DMSO-d_6) δ 170.15, 143.69, 133.50, 131.99, 128.70, 121.33, 110.26, 104.87. FTIR, cm^{-1}: 3263 (-NH-), 3152 (C-H aromatic), 1630 (aromatic C=C), 1584 (aromatic C=N), 12360 (C=S), 668 (aromatic C-Br). HRMS (+ESI-TOF) m/z: [M^+] calcd for $C_{10}H_8BrN_3S$ 280.9622; found 280.9620.

^{1}H NMR of compound 24

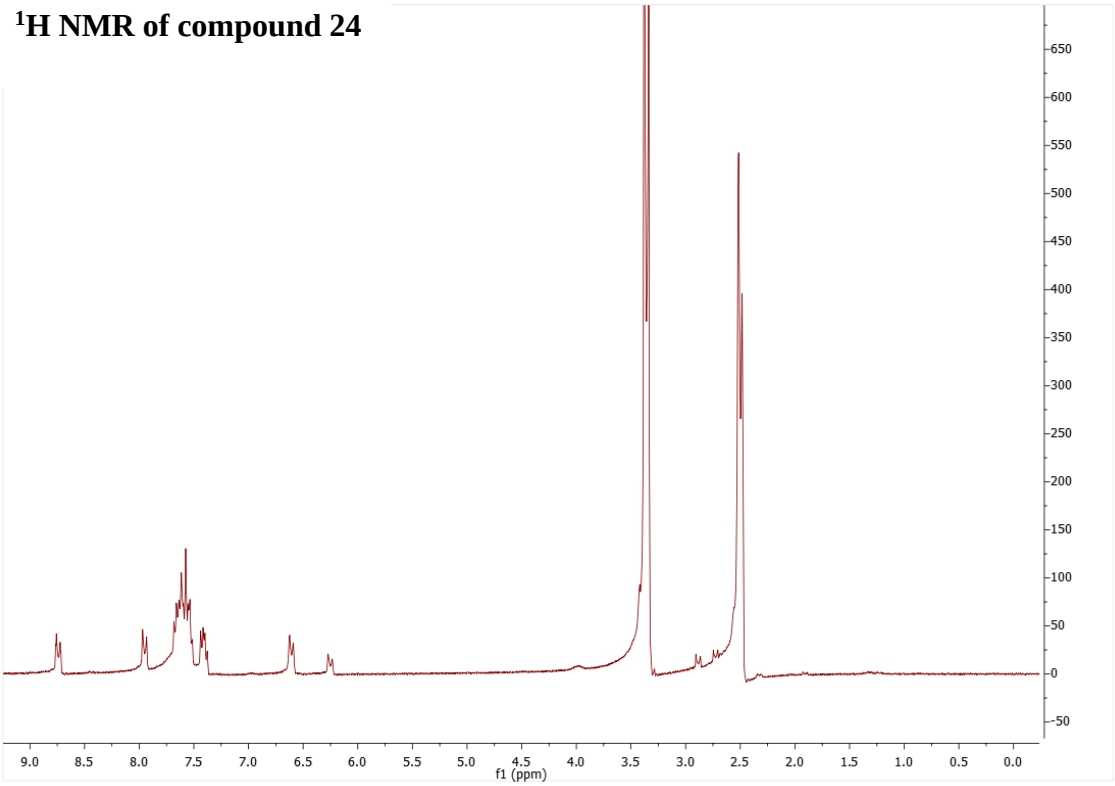

^{13}C NMR of compound 24

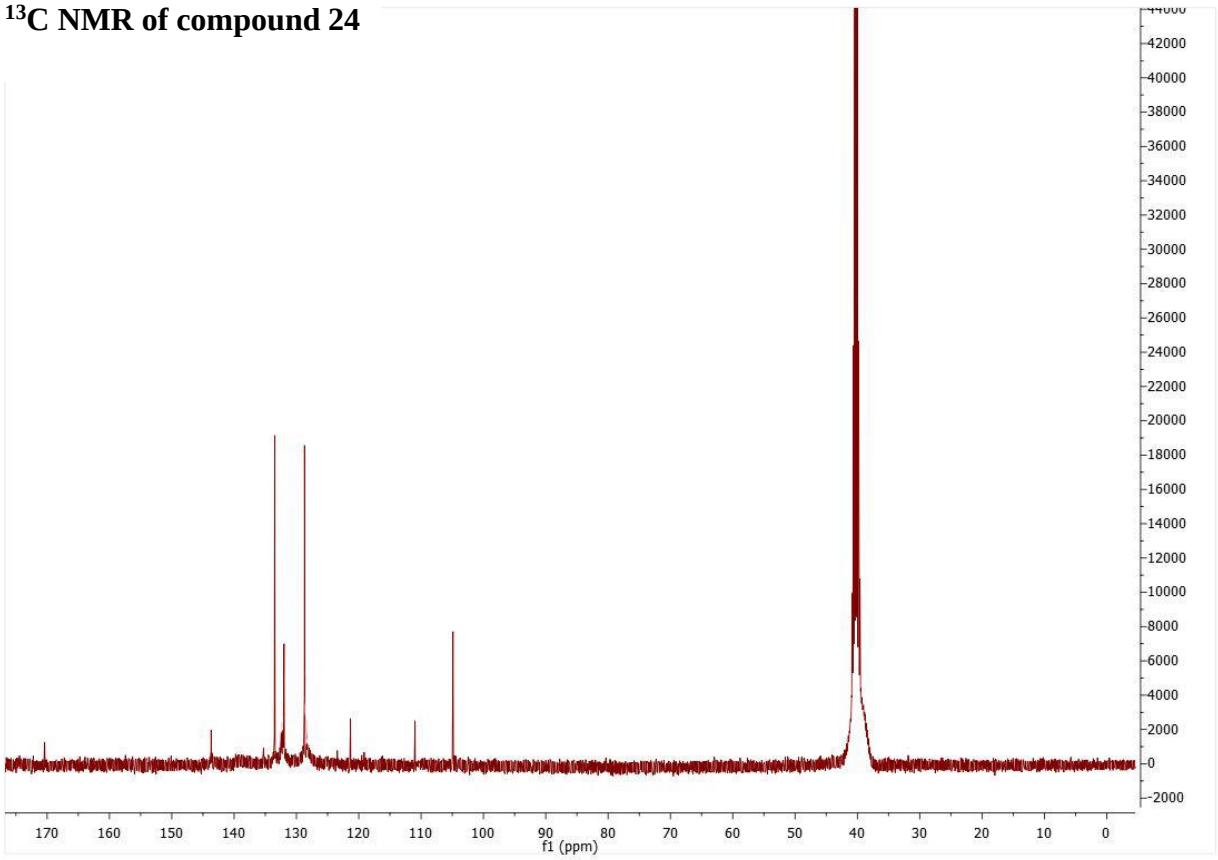

HRMS for compound **24**
Monoisotopic Mass: 280.9616823
Found: 280.9620
Chemical Formula: $C_{10}H_8BrN_3S$
M+

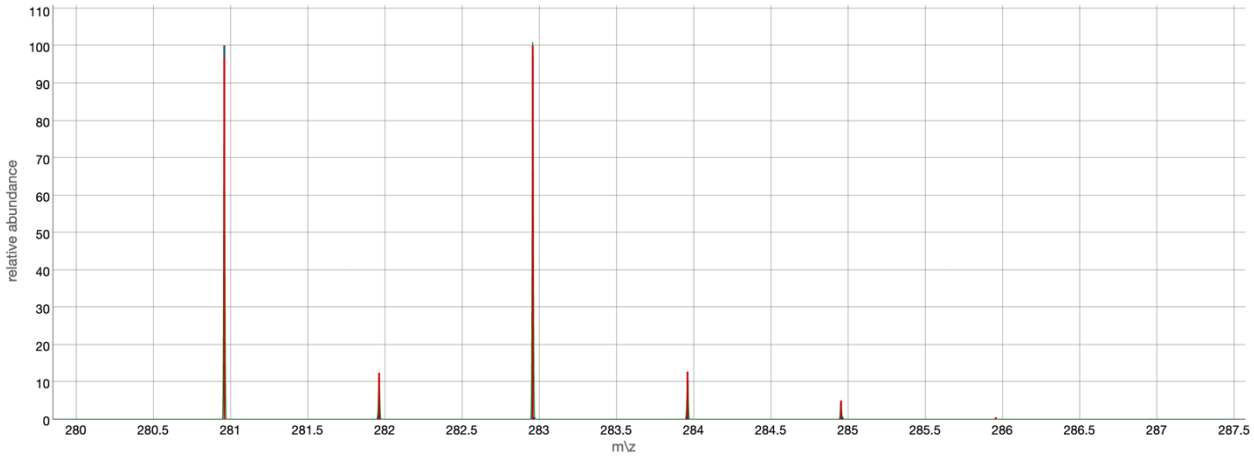

N-(4-methoxyphenyl)-1H-pyrazole-1-carbothioamide (25)

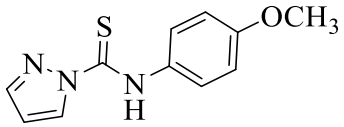

25 (65%)

A mixture of 1H-pyrazole (206 mg, 3.03 mmol) and 4-Methoxyphenyl isothiocyanate (500mg, 3.03 mmol) were mixed in DMF. Anhydrous potassium carbonate (321 mg, 3.03 mmol) was added to the reaction and stirred at room temperature for 20 hours. The reaction was monitored by TLC (33% EtOAc/hexanes). K_2CO_3 was filtered off by gravity filtration. DMF was removed in vacuum. Resulting crude mixture was gluey and retained on the glass wall. Product was recrystallized with methanol to retrieve a pale yellowish solid product **25** (65%). ^{1}H NMR (400 MHz, DMSO-d_6) δ 8.76 (s, 1H), 7.45 (s, 1H), 7.05 (d, J = 8.0 Hz, 2H), 6.78 (d, J = 8.8 Hz, 2H), 6.22 (s, 1H), 3.70 (m, 3H). ^{13}C NMR (101 MHz, DMSO-d_6) δ 173.45, 156.67, 146.35, 133.82, 128.15, 123.66, 114.84, 109.64, 79.93. FTIR, cm^{-1}: 3272 (-NH-), 3125(C-H aromatic), 2840 (C-H), 1651(aromatic C=C), 1490 (aromatic C=N), 1250 (C=S), 1234 (C-O). HRMS (+ESI-TOF) m/z: [M^+] calcd for $C_{11}H_{11}N_3OS$ 233.0623; found 233.0623.

^{1}H NMR of compound 25

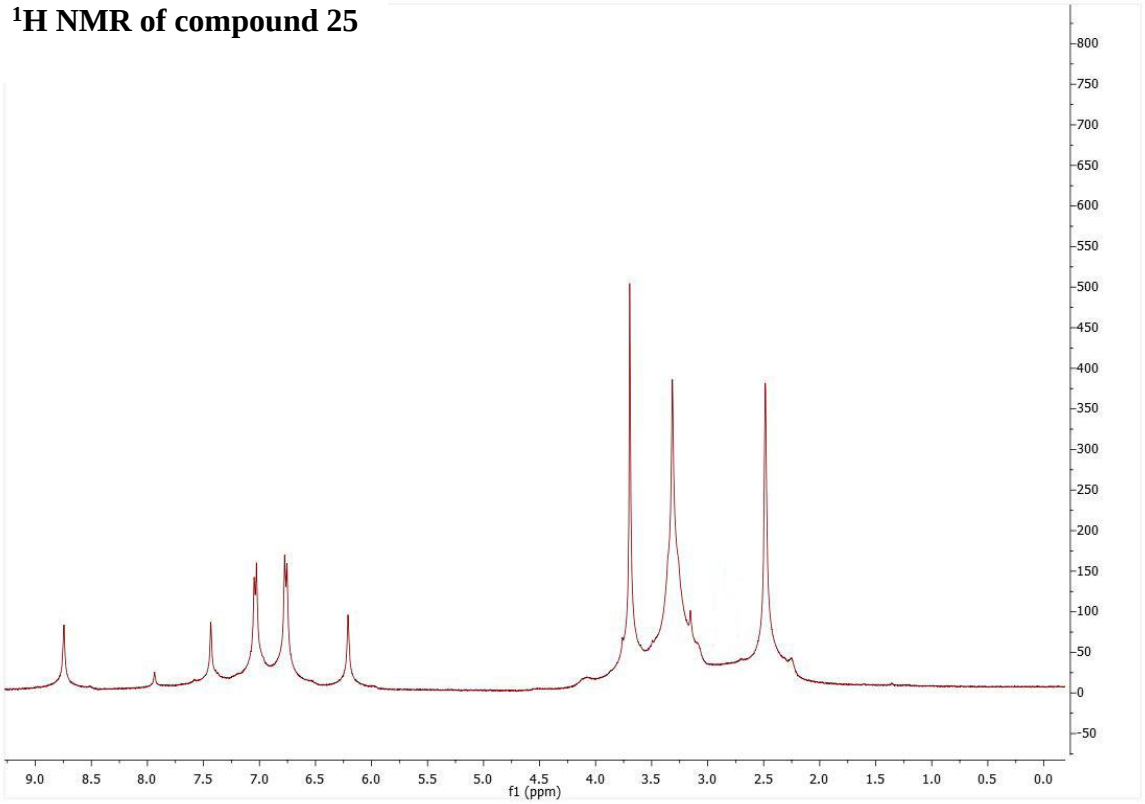

^{13}C NMR of compound 25

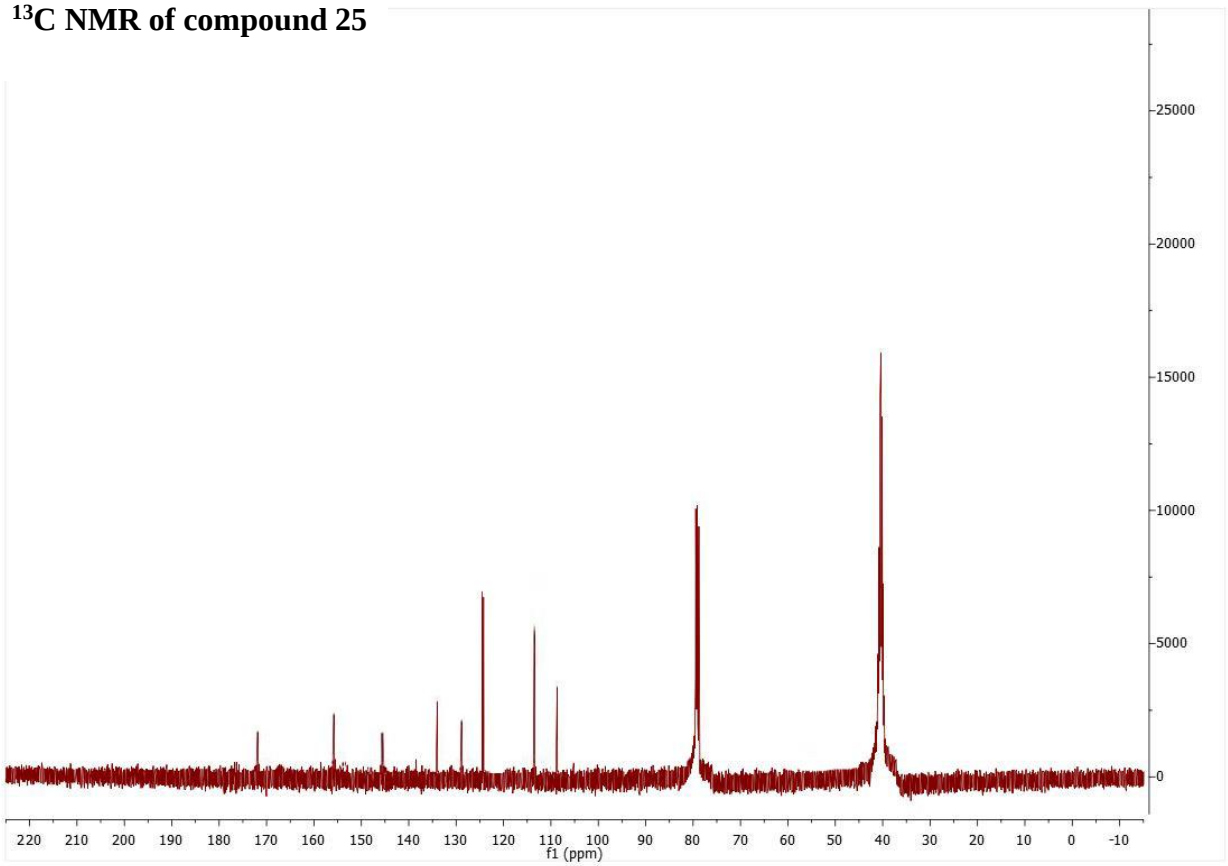

HRMS for compound **25**
Monoisotopic Mass: 233.0617342
Found: 233.0623
Chemical Formula: $C_{11}H_{11}N_3OS$
M+

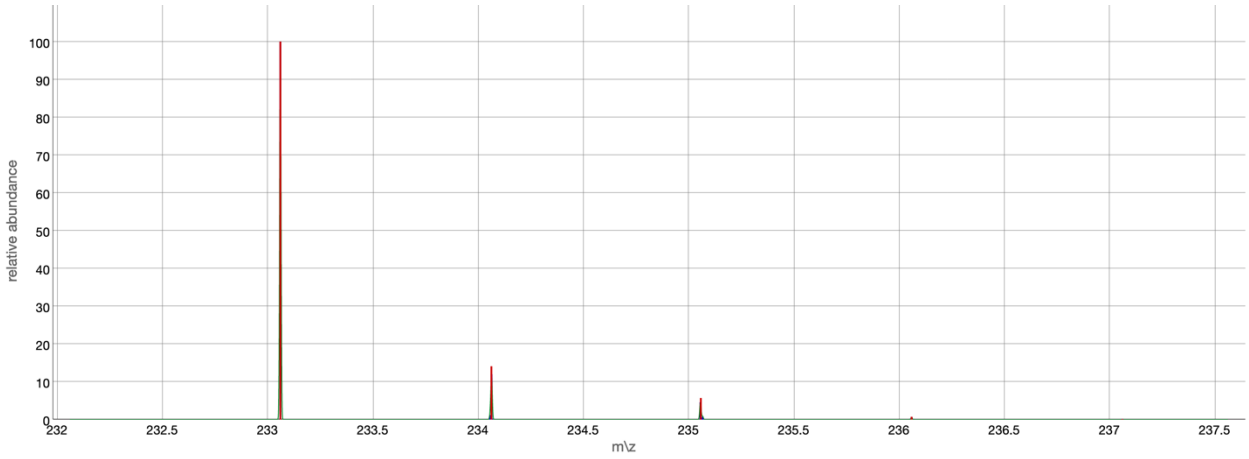

N-(p-tolyl)-1H-pyrazole-1-carbothioamide (26)

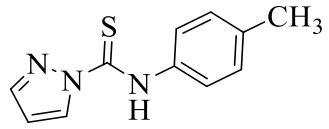

26 (68%)

A mixture of 1H-pyrazole (228 mg, 3.34 mmol) and 4-Tolyl isothiocyanate (500mg, 3.34 mmol) were mixed in DMF. Anhydrous potassium carbonate (355 mg, 3.34 mmol) was added to the reaction and stirred at room temperature for 20 hours. The reaction was monitored by TLC (33% EtOAc/hexanes). K_2CO_3 was filtered off by gravity filtration. DMF was removed *in vacuum*. Resulting crude mixture was orange color and retained on the glass wall. Product was recrystallized with methanol washed with cold DCM to retrieve off-white solid product **26** (68%). ^{1}H NMR (600 MHz, DMSO-d_6) δ 8.75 (d, J = 2.8 Hz, 1H), 7.97 (d, J = 1.6 Hz, 1H), 7.50 (m, 2H), 7.25 (m, 2H), 6.63 (dd, J = 2.8, 1.7 Hz, 1H), 2.33 (s, 3H). ^{13}C NMR (151 MHz, DMSO-d_6) δ 174.62, 143.66, 132.32, 130.81, 129.42, 125.91, 110.32, 104.67, 21.17. FTIR, cm^{-1}: 3277 (-NH-), 3119 (C-H aromatic), 2914 (aliphatic C-H), 1658 (aromatic C=C), 1584 (aromatic C=N), 1240 (C=S), 1516 (C=C-C). HRMS (+ESI-TOF) m/z: [M^+] calcd for $C_{11}H_{11}N_3S$ 217.0674; found 217.0671.

^{1}H NMR of compound 26

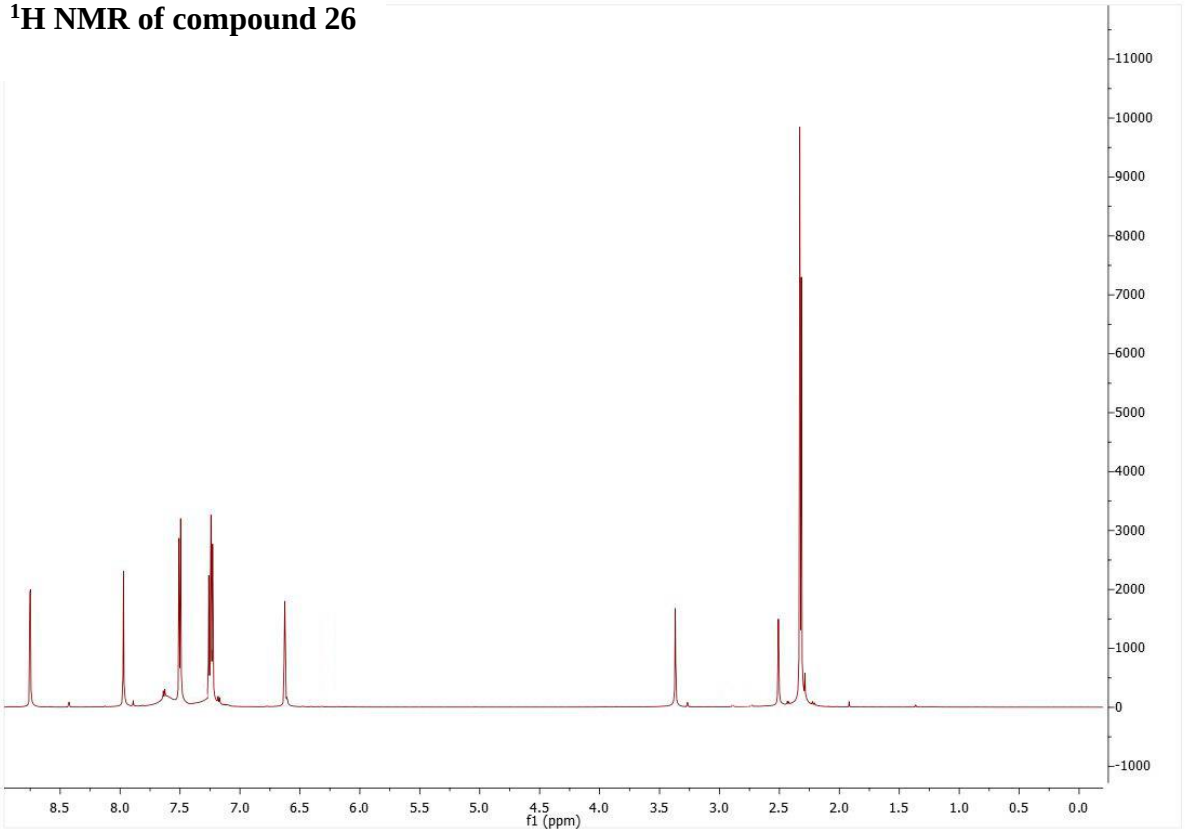

^{13}C NMR of compound 26

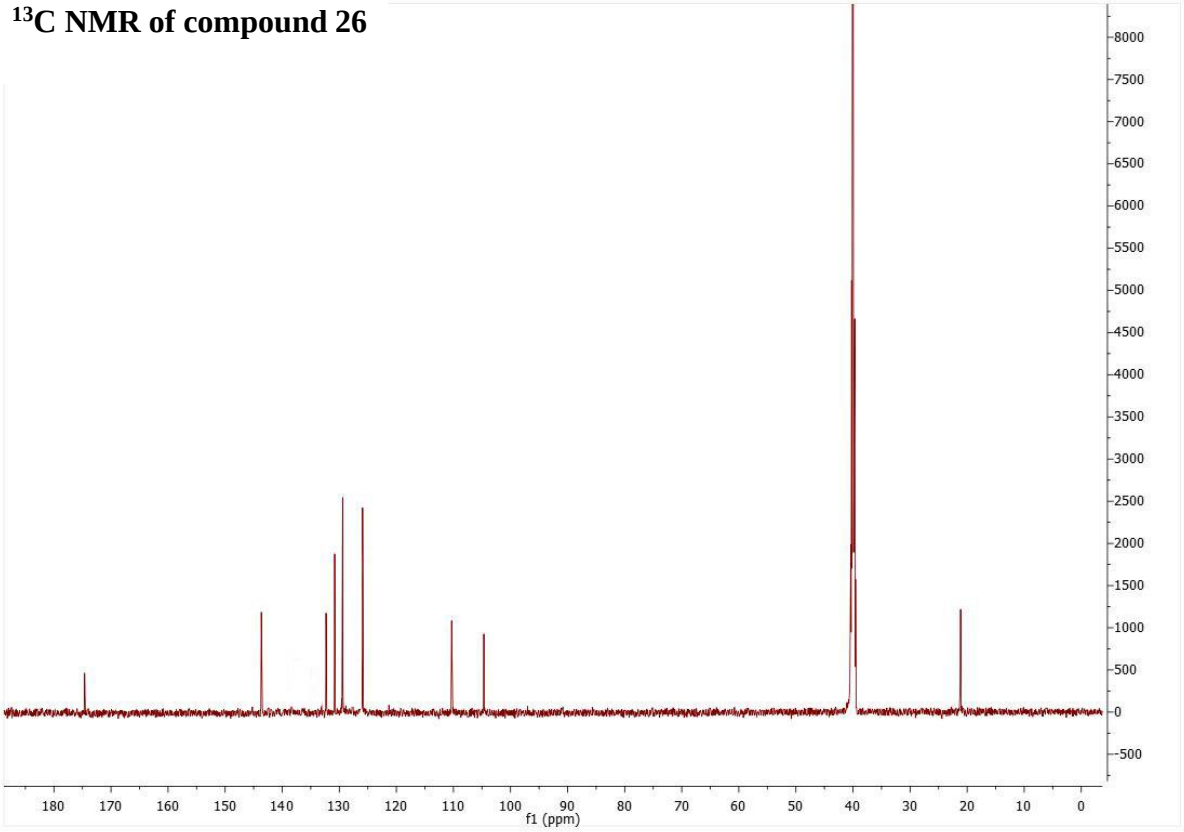

HRMS for compound **26**
Monoisotopic Mass: 217.0668195
Found: 217.0671
Chemical Formula: $C_{11}H_{11}N_3S$
M+

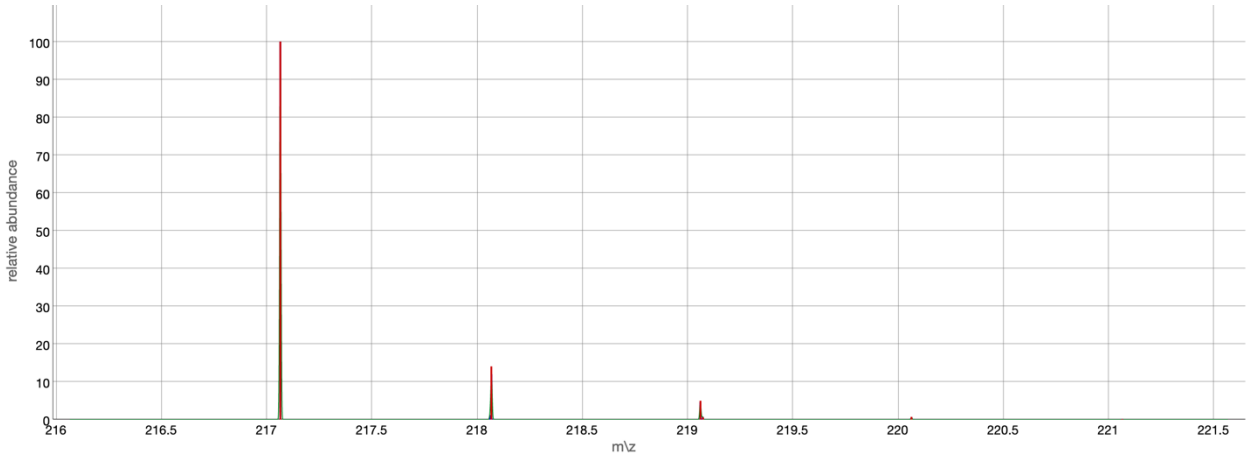

3-amino-N-(4-nitrophenyl)-1H-pyrazole-1-carbothioamide (27)

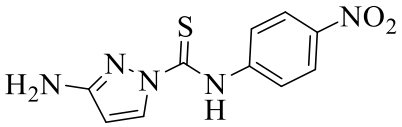

27 (66%)

1H-pyrazol-3-amine (230 mg, 2.77 mmol) was dissolved in DCM and stirred in a 100 mL round bottom flask. 4-Nitrophenyl isothiocyanate (500 mg, 2.77 mmol, 1 eq) was dissolved in DCM separately and added to the stirring reaction dropwise. The reaction was then refluxed for 20 hours at 60 ˚C. The reaction was monitored by TLC (DCM/ methanol 50:2). All volatile components were evaporated under vacuum and resulting crude product was purified by flash column chromatography (DCM/methanol 1% - 10%) to afford 66% yield of **27** as a yellow color solid. ^{1}H NMR (600 MHz, DMSO-d_6) δ 11.35 (s, 1H), 8.45 (d,1H), 8.26 (d, 2H), 8.06 (d, 2H), 6.05 (d, 1H), 5.85 (s, 2H). ^{13}C NMR (151 MHz, DMSO-d_6) δ 172.90, 159.33, 144.98, 144.54, 133.27, 125.10, 124.44, 103.37.

^{1}H NMR of compound 27

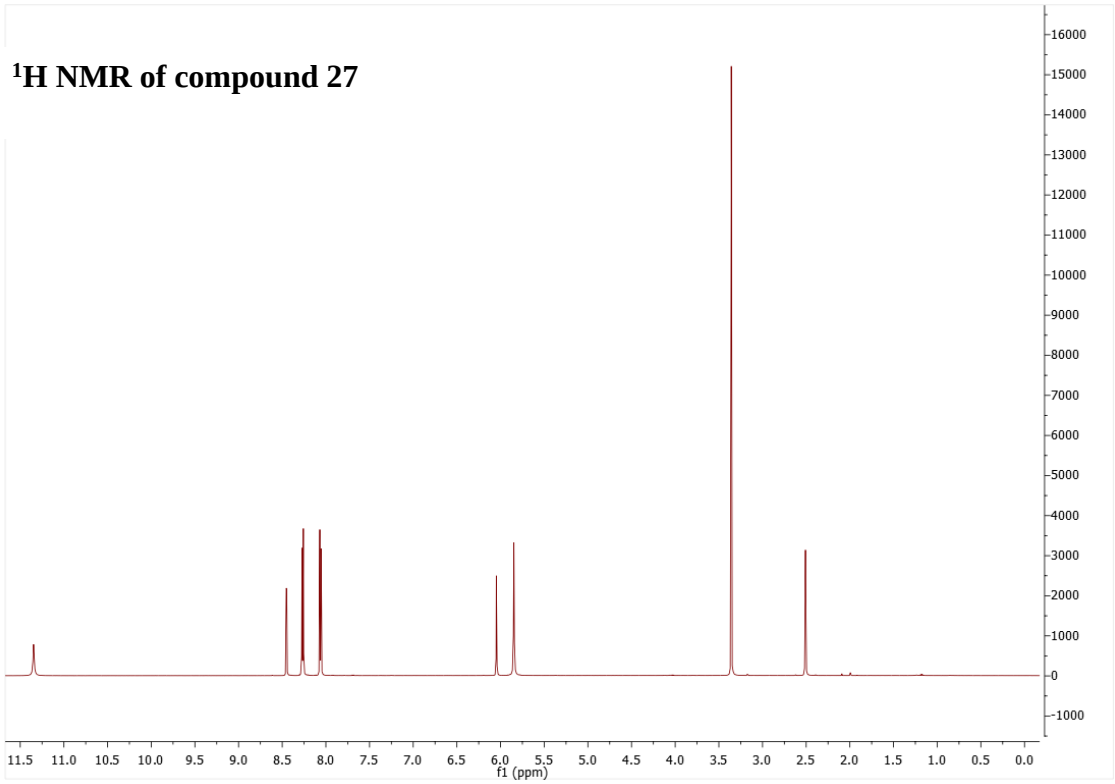

^{13}C NMR of compound 27

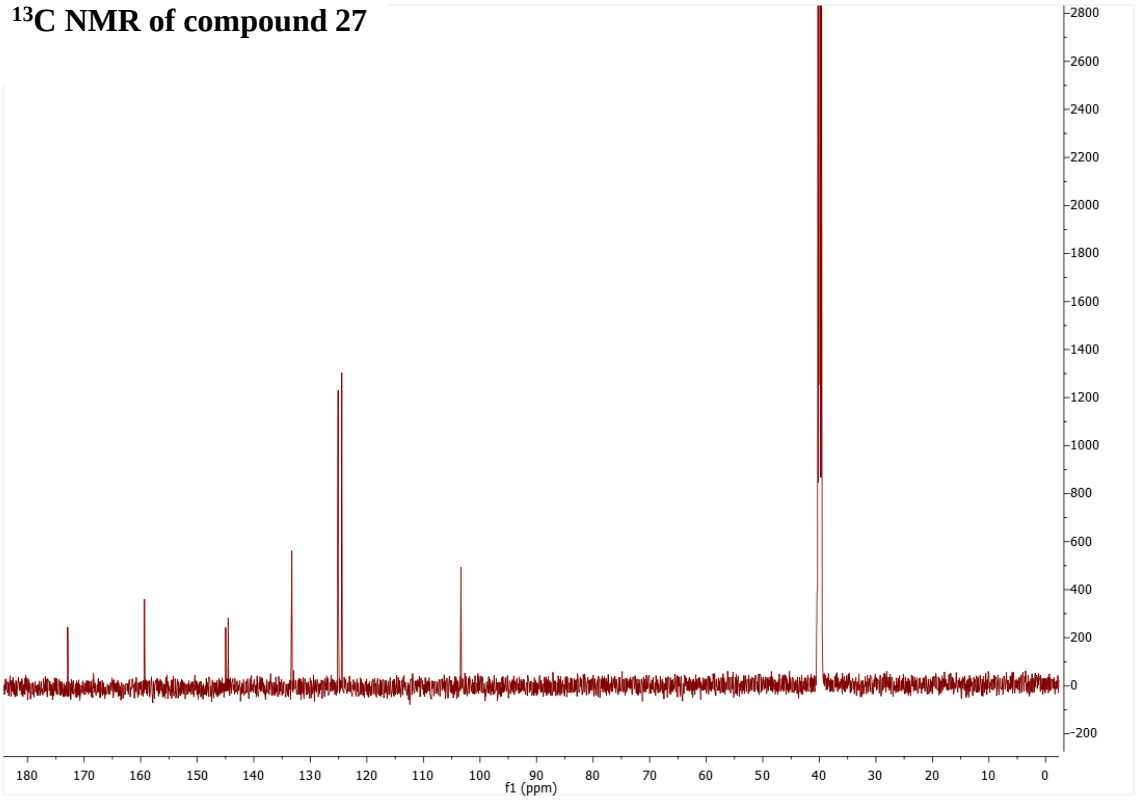

MS of compound **27**

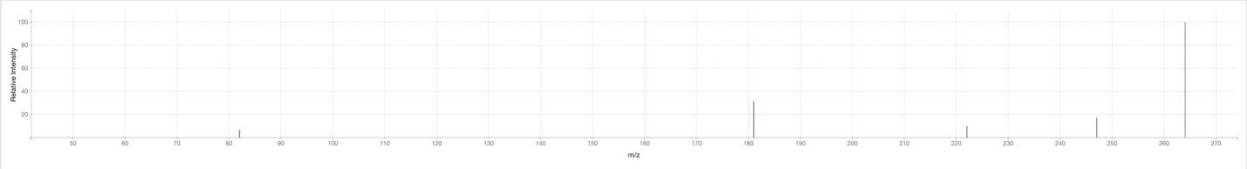

Peak intensity	Mass	Formula
100%	264 [M^+H^+]	$C_{10}H_9N_5O_2S$
68%	181[H^+]	$C_7H_4N_2O_2S$
26%	82	$C_3H_4N_3$

3-amino-N-(4-fluorophenyl)-1H-pyrazole-1-carbothioamide (28).

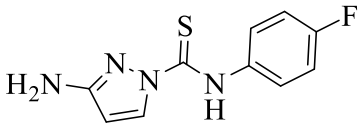

28 (55%)

1H-pyrazol-3-amine (271 mg, 3.26 mmol) was dissolved in DCM and stirred in a 100 mL round bottom flask. 4-Fluorophenyl isothiocyanate (500 mg, 3.26 mmol, 1 eq) was dissolved in DCM separately and added to the stirring reaction dropwise. The reaction was then refluxed for 20 hours at 60 °C and solid sedimentation was observed during refluxing. The reaction was monitored by TLC (DCM/ methanol 50:2). All volatile component was evaporated under vacuum and resulting crude product was purified by flash column chromatography (100% DCM) to afford 55% yield of **28,** off-white to pale yellow color solid. ^{1}H NMR (400 MHz, DMSO-d_6) δ 7.74 (s, 1H), 7.60 (dt, J = 9.4, 4.8 Hz, 2H), 7.21 (td, J = 8.9, 4.9 Hz, 2H), 6.02 (s, 1H). ^{13}C NMR (151 MHz, DMSO-d_6) δ 177.22, 160.81, 149.81, 135.73 (d, J = 2.9 Hz), 130.15, 127.18 (d, J = 8.3 Hz), 115.61 (d, J = 22.4 Hz), 94.70. FTIR, cm^{-1}: 3332 (-NH_2), 3166 (-NH-), 3062 (C-H aromatic), 1608 (aromatic C=C), 1579 (aromatic C=N), 1273 (C=S), 1184 (aromatic C-F). HRMS (+ESI-TOF) m/z: [M^+] calcd for $C_{10}H_9FN_4S$ 236.0532; found 236.0530.

^{1}H NMR of compound 28

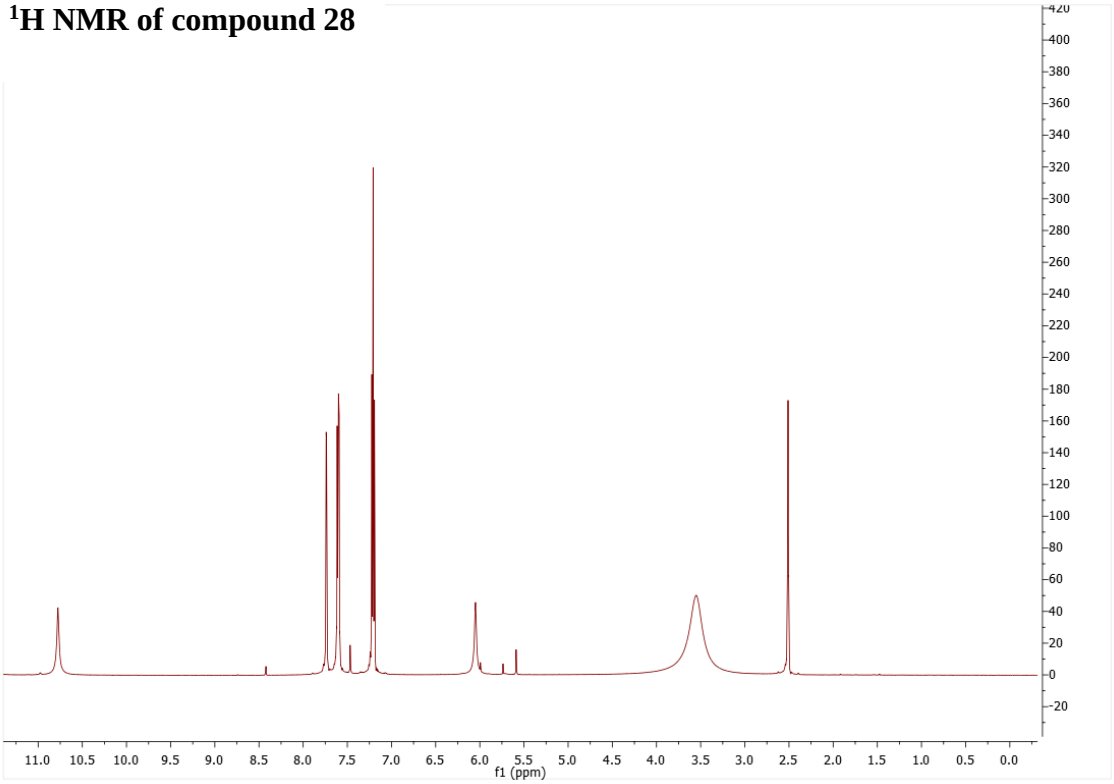

^{13}C NMR of compound 28

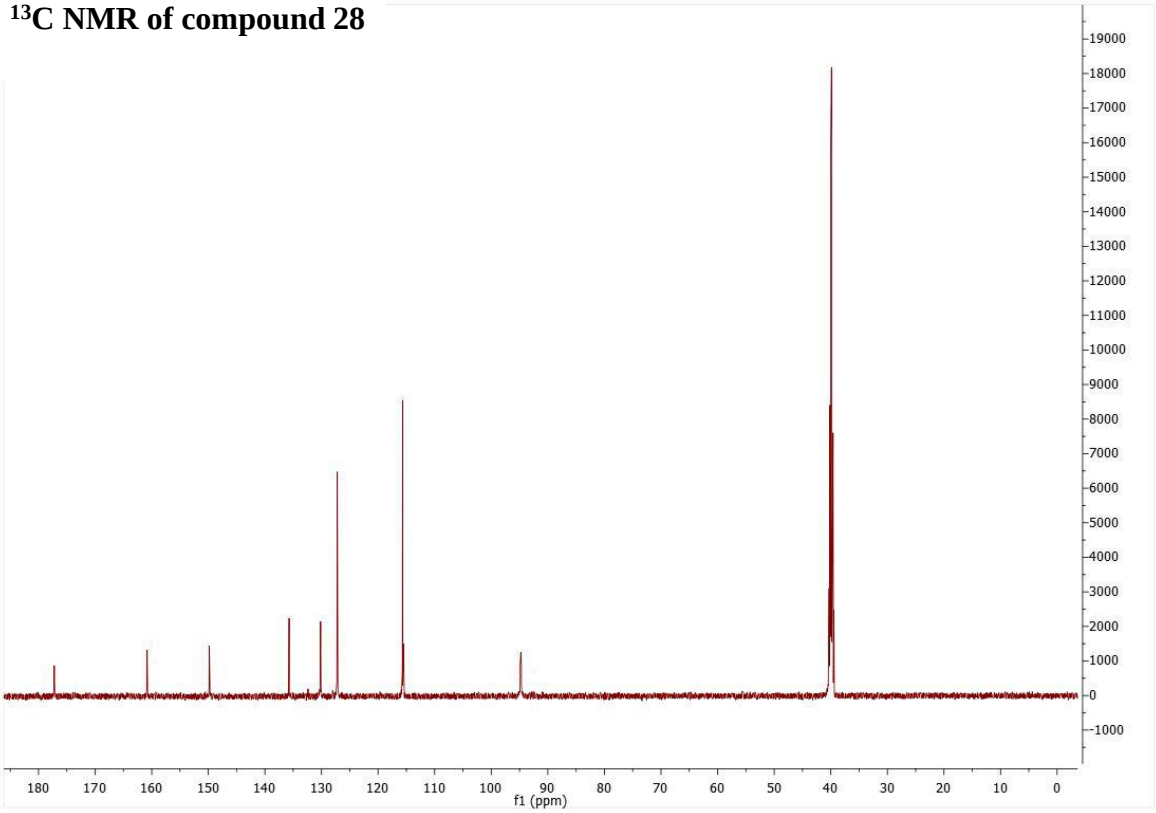

HRMS for compound **28**
Monoisotopic Mass: 236.0526467
Found: 236.0530.
Chemical Formula: $C_{10}H_9FN_4S$
M+

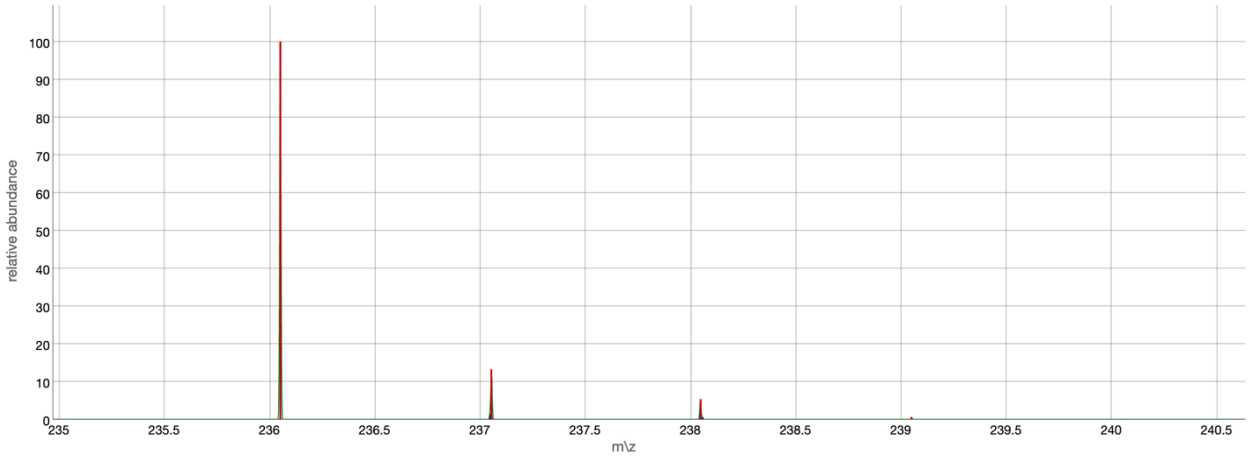

3-amino-N-(4-bromophenyl)-1H-pyrazole-1-carbothioamide (29).

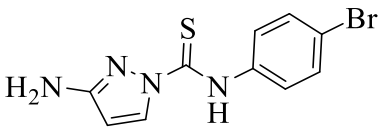

29 (50%)

1H-pyrazol-3-amine (194 mg, 2.34 mmol) was dissolved in DCM and stirred in a 100 mL round bottom flask. 4-Bromophenyl isothiocyanate (500 mg, 2.34 mmol, 1 eq) was dissolved in DCM separately and added to the stirring reaction dropwise. The reaction was then refluxed for 20 hours at 60 ˚C. The reaction was monitored by TLC (DCM/ methanol 50:2). All volatile components were evaporated under vacuum and resulting crude product was purified by flash column chromatography (100% DCM) to afford 50% yield of **29,** pale yellow color solid. ^{1}H NMR (400 MHz, DMSO-d_6) δ 7.73 (d, J = 3.1 Hz, 1H), 7.60 (d, 2H), 7.54 (d, 2H), 6.02 (s, 1H). ^{13}C NMR (151 MHz, DMSO-d_6) δ 176.66, 149.72, 138.84, 131.78, 130.20, 126.53, 117.75, 94.80. FTIR, cm^{-1}: 3361, 3338 (-NH_2), 3176 (-NH-), 3047 (C-H aromatic), 2960, 2920 (CH pyrazole), 1581, (aromatic C=C), 1533 (aromatic C=N), 1264 (C=S), 701 (aromatic C-Br). HRMS (+ESI-TOF) m/z: [M^+] calcd for $C_{10}H_9BrN_4S$ 295.9731; found 295.9734.

^{1}H NMR of compound 29

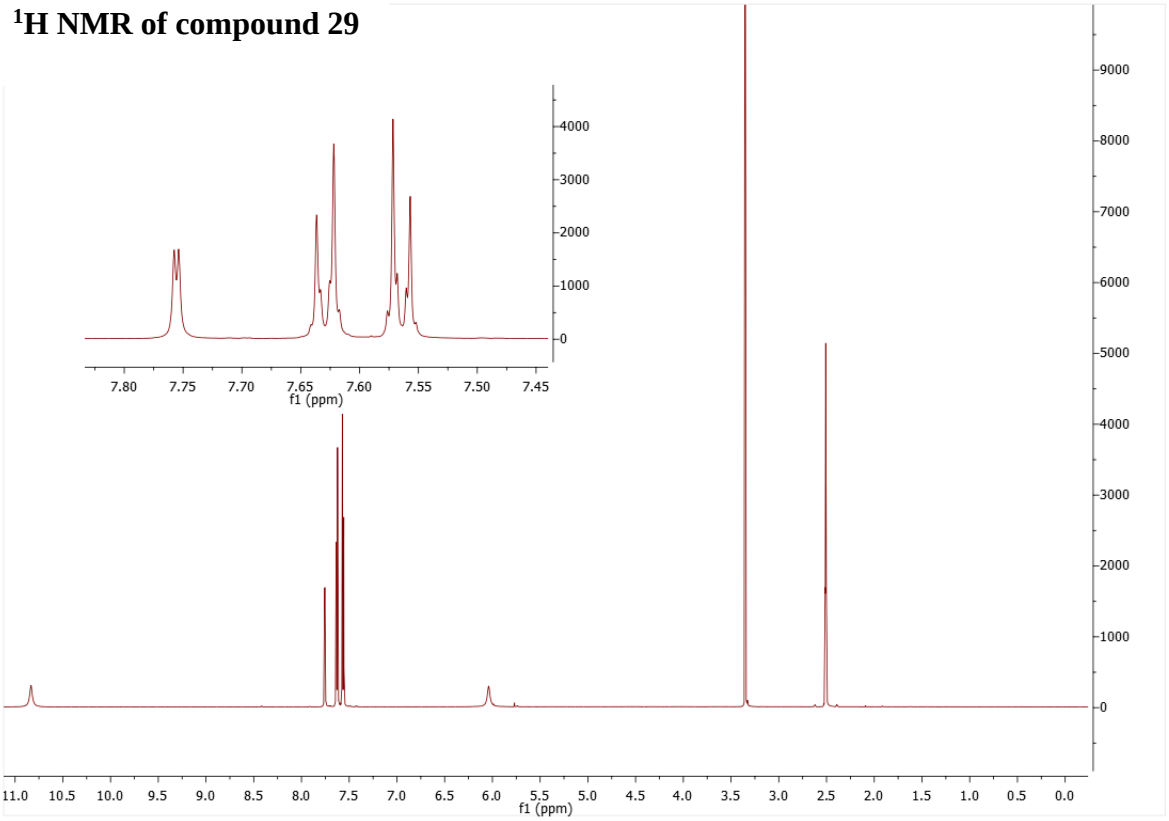

^{13}C NMR of compound 29

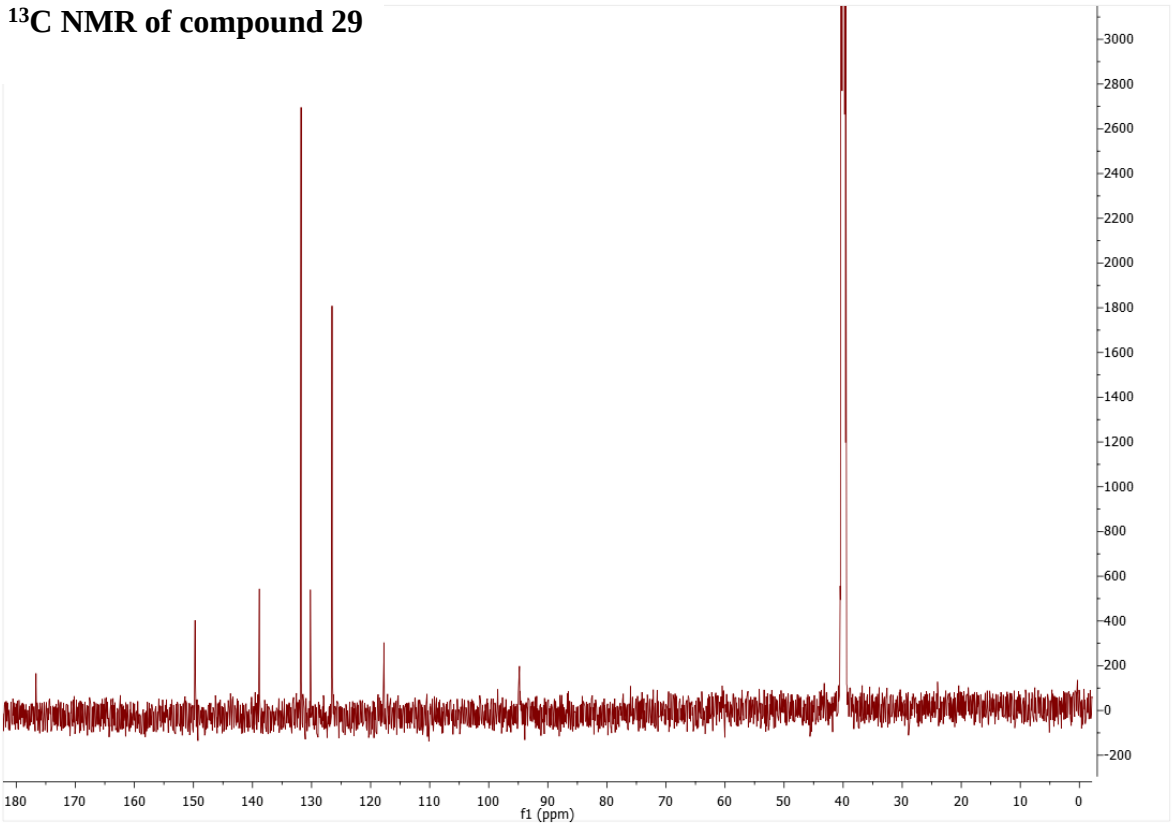

HRMS for compound **29**
Monoisotopic Mass: 295.9725814
Found: 295.9734
Chemical Formula: $C_{10}H_9BrN_4S$
M+

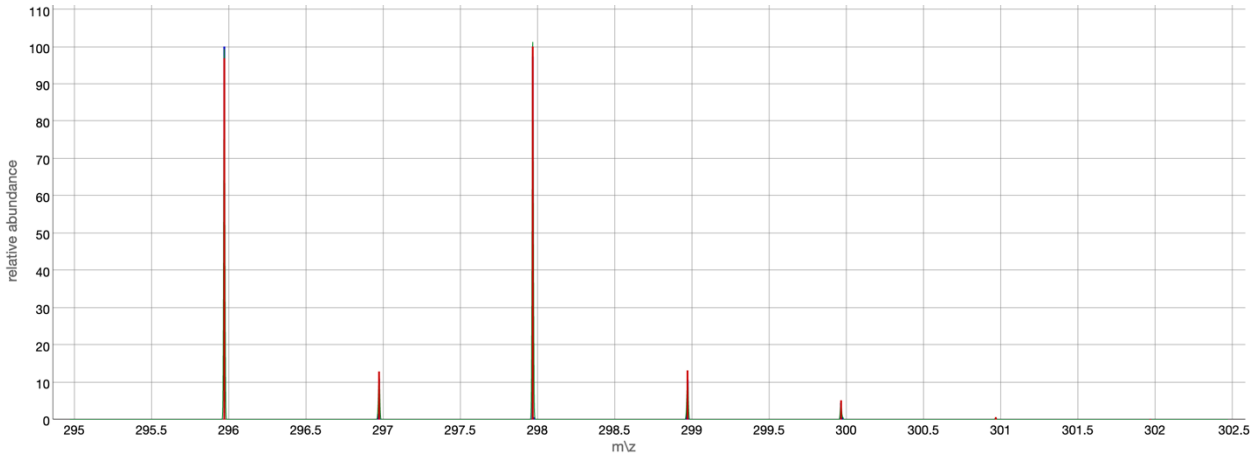

3-amino-N-(4-methoxyphenyl)-1H-pyrazole-1-carbothioamide (30).

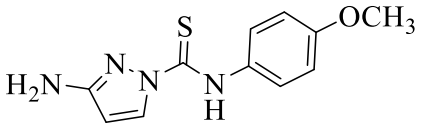

30 (75%)

1H-pyrazol-3-amine (251 mg, 3.03 mmol) was dissolved in DCM and stirred in a 100 mL round bottom flask. 4-Methoxyphenyl isothiocyanate (450 mg, 3.03 mmol, 1 eq) was dissolved in DCM separately and added to the stirring reaction dropwise. The reaction was then refluxed for 20 hours at 60 °C. The reaction was monitored by TLC (100% DCM). All volatile components were evaporated under vacuum and resulting crude product was purified by flash column chromatography (100% DCM) to afford 75% yield of **30,** off-white solid. ^{1}H NMR (400 MHz, DMSO-d_6) δ 7.73 (d, J = 2.4 Hz, 1H), 7.44 (d, J = 8.5 Hz, 2H), 6.93 (d, 2H), 6.01 (s, 1H), 3.76 (s, 3H). ^{13}C NMR (101 MHz, DMSO-d_6) δ 177.36, 157.56, 150.18, 132.52, 130.29, 126.85, 114.33, 94.83, 55.94. FTIR, cm^{-1}: 3413 (-NH_2), 3184 (-NH-), 3051 (C-H aromatic), 2929 (C-H), 1583 (aromatic C=C), 1535 (aromatic C=N), 1250 (C=S), 1232 (C-O). HRMS (+ESI-TOF) m/z: [M^+] calcd for $C_{11}H_{12}N_4OS$ 248.0730; found 248.0731.

^{1}H NMR of compound 30

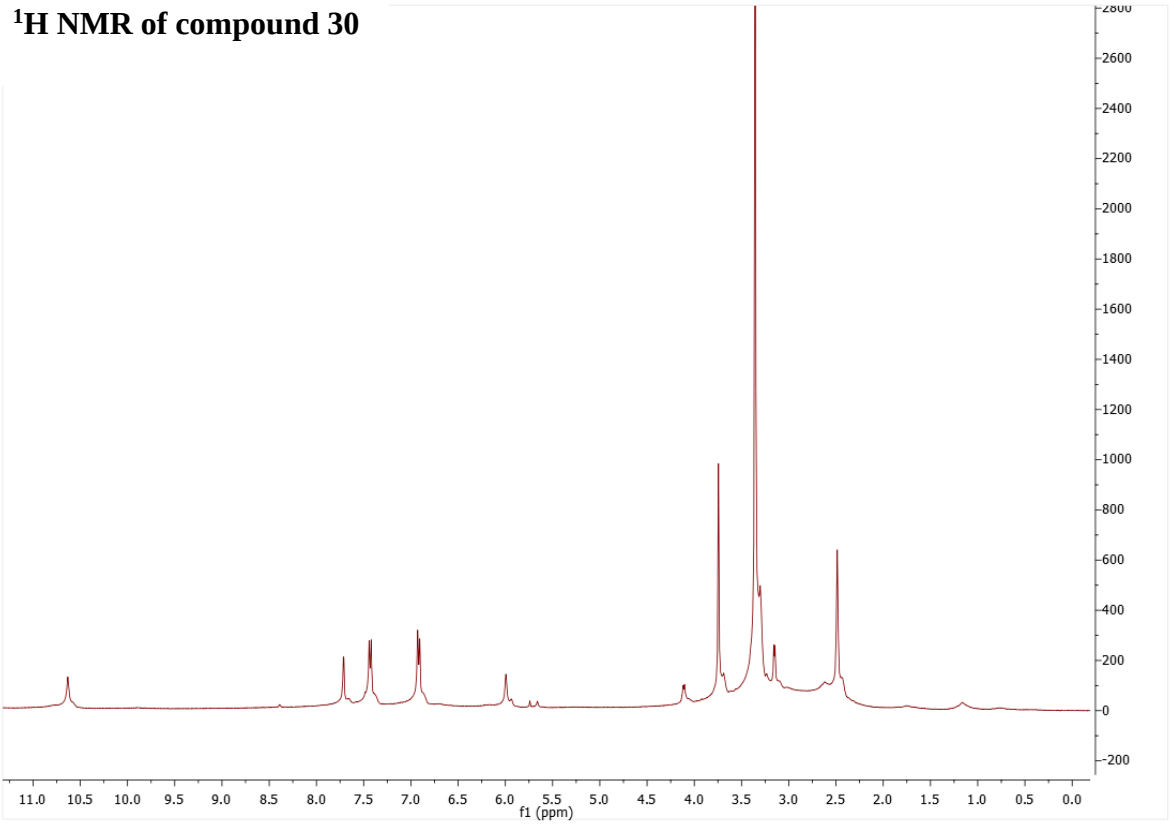

^{13}C NMR of compound 30

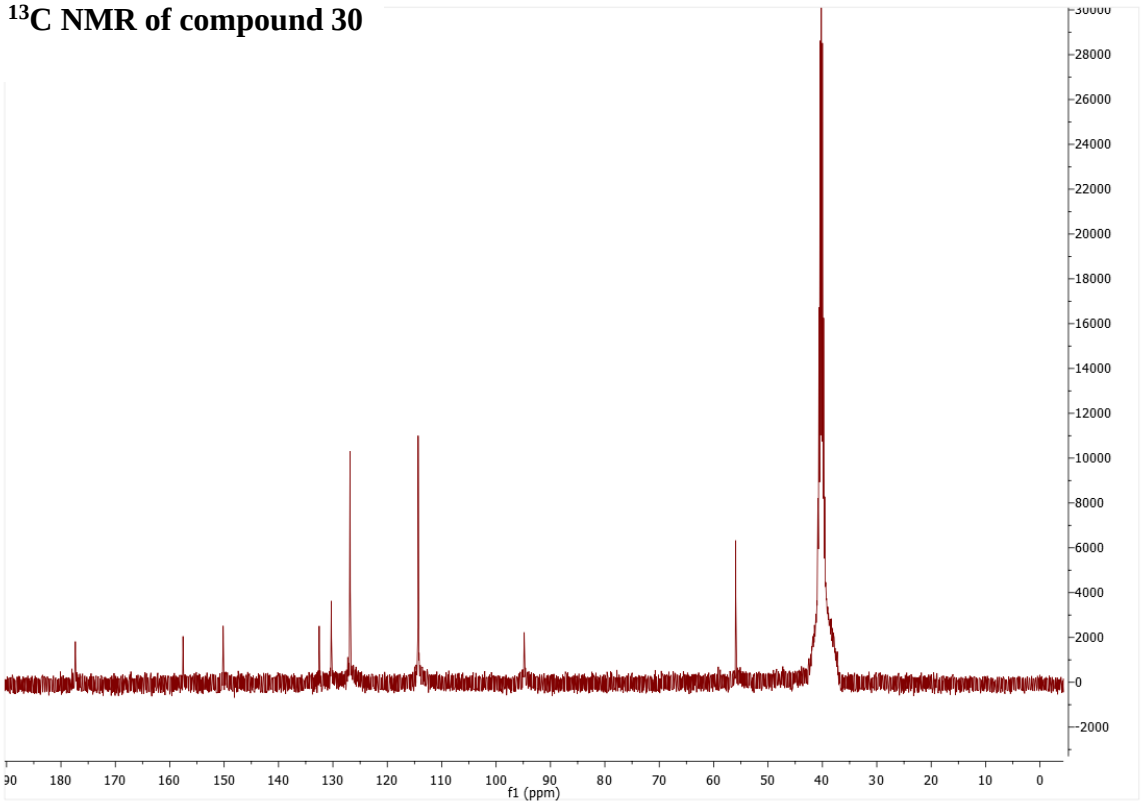

HRMS for compound **30**
Monoisotopic Mass: 248.0726332
Found: 248.0731
Chemical Formula: $C_{11}H_{12}N_4OS$
M+

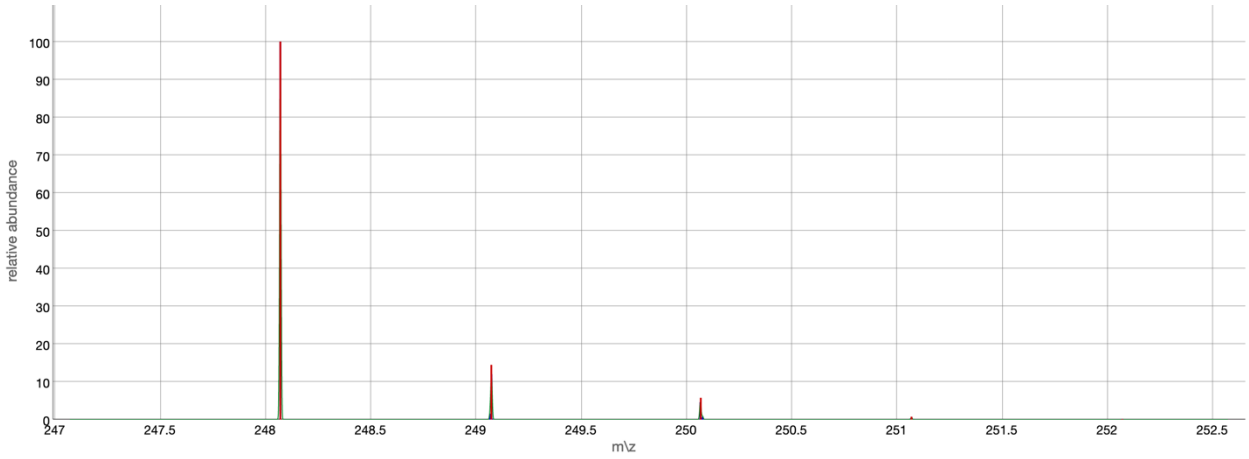

3-amino-N-(p-tolyl)-1H-pyrazole-1-carbothioamide (31)

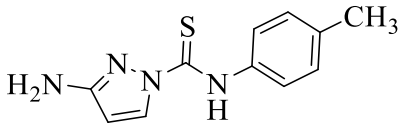

31 (62%)

1H-pyrazol-3-amine (278 mg, 3.35 mmol) was dissolved in DCM and stirred in a 100 mL round bottom flask. 4-Tolyl isothiocyanate (500 mg, 3.35 mmol, 1 eq) was dissolved in DCM separately and added to the stirring reaction dropwise. The reaction was then refluxed for 20 hours at 60 ˚C. The reaction was monitored by TLC (DCM/ methanol 50:2). All volatile components were evaporated under vacuum and the resulting crude product was purified by flash column chromatography (100% DCM) to afford 62% yield of **31,** off-white solid. ^{1}H NMR (400 MHz, DMSO-d_6) δ 7.73 (d, J = 2.0 Hz, 1H), 7.47 (dd, J = 8.3, 2.0 Hz, 2H), 7.17 (d, 2H), 6.01 (s, 1H), 2.29 (d, J = 1.9 Hz, 3H). ^{13}C NMR (101 MHz, DMSO-d_6) δ 176.97, 150.15, 137.11, 135.13, 129.60, 124.88, 102.22 94.87, 21.23. FTIR, cm^{-1}: 3374 (-NH_2), 3185 (-NH-), 3046 (C-H aromatic), 2980 (aliphatic C-H), 1573 (aromatic C=C), 1537 (aromatic C=N), 1250 (C=S), 1520 (C=C-C). HRMS (+ESI-TOF) m/z: [M^+] calcd for $C_{11}H_{12}N_4S$ 232.0783; found 232.0781.

^{1}H NMR of compound 31

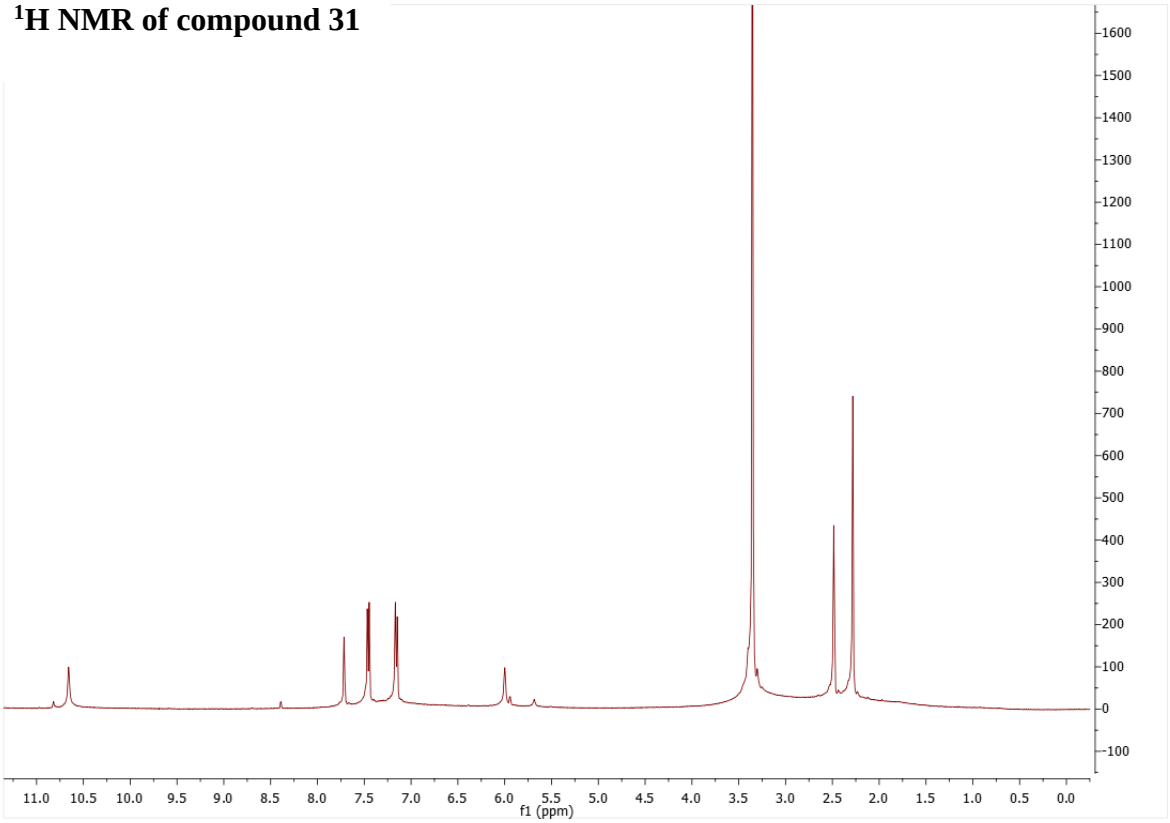

^{13}C NMR of compound 31

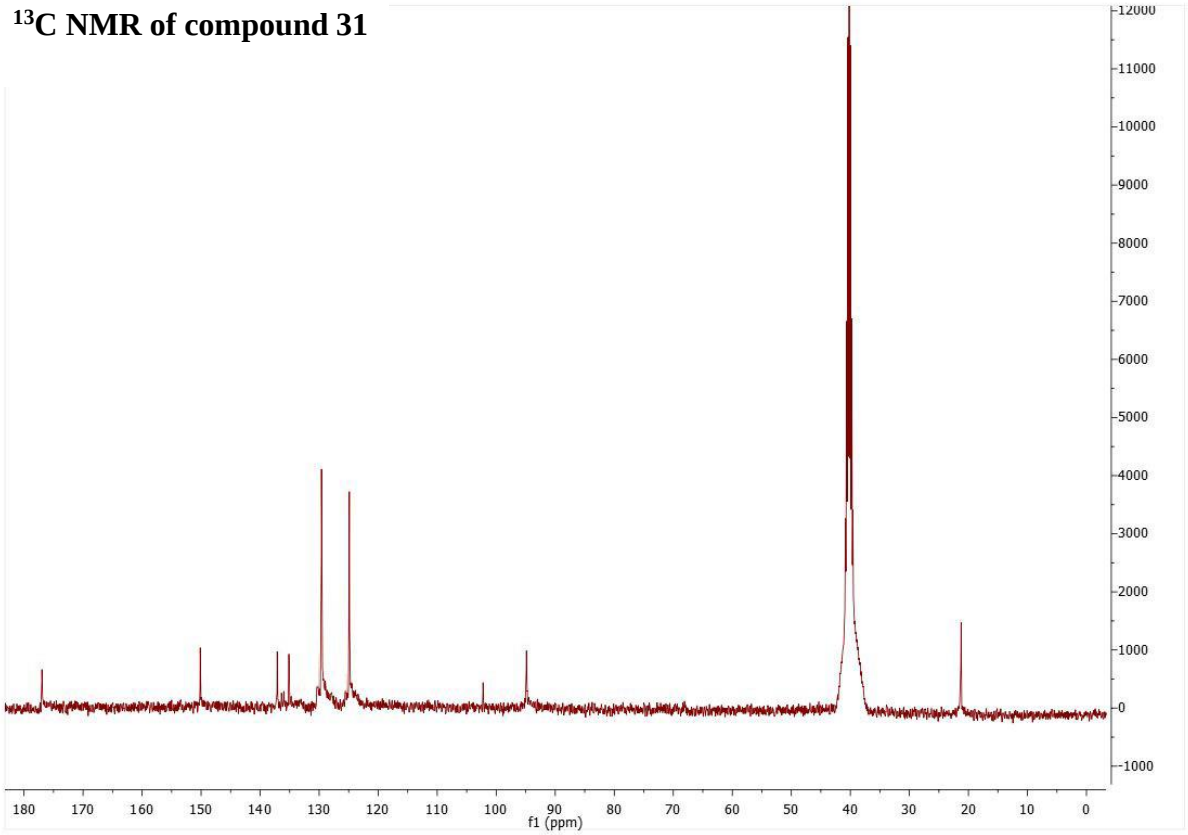

HRMS for compound **31**
Monoisotopic Mass: 232.0777186
Found: 232.0781
Chemical Formula: $C_{11}H_{12}N_4S$
M+

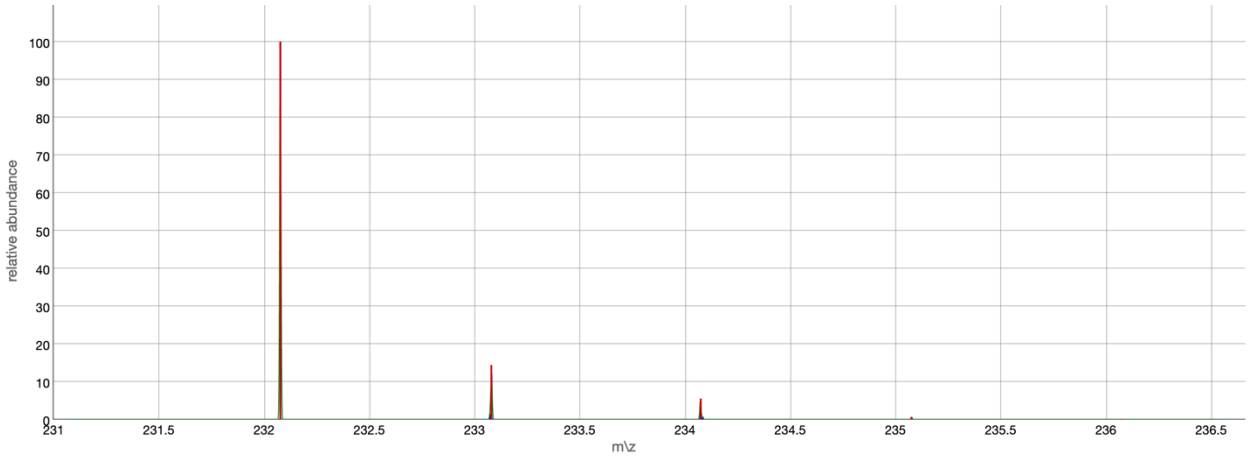

4-nitro-1H-pyrazole (32)

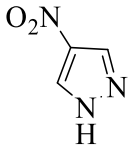

85%

32

Pyrazole (1 g, 14.69 mmol) was measured in to a 100 mL round bottom flask and dissolved in 5 mL of H_2SO_4 (after 10 min pyrazole was fully dissolved). Afterwards, the solution was heated to 60 $^{\circ}$C and 1.1 eq of (1.46 mL) conc. HNO_3 was added dropwise followed by stirring for 90 min at 60 $^{\circ}$C. After 90 min, the product solution was poured into 15 g of ice/water. The product was obtained as a white color solid precipitate (85%). To obtain the second crop, the mother liquor was extracted with ethyl acetate thrice, combined organic layers were washed with $NaHCO_3$/ brine and finally dried over sodium sulfate followed by concentration in *vacuum*. ^{1}H NMR (400 MHz, DMSO-d_6) δ 13.32 (bs, 1H), 8.86 (s, 1H), 8.23 (s, 1H). ^{13}C NMR (101 MHz, DMSO-d_6) δ 136.10, 130.01.

^{1}H NMR of compound 32

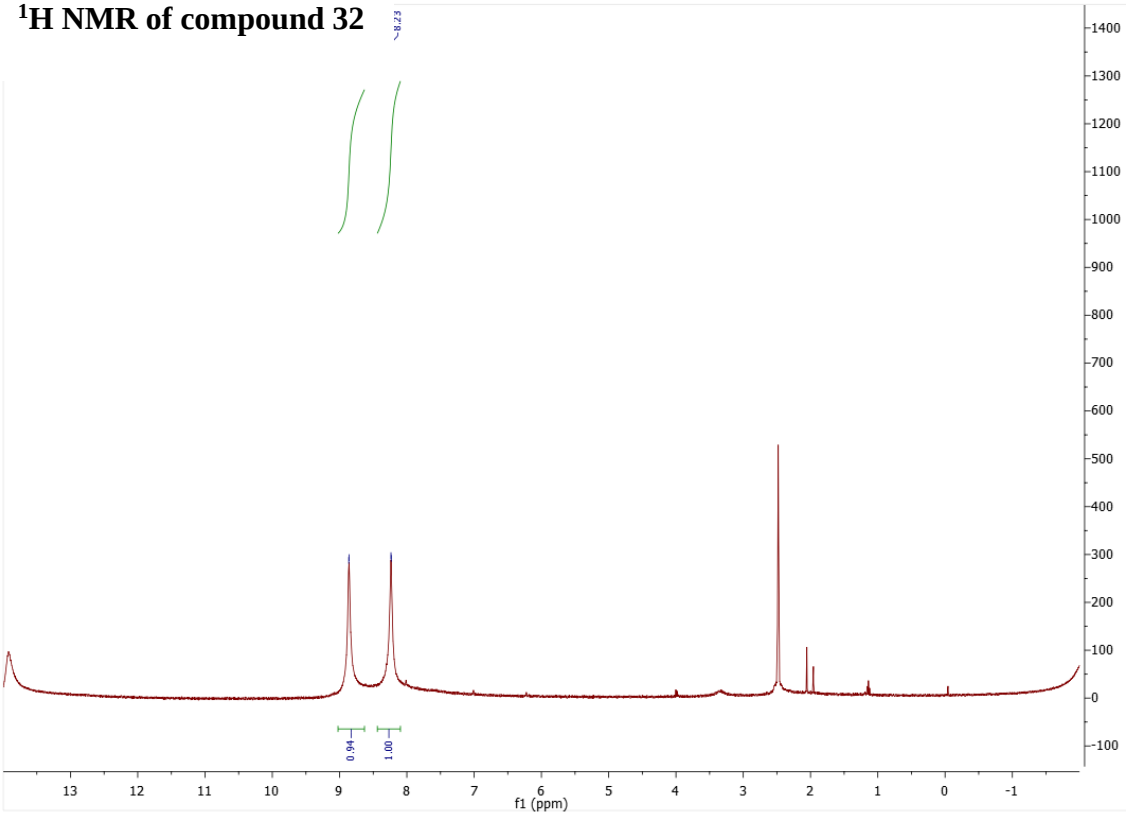

^{13}C NMR of compound 32

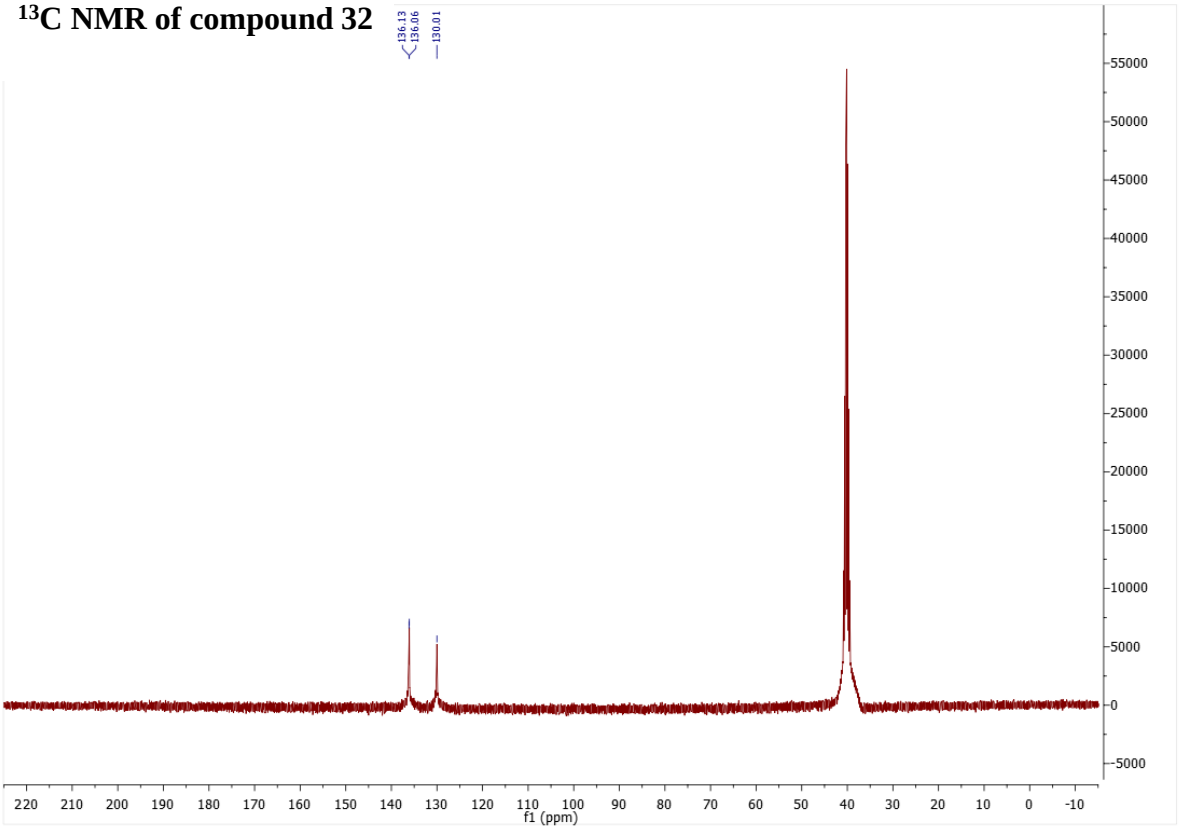

MS of compound **32**

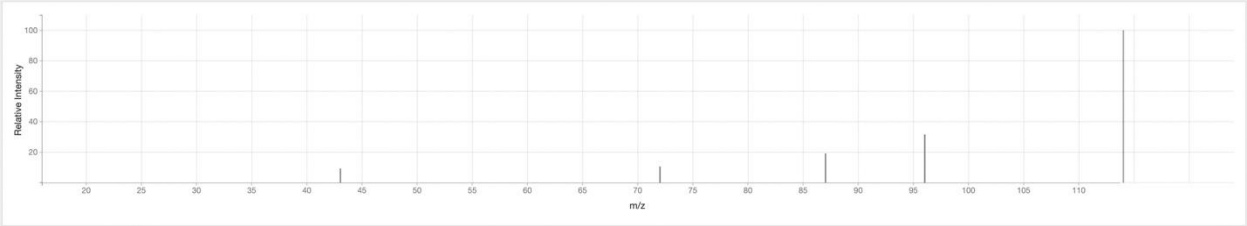

Peak intensity	Mass	Formula
100%	114 [M^+H^+]	$C_3H_3N_3O_2$
31%	72 [H^+]	C_2HNO_2
19%	69	C_2HN_2O
11%	43	CH_3N_2

N-(4-chlorophenyl)-4-nitro-1H-pyrazole-1-carbothioamide (33)

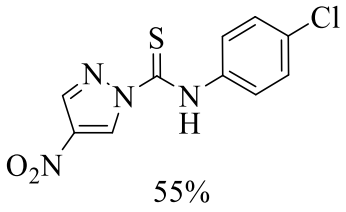

55%

33

4-nitro-1H-pyrazole (75.4 mg, 0.66 mmol) was syringed to a suspension of sodium hydride (26.4 mg, 0.66 mmol, 1 eq) in 10mL of THF (under Ar gas). Afterwards, the solution was allowed to stir at room temperature under argon for three hours. 4-chlorophenyl isothiocyanate (112 mg, 0.66 mmol) was then added and the solution was kept stirring overnight. The reaction was concentrated to dryness and recrystallized using hexane, yielding the product **33** as an off-white solid (55%). ^{1}H NMR (400 MHz, DMSO-d_6) δ 9.46 (d, J = 3.6 Hz, N-H), 8.24 (s, J = 3.7 Hz, 1H), 7.98 (s, J = 3.7 Hz, 1H), 7.25 (dd, J = 8.8, 3.6 Hz, 2H), 7.12 (dd, J = 8.7, 3.6 Hz, 2H). ^{13}C NMR (151 MHz, DMSO-d_6) δ 166.68, 151.46, 136.64, 135.49, 129.15, 128.18, 125.56, 124.68. FTIR, cm^{-1}: 3388 (-NH-), 3100 (C-H aromatic), 1652 (aromatic C=C), (aromatic C=N), 1254 (C=S), 760 (aromatic C-Cl), 1479 and 1275 (N=O). HRMS (+ESI-TOF) m/z: [M^+] calcd for $C_{10}H_7ClN_4O_2S$ 281.9978; found 281.9980.

^{1}H NMR of compound 33

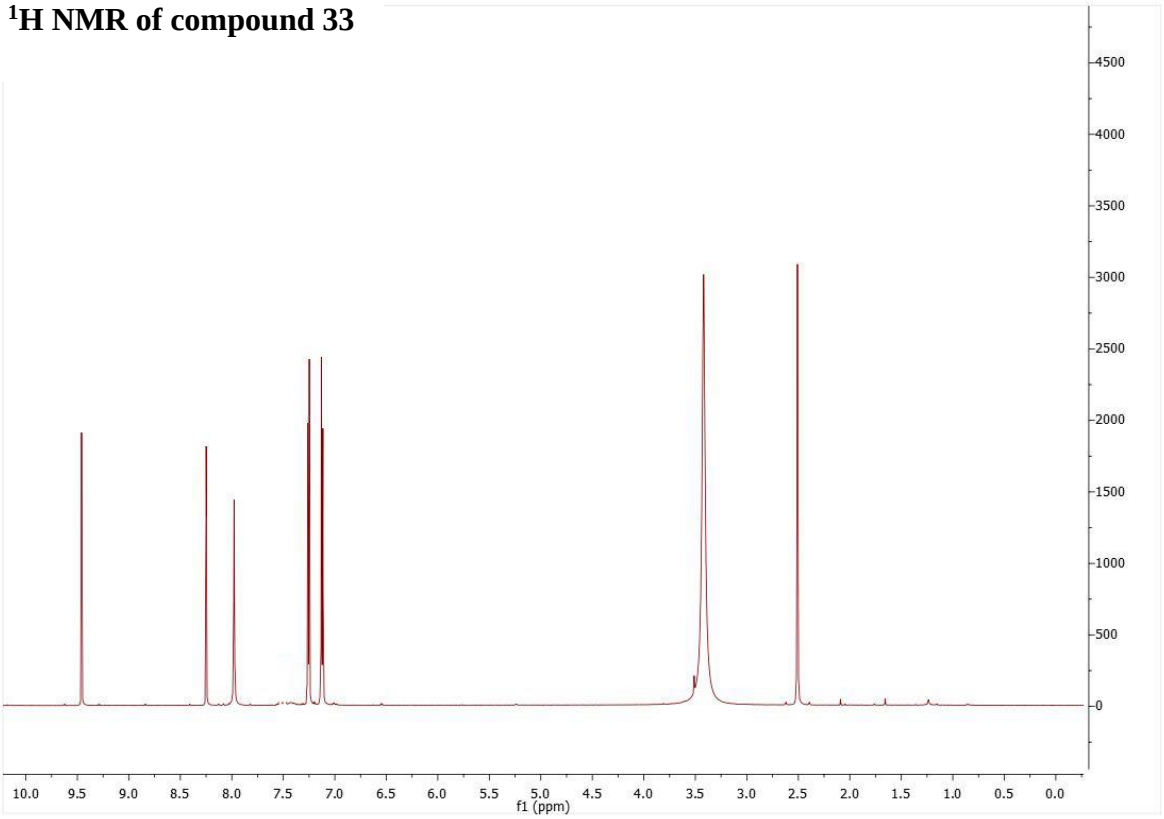

^{13}C NMR of compound 33

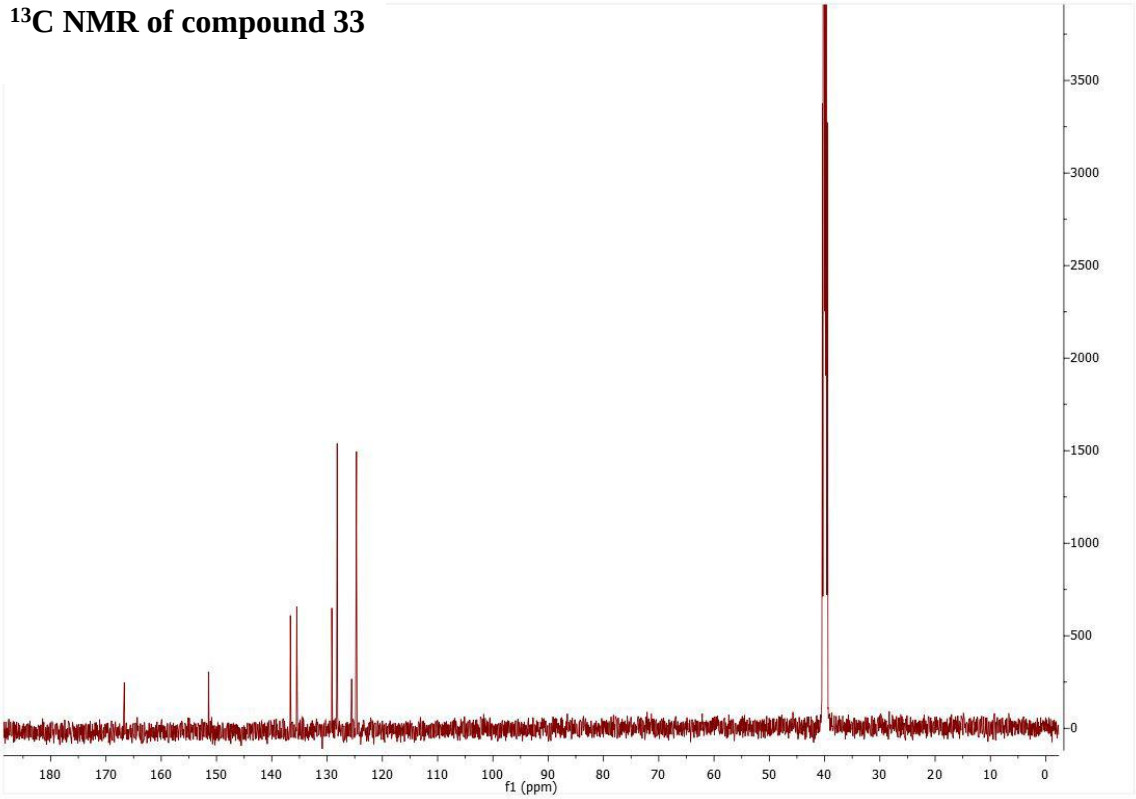

HRMS for compound **33**
Monoisotopic Mass: 281.9972754
Found: 281.9980
Chemical Formula: $C_{10}H_7ClN_4O_2S$
M+

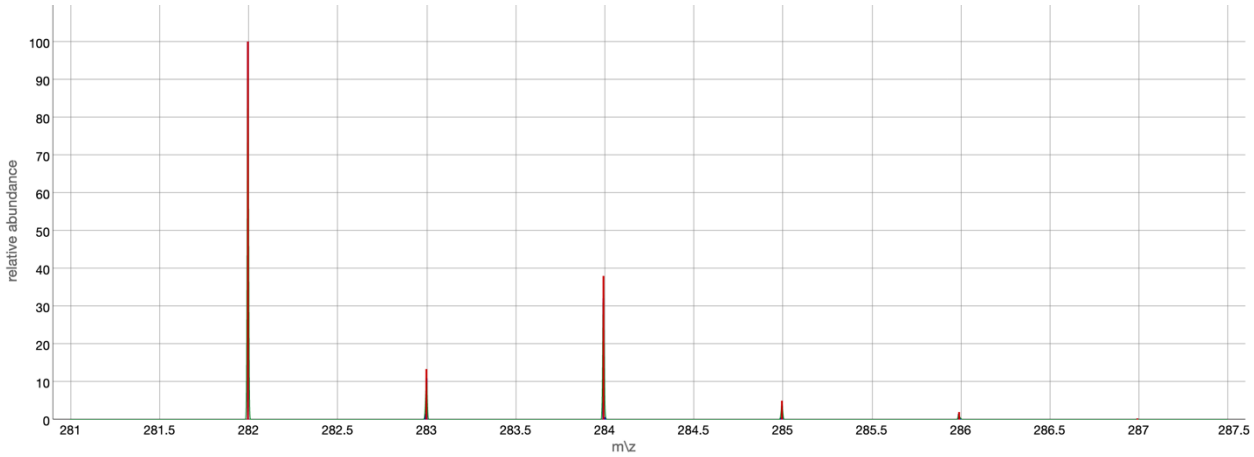

4-amino pyrazole (34)

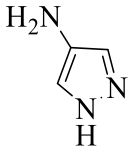

86%

34

4-amino pyrazole was prepared according to the literature method. 4-nitro-1*H*-pyrazole (100 mg, 0.88 mmol) was dissolved in 3 mL of EtOH/H_2O and transferred to a 100 mL round bottom flask equipped with a stir bar. While the reaction stirred, 20 eq (18.9 mmol, 1.056 g) of Fe powder (suspension in 10 mL of EtOH/H_2O) was added and heated the system to 95 $^{\circ}$C. At 95 $^{\circ}$C, 200 µL of conc. HCl was added dropwise and refluxed at same temperature for 90 min. The reaction was monitored by TLC (50% EtOAc/hexanes). Then, the reaction mixture was filtered hot by gravity filtration and followed by the filtration through celite pad. The filtrate was purified by flash column chromatography (EtOAc/hexanes 10% - 40%) to afford 86% yield. ^{1}H NMR (600 MHz, DMSO-d_6) δ 7.92 (s, 2H), 4.18 (s, 2H). ^{13}C NMR (151 MHz, DMSO-d_6) δ 128.74, 125.47, 123.42.

^{1}H NMR of compound 34

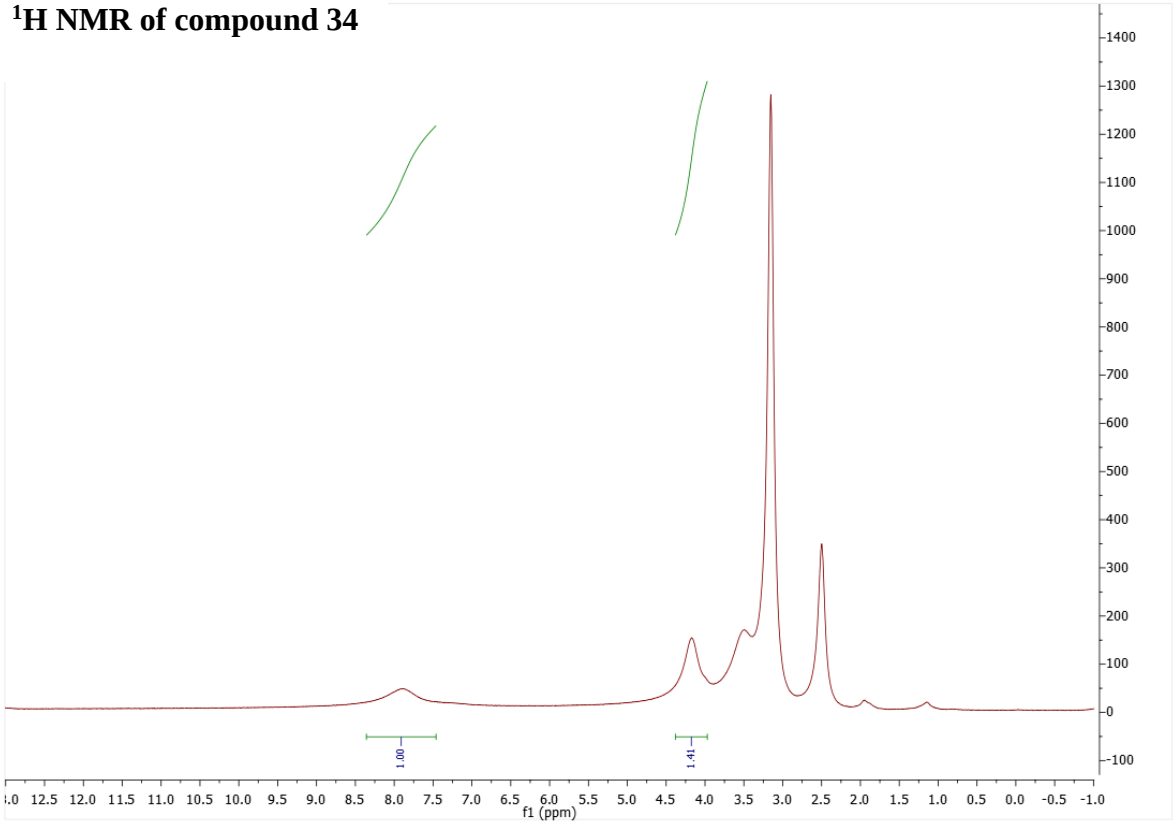

^{13}C NMR of compound 34

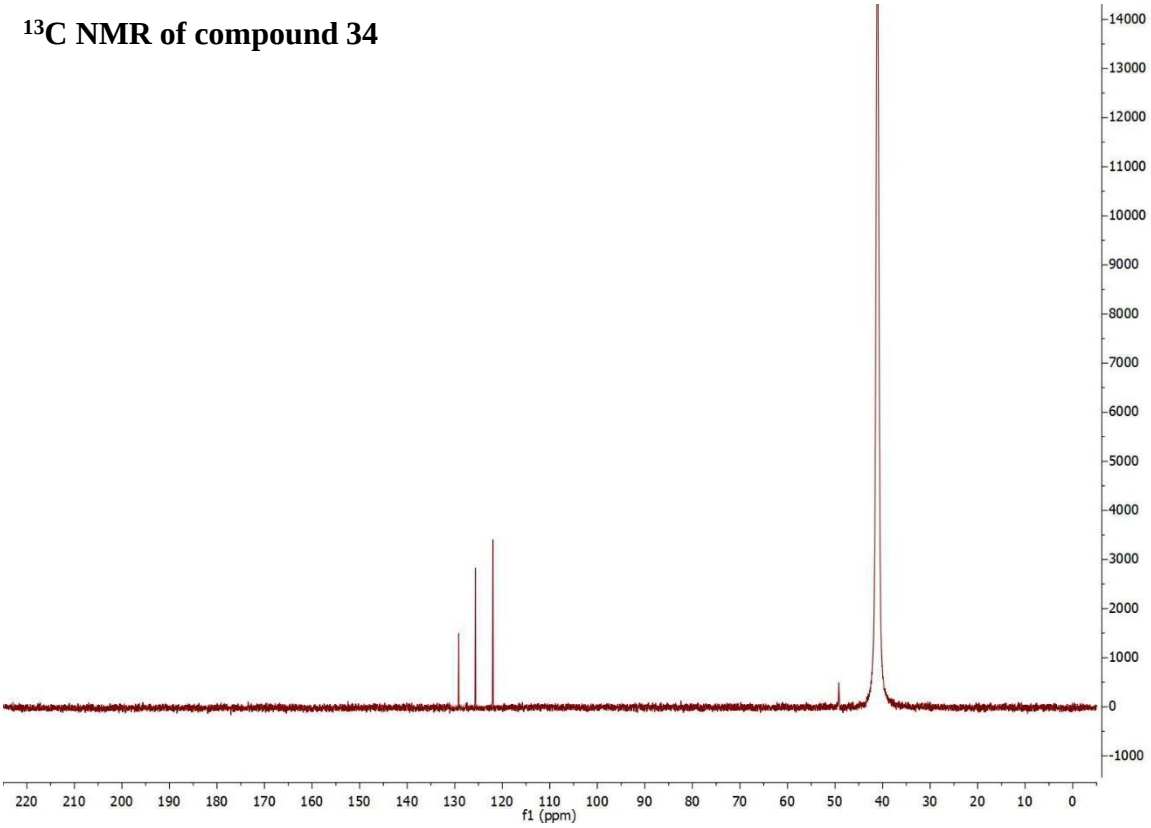

MS of compound **34**

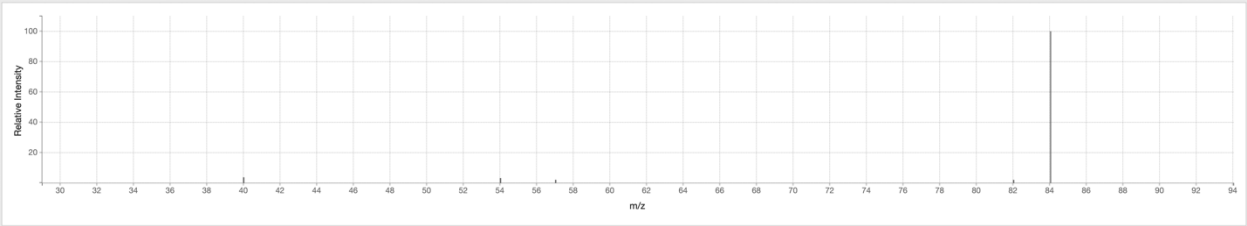

Peak intensity	Mass	Formula
100%	84 [M^+H^+]	$C_3H_5N_3$
2%	57	$C_2H_5N_2$
2%	54	C_3H_4N
4%	43	C_2H_2N

4-amino-N-(4-chlorophenyl)-1H-pyrazole-1-carbothioamide (35)

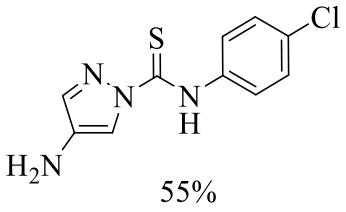

55%

35

1H-pyrazol-4-amine, **10** (325 mg, 3.92 mmol) was dissolved in DMF and stirred in a 100 mL round bottom flask. Potassium carbonate (416 mg, 3.92 mmol, 1 eq) was placed in the reaction mixture and stirred vigorously. 4-chlorophenyl isothiocyanate (665 mg, 3.92 mmol) was added and stirred for 18 hours. The reaction was monitored by TLC (25% EtOAc/hexanes). Potassium carbonate solid was filtered off by gravity filtration. DMF was evaporated in *vacuum.* The resulting crude product was purified by flash column chromatography (100% hexane to 10% ethyl acetate/hexane) to afford 55% yield of **35,** off-white to pale yellow color solid. ^{1}H NMR (600 MHz, Chloroform-*d*) δ 8.81 (m, NH), 7.34 (d, *J* = 8.2 Hz, 2H), 7.29 (s, 1H), 7.26 (m, 2H), 4.17 (d, *J* = 9.9 Hz, 1H). ^{13}C NMR (151 MHz, Chloroform-*d*) δ 189.45, 139.87, 135.41, 130.83, 129.19, 124.52 122.93, 117.47. FTIR, cm^{-1}: 3234, 3170 (-NH_2), 3104 (-NH-), 3055(C-H aromatic), 2919 (CH pyrazole), 1590, (aromatic C=C), 1544 (aromatic C=N), 1200 (C=S), 650 (aromatic C-Cl). HRMS (+ESI-TOF) m/z: [M^+] calcd for $C_{10}H_9ClN_4S$ 252.0236; found 252.0232.

[1] HNMR of compound 35

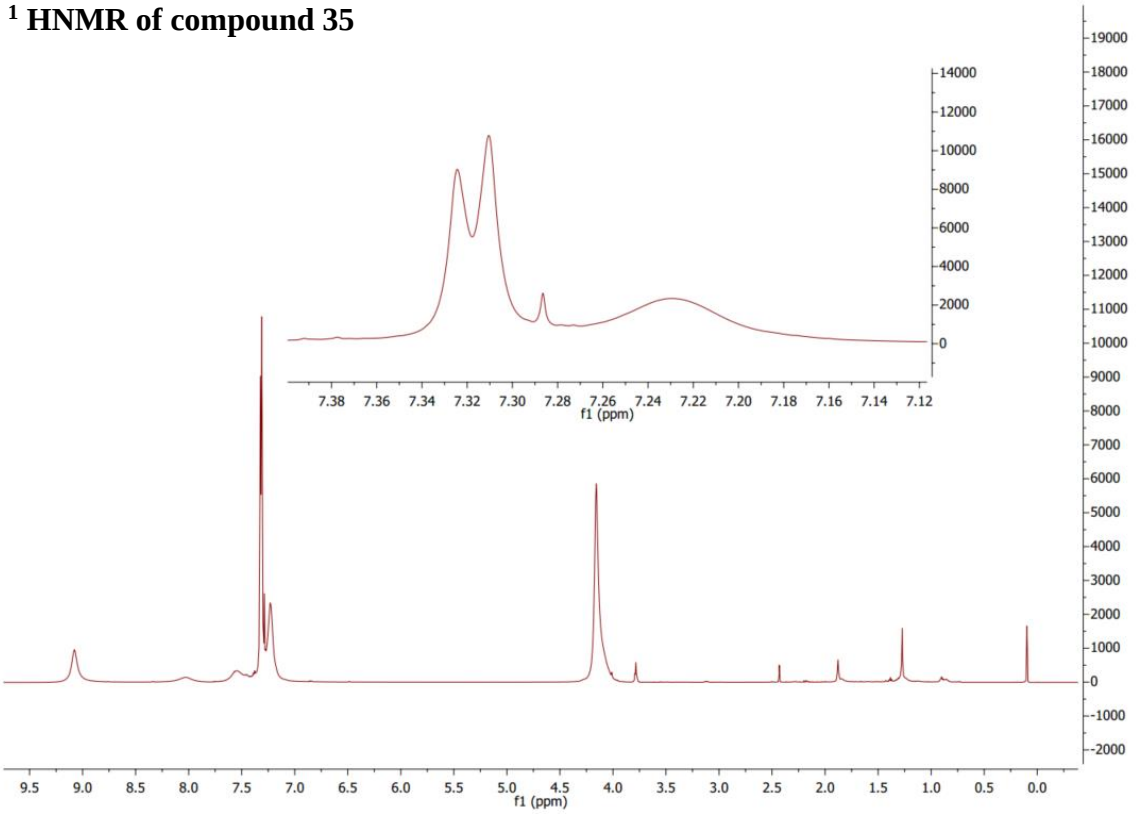

[13]C NMR of compound 35

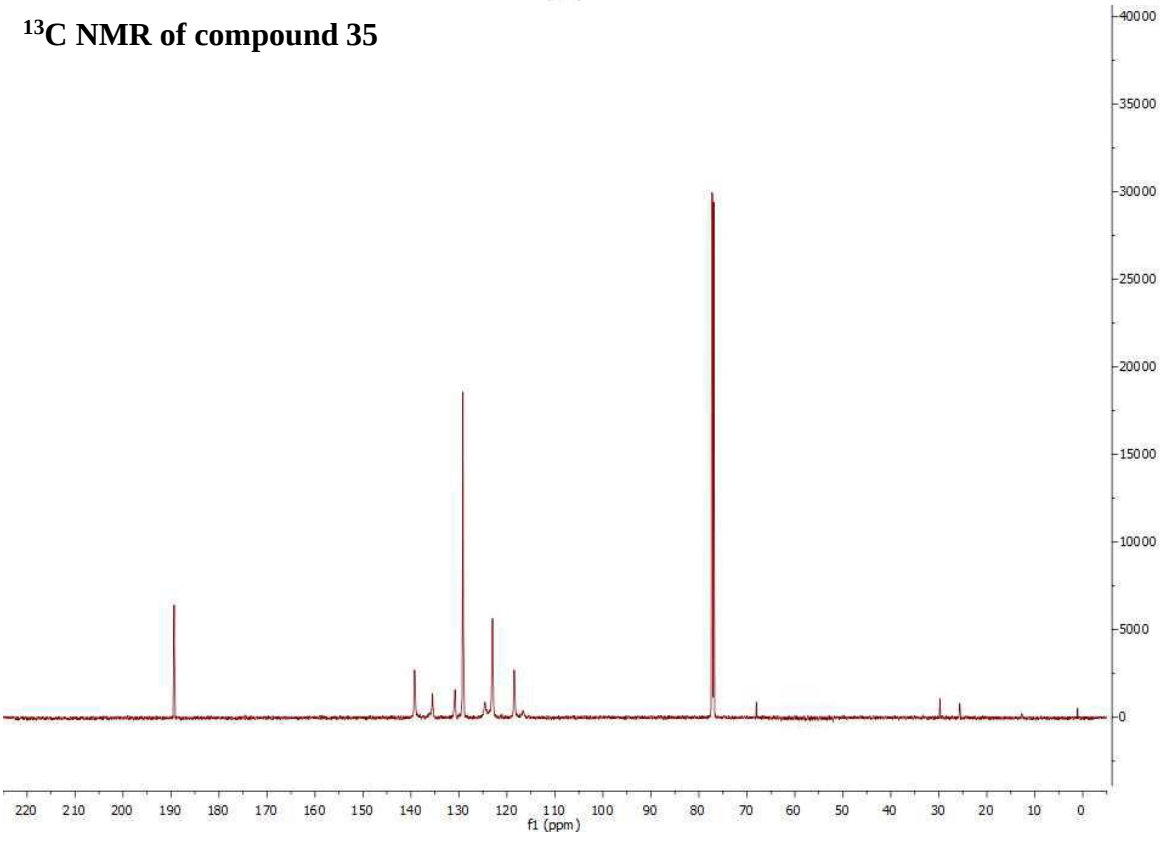

HRMS for compound **35**
Monoisotopic Mass: 252.0230962
Found: 252.0232
Chemical Formula: $C_{10}H_9ClN_4S$
M+

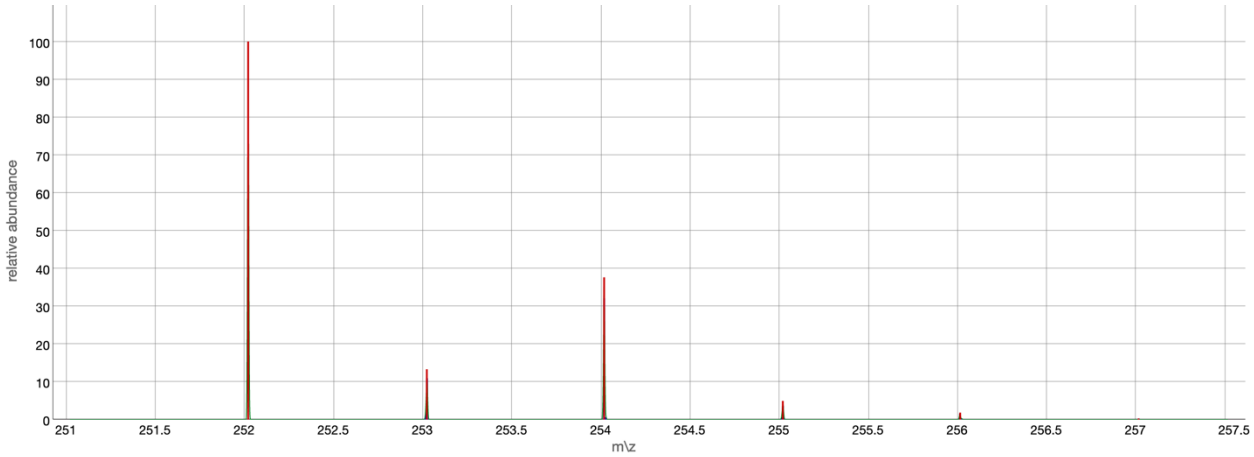

1H-pyrazole-3-carboxylic acid (36)

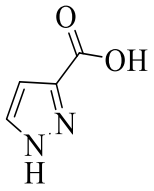

85%

36

765.8 mg (9.33mmol) of 3-methyl-1H-pyrazole was dissolved in 10mL of distilled water. 3.140g (eq. 2.2, 20.52mmol) of $KMnO_4$ was dissolved in 20mL of distilled water separately. At room temperature, both the reagents were mixed and refluxed for 4hr. TLC was done in the solvent mixture of DCM/MeOH (20:1) and visualized with potassium permanganate stain (unreacted 3-methyl-1H-pyrazole at R_f= 0.3 and new product spot was retained on the baseline). Once the reaction completion was monitored, the solution was evaporated to a small volume. Recrystallization was performed in pH 2 and let the crude mixture stands for 1 hour at 4 ^{O}C. Resulting white solid precipitate was filtered by vacuum filtration and washed with cold water. Received **36** as white solid 85%. ^{1}H NMR (400 MHz, Deuterium Oxide) δ 7.74 (d, *J* = 2.1 Hz, 1H), 6.83 (d, *J* = 2.1 Hz, 1H).

^{1}H NMR of compound 36

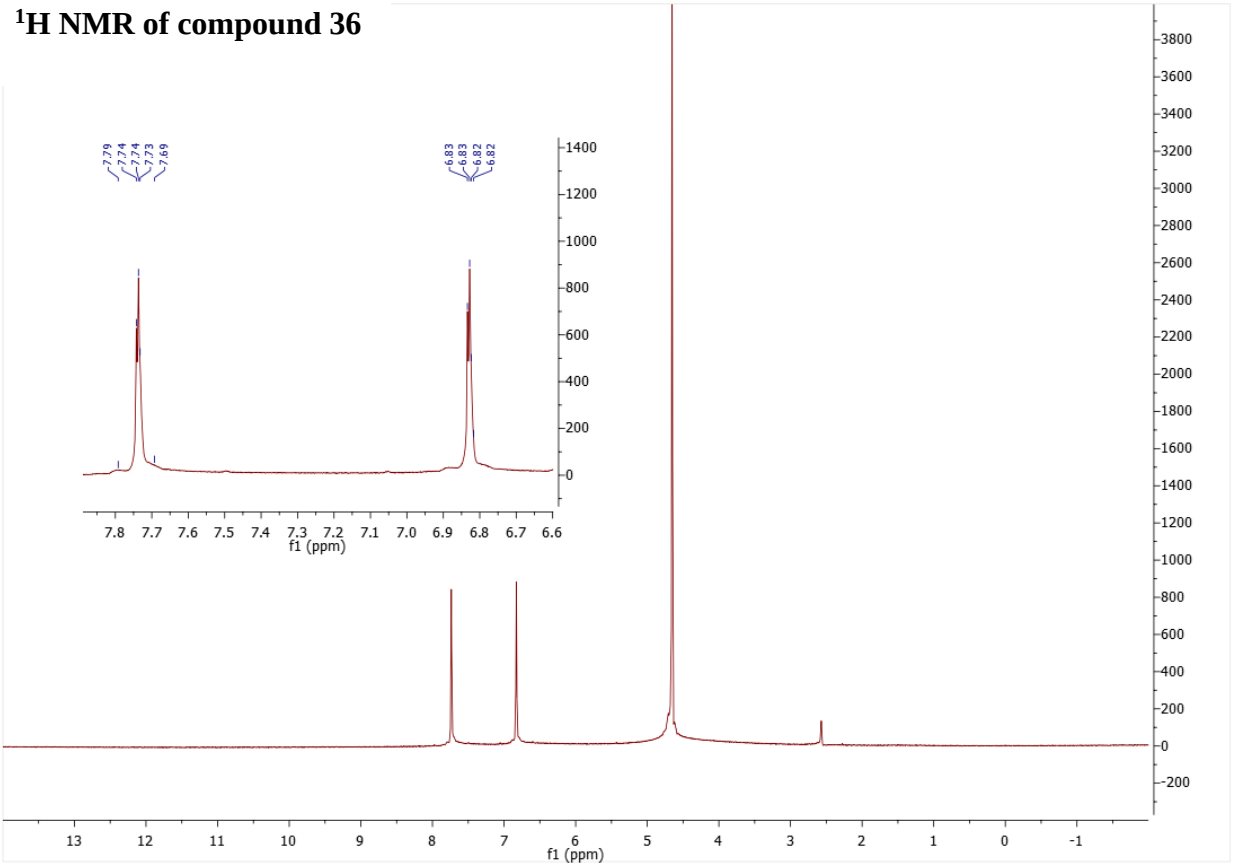

MS of compound **36**

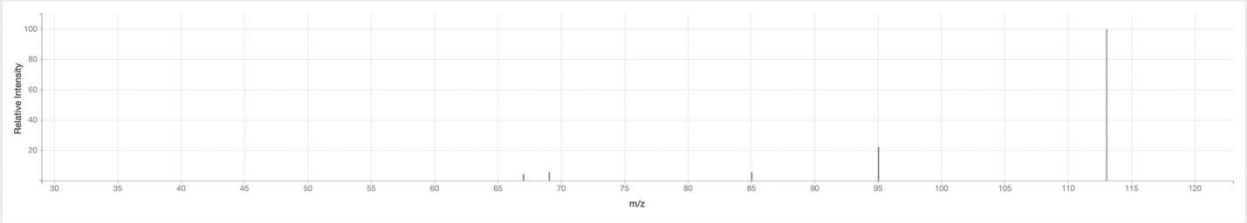

Peak intensity	Mass	Formula
100%	113 [M^+H^+]	$C_4H_4N_2O_2$
22%	95	$C_4H_3N_2O$
2%	85	$C_4H_5O_2$
5%	69	$C_3H_5N_2$

Methyl 1H-pyrazole-3-carboxylate (37)

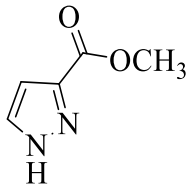

68%

37

400.9 mg (3.58 mmol) of 1H-pyrazole-3-carboxylic acid was dissolved in MeOH and cooled down to -78 °C with Dry Ice and acetone. Then 2 eq. of $SOCl_2$ wad added to the cooled reaction in dropwise. The reaction mixture was stirred at cooled temperature for 15- 30 min followed by the reflux at 70 -80 °C overnight. TLC was done in the solvent mixture of DCM/MeOH (20:1) and visualized under UV light. After stirring overnight, the reaction mixture was light yellow color clear solution. MeOH was evaporated in vacuum and diluted again with cold distilled water. After that it was extracted three times with EtOAC. Organic layer was dried over anhydrous $MgSO_4$. Solvent was removed in vacuum to receive the crude product in 68%. ^{1}H NMR (600 MHz, Chloroform-*d*) δ 7.94 (d, *J* = 2.6 Hz, 1H), 6.84 (d, *J* = 2.4 Hz, 1H), 3.87 (s, 3H). ^{13}C NMR (151 MHz, Chloroform-*d*) δ 160.90, 140.53, 132.79, 108.31, 52.42.

^{1}H NMR of compound 37

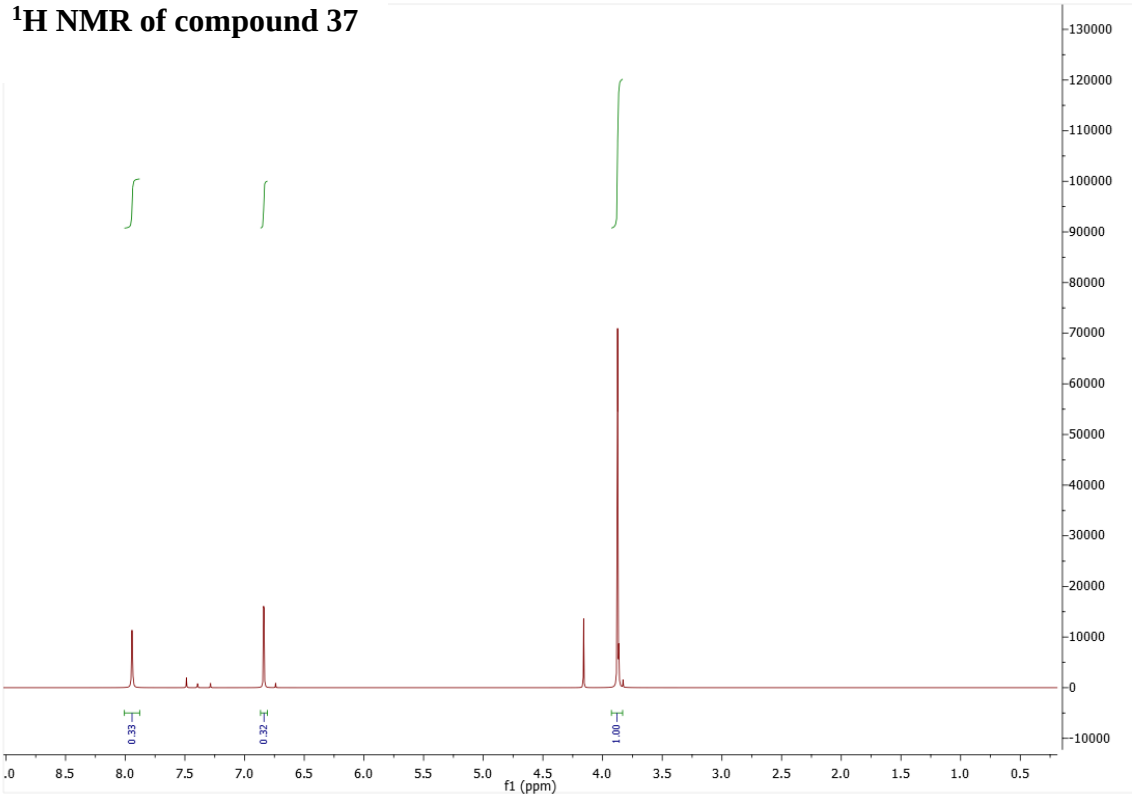

^{13}C NMR of compound 37

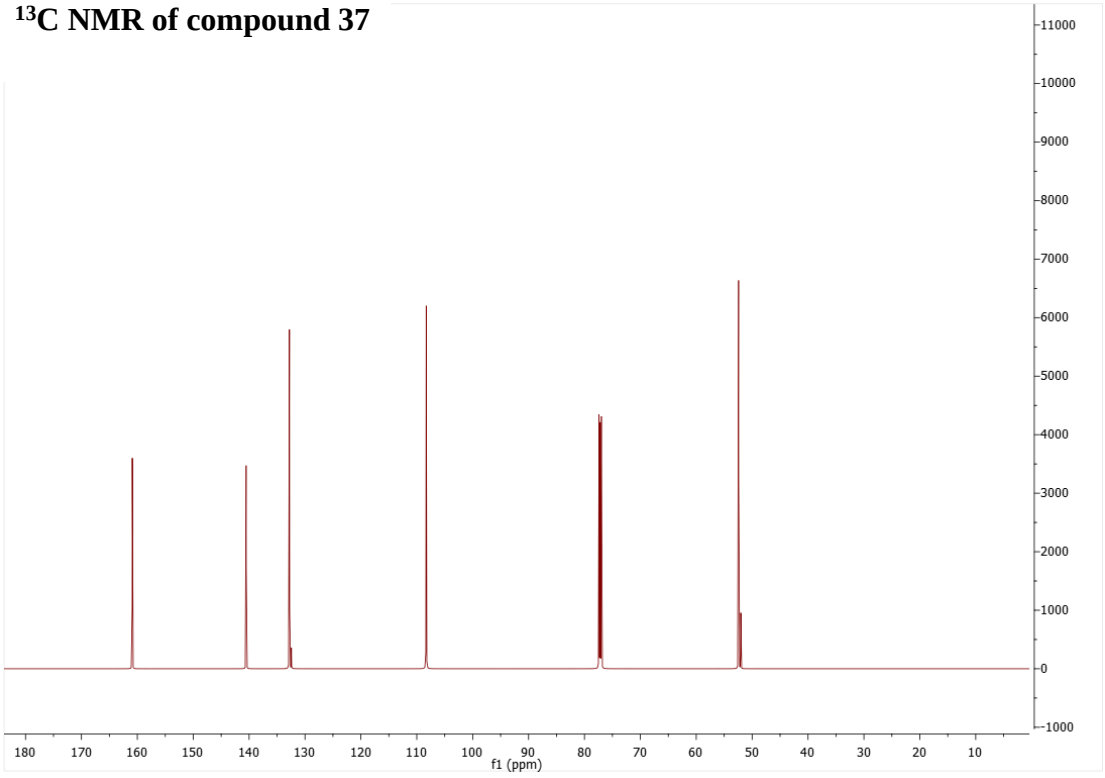

Methyl 1-((4-chlorophenyl)carbamothioyl)-1H-pyrazole-3-carboxylate (38)

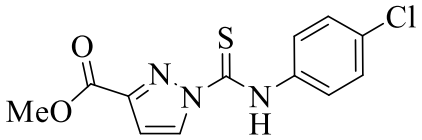

20%

38

Methyl 1H-pyrazole-3-carboxylate (214.7 mg, 1.70 mmol) was dissolved in DCM and stirred in a 100 mL round bottom flask. 4-chlorophenyl isothiocyanate (289 mg, 1.70 mmol, 1 eq) was dissolved in DCM separately and added to the stirring reaction dropwise. The reaction was then refluxed for 20 hours at 60 °C. The reaction was monitored by TLC (EtOAc/ Hexane 25%). All volatile components were evaporated under vacuum and resulting crude product was purified by flash column chromatography (100% DCM) to afford 20% yield of **38,** off-white solid. ^{1}H NMR (600 MHz, DMSO-d_6) δ 9.99 (s, NH), 7.87 (s, 1H), 7.50 (d, 2H), 7.39 (d, 2H), 6.75 (s, J = 2.2 Hz, 1H), 3.79 (s, 3H). ^{13}C NMR (151 MHz, DMSO-d_6) δ 180.17, 163.04, 143.11, 138.79, 130.47 (d, J = 27.5 Hz), 128.83, 128.28, 125.77, 107.92, 51.88.

^{1}H NMR of compound 38

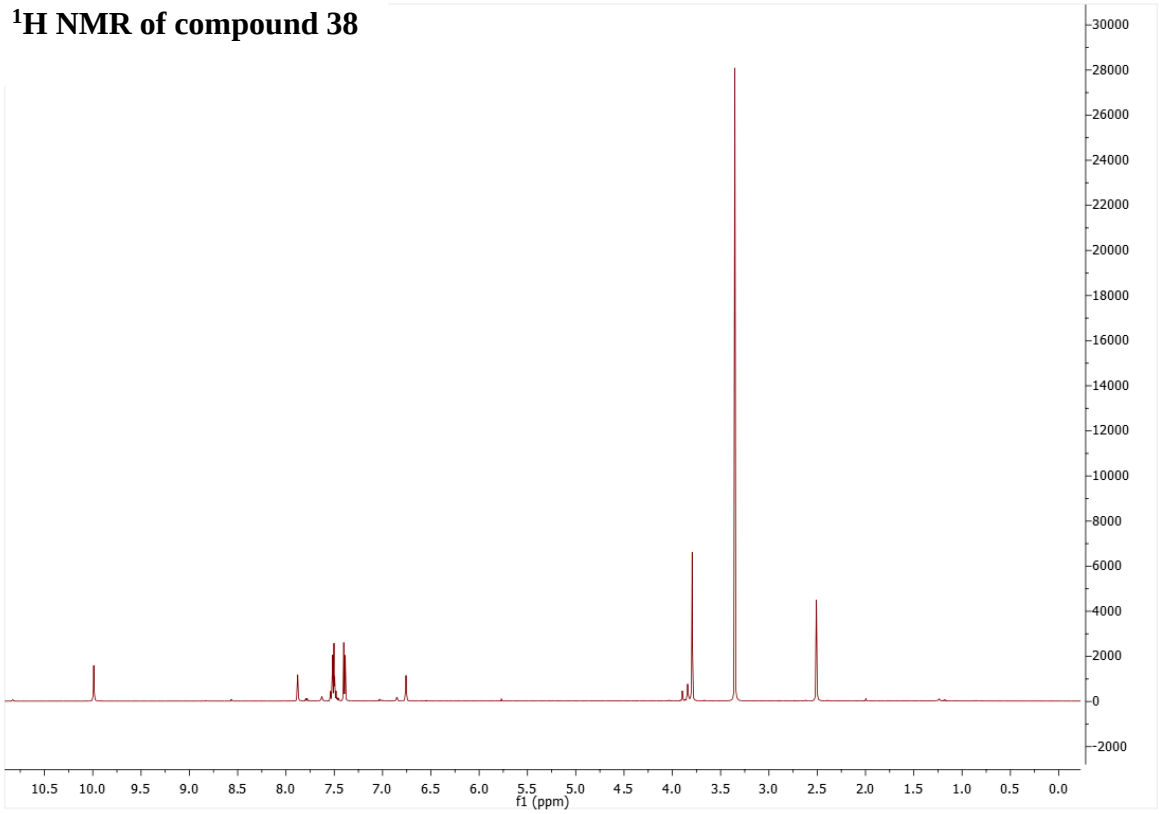

^{13}C NMR of compound 38

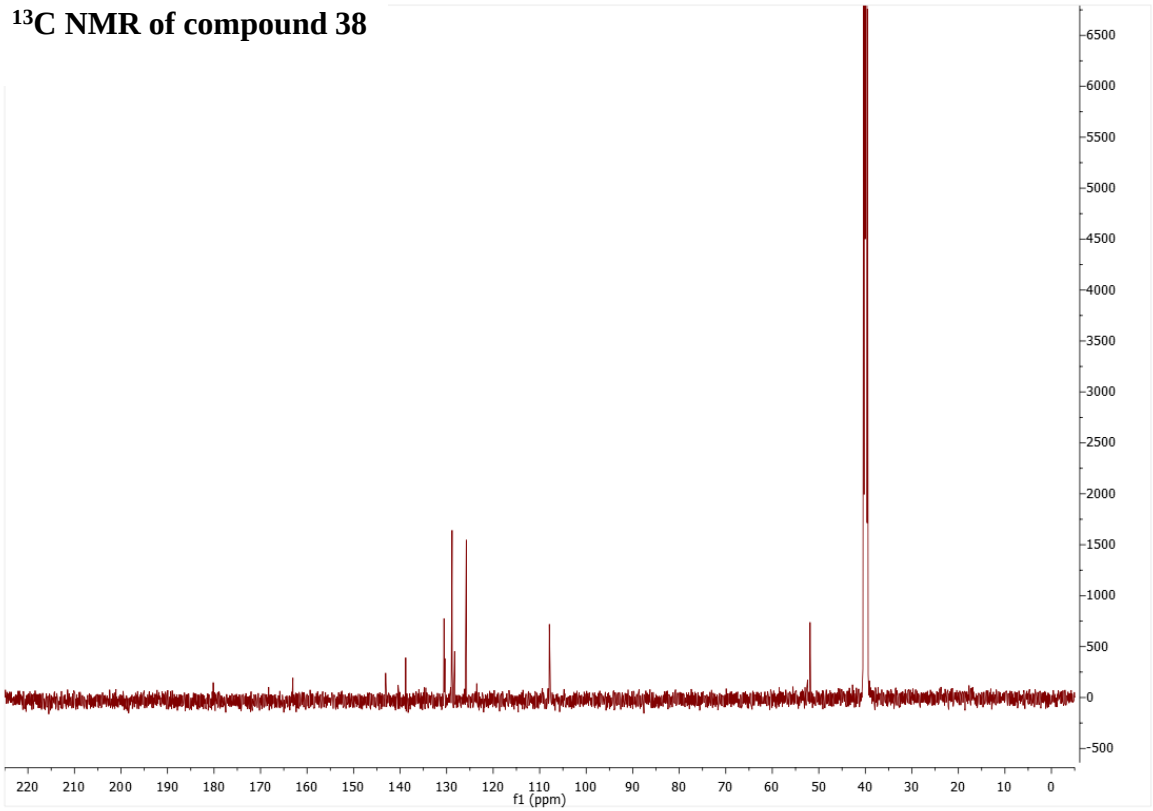

1H-pyrazol-3-ol (39)

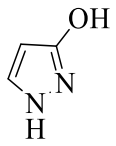

99%

39

1g (8.612 mmol) of methyl-3-methoxyacrylate dissolved in MeOH was added with stirring solution of 1.1 eq. of hydrazine monohydrate (474.22 mg, 9.473 mmol). The reaction was refluxed for 2 hr. TLC was done in 50% EtOAc/hexane system and visualized under UV. All volatile components were removed in vacuum to obtain a pale yellow solid 99%. ^{1}H NMR (600 MHz, DMSO-d_6) δ 7.35 (s, 1H), 5.43 (s, 1H). ^{13}C NMR (151 MHz, DMSO-d_6) δ 161.42, 130.66, 89.57.

^{1}H NMR of compound 39

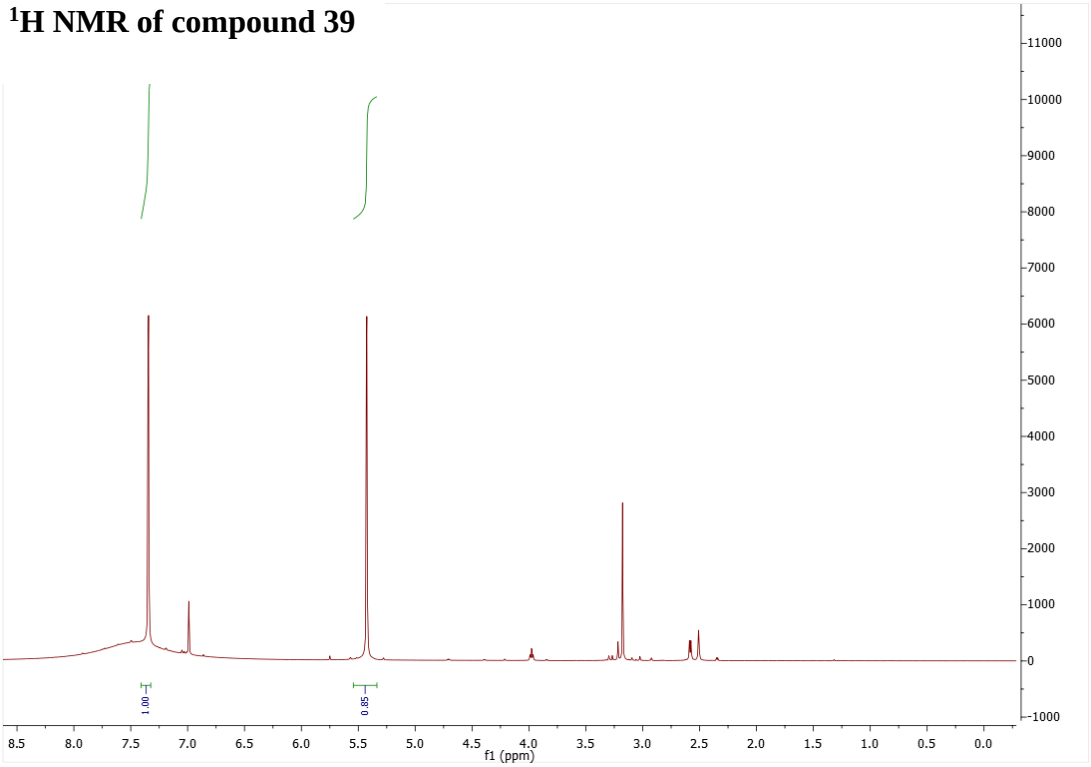

^{13}C NMR of compound 39

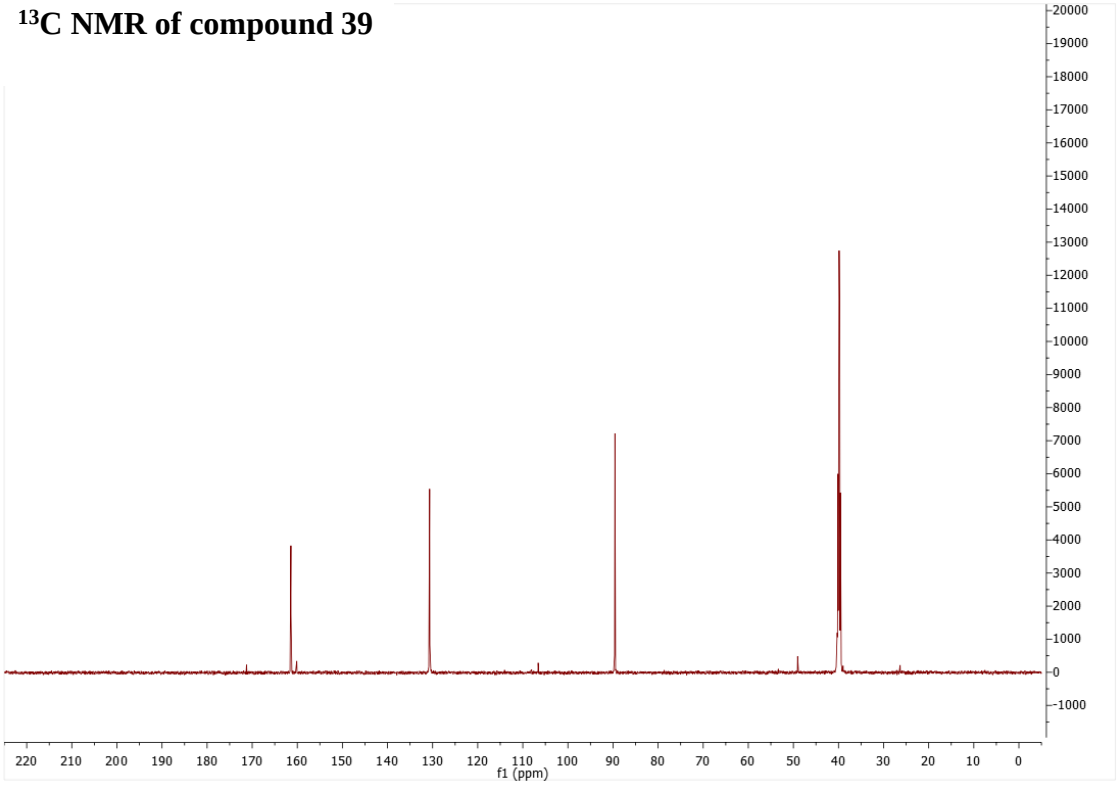

MS of compound **39**

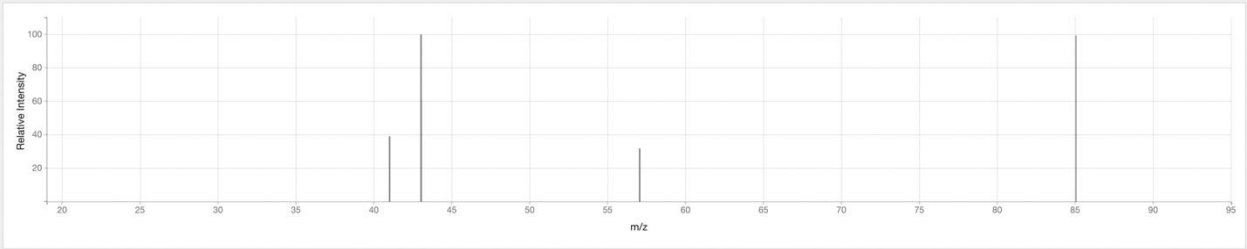

Peak intensity	Mass	Formula
98%	85 [M^+H^+]	$C_3H_5N_2O$
11%	57	$C_2H_5N_2$
100%	43	CH_3N_2
40%	41	C_2HO

1-(3-hydroxy-1H-pyrazol-1-yl)ethan-1-one (40)

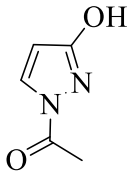

87%

40

A solution of 2 g (23.79 mmol) of 1H-pyrazol-3-ol dissolved in anhydrous pyridine was heated to 95 °C. The solution of acetic anhydride (24.89 mmol, 2.35 mL) in pyridine (5mL) was added to the stirring mixture dropwise over 20 min. Then, the reaction was stirred at 95 °C for 2 hr. TLC was done in 50% EtOAc/ hexane system. All the volatile components were removed in vacuum and resulting slurry was charged with 25 mL of diethyl ether. Slurry was stirred at room temp overnight. A crashed out solid was observed on the following day. Pale yellow color solid was filtered out by vacuum filtration. Obtained pale yellow solid 87%. ^{1}H NMR (400 MHz, DMSO-d_6) δ 8.11 (d, J = 3.0 Hz, 1H), 5.99 (d, J = 3.0 Hz, 1H), 2.45 (d, J = 3.1 Hz, 3H). ^{13}C NMR (101 MHz, DMSO-d_6) δ 168.66, 164.66, 130.53, 100.61, 22.08.

^{1}H NMR of compound 40

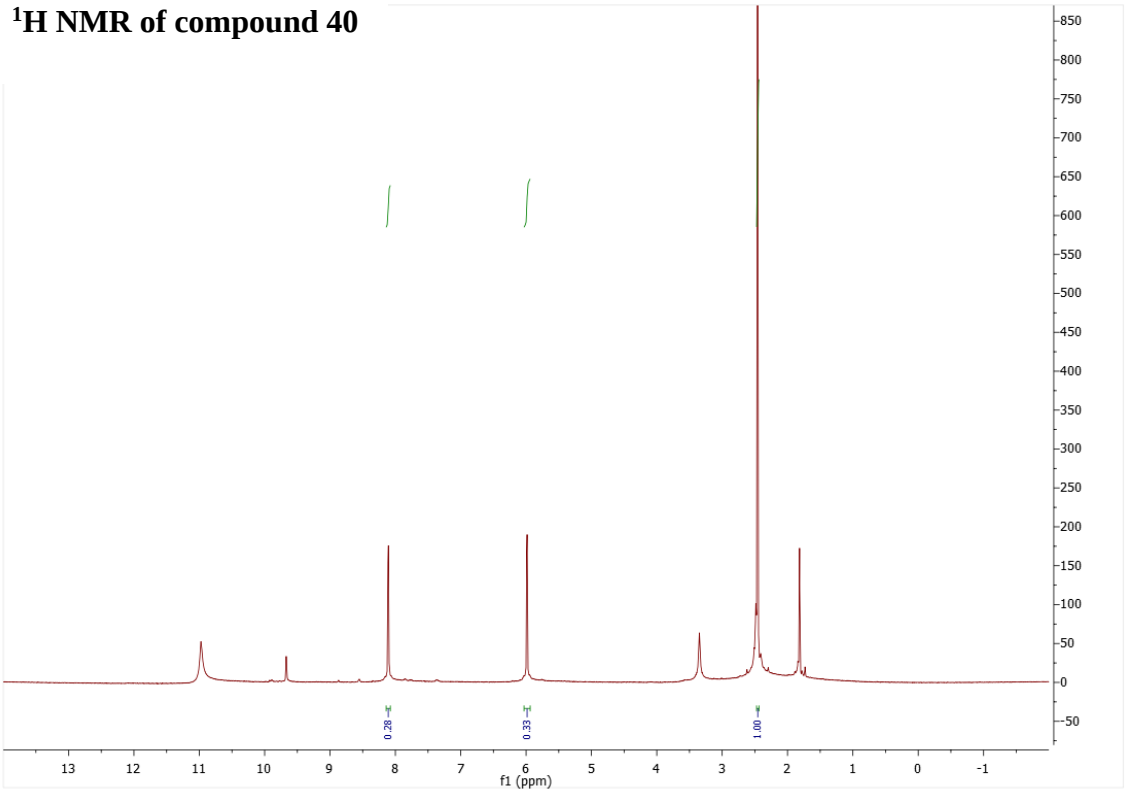

^{13}C NMR of compound 40

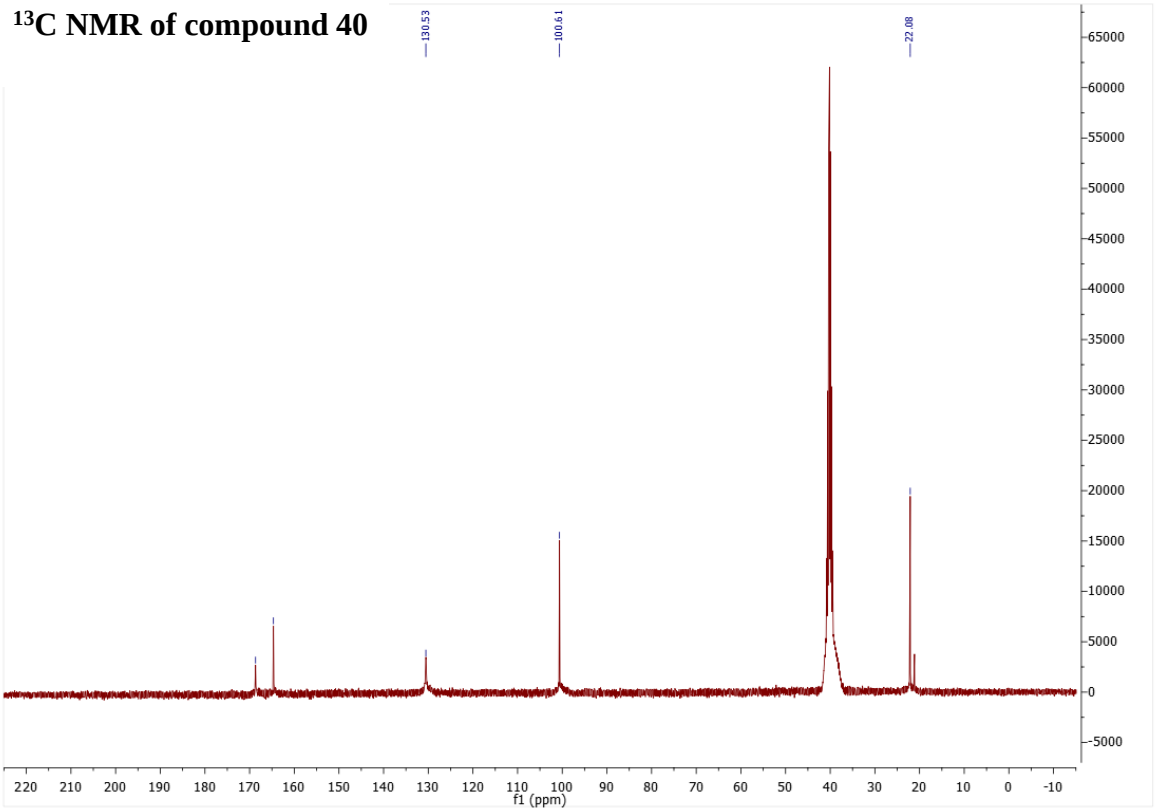

MS of compound **40**

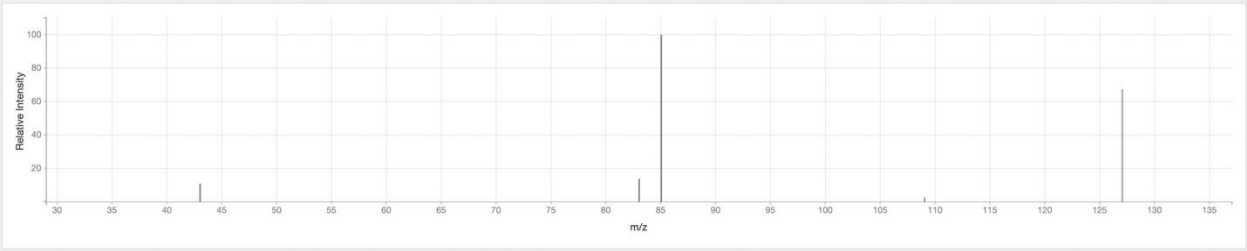

Peak intensity	Mass	Formula
68%	127 [M^+H^+]	$C_5H_7N_2O_2$
100%	57	$C_3H_5N_2O$

1-(3-(benzyloxy)-1H-pyrazol-1-yl)ethan-1-one (41)

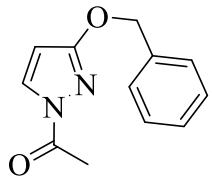

77%

41

The suspension of previous product **40** (1.0135 g, 8.04 mmol) and benzyl bromide (1.51 g, 8.844 mmol 1.1 eq) in DMF was poured into a round bottom flask and K_2CO_3 (1.482 g, 10.72 mmol, 1.33 eq) was also added. The reaction mixture was stirred for 10 h at room temperature. DMF was removed with vacuum distillation and resulting slurry was diluted with EtOAc and water. The organic phase was washed with brine (3 times) followed by drying over sodium sulfate. EtOAc was evaporated under vacuum and crude product was purified by flash column chromatography (5%-10% EtOAC/Hexane). TLC was done in 25% (EtOAc/Hexane). Purified product **41** was delivered as white color solid (77%). ^{1}H NMR (600 MHz, Chloroform-*d*) δ 8.09 (d, *J* = 3.1 Hz, 1H), 7.49 (d, *J* = 7.4 Hz, 2H), 7.42 (dd, *J* = 8.2, 6.6 Hz, 2H), 7.40 – 7.36 (m, 1H), 7.29 (s, 1H), 6.02 (d, *J* = 3.1 Hz, 1H), 5.31 (s, 2H). ^{13}C NMR (151 MHz, Chloroform-*d*) δ 168.85, 165.09, 136.27, 129.83, 128.57, 128.34, 128.23, 99.63, 70.94, 21.57.

^{1}H NMR of compound 41

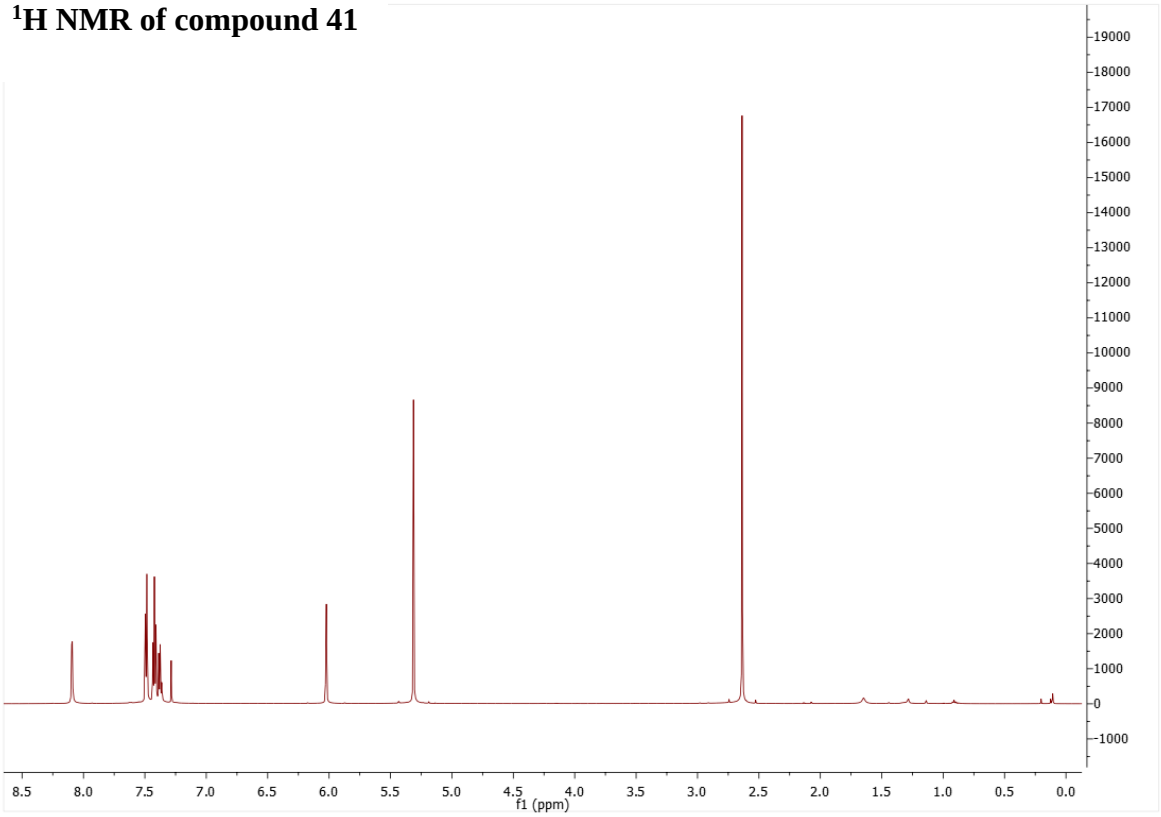

^{13}C NMR of compound 41

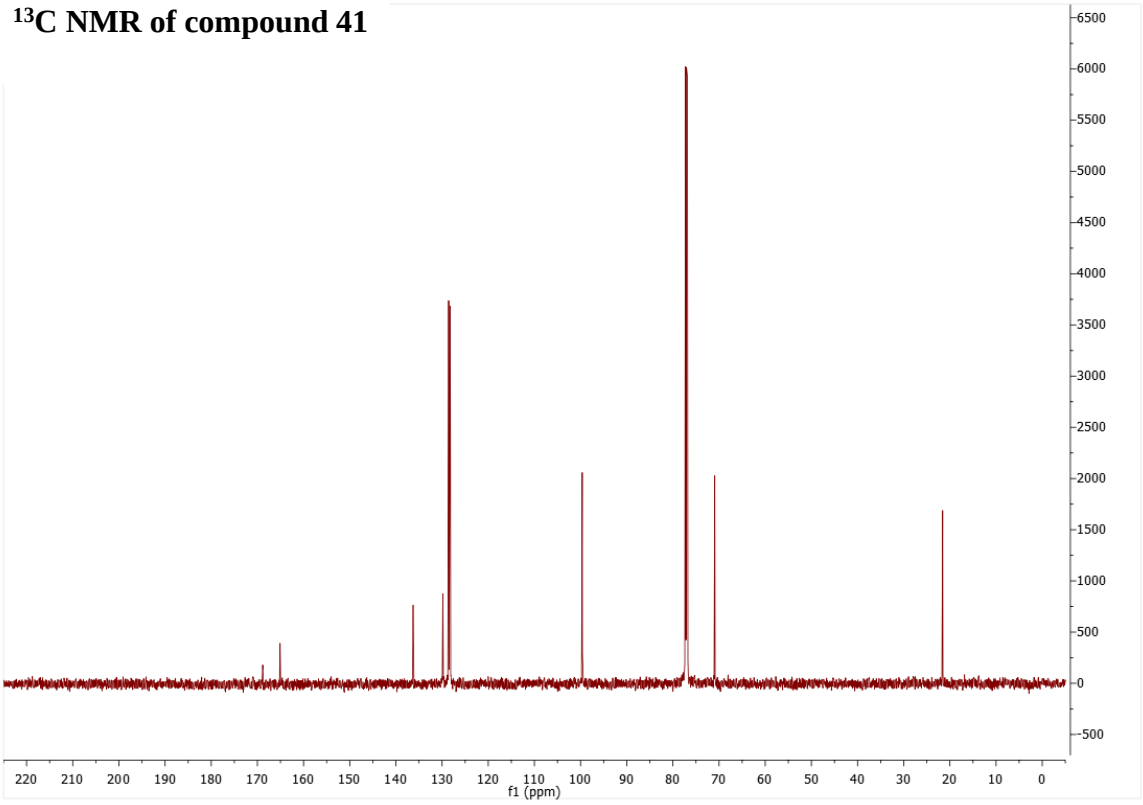

MS of compound **41**

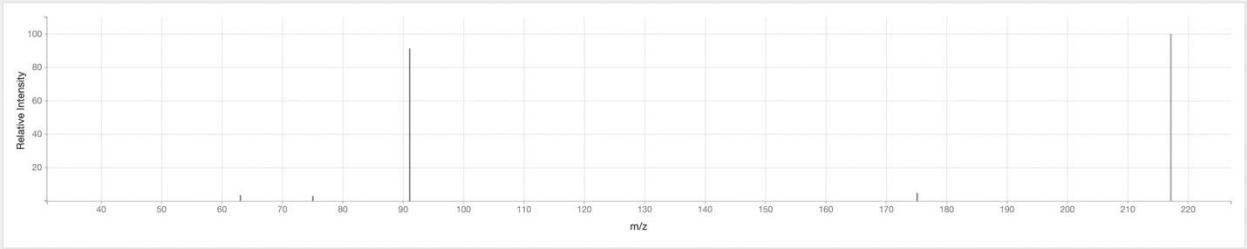

Peak intensity	Mass	Formula
100%	217 [M^+H^+]	$C_{12}H_{13}N_2O_2$
91%	57	C_7H_7

3-(benzyloxy)-1H-pyrazole (42)

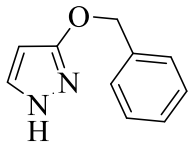

80%

42

Compound **41** was dissolved in a mixture of MeOH/THF (2:3 v/v) and 10% NaOH (in H_2O) was added. The reaction mixture was stirred for 5 h at room temperature. The reaction was monitored with TLC 25% (EtOAc/Hexane). The volatile components were evaporated under vacuum and diluted with EtOAc and water. Aqueous phase was washed three times with EtOAc. Combined organic phase was washed with brine (3 times) and dried over sodium sulfate. EtOAc was evaporated *in vacuum* to obtain off-white solid 3-(benzyloxy)-1H-pyrazole (80%). ^{1}H NMR (600 MHz, Chloroform-*d*) δ 11.33 (bs, 1H), 7.54 (d, 1H), 7.47 (t, 1H), 7.42 (tt, 1H), 7.34 (d, *J* = 2.4 Hz, 1H), 5.85 (d, *J* = 2.4 Hz, 1H), 5.32 (s, 2H). ^{13}C NMR (151 MHz, Chloroform-*d*) δ 163.61, 137.09, 130.58, 128.68, 128.17, 127.81, 90.32, 71.32.

^{1}H NMR of compound 42

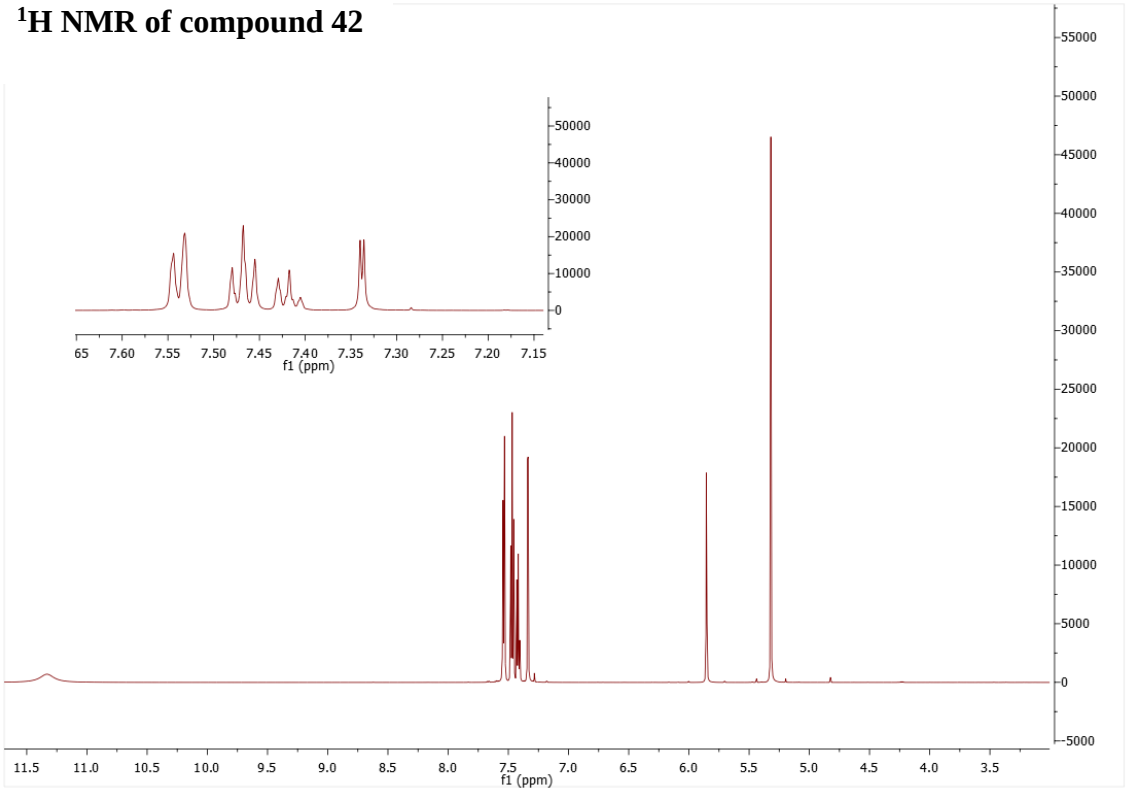

^{13}C NMR of compound 42

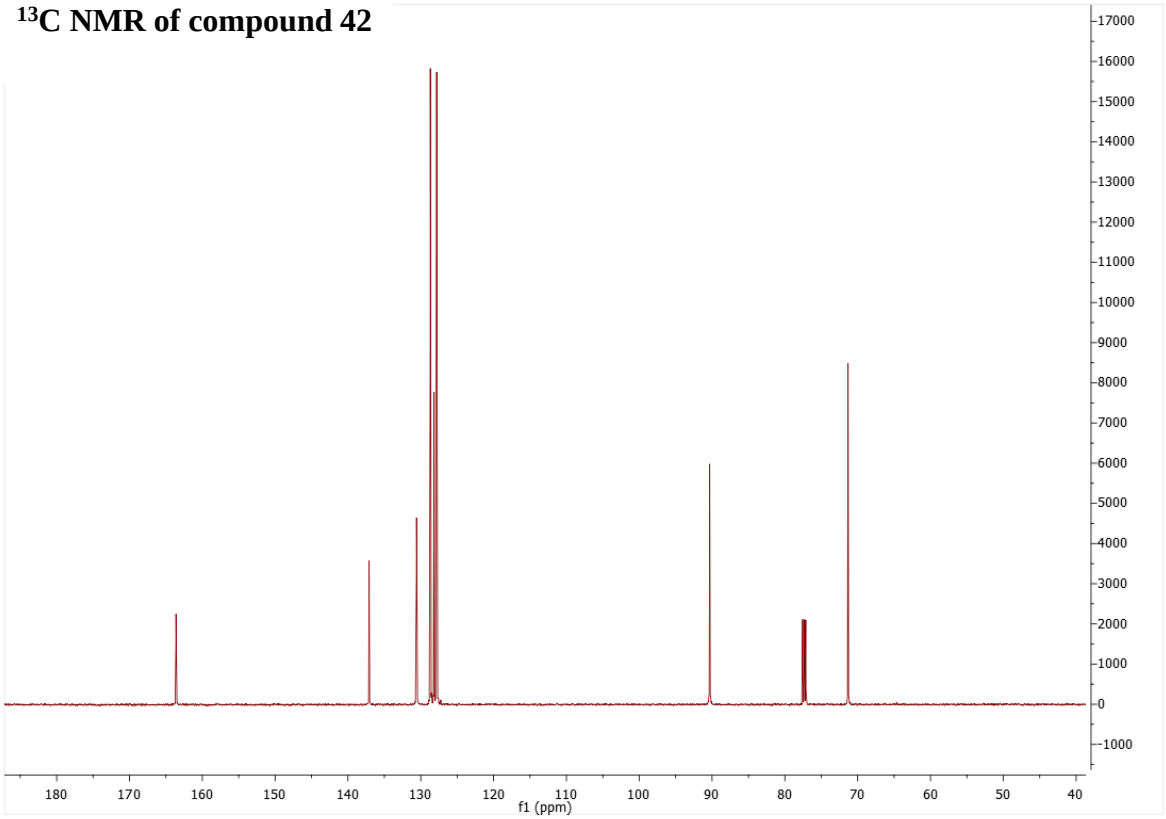

MS of compound **42**

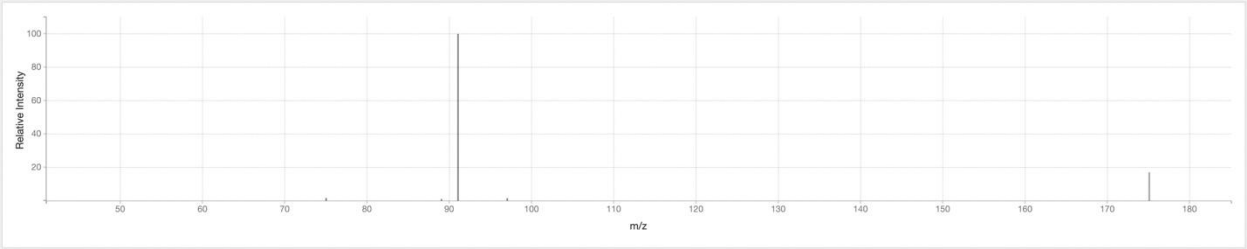

Peak intensity	Mass	Formula
18%	175 [M^+H^+]	$C_{12}H_{13}N_2O_2$
100%	91	C_7H_7

3-(benzyloxy)-N-(4-chlorophenyl)-1H-pyrazole-1-carbothioamide (43).

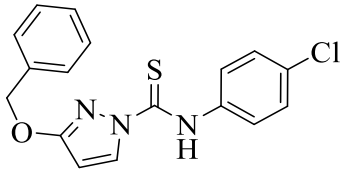

49%

43

3-(benzyloxy)-1H-pyrazole **(17)** (400 mg, 2.30 mmol) was dissolved in dry THF and transferred into a round bottom flask that was previously charged with K_2CO_3 (317.8 mg, 2.30 mmol). The reaction mixture was stirred vigorously for 1 hour at 50 °C. Then 4-chlorophenyl isothiocyanate (390 mg, 2.30 mmol) was added and stirred for 18 hours at room temp. The reaction was monitored by TLC (25% EtOAc/hexanes). Potassium carbonate solid was filtered off by gravity filtration. DMF was evaporated in *vacuum.* Resulting crude product was purified by flash column chromatography (100% hexane to 5% ethyl acetate/hexane) to afford 49% yield of **43,** off-white colored solid. ^{1}H NMR (600 MHz, Chloroform-*d*) δ 10.24 (s, N-H), 8.61 (t, *J* = 3.3 Hz, 1H), 7.73 (dd, *J* = 8.7, 3.2 Hz, 2H), 7.49 (dd, *J* = 7.9, 2.9 Hz, 2H), 7.42 (dddd, *J* = 15.0, 13.0, 8.4, 4.5 Hz, 5H), 6.07 (t, *J* = 3.3 Hz, 1H), 5.33 (d, *J* = 3.2 Hz, 2H).^{13}C NMR (151 MHz, Chloroform-*d*) δ 173.04, 164.78, 135.83, 133.02, 132.08, 129.12, 128.71, 128.54, 127.99, 125.25, 99.46, 71.37. FTIR, cm^{-1}: 3294 (-NH-), 3010 (C-H aromatic), 2929 (aliphatic C-H), 1558 (aromatic C=C), 1502 (aromatic C=N), 1246 (C=S), 762 (aromatic C-Cl), 1342 and 1002 (alkyl aryl C-O-C). HRMS (+ESI-TOF) m/z: [M^+] calcd for $C_{17}H_{14}ClN_3OS$ 343.0546; found 343.0548.

^{1}H NMR of compound 43

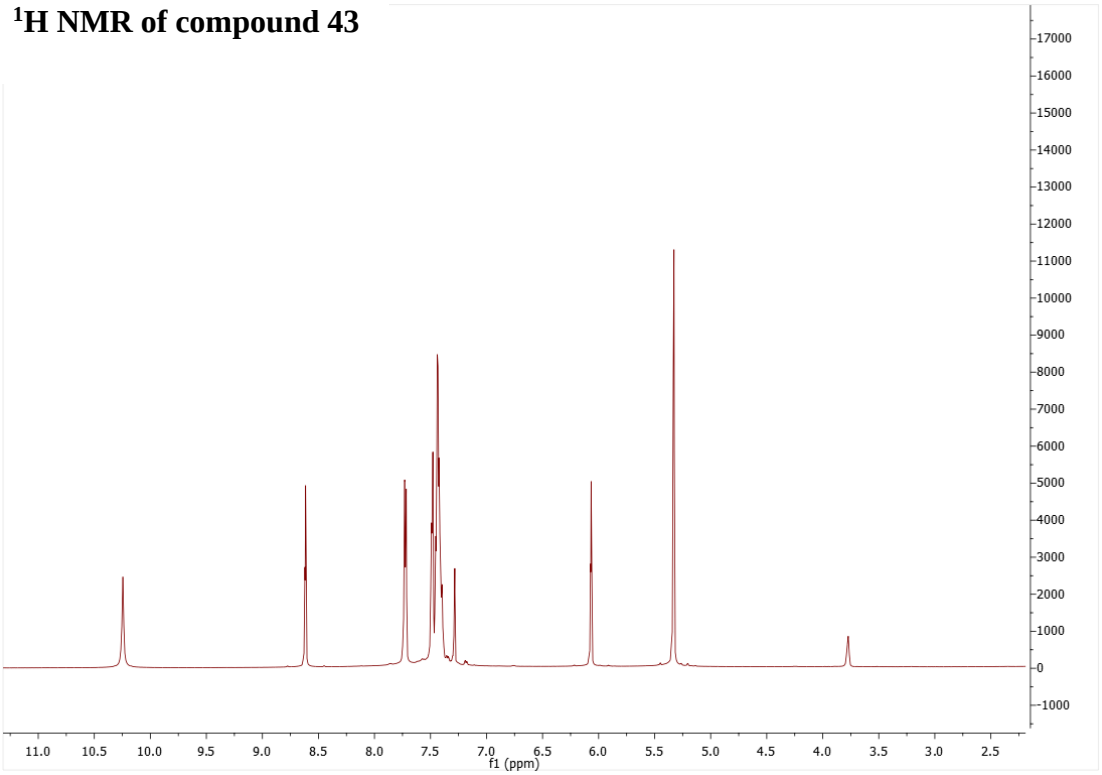

^{13}C NMR of compound 43

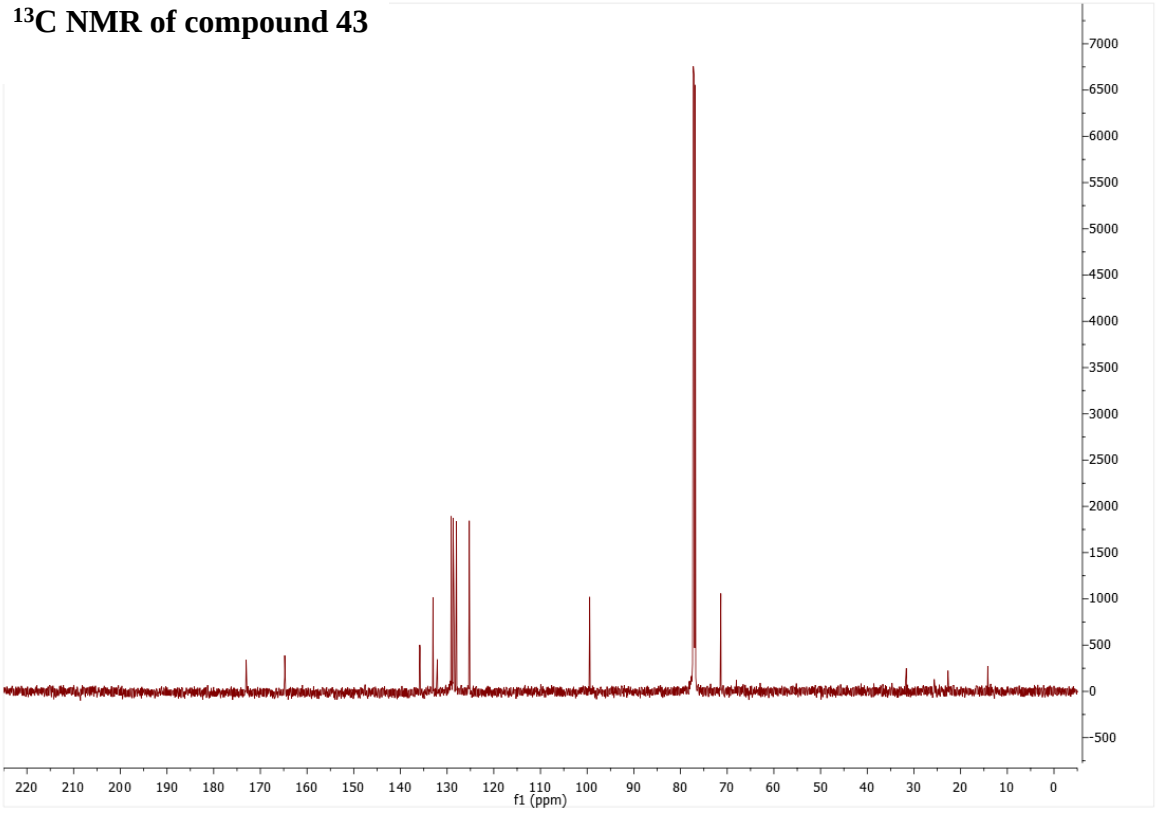

HRMS for compound **43**
Monoisotopic Mass: 343.054062
Found: 343.0548
Chemical Formula: $C_{17}H_{14}ClN_3OS$
M+

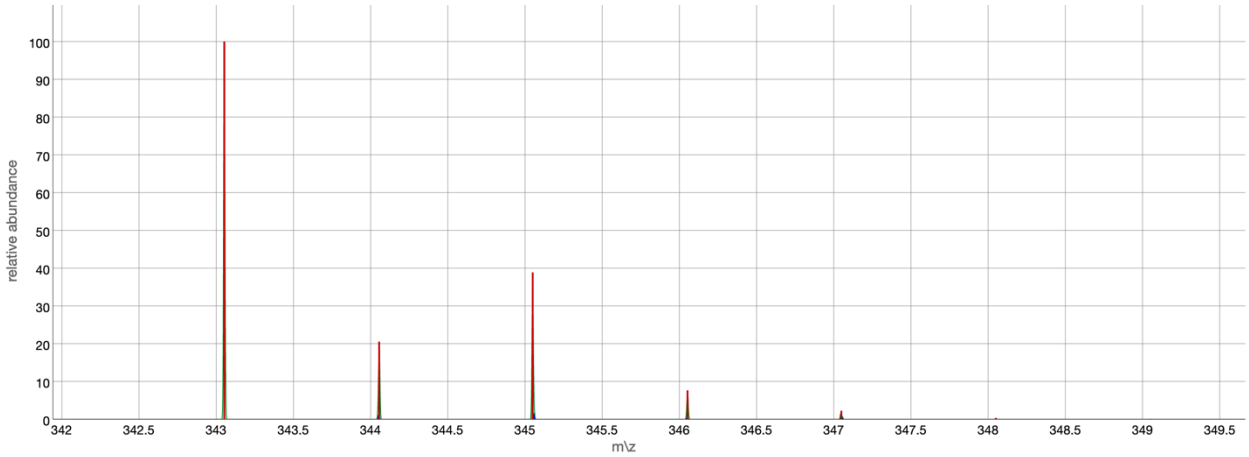

1-(bromomethyl)-4-nitrobenzene (44)

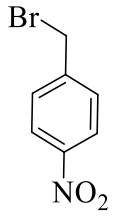

43%

44

2g (11.7 mmol) of benzyl bromide was cooled to 5°C and 1.4 mL of concentrated H_2SO_4 was added while it was being stirred. 0.7 mL of HNO_3 was added to it dropwise over 10 min. The reaction was allowed to reach to room temperature while stirring. Once room temperature was reached, it was stirred for another 2 hr. At this point, it gave dark orange colored viscous solution. Some crushed ice was added to this mixture and a bright yellow colored solid crashed out. Solids were vacuum filtered and washed three times with cold distilled water. TLC was done in 25% EtOAc/ hexane system and visualized under UV. Solids were oven dried to remove all the moisture. Final product was pale yellow color solid in 43%.

H NMR (400 MHz, DMSO-d6) δ 8.21 (d, J = 8.7 Hz, 2H), 7.72 (d, J = 8.7 Hz, 2H), 4.93 (s, 0H), 4.81 (s, 2H).

^{1}H NMR of compound 44

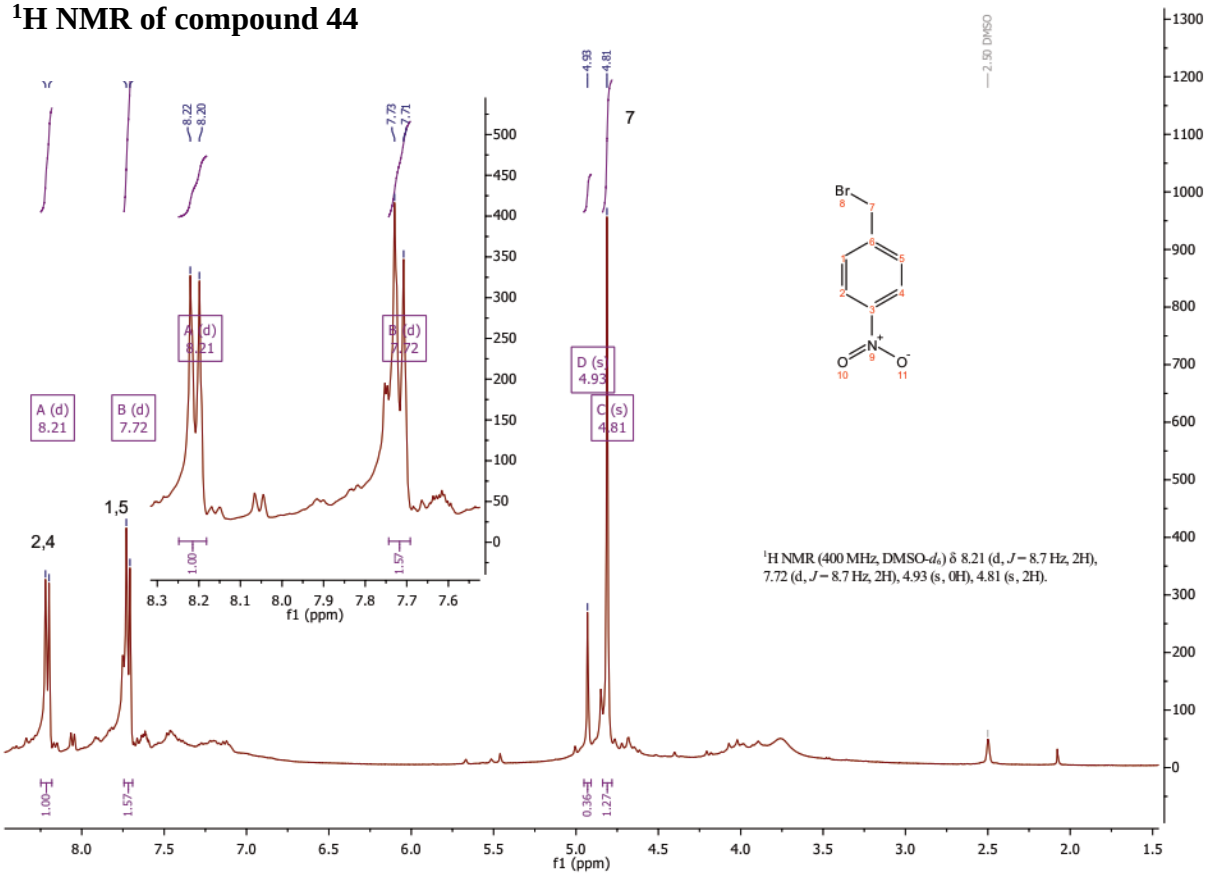

N-(4-chlorophenyl)-3-((4-nitrobenzyl)oxy)-1H-pyrazole-1-carbothioamide (45)

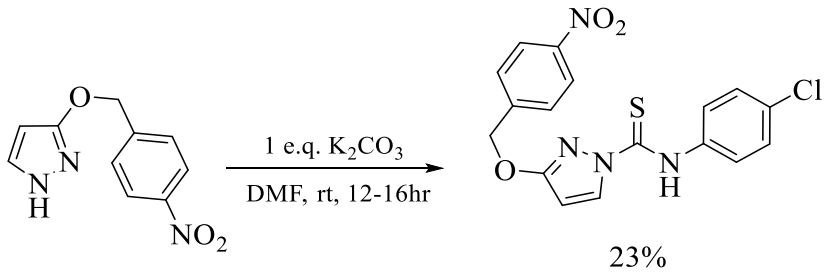

23%

45

269.6 mg (1.23 mmol) of 3-((4-nitrobenzyl)oxy)-1H-pyrazole dissolved in DMF was mixed with 1 eq. (208 mg, 1.23 mmol) of 4-chlorophenyl isothiocyanate in DMF. 1 eq. of K_2CO_3 was added to the reaction mixture. After that, it was mixed at room temp overnight. TLC was performed 25% EtOAc/ hexane system and visualized under UV. After reaction completion, potassium carbonate was filtered off and DMF was evaporated under vacuum. Resulting crude product was purified with column chromatography to obtain off-white product in 23%. ^{1}H NMR (600 MHz, DMSO-d_6) δ 11.42 (s, 1H), 8.62 (d, J = 3.0 Hz, 1H), 8.28 (m, 2H), 7.77 (m, 2H), 7.63 (m, 2H), 7.51 (m, 2H), 6.35 (d, J = 3.0 Hz, 1H), 5.56 (s, 2H). ^{13}C NMR (151 MHz, DMSO-d_6) δ 174.40, 164.67, 147.69, 144.49, 137.52, 134.26, 131.28, 129.25, 128.97, 128.20, 124.16, 99.39, 69.88.

^{1}H NMR of compound 45

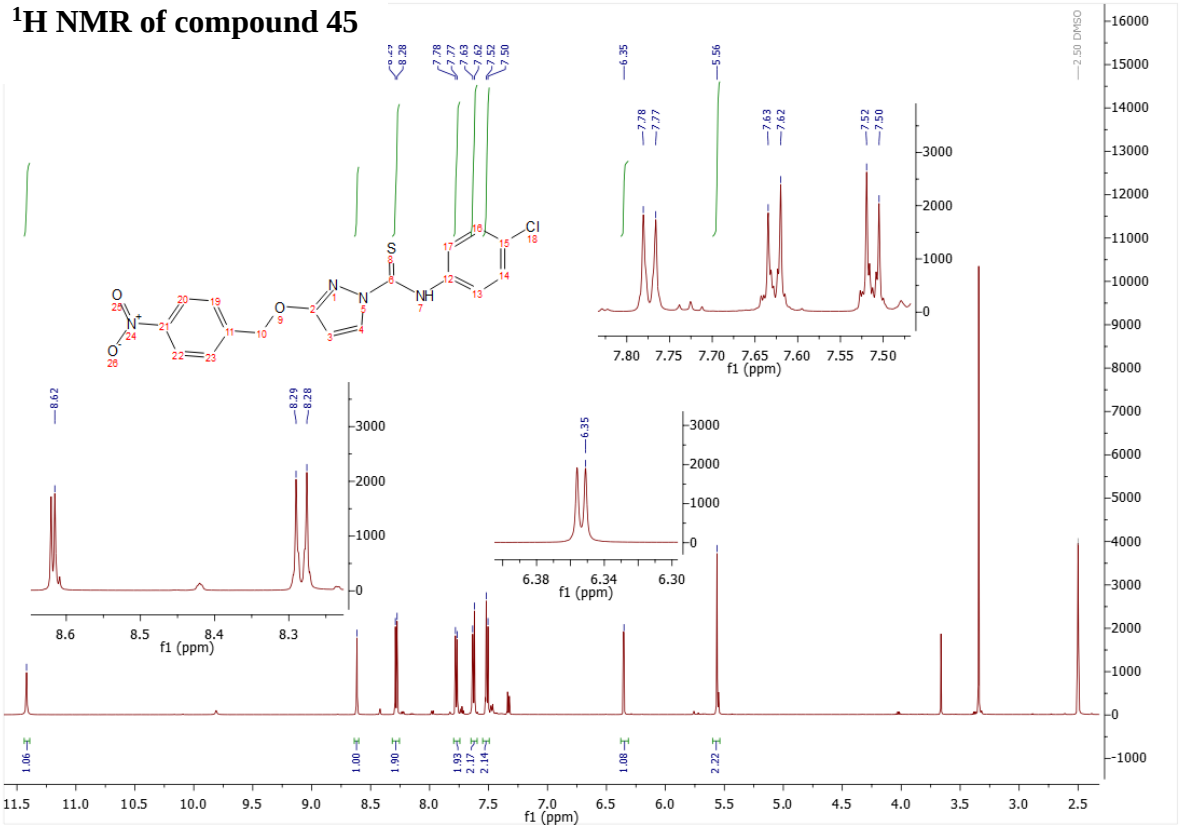

^{13}C NMR of compound 45

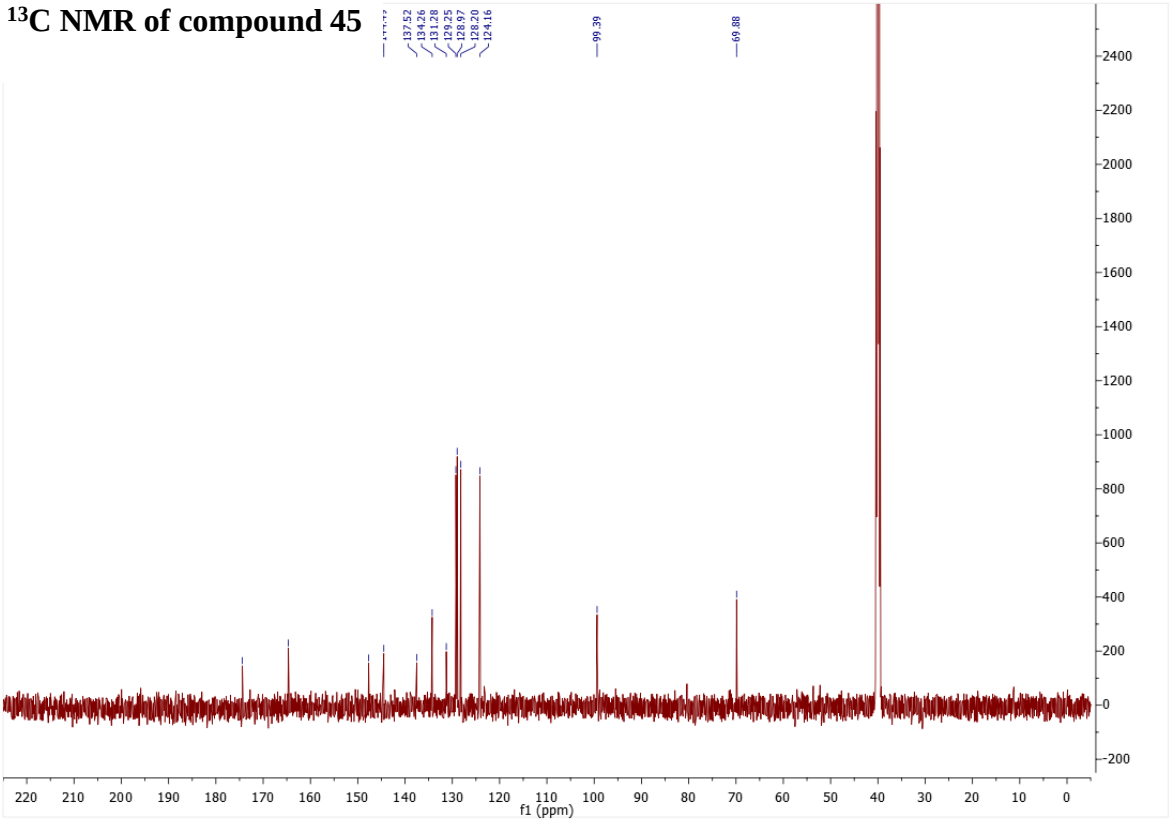

N-(4-chlorophenyl)-3-methyl-1H-pyrazole-1-carbothioamide (46).

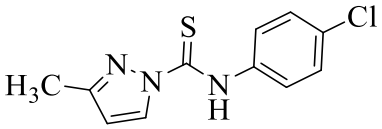

76%
46

3-methyl-1H-pyrazole (213 mg, 2.59 mmol) was dissolved in DCM and stirred in a 100 mL round bottom flask. 4-chlorophenyl isothiocyanate (440 mg, 2.6 mmol, 1 eq) after being dissolved in DCM was added to the reaction dropwise and stirred for 20 hours at room temperature. The reaction was monitored by TLC (25% EtOAc/hexanes). There was a solid precipitate in the slightly orange colored solution. Precipitate was isolated by gravity filtration and washed several times with cold dichloromethane. Resulting solid precipitate was re-crystallized with MeOH. Obtained off-white colored solid, **46** (76.1%) was oven dried. ^{1}H NMR (400 MHz, DMSO-d_6) δ 11.70 (s, J = 4.5 Hz, 1H), 8.63 (s, J = 2.8 Hz, 1H), 7.66 (d, J = 6.1 Hz, 2H), 7.48 (d, J = 6.1 Hz, 2H), 6.46 (s, J = 2.8 Hz, 1H), 2.33 (s, J = 5.1 Hz, 3H). ^{13}C NMR (101 MHz, DMSO-d_6) δ 174.28, 152.93, 137.11, 132.51, 129.87, 128.37, 127.74, 127.46, 110.72, 103.59, 13.61. FTIR, cm^{-1}: 3278 (-NH-), 3050 (C-H aromatic), 2921 (aliphatic C-H), 1587(aromatic C=C), 1534 (aromatic C=N), 1189 (C=S), 694 (aromatic C-Cl). HRMS (+ESI-TOF) m/z: [M^{+}] calcd for $C_{11}H_{10}ClN_3S$ 251.0284; found 251.0283.

^{1}H NMR of compound 46

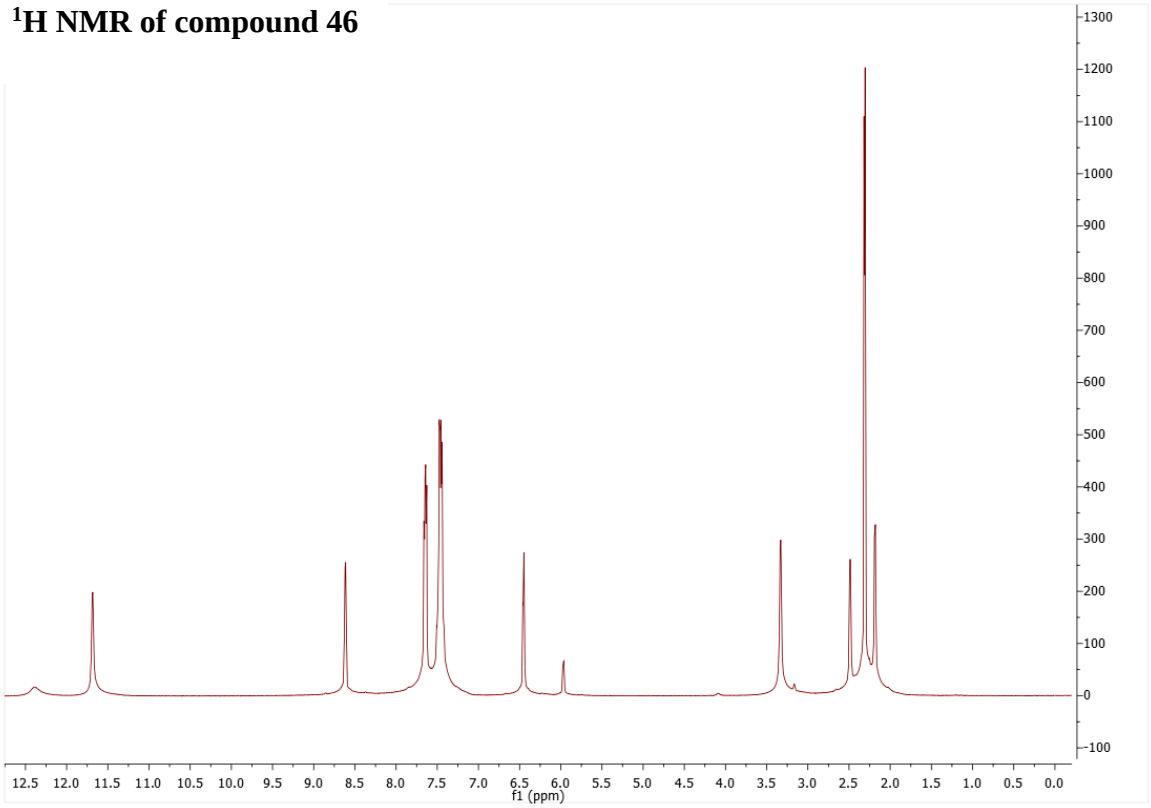

^{13}C NMR of compound 46

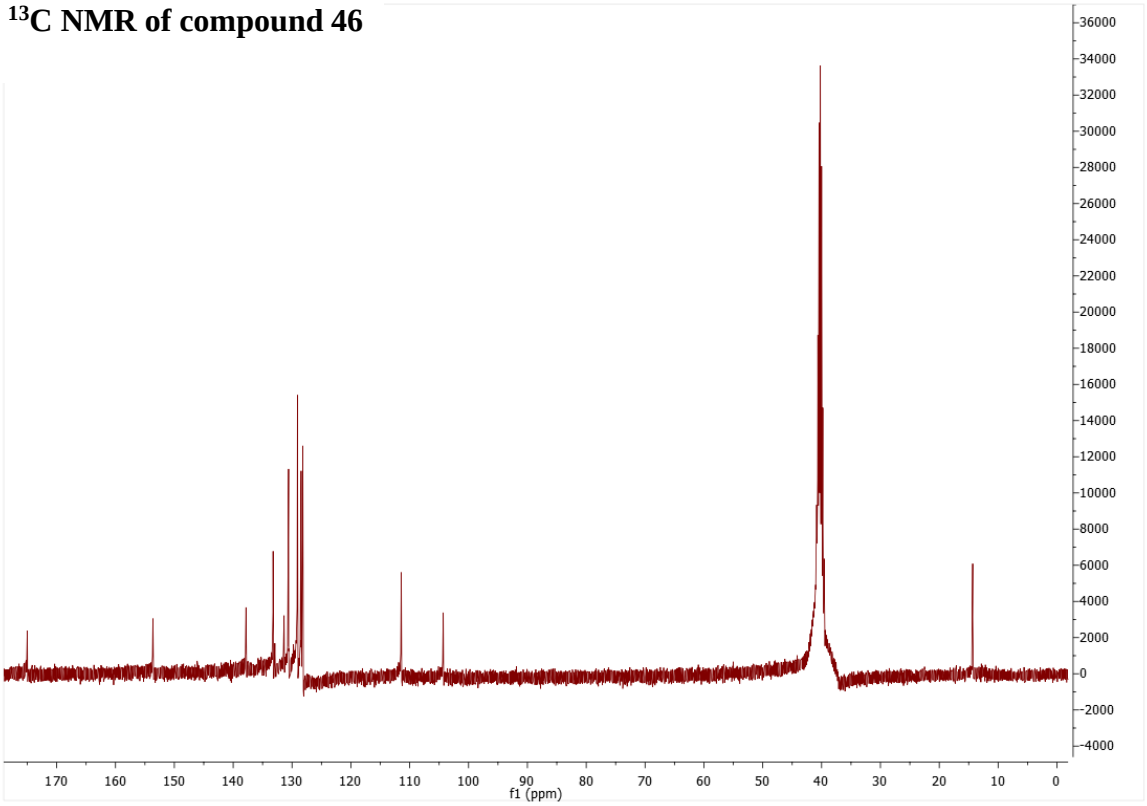

HRMS for compound **46**
Monoisotopic Mass: 251.0278472
Found: 251.0283
Chemical Formula: $C_{11}H_{10}ClN_3S$
M+

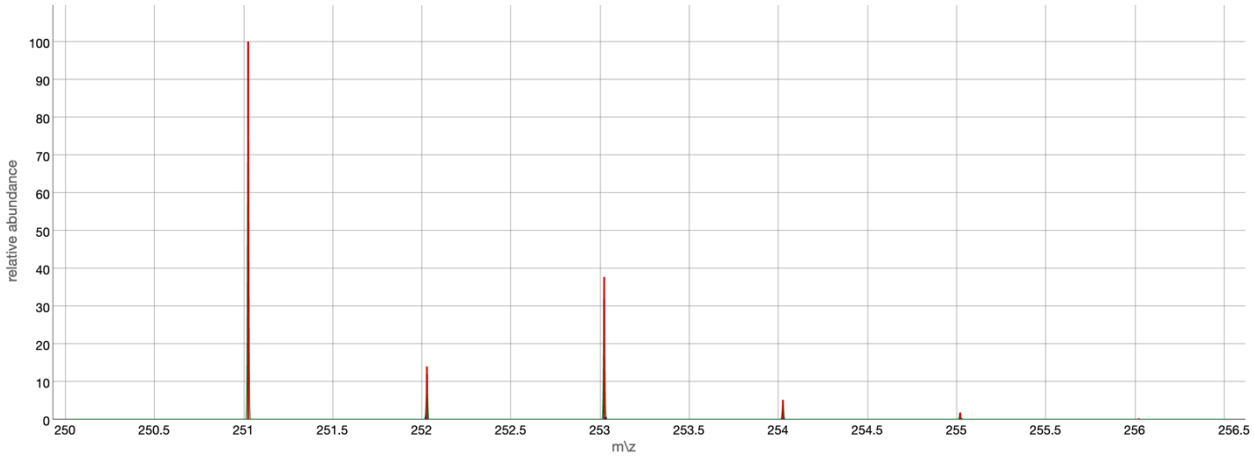

1-adamantylhydrazine (47)

88%
47

Ivory color (literature states white to yellow) 1-bromoadamantane (200 mg, 0.93 mmol) was measured on a weighing paper and it was transferred to a 150 mL, one-necked, round bottomed flask with a magnetic stirring bar using a powder funnel. Then the round bottomed flask was charged with excess amount (25 mL) of hydrazine monohydrate which acts as the solvent and reactant (no other solvents were required here). 1-bromoadamantane does not dissolve in hydrazine at this point and there was a dispersion that occurred in the reaction vessel. Mineral oil bath was equipped to reflux the reaction at 125 °C – 135 °C. Inside the reaction vessel, temperature was 110 °C. The refluxing temperature is crucial because the reaction refluxed below 100 °C delivered both the product and unreacted 1-bromoadamantyl. Temperature was taken only from the oil bath. Reaction was refluxed for 8 – 12 hours. During reflux, 1-bromoadamantane was completely dissolved in hydrazine and reaction mixture was very light-yellow color clear solution. Thin Layer Chromatography (TLC) was done in 50% EtOAc/hexane system and spots were visualized with phosphomolybdic Acid (PMA) as 1-bromoadamantane was not visible under short wavelength of ultraviolet (UV). The starting material 1-bromoadamantane gave a dark spot on a light green background at R_f = 0.90 whereas the product spot was not significantly visible as a dark spot, which indicates the formation of a new product.

The reaction mixture was cooled to room temperature followed by an addition of 45% KOH solution (when the reaction was cooling, the formerly clear solution turned cloudy as the adamantyl

product possesses low solubility in hydrazine monohydrate). Washing with 45% KOH assists in dissolving excessive hydrazine left in the crude mixture. At this point, the reaction mixture was less cloudy and became an off-white opaque solution. It was transferred to a separatory funnel and extracted with diethyl ether three times. Due to the hydrophobic adamantyl moiety, the product tends to move to organic layer (diethyl ether). The organic layer was dried over anhydrous sodium sulfate (the original literature stated to use anhydrous magnesium sulfate, however it is wise to use basic conditions as the molecule consists of hydrazine moiety). Upon the addition of anhydrous sodium sulfate, product solution was became clear, which was concentrated *in vacuum* to reduce a quarter of the solvent. Then it was charged with concentrated hydrochloric acid to obtain 1-adamantylhydrazine chloride salt which is more stable than the 1-adamantylhydrazine. Upon the addition of the acid, white colored solid product crashed out. The solid product was isolated by gravity filtration and dried in high vacuum. The original literature states to conduct recrystallization of this white solid using isopropanol, but it could lead to some product loss as the desired product shows considerable solubility in isopropanol. Without recrystallization the yield was > 88% and with recrystallization it was diminished to ~ 53%. NMR samples were prepared for the 1-adamantylhydrazine and its' salt in DMSO-D_6. And the products were analyzed with UPLC-MS and it clearly showed the presence of 1-adamantylhydrazine as molecular peak of 166.27. Melting points observed did not fit with the literature values.

^{1}H NMR (DMSO-D_6, 400 MHz): δ = 2.11 (s, 3H), 1.78 (s, 6H), 1.59 (m, 6H). ^{13}C NMR (101 MHz, DMSO-d_6) δ 45.72, 37.05, 35.88, 30.50, 28.65. FTIR: 2891 (w,s), 2709 (w,s), 2549 (m,b), 1480 (m,s), 1085 (m,s).

^{1}H NMR of compound 47

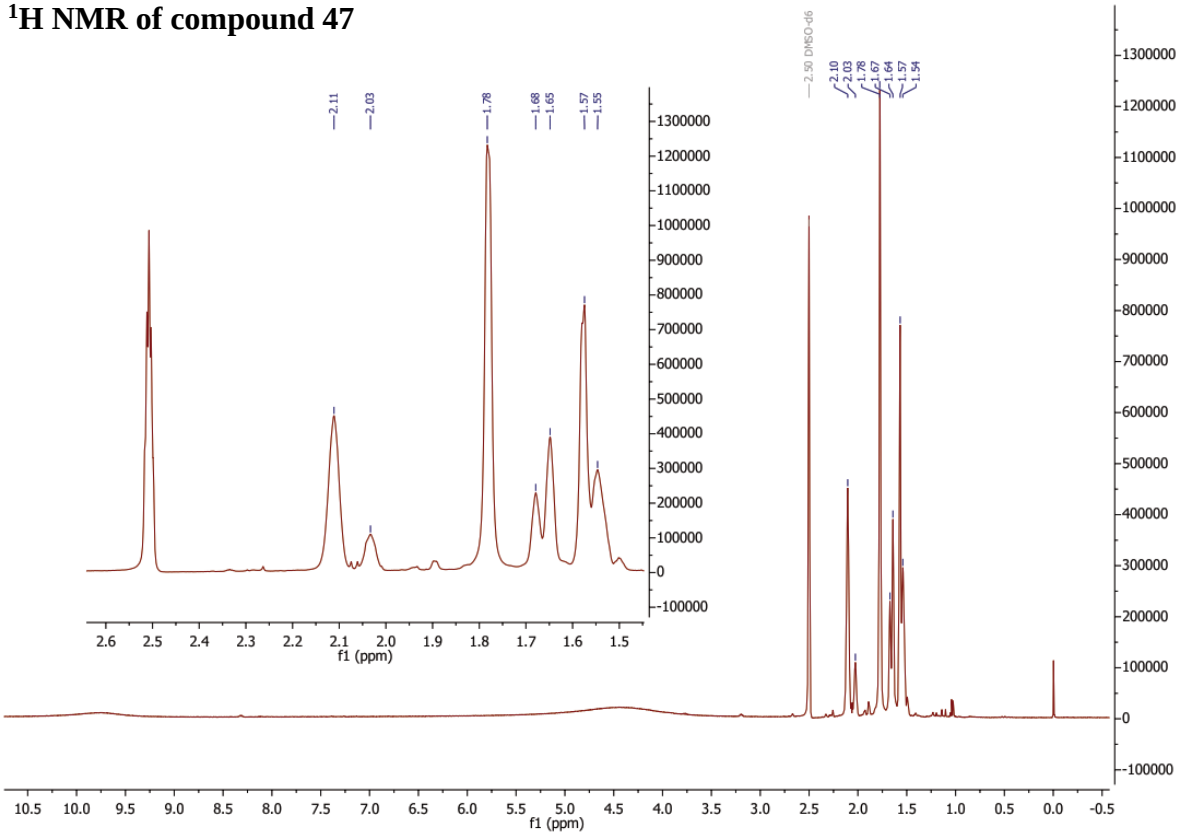

^{13}C NMR of compound 47

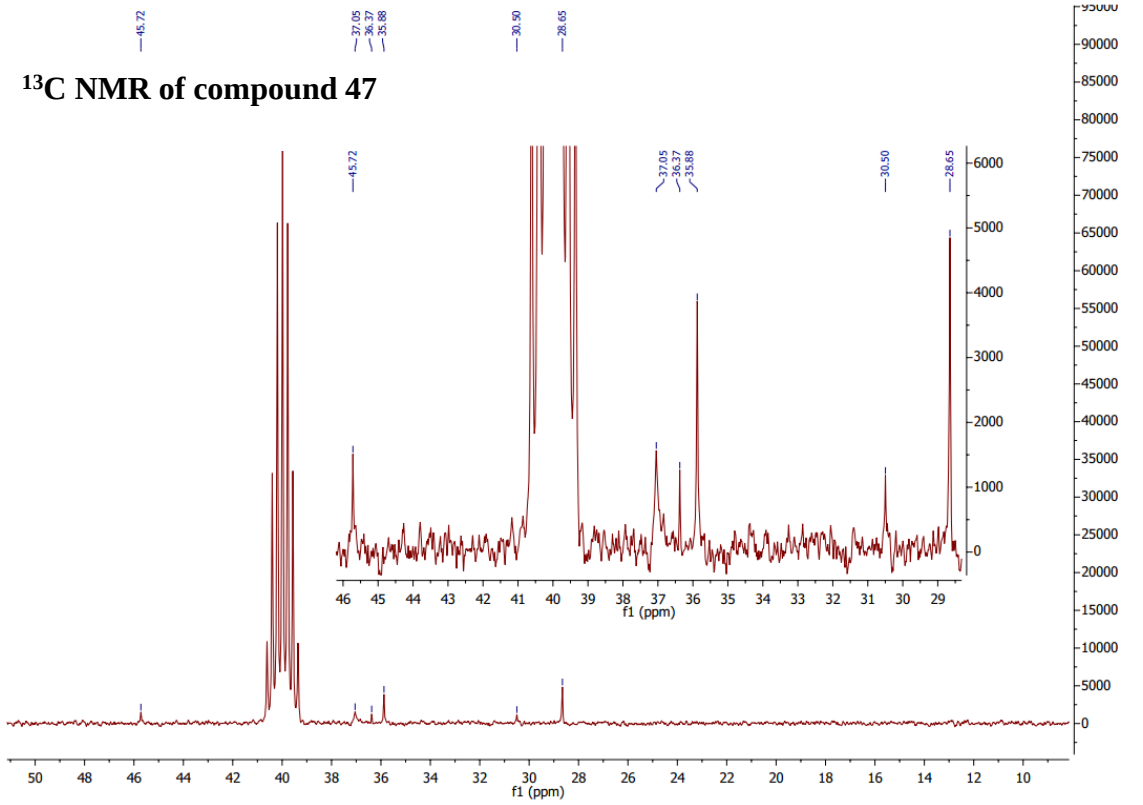

MS of compound **47**

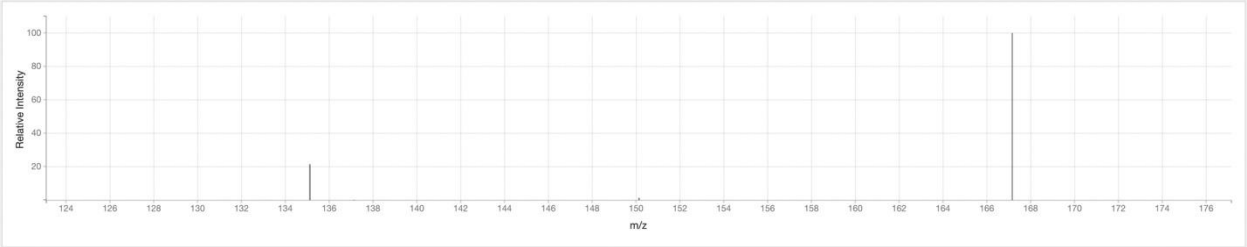

Peak intensity	Mass	Formula
100%	167 [M^+H^+]	$C_{10}H_{19}N_2$
22%	135	$C_{10}H_{15}$

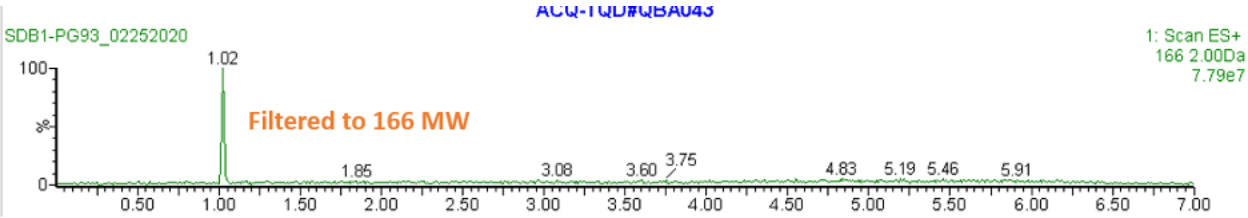

UPLC-MS chromatography data of the final product, 1-adamantylhydrazine

1-(Adamantan-1-yl)-1H-pyrazol-3-amine using 1-adamantylhydrazine (48)

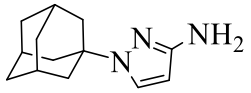

43%

48

2-chloroacrylonitrile (1 eq.) was measured into 150 mL round bottom flask and dispersed with 5 mL of distilled water. Separately, K_2CO_3 and $NaHCO_3$ (1:2) were dissolved in distilled water and mixed, followed by their addition to the acrylonitrile solution. Then 1-adamantylhydrazin hydrochloride (1eq) salt was dissolved in distilled water and transferred to the original mixture which was stirred overnight. According to the original protocol, the product was meant to be extracted by EtOAc three times. However, from previous experiences, it is wise to perform a continuous extraction to collect the desired product from the aqueous layer as pyrazolic compounds tend to show considerable hydrophilic behavior. Finally, the organic layer was dried *in vacuum* and purified by flash column chromatography (5% - 25% EtOAc/ Hexane) to obtain a dark orange colored thick, oily liquid, 43%.

^{1}H NMR (400 MHz, Chloroform-*d*) δ 7.47 (d, *J* = 14.3 Hz, 1H), 6.36 (d, *J* = 14.3 Hz, 1H), 6.06 (s, 1H), 2.23 (m, 3H), 1.77 (m, 6H), 1.28 (s, 6H).

^{13}C NMR (101 MHz, Chloroform-*d*) δ 160.39, 146.58, 106.20, 42.73, 40.20, 36.32, 29.55.

FTIR: 3318.16 (w,b), 2904 (m, s), 2849 (m,s), 1683 (w,s), 1542 (w.s), 743 (m,s).

^{1}H NMR of compound 48

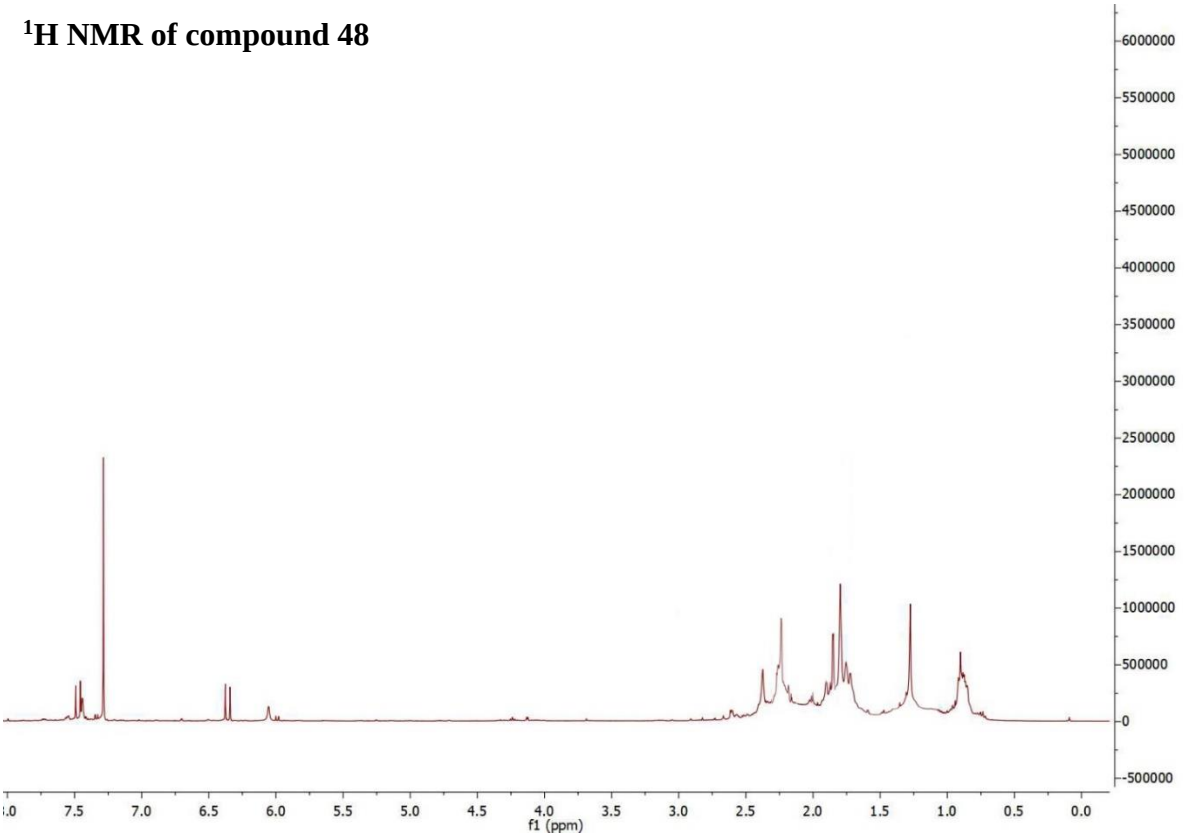

^{13}C NMR of compound 48

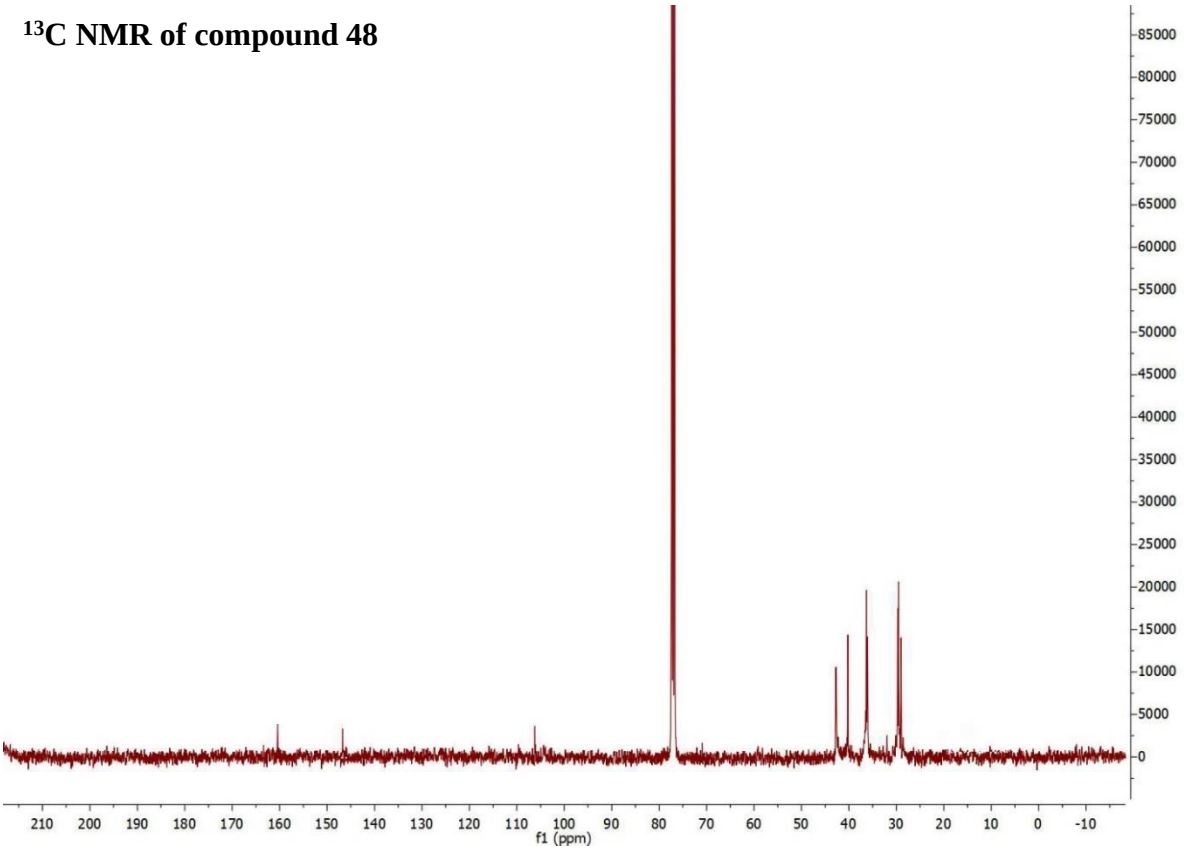

MS of compound **48**

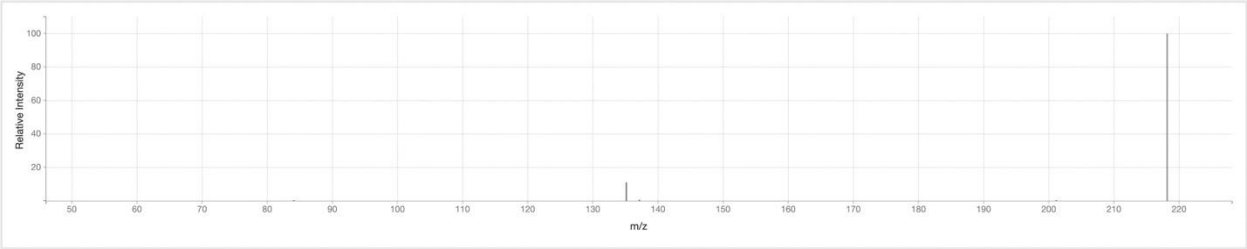

Peak intensity	Mass	Formula
100%	218 [M^+H^+]	$C_{13}H_{20}N_3$
12%	135	$C_{10}H_{15}$

4-bromo-1H-pyrazole (49)

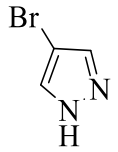

79%
49

500 mg (7.34 mmol) of pyrazole was dissolved in 15 mL of distilled water and stirred vigorously. 1 eq. (1.3 g, 7.34 mmol) of N-bromosuccinimide was dispersed in distilled water and was added to the stirring mixture. Reaction was stirred for 3h at room temperature and the reaction completion was monitored by TLC. TLC was done in 75% EtOAC/ hexane system and spots were visualized with PAM. The organic layer was extracted to DCM (three times) and dried over anhydrous sodium sulfate. The crude product was concentrated *in vacuum* before proceeding to column chromatography. Column chromatography was initiated with 30% EtOAC/ hexane and gradually increased to 75% EtOAC/ hexane. Received white solid 79% yield. ^{1}H NMR (DMSO-$D_{6,}$ 600 MHz,) δ 7.96 (s, 1H), 7.58 (s, 1H). ^{13}C NMR (151 MHz, DMSO-d_6) δ 139.45, 129.24, 92.20.

^{1}H NMR of compound 49

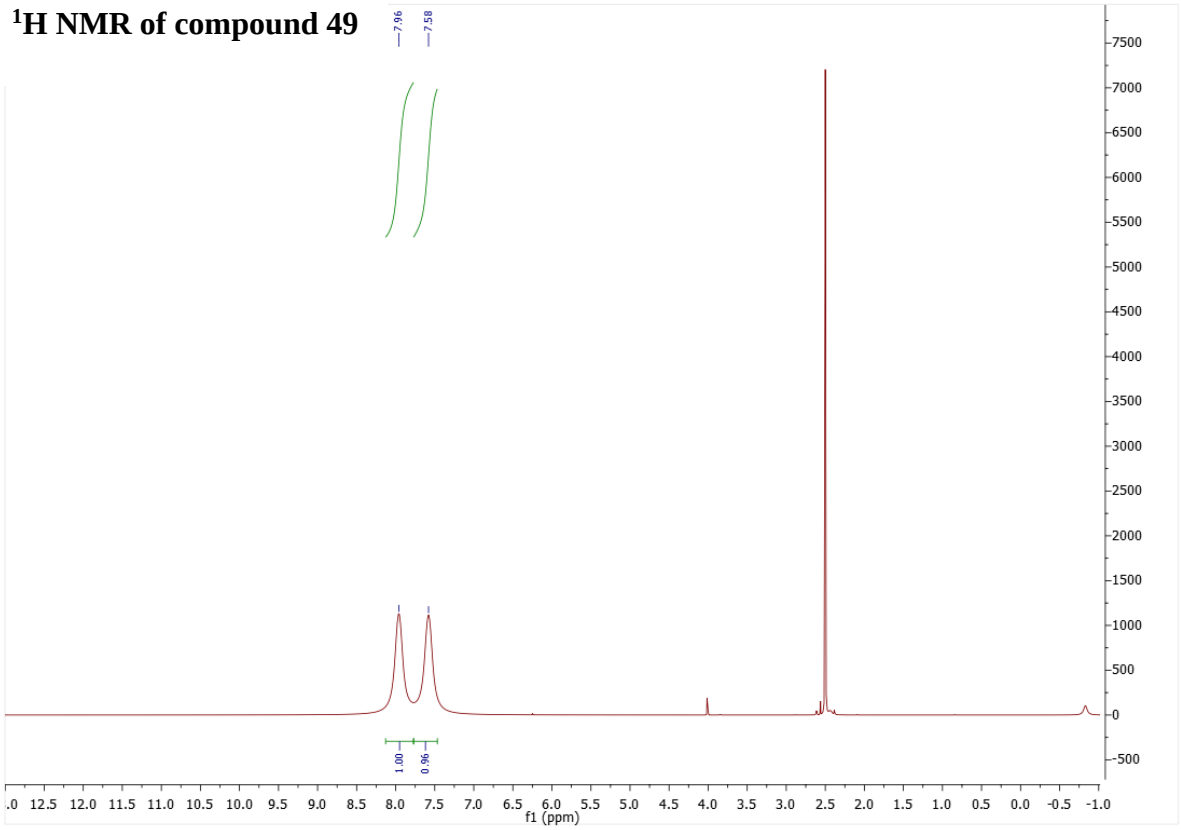

^{13}C NMR of compound 49

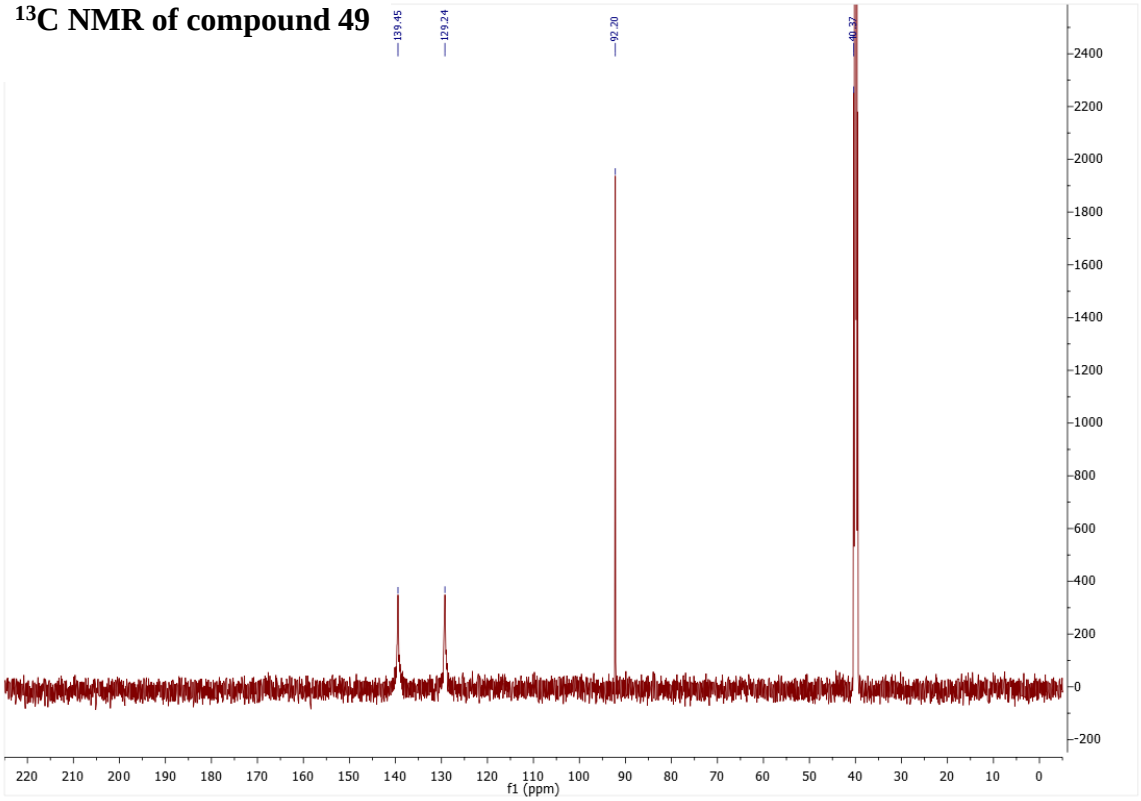

1H,1'H-4,4'-bipyrazole (50)

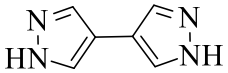

97%
50

267.1 mg (eq. 0.3) of $Ni(PPh_3)_2Cl_2$ was dispersed in dry THF and into this mixture, 350 mg (eq. 1) of Et_4NI in THF was added and stirred. 133.5 mg (eq. 1.3) of Zn dust was added to the mixture and stirring was continued for 30 min at room temperature. Afterwards the reaction temperature was increased to 50 ºC. At this temperature, 200 mg (eq. 1) of compound **49** was added to the reaction and was stirred for 14h. Initially the reaction mixture was a dark brown color and upon addition of **49**, the color did not change. After 14h, the reaction was basified using 2M of ammonium hydroxide to pH 11. Then a dark brown colored solid precipitate occurred. This solid was filtered off and the aqueous green filtrate was collected and concentrated *in vacuum* before proceeding to the extraction with EtOAC. The extracted organic layer was dried over $MgSO_4$ and a crude organic layer was again concentrated *in vacuum.* The obtained slurry was diluted again with water and extracted to EtOAC (three times). The combined organic layer was dried over anhydrous $MgSO_4$ and it was concentrated *in vacuum* to obtain an off-white colored solid in 97% yield. ^{1}H NMR (DMSO-D_6, 600 MHz,) δ 7.62 (dd, *J* = 11.3, 7.4 Hz, 1H), 7.55 (dd, *J* = 7.8, 3.0 Hz, 1H). ^{13}C NMR (151 MHz, DMSO-d_6) δ 133.53, 132.85, 132.52, 131.96, 129.24.

^{1}H NMR of compound 50

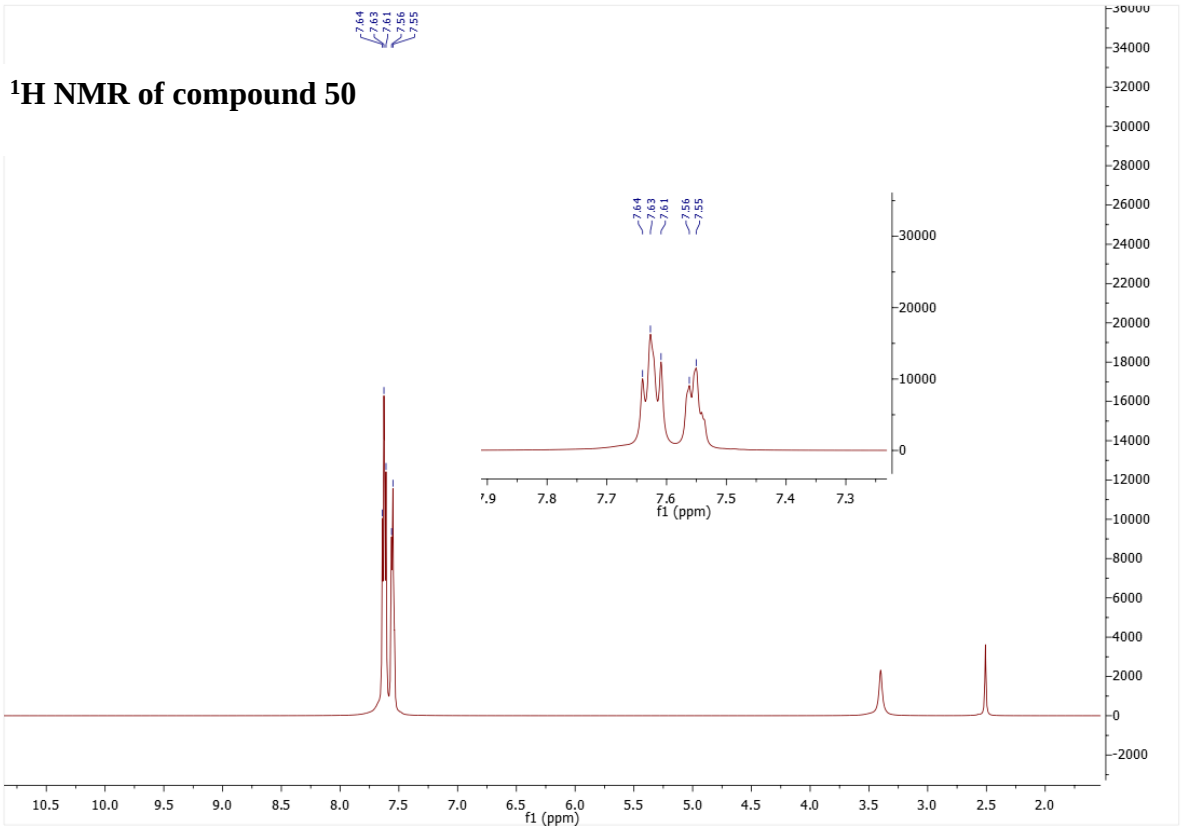

^{13}C NMR of compound 50

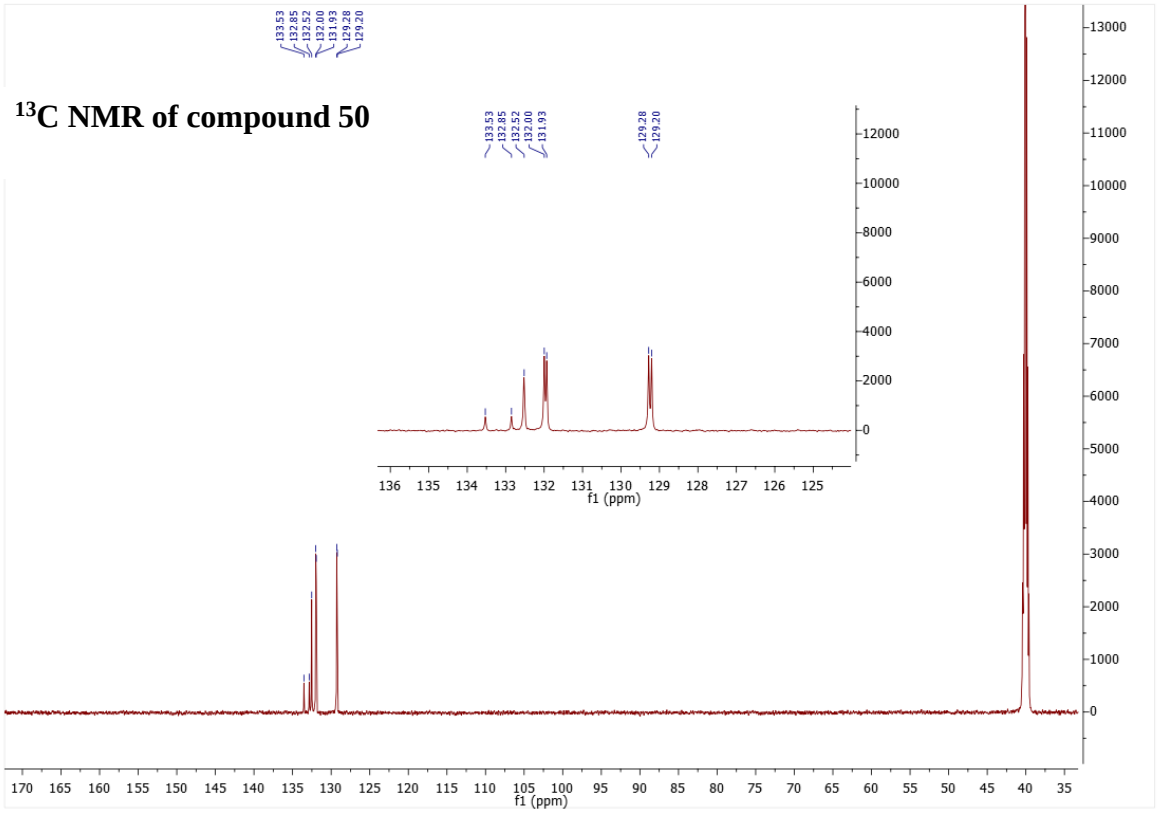

N1,N1'-bis(4-chlorophenyl)-1H,1'H-[4,4'-bipyrazole]-1,1'-bis(carbothioamide) (51)

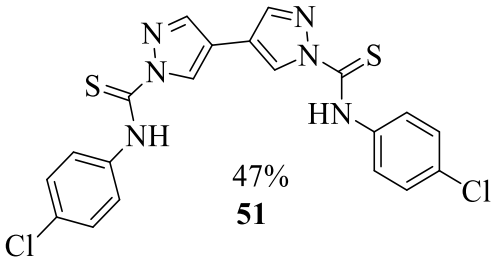

47%

51

60.5 mg (0.45 mmol) of compound **50** dissolved in DMF was charged into a round bottom flask and eq. 2 (125 mg) of K_2CO_3 was added to the stirring mixture. This mixture was stirred 20 min before the addition of 4-chlorophenyl isothiocyanate. Afterward, eq. 2 (0.9 mmol, 153 mg) of 4-chlorophenyl isothiocyanate in DMF was added to reaction mixture. It was stirred at room temperature overnight. TLC was done in 50% EtOAC/ hexane system and spots were visualized under UV. Flash column was performed to isolate the desired solid product in 47% yield. ^{1}H NMR (400 MHz, DMSO-d_6) δ 8.88 (s, 2H), 7.63 (s, 2H), 7.57 (s, 2H), 7.48 (d, J = 8.9 Hz, 4H), 7.33 (d, J = 8.8 Hz, 4H).

^{1}H NMR of compound 51

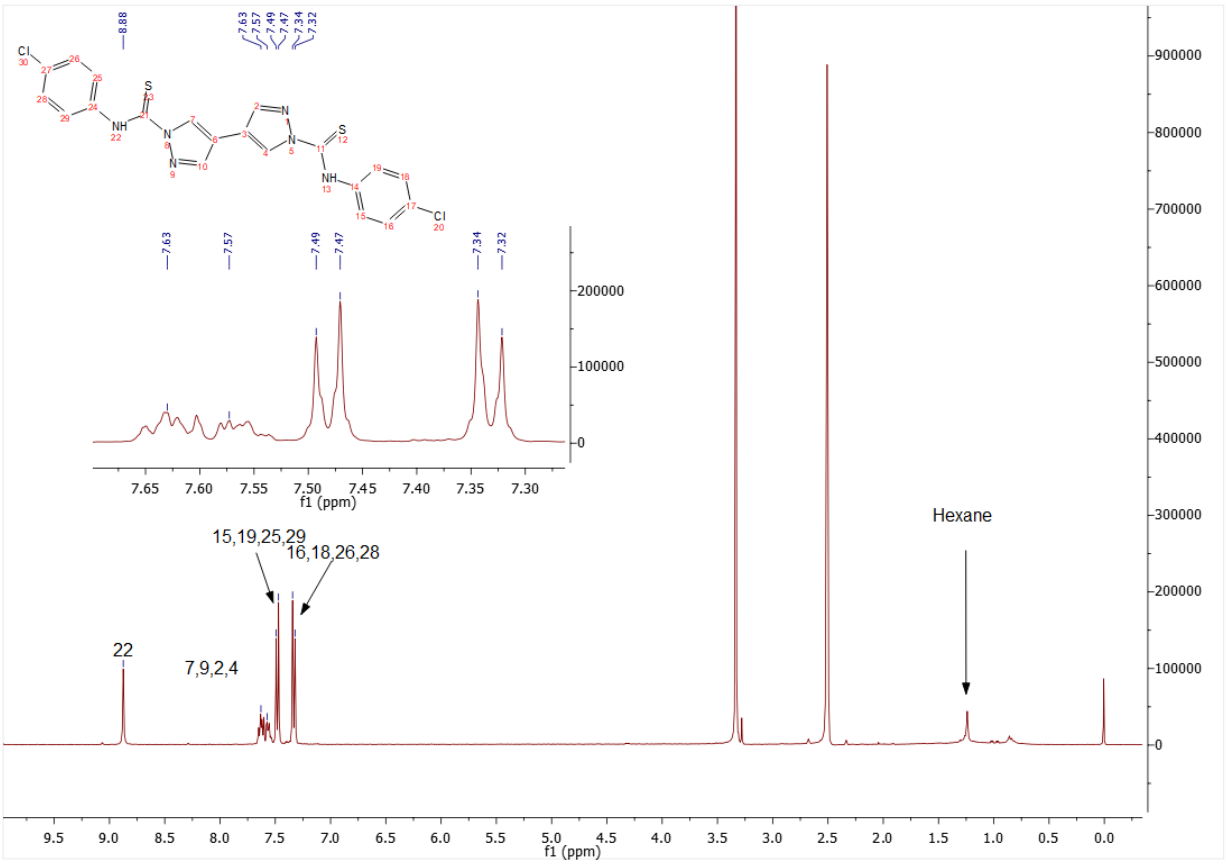

4-bromo-N-(4-chlorophenyl)-1H-pyrazole-1-carbothioamide (52)

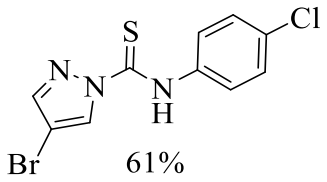

52

148.6 mg (1.01 mmol) of compound **49** dissolved in DMF was charged into a 100 mL round bottom flask and eq. 1 (139 mg) of K_2CO_3 was added to this stirring mixture. 4-chlorophenyl isothiocyanate (177 mg, 1.01 mmol, 1 eq) dissolved in DMF was added to the reaction and stirred overnight at room temperature. The reaction was monitored by TLC (25% EtOAc/hexanes) and visualized under UV light. After reaction completion, potassium carbonate was filtered off and DMF was evaporated under vacuum. The resulting crude product was purified with column chromatography (column was initiated with 10% EtOAC/ hexane system) to obtain off-white product in 61% yield. ^{1}H NMR (600 MHz, DMSO-d_6) δ 12.00 (s, 1H), 8.93 (s, 1H), 8.17 (s, 1H), 7.66 (d, J = 8.7 Hz, 2H), 7.51 (d, J = 8.7 Hz, 2H). ^{13}C NMR (151 MHz, DMSO-d_6) δ 173.89, 144.00, 139.48, 137.40, 132.10, 129.03, 127.89, 98.45.

^{1}H NMR of compound 52

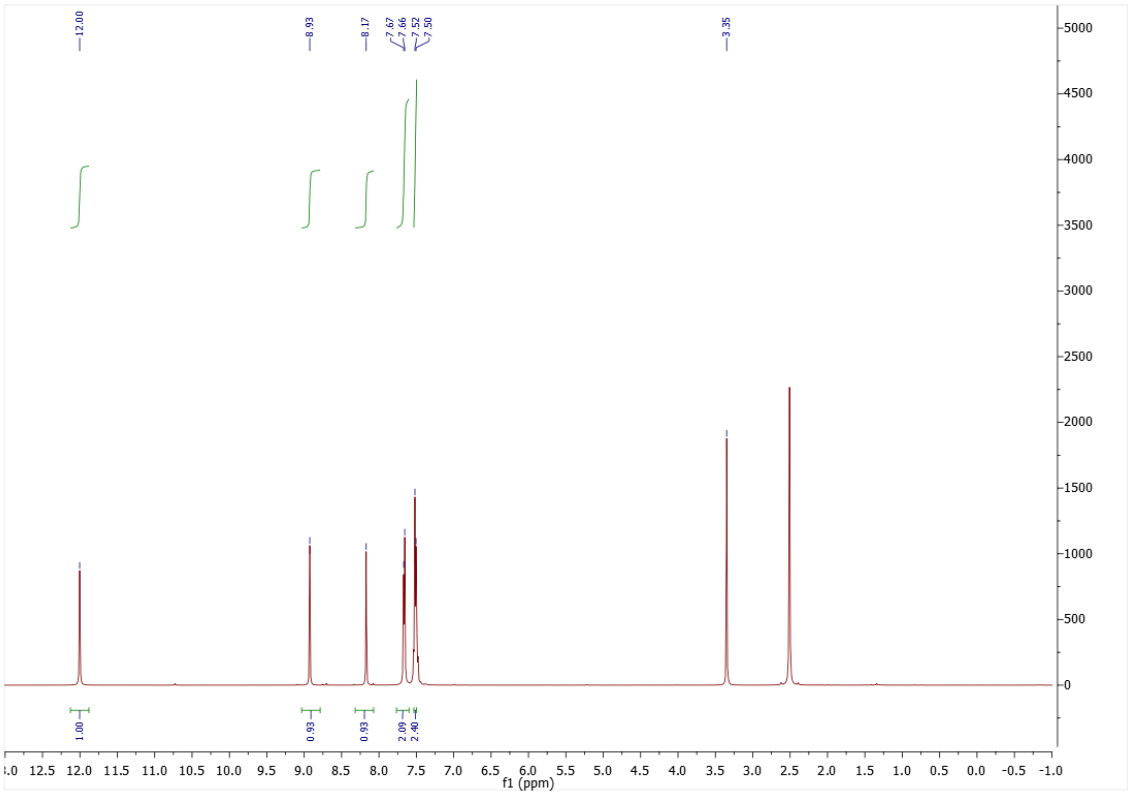

^{13}C NMR of compound 52

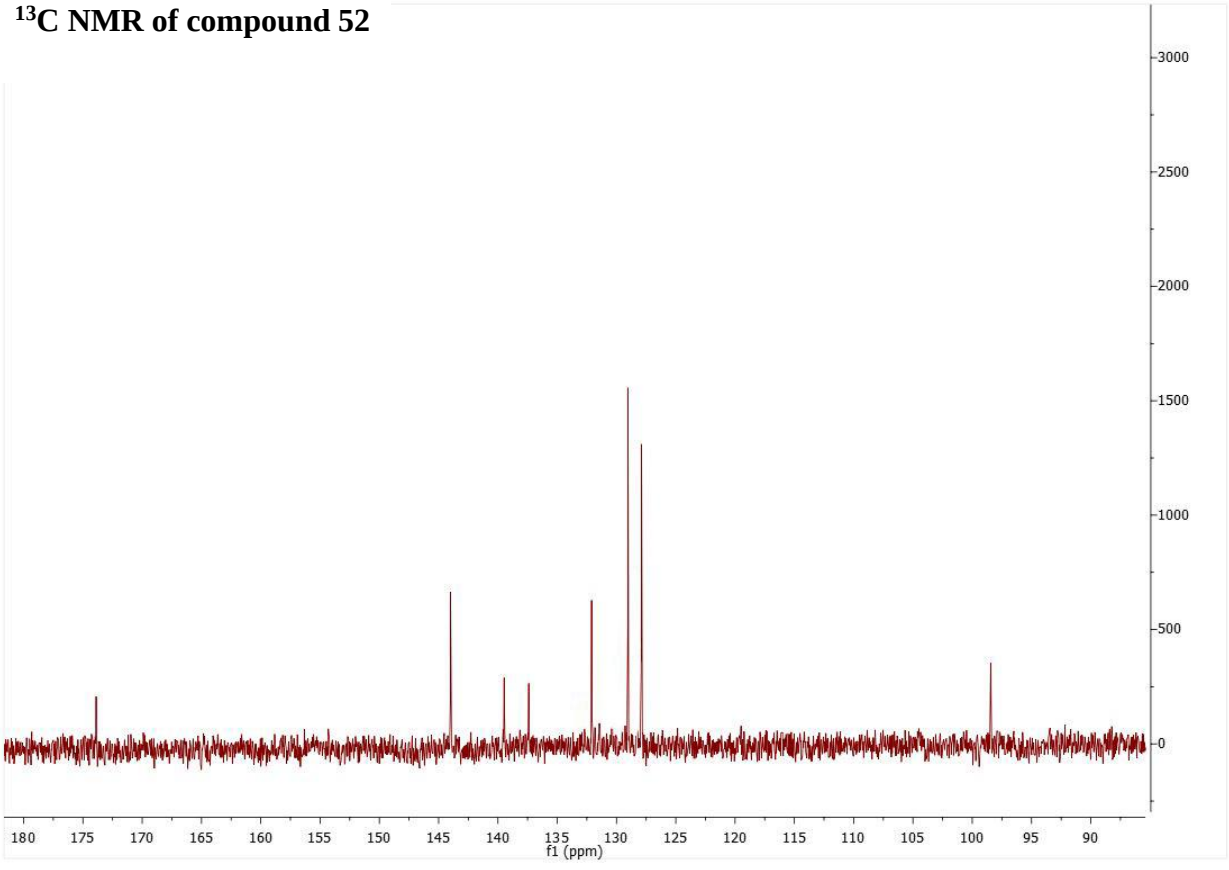

2-isothiocyanato-1,3-dimethylbenzene (53)

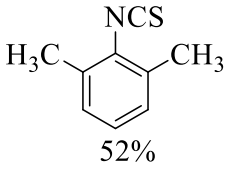

52%

53

2g (16.5 mmol) of 2,6-dimethyl aniline was measured into a 150 mL round bottom flask and was diluted with 10 mL of distilled water. While it was stirring, eq. 2 (4.56 g, 33.0 mmol) of K_2CO_3 was added to the reaction mixture. Then eq. 1.2 (19.8 mmol, 1.51 g) of CS_2 was added dropwise and stirred 4h at room temperature. After 4h, the reaction mixture was cooled down in an ice bath (0-5 ºC) and eq. 0.5 (1.52 g) of TCT was added and stirring continued for additional 30 min. In 30 min, the reaction was basified to pH 11 using 6N NaOH solution. The organic mixture was extracted using DCM (three times) and the combined organic layer was dried over anhydrous sodium sulfate. DCM was evaporated *in vacuum*. TLC was done in 25% EtOAC/ hexane system and spots were visualized under UV. PET ether was used to pack and run the column chromatography to isolate the oily product in 52% yield. ^{1}H NMR (600 MHz, DMSO-d_6) δ 7.14 (m, 3H), 2.29 (s, 6H). ^{13}C NMR (151 MHz, DMSO-d_6) δ 135.13, 129.02, 128.59, 127.89, 18.61. One peak is missing or overlapped in ^{13}C NMR spectrum.

^{1}H NMR of compound 53

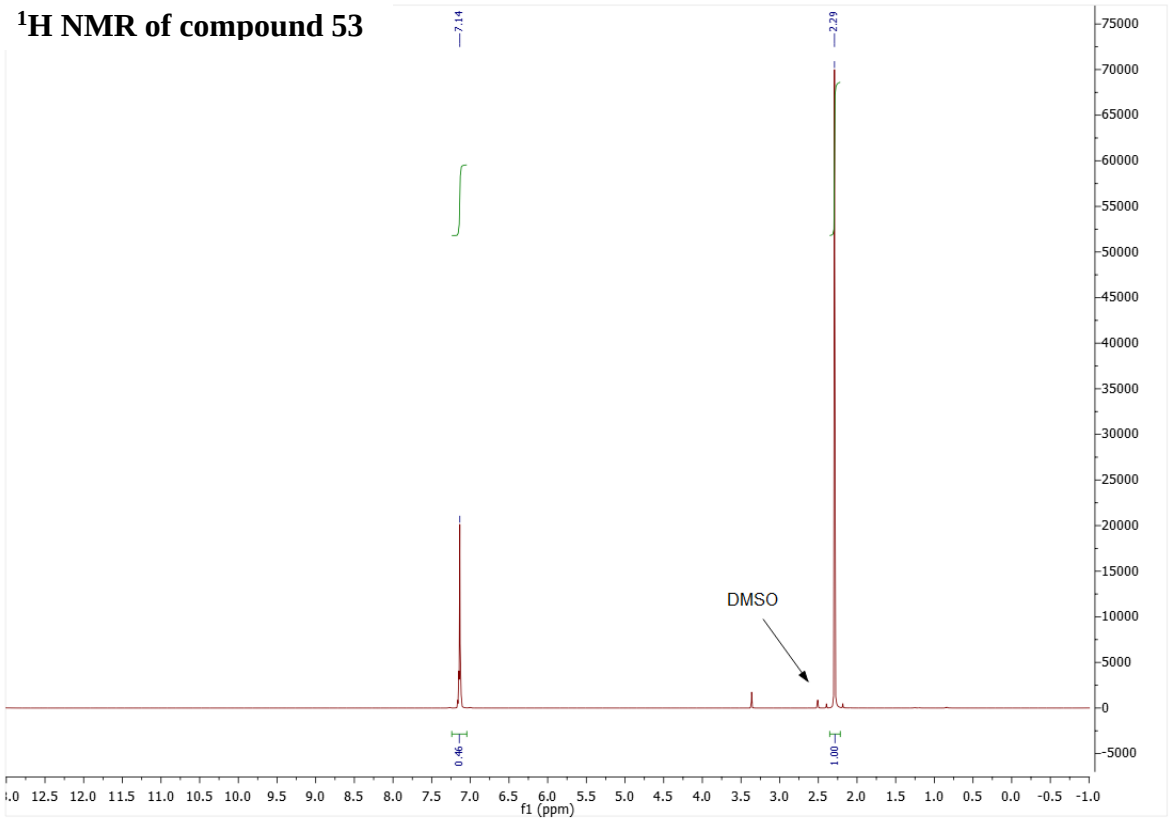

^{13}C NMR of compound 53

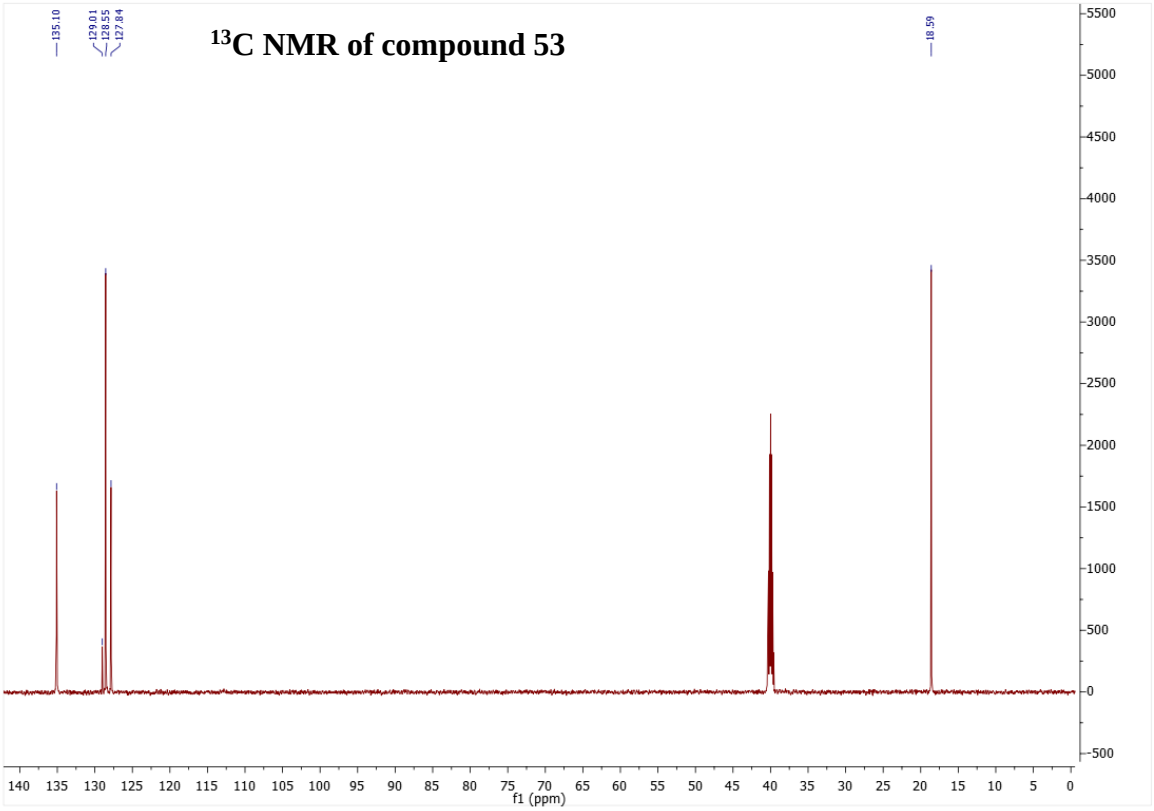

N-(2,6-dimethylphenyl)-1H-pyrazole-1-carbothioamide (54)

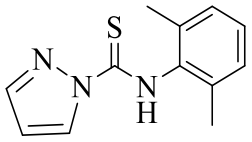

74%

54

126 mg (1.84 mmol) of pyrazole dissolved in DMF was charged into a 100 mL round bottom flask and eq. 1 (254 mg, 1.84 mmol) of K_2CO_3 was added to this stirring mixture. Compound **53** (300 mg, 1.84 mmol, 1 eq) dissolved in DMF was added to the reaction and stirred overnight at room temperature. The reaction was monitored by TLC (50% EtOAc/hexanes) and visualized under UV light. After reaction completion, potassium carbonate was filtered off and DMF in filtrate was evaporated under vacuum. The resulting crude product was purified with column chromatography (5 – 15% EtOAc/ hexane). Obtained pale yellow solid in 74% yield. ^{1}H NMR (600 MHz, DMSO-d_6) δ 11.60 (s, 1H), 8.73 (dd, J = 2.8, 0.8 Hz, 1H), 7.98 (dd, J = 1.7, 0.6 Hz, 1H), 7.18 (d, J = 3.6 Hz, 2H), 7.15 (s, 1H), 6.62 (dd, J = 2.8, 1.6 Hz, 1H), 2.16 (s, 6H). ^{13}C NMR (151 MHz, DMSO-d_6) δ 175.36, 143.99, 135.73, 132.26, 128.64, 128.43, 128.09, 110.15, 18.09.

^{1}H NMR of compound 54

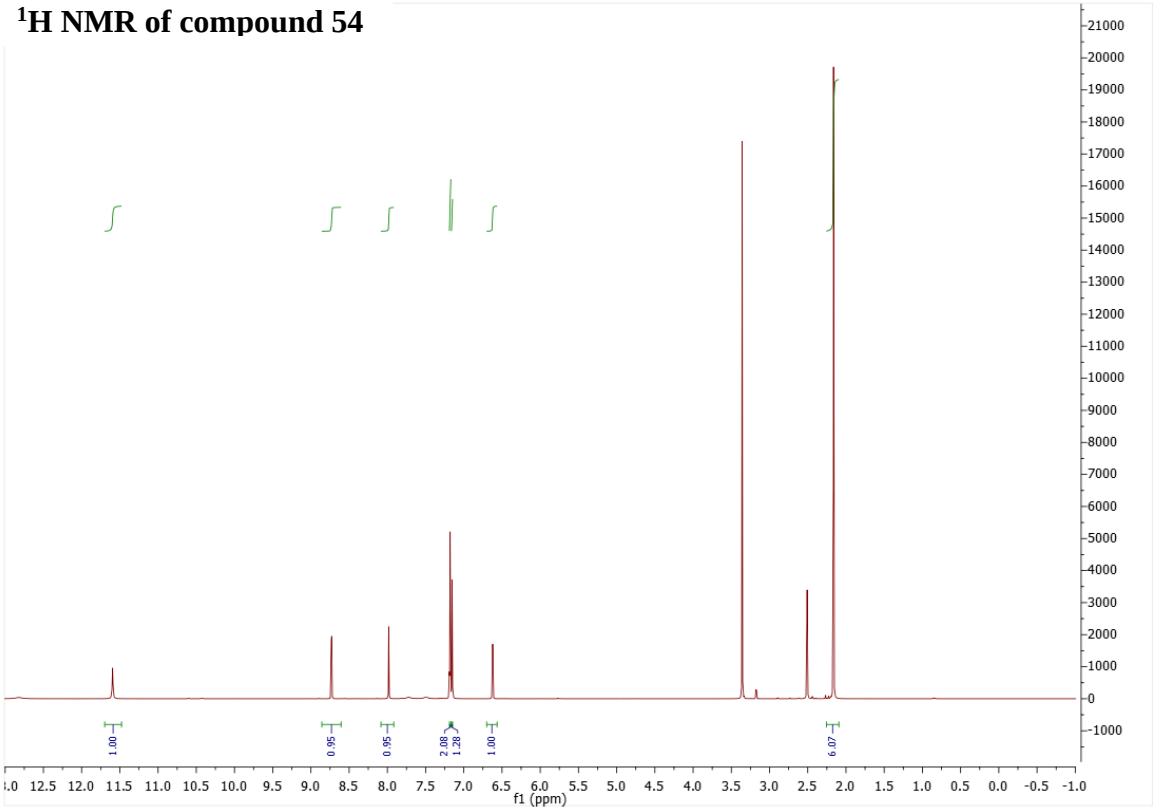

^{13}C NMR of compound 54

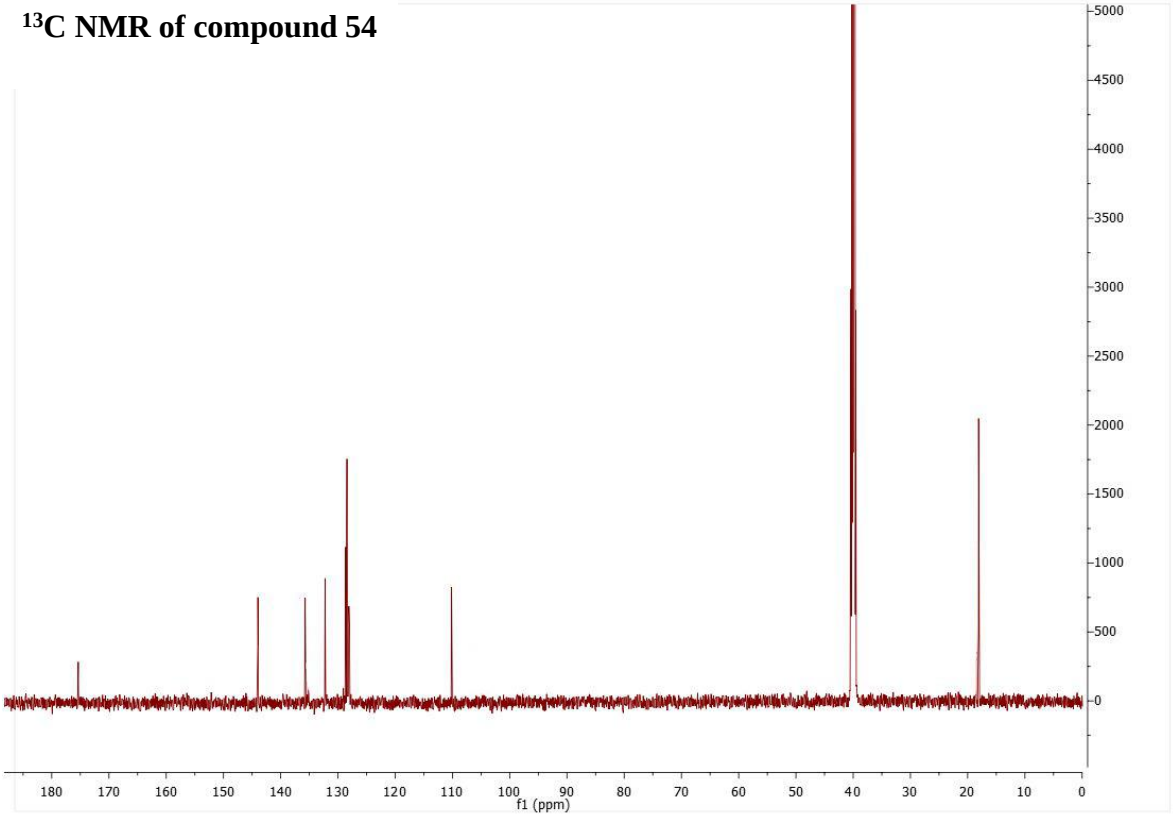

N-(2,6-dimethylphenyl)-3-methyl-1H-pyrazole-1-carbothioamide (55)

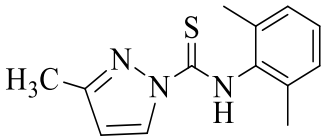

48%

55

143 mg (1.93 mmol) of 3-methyl pyrazole dissolved in DMF was charged into a 100 mL round bottom flask and eq. 1 (266 mg, 1.93 mmol) of K_2CO_3 was added to this stirring mixture. Compound **53** (314 mg, 1.93 mmol, 1 eq) dissolved in DMF was added to the reaction and stirred overnight at room temperature. The reaction was monitored by TLC (25% EtOAc/hexanes) and visualized under UV light. After reaction completion, the potassium carbonate was filtered off and DMF in filtrate was evaporated under vacuum. Resulting crude product was purified with column chromatography (started with 100% hexane and gradually increased the polarity to 15% EtOAc/ hexane) to receive white solid product in 48% yield. ^{1}H NMR (400 MHz, DMSO-d_6) δ 11.42 (s, 1H), 8.62 (d, J = 2.8 Hz, 1H), 7.16 (t, 1H), 7.12 (d, J = 9.0 Hz, 2H), 6.45 (d, J = 2.8 Hz, 1H), 2.33 (s, 3H), 2.15 (s, 6H). ^{13}C NMR (101 MHz, DMSO-d_6) δ 175.21, 153.42, 136.85, 135.78, 132.87, 128.37, 127.97, 110.69, 18.13, 14.16.

^{1}H NMR of compound 55

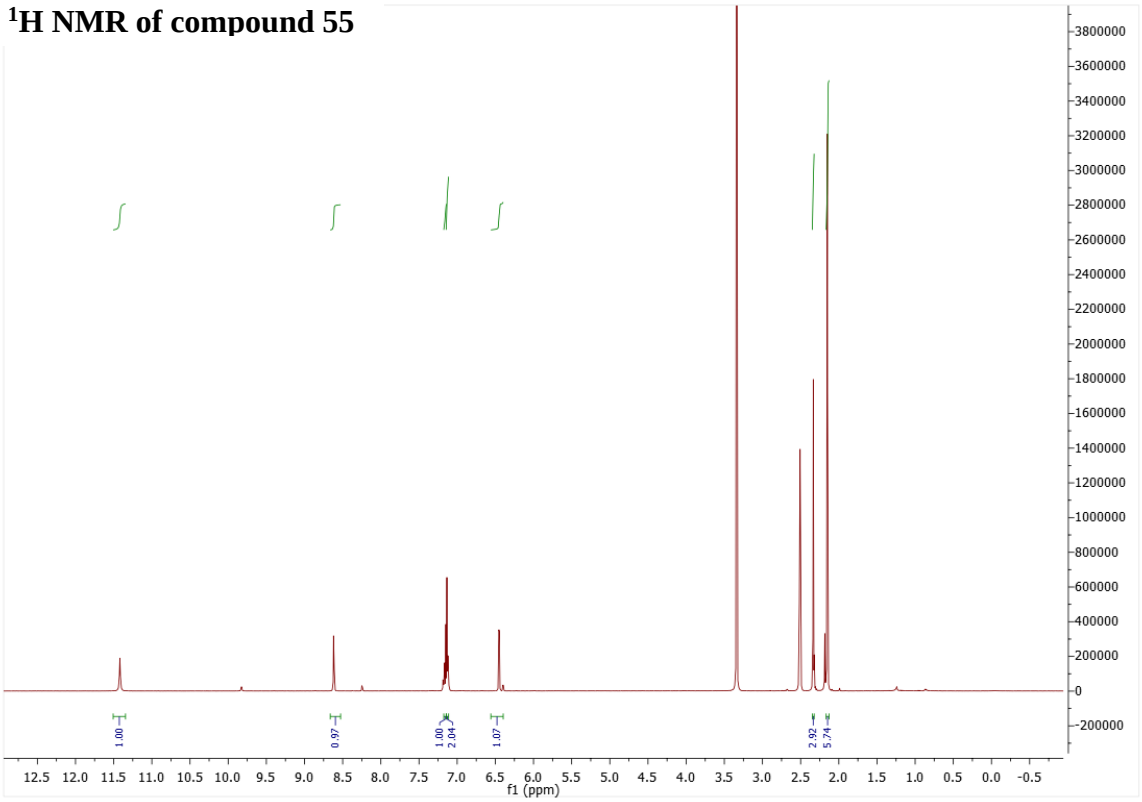

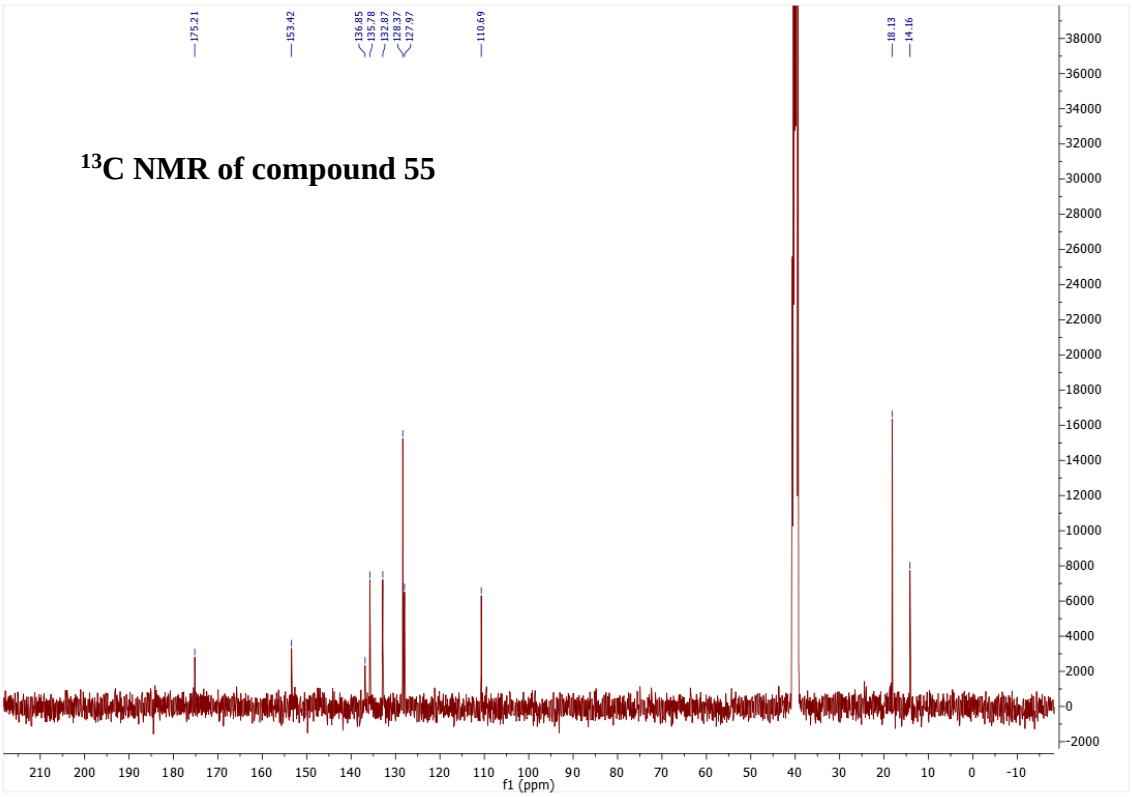

^{13}C NMR of compound 55

4-bromo-N-(2,6-dimethylphenyl)-1H-pyrazole-1-carbothioamide (56)

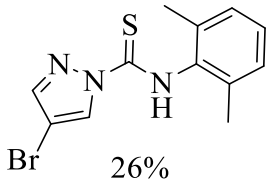

26%

56

200 mg (1.36 mmol) of 4-bromo pyrazole dissolved in DMF was charged into a 100 mL round bottom flask and eq. 1 (188 mg, 1.36 mmol) of K_2CO_3 was added to this stirring mixture. Compound **53** (222 mg, 1.36 mmol, 1 eq) dissolved in DMF was added to the reaction and stirred overnight at room temperature. The reaction was monitored by TLC (25% EtOAc/hexanes) and visualized under UV light. After reaction completion, the potassium carbonate was filtered off and DMF in filtrate was evaporated under vacuum. Resulting crude product was purified with column chromatography (started with 100% hexane) to receive off white solid product in 26% yield. ^{1}H NMR (400 MHz, DMSO-d_6) δ 11.66 (s, 1H), 8.89 (s, 1H), 8.14 (s, 1H), 7.17 (m, 3H), 2.15 (s, 6H). ^{13}C NMR (101 MHz, DMSO-d_6) δ 174.31, 144.11, 136.46, 135.68, 131.93, 128.49, 128.26, 98.08, 18.00.

^{1}H NMR of compound 56

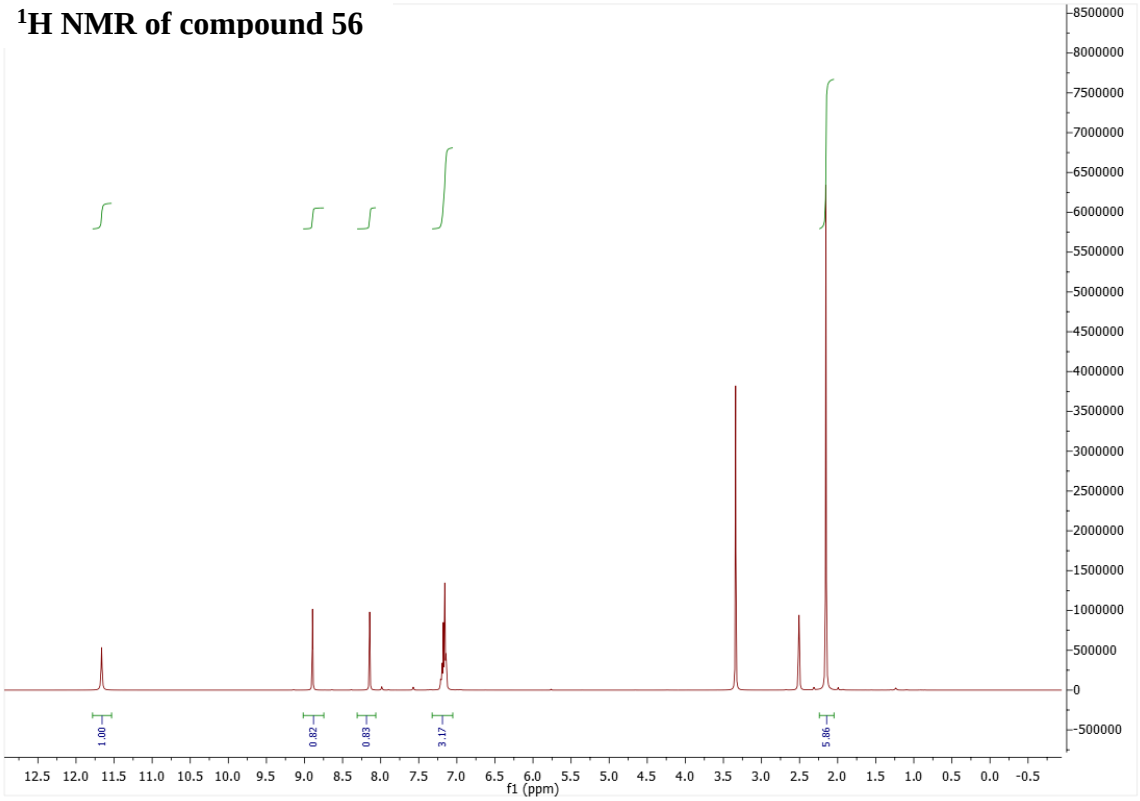

^{13}C NMR of compound 56

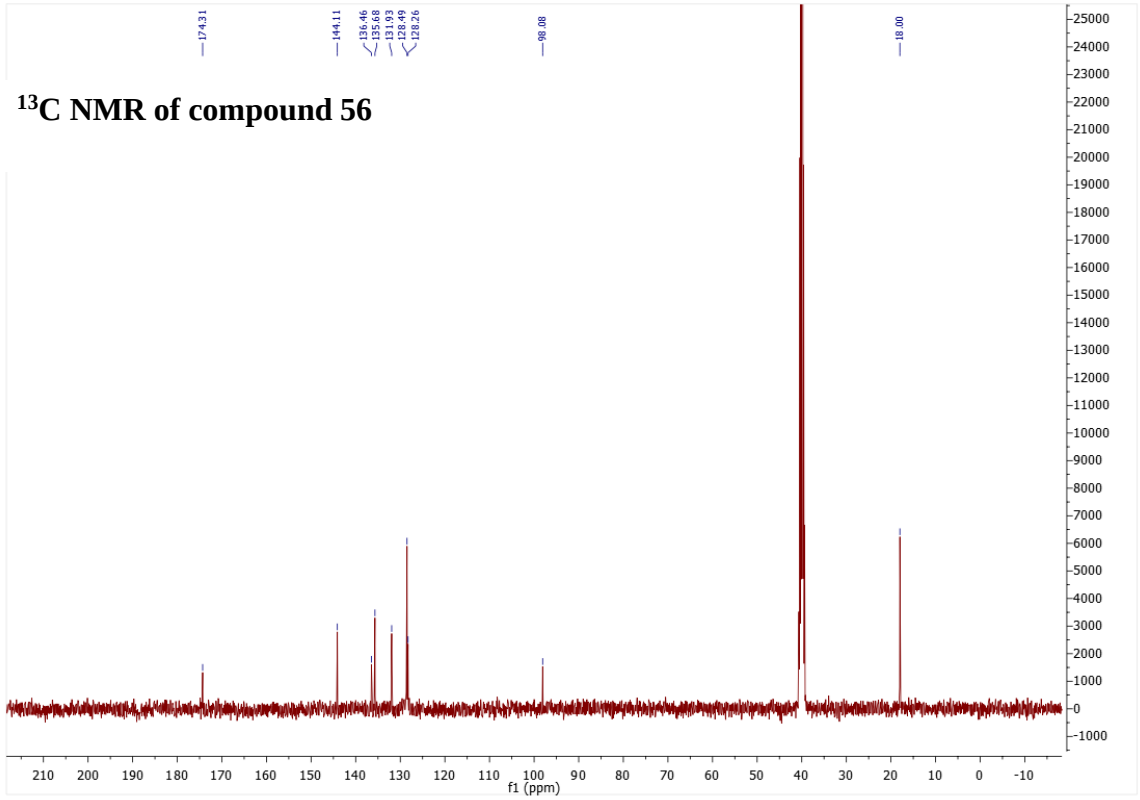

3-(benzyloxy)-N-(2,6-dimethylphenyl)-1H-pyrazole-1-carbothioamide (57)

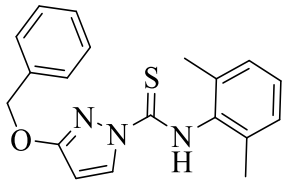

42%

57

174.8 mg (1.00 mmol) of 4-bromo pyrazole dissolved in DMF was charged into a 100 mL round bottom flask and eq. 1 (138.8 mg, 1.00 mmol) of K_2CO_3 was added to this stirring mixture. Compound **53** (164 mg, 1.00 mmol, 1 eq) dissolved in DMF was added to the reaction and stirred overnight at room temperature. The reaction was monitored by TLC (15% EtOAc/hexanes) and visualized under UV light. After reaction completion, the potassium carbonate was filtered off and DMF in filtrate was evaporated under vacuum. Resulting crude product was purified with column chromatography (started with 100% hexane) to receive off white solid product in 42% yield. ^{1}H NMR (600 MHz, Chloroform-*d*) δ 9.73 (s, 1H), 8.61 (d, *J* = 3.0 Hz, 1H), 7.549 (m, 2H), 7.43 (m, 2H), 7.39 (m, 1H), 7.25 (dd, *J* = 8.3, 6.7 Hz, 1H), 7.19 (d, *J* = 7.8 Hz, 2H), 6.06 (d, *J* = 3.0 Hz, 1H), 5.32 (d, *J* = 1.2 Hz, 2H), 2.32 (s, 6H). ^{13}C NMR (151 MHz, Chloroform-*d*) δ 174.93, 164.94, 136.19, 135.95, 134.62, 133.13, 128.65, 128.41, 128.09, 98.92, 71.24, 53.47, 18.28.

^{1}H NMR of compound 57

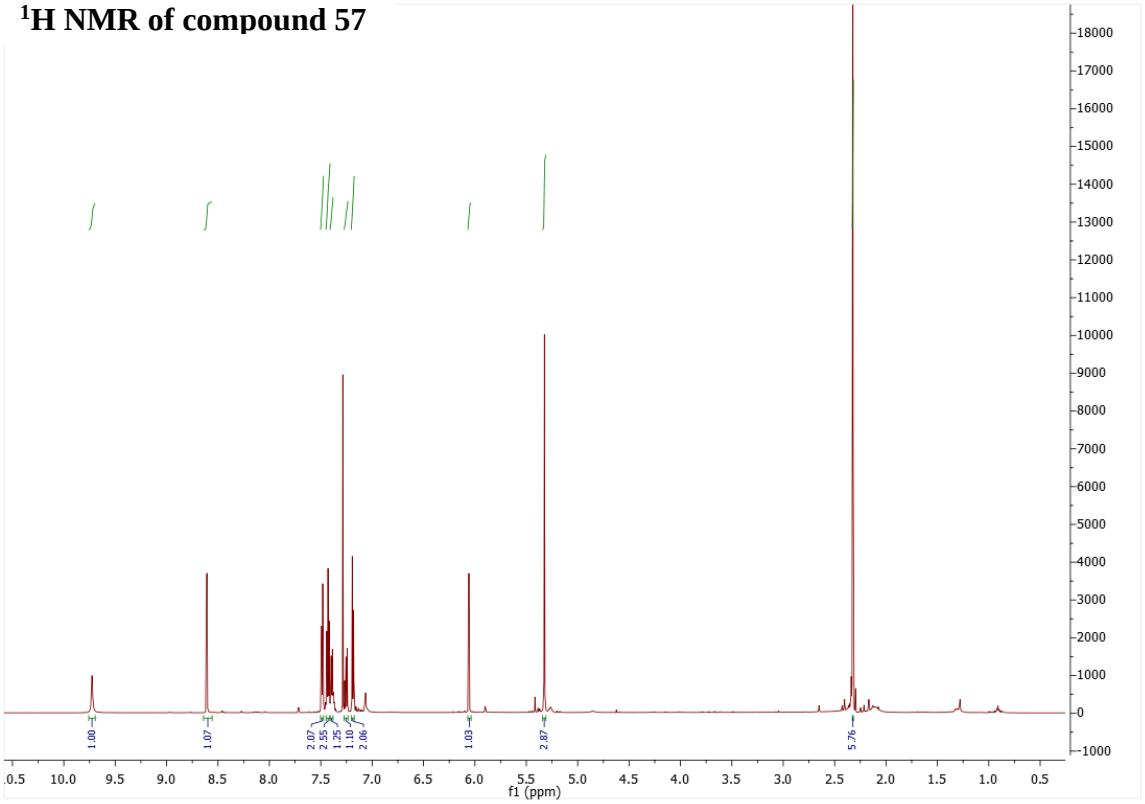

^{13}C NMR of compound 57

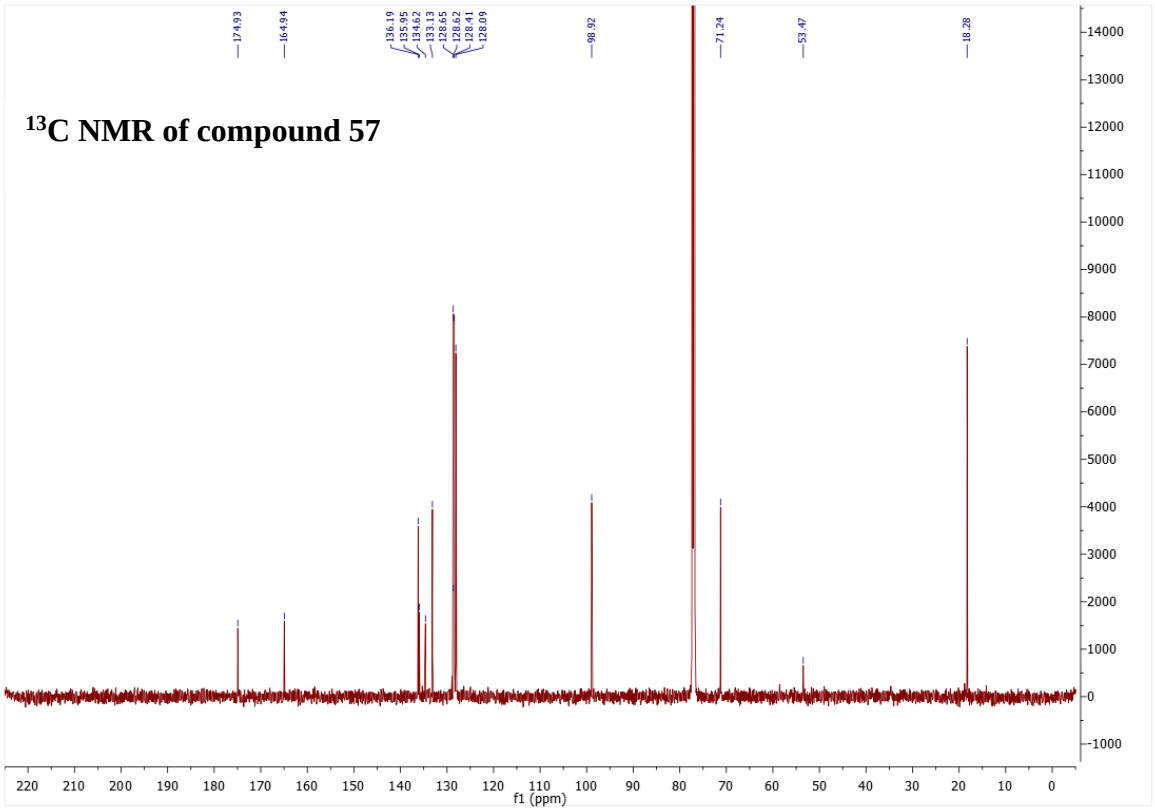

Appendix A - MIC Measurements

Activity of the Newly Synthesized Pyrazolyl-Thioureas and -Carbothioamides Against a MRSA Clinical Isolate

NNSN compounds were tested against both *Staphylococcus aureus* strain Newman, a clinical isolate[232] and *S. aureus* strain Lac, a USA300 typed MRSA clinical isolate, as previously described.[115, 135]

MIC testing was performed in the group of Prof. Dr. Frank Wolschendorf and since 2018 in the group of Prof. Dr. Olaf Kutsch in the Departments of Medicine and Microbiology at the University of Alabama at Birmingham. The testing conditions were designed to mimic the chemical conditions in activated phagosomes (50 μM of copper I under reductive conditions. As described below Cu(II)SO_4 will be immediately reduced to Cu(I) under these conditions. The former is used because it is much easier to handle when setting up biological assays).

The procedure for MIC testing is described in detail in reference.[134] It is quoted verbatim below:

Determination of minimum inhibitory concentration (MIC)

"For the assays, compounds and the indicated metals salts were mixed in RPMI medium without phenol red (Corning) and then distributed or further diluted in 96-well plates to reach final concentrations as indicated. Metal concentrations and BCS were kept constant from well to well, at 50 μM, while compound concentrations in DMSO were titrated in 2-fold increments down from 10 mM unless indicated otherwise.

Bacteria harvested from exponentially growing cultures were first washed and diluted in RPMI and then distributed to each well for a final assay OD_{600} of 0.005 (~ 5 x 10^6 cells per ml). Sterility

controls and no compound controls containing either only media or media supplemented with 50 μM $CuSO_4$ x 6 H_2O (Acros) were present on each challenge plate. Plates were sealed with parafilm or placed in a sealed plastic bag to reduce evaporation and edge effects and kept at 37 ^oC overnight after which OD_{600} readings were taken on a plate reader (Cytation 3, BioTek). Values were blank subtracted and normalized to the appropriate no drug controls. MIC was defined as the lowest concentration at which growth was reduced by at least 90% in comparison to the untreated controls." (quoted verbatim from reference 106) MIC was determined by addition of resazurin, a metabolic indicator, using 10% conversion of a blank subtracted and normalized value as the cutoff.

The wavelength of λ=600 nm was selected for these assays because the light scattering from growing Staphylococcus Aureus cultures can be detected there. Note that $CuSO_4$ and $CuCl_2$ boosted the activity of selected NNSN compounds in an identical manner. The presence copper was ascertained by complexation with bathocuproine disulfonic acid and monitored by measuring the absorption at 480 nm immediately after dissolution. Cu(II) salts were use here, because they dissolve much better in RPMI medium and can be utilized in an oxygenated atmosphere. It is noteworthy that RPMI medium contains up to 2 percent of gluthatione. The standard potential E_0 of the glutathione redox couple is −264 mV for pH 7.4, based on a value of −240 mV for pH 7.0 and a pH effect of −59 mV/pH unit. This means that Cu(II) is reduced to the Cu(I)-glutathione complex within approx. 1h after mixing. Cu(I) remains bioavailable as glutathione complex.[178] Staining of isolated S. Aureus bacteria with bathocuproine disulfonic acid failed, because there is no copper(II) in the bacteria.

As shown in the Figures below, both S. A. Newman and S. A. Lac grow in RPMI medium in the absence and presence of 50μM of $CuSO_4$ x 6 H_2O.

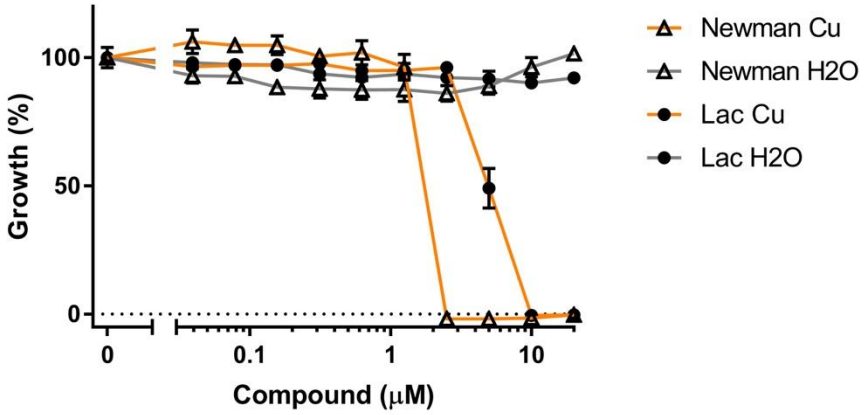

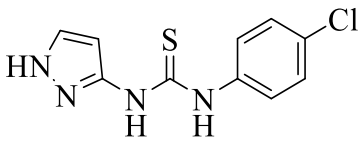

15

Figure A.1 Dose response curves were determined by diluting 1-(4-chlorophenyl)-3-(1H-pyrazol-3-yl)thiourea **15** in RPMI medium with or without 50μM copper sulfate. A logarithmic phase culture of *S. aureus* grown in Mueller Hinton broth was washed in RPMI, then diluted in fresh RPMI and added to plates for a final optical density of 0.005. The plates were incubated overnight at 37ºC. Metabolic activity was determined by adding resazurin using 10% conversion of a blank subtracted and normalized value as the cutoff.

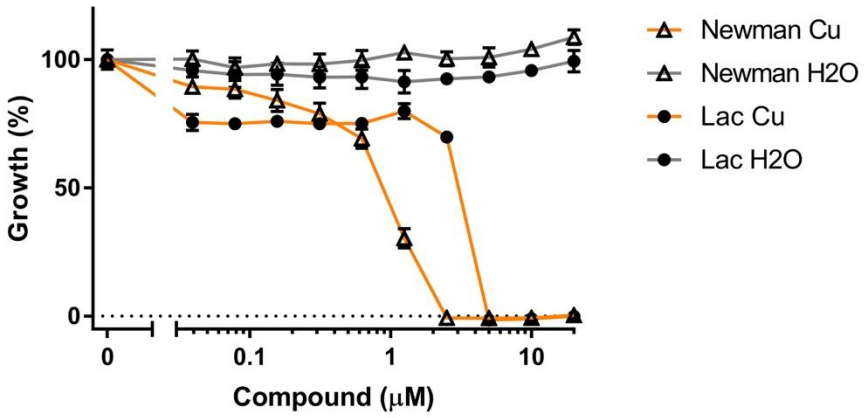

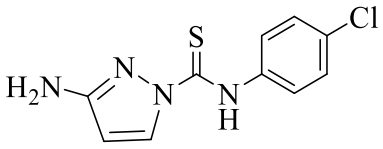

16

Figure A.2 Dose response curves were determined by diluting 3-amino-N-(4-chlorophenyl)-1H-pyrazole-1-carbothioamide **16** in RPMI medium with or without 50μM copper sulfate. A logarithmic phase culture of *S. aureus* grown in Mueller Hinton broth was washed in RPMI, then diluted in fresh RPMI and added to plates for a final optical density of 0.005. The plates were incubated overnight at 37 ºC. Metabolic activity was determined by adding resazurin using 10% conversion of a blank subtracted and normalized value as the cutoff.

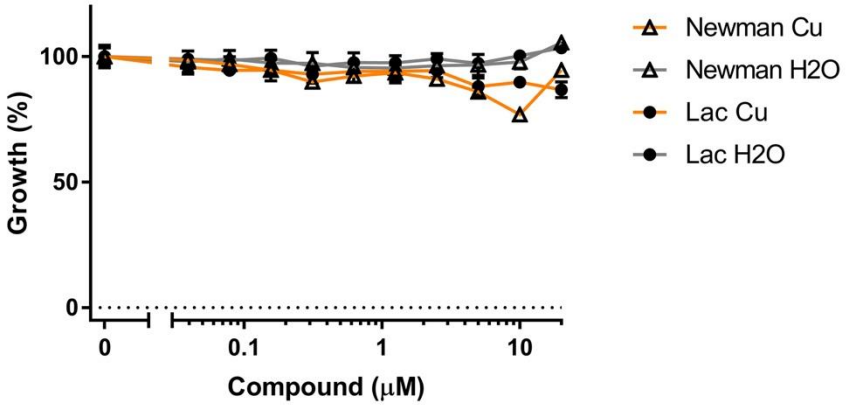

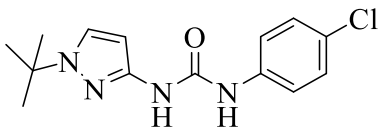

17

Figure A.3 Dose response curves were determined by diluting 1-(1-(tert-butyl)-1H-pyrazol-3-yl)-3-(4-chlorophenyl)urea **17** in RPMI medium with or without 50μM copper sulfate. A logarithmic phase culture of *S. aureus* grown in Mueller Hinton broth was washed in RPMI, then diluted in fresh RPMI and added to plates for a final optical density of 0.005. The plates were incubated overnight at 37 ºC. Metabolic activity was determined by adding resazurin using 10% conversion of a blank subtracted and normalized value as the cutoff.

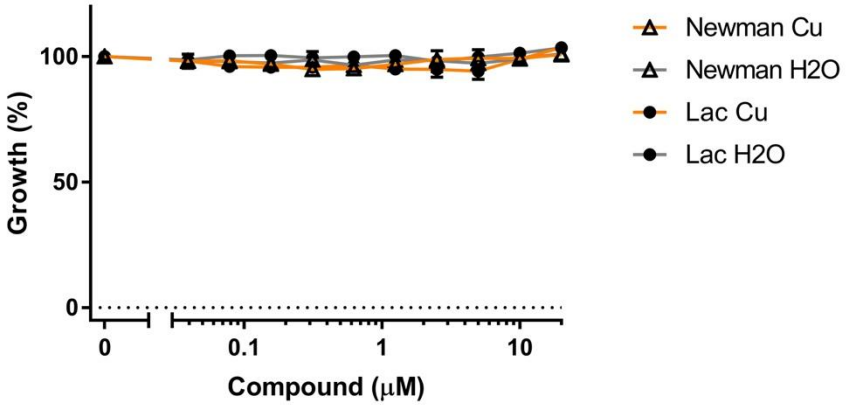

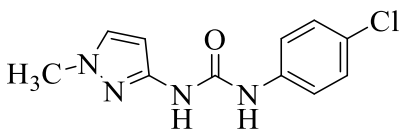

18

Figure A.4 Dose response curves were determined by diluting 1-(4-chlorophenyl)-3-(1-methyl-1H-pyrazol-3-yl) **18** in RPMI medium with or without 50μM copper sulfate. A logarithmic phase culture of *S. aureus* grown in Mueller Hinton broth was washed in RPMI, then diluted in fresh RPMI and added to plates for a final optical density of 0.005. The plates were incubated overnight at 37 ºC. Metabolic activity was determined by adding resazurin using 10% conversion of a blank subtracted and normalized value as the cutoff.

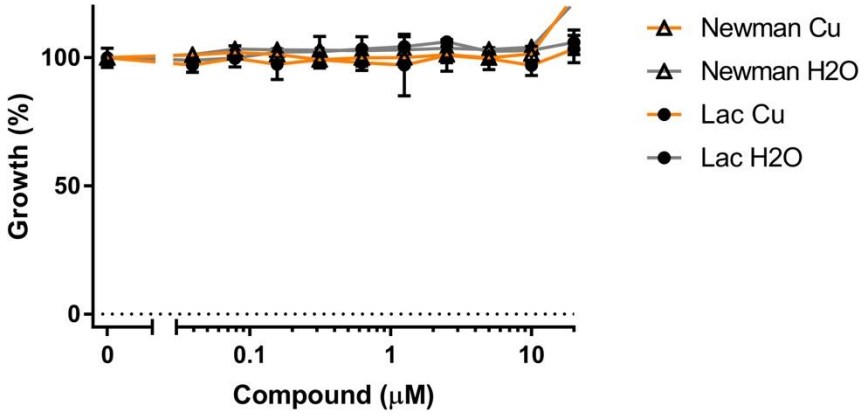

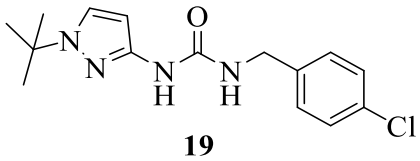

19

Figure A.5 Dose response curves were determined by diluting 1-(1-(tert-butyl)-1H-pyrazol-3-yl)-3-(4-chlorobenzyl)urea **19** in RPMI medium with or without 50μM copper sulfate. A logarithmic phase culture of *S. aureus* grown in Mueller Hinton broth was washed in RPMI, then diluted in fresh RPMI and added to plates for a final optical density of 0.005. The plates were incubated overnight at 37 ºC. Metabolic activity was determined by adding resazurin using 10% conversion of a blank subtracted and normalized value as the cutoff.

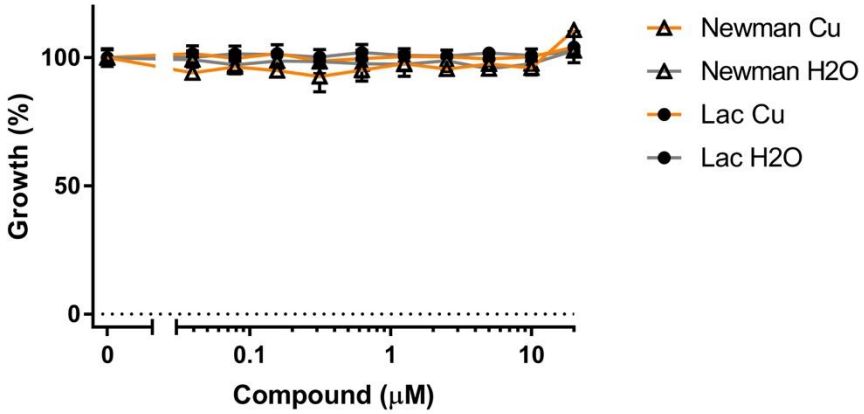

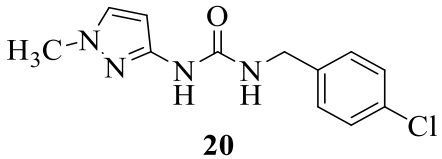

20

Figure A.6 Dose response curves were determined by diluting 1-(4-chlorobenzyl)-3-(1-methyl-1H-pyrazol-3-yl)urea **20** in RPMI medium with or without 50μM copper sulfate. A logarithmic phase culture of *S. aureus* grown in Mueller Hinton broth was washed in RPMI, then diluted in fresh RPMI and added to plates for a final optical density of 0.005. The plates were incubated overnight at 37 ºC. Metabolic activity was determined by adding resazurin using 10% conversion of a blank subtracted and normalized value as the cutoff.

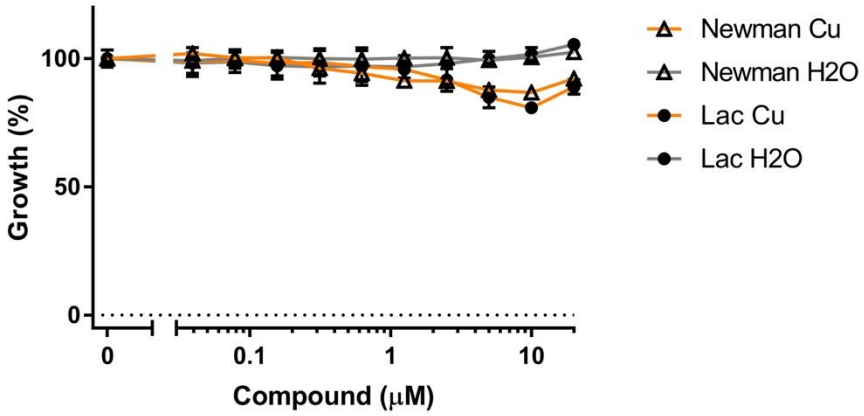

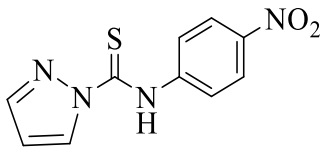

21

Figure A.7 Dose response curves were determined by diluting N-(4-nitrophenyl)-1H-pyrazole-1-carbothioamide **21** in RPMI medium with or without 50μM copper sulfate. A logarithmic phase culture of *S. aureus* grown in Mueller Hinton broth was washed in RPMI, then diluted in fresh RPMI and added to plates for a final optical density of 0.005. The plates were incubated overnight at 37 ºC. Metabolic activity was determined by adding resazurin using 10% conversion of a blank subtracted and normalized value as the cutoff.

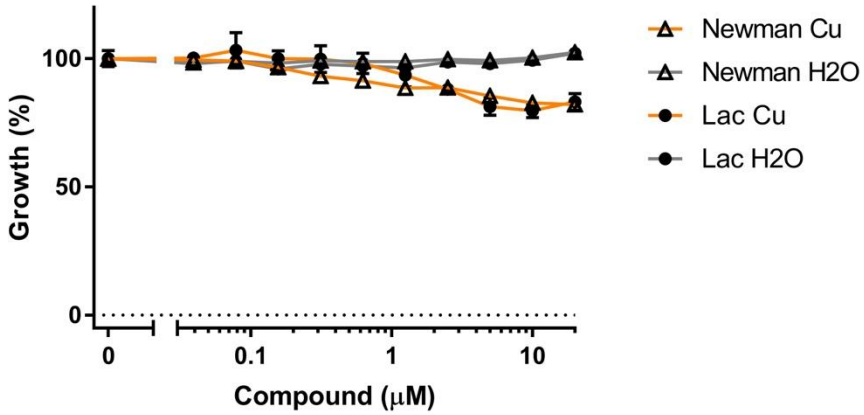

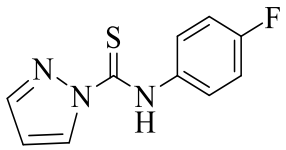

22

Figure A.8 Dose response curves were determined by diluting N-(4-fluorophenyl)-1H-pyrazole-1-carbothioamide **22** in RPMI medium with or without 50µM copper sulfate. A logarithmic phase culture of *S. aureus* grown in Mueller Hinton broth was washed in RPMI, then diluted in fresh RPMI and added to plates for a final optical density of 0.005. The plates were incubated overnight at 37 ºC. Metabolic activity was determined by adding resazurin using 10% conversion of a blank subtracted and normalized value as the cutoff.

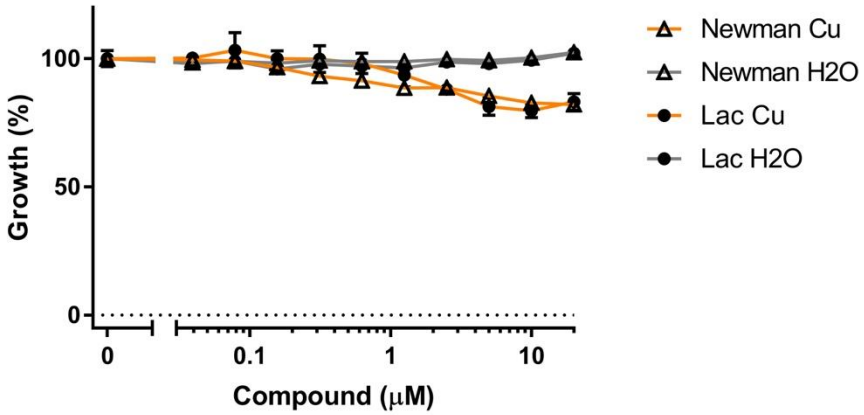

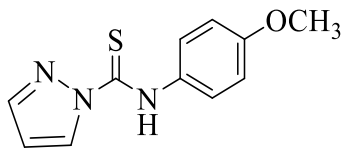

25

Figure A.9 Dose response curves were determined by diluting N-(4-methoxyphenyl)-1H-pyrazole-1-carbothioamide **25** in RPMI medium with or without 50μM copper sulfate. A logarithmic phase culture of *S. aureus* grown in Mueller Hinton broth was washed in RPMI, then diluted in fresh RPMI and added to plates for a final optical density of 0.005. The plates were incubated overnight at 37 ºC. Metabolic activity was determined by adding resazurin using 10% conversion of a blank subtracted and normalized value as the cutoff.

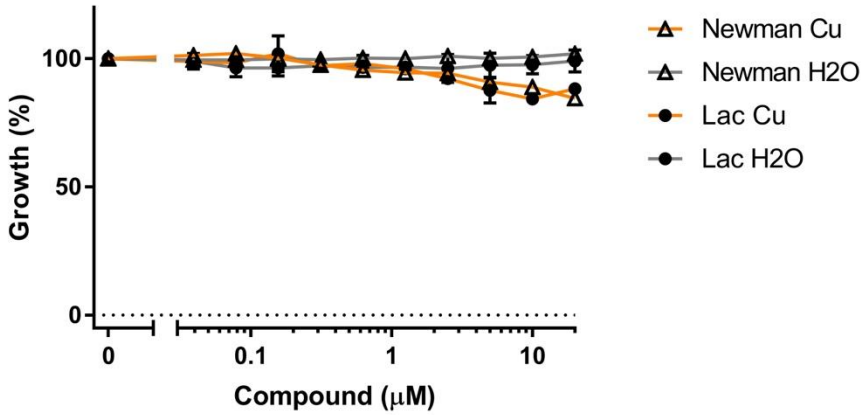

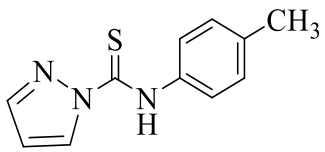

26

Figure A.10 Dose response curves were determined by diluting N-(p-tolyl)-1H-pyrazole-1-carbothioamide **26** in RPMI medium with or without 50μM copper sulfate. A logarithmic phase culture of *S. aureus* grown in Mueller Hinton broth was washed in RPMI, then diluted in fresh RPMI and added to plates for a final optical density of 0.005. The plates were incubated overnight at 37 ºC. Metabolic activity was determined by adding resazurin using 10% conversion of a blank subtracted and normalized value as the cutoff.

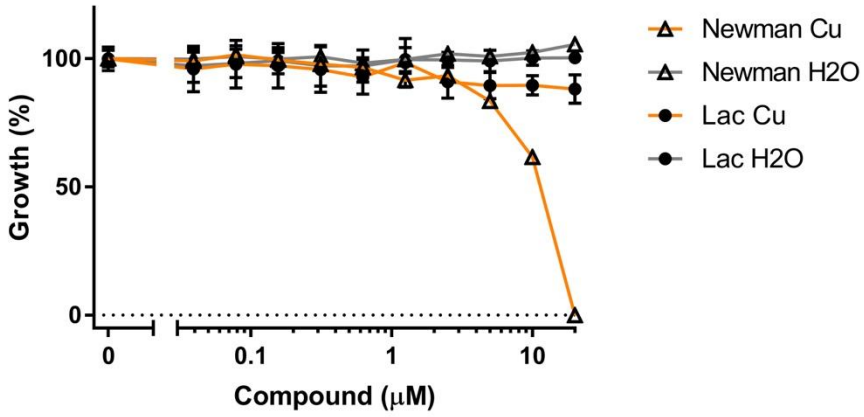

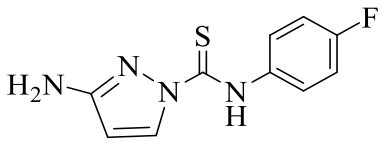

28

Figure A.11 Dose response curves were determined by diluting 3-amino-N-(4-fluorophenyl)-1H-pyrazole-1-carbothioamide **28** in RPMI medium with or without 50μM copper sulfate. A logarithmic phase culture of *S. aureus* grown in Mueller Hinton broth was washed in RPMI, then diluted in fresh RPMI and added to plates for a final optical density of 0.005. The plates were incubated overnight at 37 ºC. Metabolic activity was determined by adding resazurin using 10% conversion of a blank subtracted and normalized value as the cutoff.

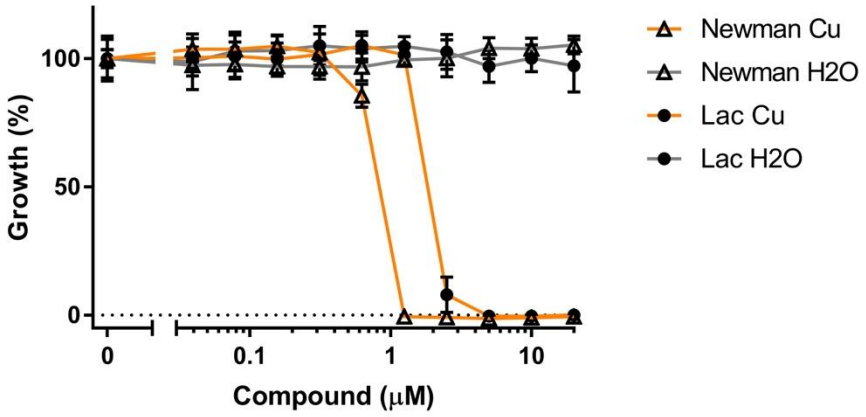

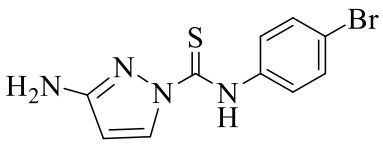

29

Figure A.12 Dose response curves were determined by diluting 3-amino-N-(4-bromophenyl)-1H-pyrazole-1-carbothioamide **29** in RPMI medium with or without 50μM copper sulfate. A logarithmic phase culture of *S. aureus* grown in Mueller Hinton broth was washed in RPMI, then diluted in fresh RPMI and added to plates for a final optical density of 0.005. The plates were incubated overnight at 37 ºC. Metabolic activity was determined by adding resazurin using 10% conversion of a blank subtracted and normalized value as the cutoff.

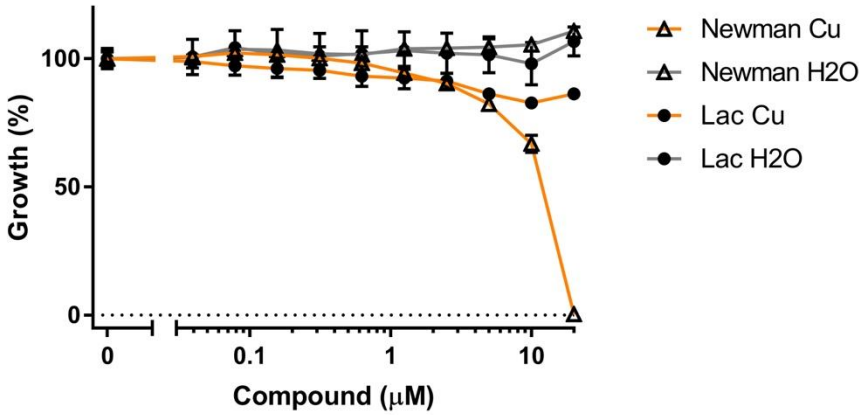

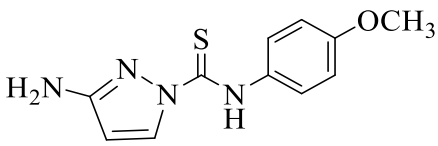

30

Figure A.13 Dose response curves were determined by diluting 3-amino-N-(4-methoxyphenyl)-1H-pyrazole-1-carbothioamide **30** in RPMI medium with or without 50μM copper sulfate. A logarithmic phase culture of *S. aureus* grown in Mueller Hinton broth was washed in RPMI, then diluted in fresh RPMI and added to plates for a final optical density of 0.005. The plates were incubated overnight at 37 ºC. Metabolic activity was determined by adding resazurin using 10% conversion of a blank subtracted and normalized value as the cutoff.

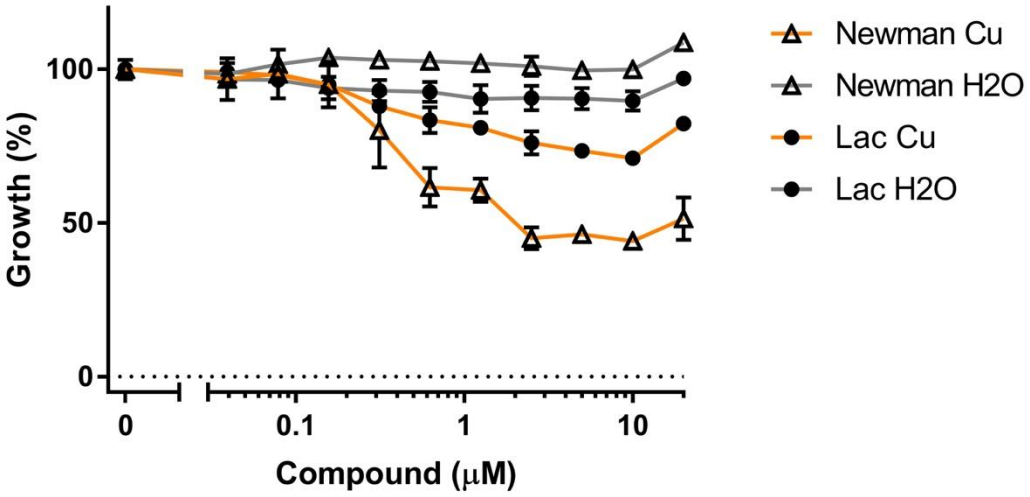

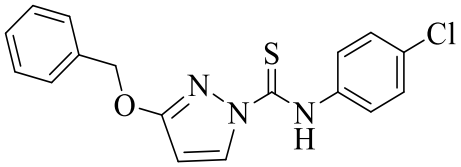

45

Figure A.14 Dose response curves were determined by diluting 3-(benzyloxy)-N-(4-chlorophenyl)-1H-pyrazole-1-carbothioamide **45** in RPMI medium with or without 50μM copper sulfate. A logarithmic phase culture of *S. aureus* grown in Mueller Hinton broth was washed in RPMI, then diluted in fresh RPMI and added to plates for a final optical density of 0.005. The plates were incubated overnight at 37 ºC. Metabolic activity was determined by adding resazurin using 10% conversion of a blank subtracted and normalized value as the cutoff.

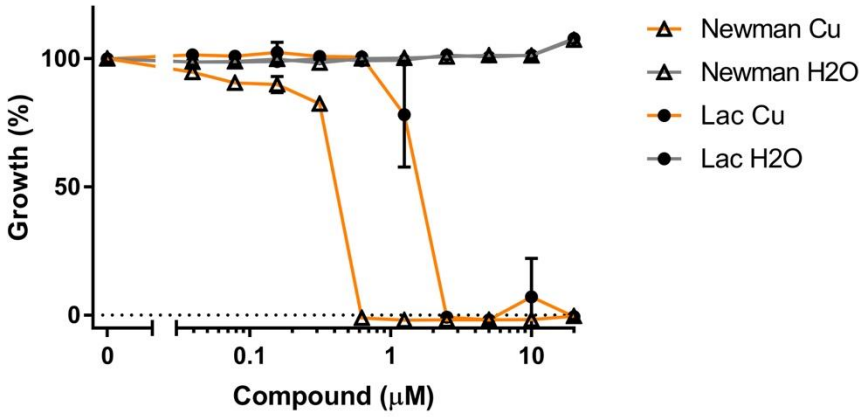

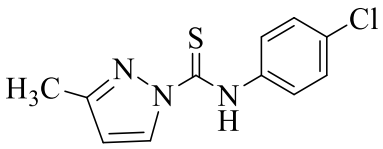

46

Figure A.15 Dose response curves were determined by diluting N-(4-chlorophenyl)-3-methyl-1H-pyrazole-1-carbothioamide **46** in RPMI medium with or without 50μM copper sulfate. A logarithmic phase culture of *S. aureus* grown in Mueller Hinton broth was washed in RPMI, then diluted in fresh RPMI and added to plates for a final optical density of 0.005. The plates were incubated overnight at 37 ºC. Metabolic activity was determined by adding resazurin using 10% conversion of a blank subtracted and normalized value as the cutoff.

A.1 Proposed mechanistic discussion for the reaction between substituted hydrazine and 2-chloroacrylonitrile.

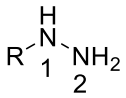

Figure A.16 Generic structure of the substituted hydrazine.

Both the nitrogen atoms show α-effect nucleophilicity[233] but the presence of an electron donating group (R group) can enhance the nucleophilicity of nitrogen 1 by inductively compared to nitrogen 2 (Fig A.16). Therefore, in hydrazine, nitrogen 1 possesses enhanced nucleophilicity. Another important factor is using of additional bases (in real experiment, $NaHCO_3$ and K_2CO_3 were used as basic additives)[188] tends to facilitate nucleophilic attack from the substituted amine of the hydrazine.[234]

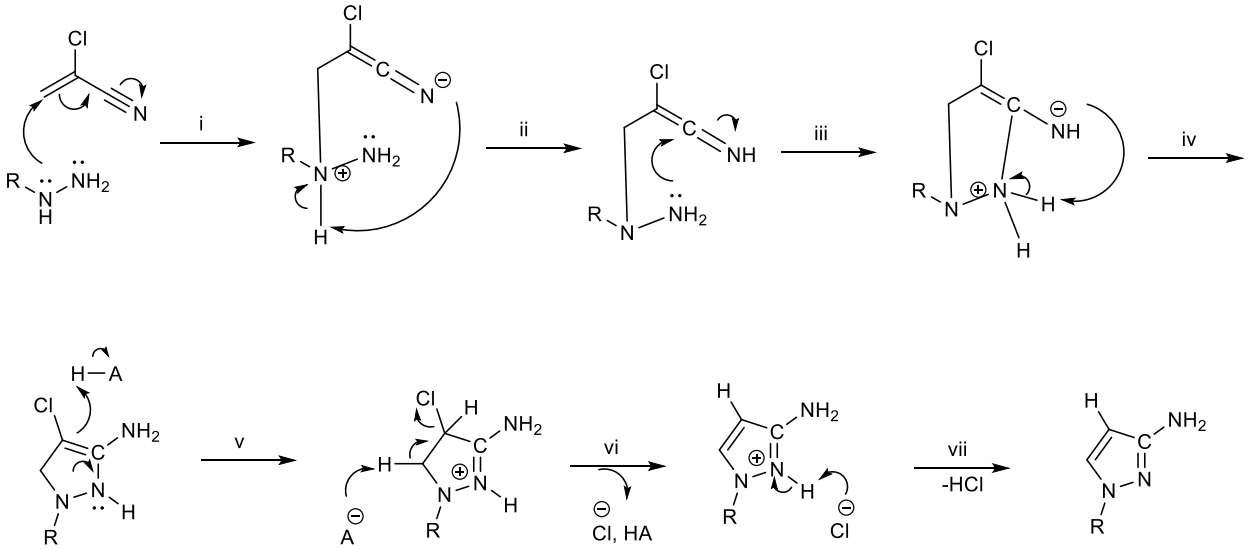

Scheme A.1 Proposed mechanism for the 3-aminopyrazole derivatives

As shown in Scheme A.1, the nitrile group shows an electron withdrawing effect, thus the terminal alkene will be more electrophilic to get attacked by the secondary amine of the hydrazine. Again, in step iii, the allene type of C is more electrophilic as the nitrogen's lone pair is not conjugated with the π electron cloud of the allene like system. After step iv, the rest of steps can be driven

forward by the fact of obtaining aromaticity of the final pyrazole product. In step vi, the base (conjugated base) can attack the proton on the carbon next to the substituted nitrogen. In accordance with an E2 mechanism (antiperiplanar orbitals) the Cl atom will leave the mother molecule. Therefore, according to this method, 3-amino pyrazole would be the predominant product.

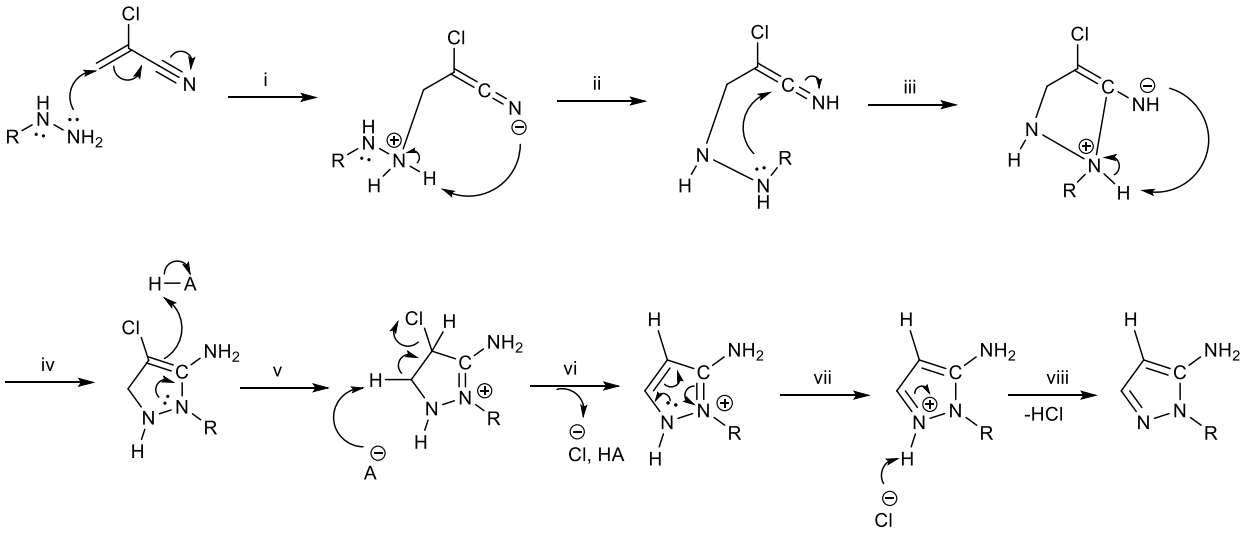

Scheme A.2 Proposed mechanism for the 5-aminopyrazole derivative.

However, if the primary amine of the hydrazine initiates the reaction, it could deliver 5-amino pyrazole as the major product, as shown in scheme A.2. According to this mechanism, the initiation step can be similar as shown in the above scheme (scheme A.1) due to the electron withdrawing effect of nitrile group. Then in step iii, the nitrogen's lone pair is not conjugated with the π electron cloud in the allene type system, thus making the center carbon more electrophilic. After step iii, the further reaction mechanism is driven to acquire aromaticity of the ring system. For this, in step vi, the most acidic proton will be abstracted by the conjugate base (resulting from step v), and the Cl atom will be leaving the ring according to an E2 mechanism (antiperiplanar) to afford the final product. Compared to the first proposed mechanism (scheme A.1), the second proposed mechanism (scheme A.2) requires a total of 8 steps to acquire aromaticity of the pyrazole. And

without any basic additives, It could show the formation of 5-aminopyrazole (Scheme A.2) as primary amine is smaller in size and easily attack the alkene (no steric hindrance). However, use of additives (bases) can shift the equilibrium to thermodynamic product side by deprotonating proton from secondary amine). Therefore, the above mechanism (scheme A.1) can be expected to be predominant and to form 3-aminopyrazole as the main product, leaving 5-aminopyrazole as the minor product.

Although it was not fully explained, the proposed scheme 1 can be supported by the two precedent papers.[234,235] In these publications, they have proposed very similar pathways for the reaction between 2-chloroacrylonitrile and hydrazine which afforded 3-aminopyrazole. According to these research publications, the hydrazine tends to attack the terminal alkene instead of the nitrile carbon.[235,234] Further more according to the general organic chemistry principals, nitrile possesses sp orbitals which has more electron density than alkene (sp^2 orbitals). So that terminal alkene is more electrophilic than nitrile C. Another possibility conjugated systems always favor to delocalize the electrons throughout the conjugated bonds. Therefore, accepting electrons to terminal alkene helps the delocalization of electrons toward nitrile group sequentially. Based on both the general concepts, nucleophilic attack on terminal alkene can be supported further.